

Towards optimal strength design of cold roll formed  
steel structural members considering manufacturing  
process effects

By:

Sangar Jamal Qadir

(BSc and MSc in civil and structural engineering)

University of Derby

Thesis submitted in partial fulfilment of the requirements  
for the degree of Doctor of Philosophy (PhD)

May 2021

# Table of Contents

<b>Table of Contents</b>	<b>ii</b>
<b>List of Figures</b>	<b>vii</b>
<b>List of Tables</b>	<b>xiii</b>
<b>Nomenclature</b>	<b>xvi</b>
<b>Declaration</b>	<b>xix</b>
<b>Abstract</b>	<b>xx</b>
<b>Acknowledgements</b>	<b>xxii</b>
<b>Publications</b>	<b>xxiii</b>
<b>Chapter 1 Introduction</b>	<b>1</b>
1.1 Background .....	1
1.2 Aim and objectives.....	7
1.3 Thesis layout .....	8
<b>Chapter 2 Literature review</b>	<b>10</b>
2.1 Cold roll forming of the manufacturing process and its typical shape defects .....	10
2.2 Manufacturing process effects in thin-walled cold formed structural members .....	15
2.2.1 Manufacturing process effects in cold formed structural column members.....	17
2.2.2 Manufacturing process effects in thin-walled structural beam members .....	49
2.2.3 Summary .....	54
2.3 Current design methods for thin-walled (CFS) members .....	56
2.3.1 Design of CFS members based on EWM in Eurocode 3.....	56
2.3.2 Design of CFS members based on DSM in AISI S100 .....	60
2.4 Optimisation of CFS section .....	67
2.5 Knowledge gap.....	71

2.6	Conclusions .....	74
<b>Chapter 3 Numerical validation of cold roll formed steel structural members</b>		<b>75</b>
3.1	Numerical Validation of cold formed steel beam member .....	75
3.1.1	Reference test programme .....	76
3.1.2	Finite Element modelling.....	79
3.1.3	Direct Strength Method.....	92
3.1.4	FE and DSM result validation.....	93
3.1.5	Conclusions.....	98
3.2	Numerical validation of cold-roll formed steel column member .....	99
3.2.1	Introduction.....	99
3.2.2	Experimental investigation .....	99
3.2.3	Development of FE models .....	101
3.2.4	Column member FE model's arrangement .....	101
3.2.5	Material model .....	102
3.2.6	FE model result validation .....	103
3.2.7	Conclusions.....	105
<b>Chapter 4 Parametric study of CFS longitudinally stiffened channel sections under bending</b>		<b>106</b>
4.1	Introduction .....	106
4.2	Description of investigated section dimensions and parameters.....	107
4.3	Parametric study and optimisation results.....	108
4.3.1	Effect of the position of the web stiffener <b><math>h_1/h</math></b> .....	108
4.3.2	Effect of the depth of the web stiffener <b><math>h_2/h</math></b> .....	112

4.3.3	Effect of the position of the peak of the web stiffener $h3/h$ .....	114
4.3.4	Effect of the width of the web stiffener $b1/b$ .....	116
4.3.5	Effect of the position of the flange stiffeners $b2/b$ .....	119
4.3.6	Effect of the size of the flange stiffeners $d/b$ .....	121
4.3.7	Effect of the number of stiffeners .....	123
4.3.8	Optimisation results .....	126
4.4	Conclusions .....	127
<b>Chapter 5 Parametric study of longitudinally stiffened CFS zed sections under bending</b>		<b>130</b>
5.1	Introduction .....	130
5.2	Description of investigated section dimensions and parameters.....	130
5.3	Parametric study and optimisation results.....	132
5.3.1	Effect of the position of the web stiffener $h1/h$ .....	132
5.3.2	Effect of the depth of the web stiffener $h2/h$ .....	136
5.3.3	Effect of the position of the peak of the web stiffener $h3/h$ .....	138
5.3.4	Effect of the width of the web stiffener $b1/b$ .....	140
5.3.5	Effect of the position of the flange stiffeners $b2/b$ .....	143
5.3.6	Effect of the size of the flange stiffeners $d/b$ .....	145
5.3.7	Effect of the number of stiffeners .....	147
5.3.8	Optimisation results .....	150
5.4	Conclusions .....	151
<b>Chapter 6 Finite Element modelling Optimisation of CFS longitudinally stiffened channel sections under bending</b>		<b>154</b>
6.1	Introduction .....	154

6.2	Finite Element modelling .....	155
6.3	Optimisation Method.....	156
6.3.1	Flow chart for FE modelling and Optimisation .....	158
6.3.2	Design OF Experiment .....	159
6.3.3	Response surface.....	160
6.3.4	Optimisation.....	162
6.4	Results and discussion.....	163
6.4.1	Design of experiment quality metrics .....	164
6.4.2	Response surface results .....	165
6.4.3	Optimisation results .....	169
6.5	Conclusions .....	177
<b>Chapter 7 Finite Element modelling Optimisation of CFS longitudinally stiffened zed sections under bending</b>		<b>184</b>
7.1	Introduction .....	184
7.2	Finite Element modelling.....	185
7.3	Optimisation Method.....	185
7.4	Results and discussion.....	188
7.4.1	Design OF Experiment quality metrics.....	188
7.4.2	Response surface results .....	189
7.4.3	Optimisation results .....	194
7.5	Conclusions .....	204
<b>Chapter 8 The influence of cold work effects on material properties and flexural strength of CFS beam sections</b>		<b>206</b>
8.1	Introduction .....	206

8.2	The cold work effects on mechanical properties of CFS sections .....	207
8.2.1	Tensile coupon tests carried out in this research .....	207
8.2.2	Predictive models.....	211
8.3	Finite Element modelling and optimisation .....	213
8.3.1	Tensile test .....	213
8.3.2	Four-point beam bending test .....	213
8.4	Optimisation.....	216
8.5	Results and discussion.....	222
8.5.1	Tensile coupon test carried out in this research .....	222
8.5.2	Comparisons of predictive models with measured increased yield stresses....	233
8.5.3	FE modelling.....	234
8.6	Conclusions .....	244
<b>Chapter 9</b>	<b>Conclusions</b>	<b>246</b>
9.1	Numerical validation .....	246
9.2	Parametric study and current design standards .....	248
9.3	New design optimisation approach .....	251
9.4	Experimental measurement and material testing .....	253
9.5	Recommendations for future research.....	254
<b>Appendices</b>		<b>256</b>
<b>Appendix A</b>		<b>256</b>
<b>Appendix B</b>		<b>265</b>
<b>Appendix C</b>		<b>271</b>
<b>Appendix D</b>		<b>274</b>
<b>References</b>		<b>276</b>

## List of Figures

Figure 1.1: Photo of different cold rolled formed steel channel and zed beams, commonly used in industrial roof systems (Hadley Industries plc.) .....	2
Figure 1.2: Typical cold roll formed steel sections for structural members: channel section with stiffeners (a), zed section with stiffeners (b), zed section with complex stiffeners (c), and photo of different cold rolled formed sections (d) (Hadley Industries plc.) .....	4
Figure 2.1: Example of cold-formed cross-sections gathered for column members .....	17
Figure 2.2: Local, distortional and global imperfections .....	18
Figure 2.3: LI effects from two manufacturing process types on peak load [35-45].....	22
Figure 2.4: DI effects from two manufacturing process types on peak load [35-45] .....	23
Figure 2.5: LI effects of different cross-sections on peak load [35-45].....	24
Figure 2.6: DI effects of different cross-sections on load-carrying capacity [35-45].....	25
Figure 2.7: FRS and MRS through wall thickness of a plate [46] .....	29
Figure 2.8: Flat regions FRS effects from CR & PB on peak load [35, 36, 38, 41, 59] .....	36
Figure 2.9: Flat regions MRS effects from CR & PB on peak load [35, 36, 38, 41, 59].....	36
Figure 2.10: Corner regions FRS effects from CR & PB on peak load [35, 36, 38, 41, 59] .....	37
Figure 2.11: Corner regions MRS effects from CR & PB on peak load [35, 36, 38, 41, 59].....	38
Figure 2.12: Stress-strain diagram for flat and corner region of a section .....	39
Figure 2.13: % yield strength increases effects from CR & PB on peak load [35, 36, 38, 41, 56, 58, 59] .....	41
Figure 2.14: % yield strength increases effects of different sections on peak load [35, 36, 38, 41, 56, 58, 59] .....	42
Figure 2.15: Example of cold-formed cross-sections collected for beam member .....	49
Figure 2.16: EWM simplified stress distribution.....	57

Figure. 3.1. A typical four-point bending test setup with channel sections.....	78
Figure 3.2. Cross section and dimensions (in mm) of the beam specimens used in experimental tests: (a) channel section, and (b) zed section. ....	78
Figure 3.3. Finite Element symmetry model with boundary conditions and closer view of the mesh of the channel section (in the box). ....	80
Figure 3.4. Engineering stress-strain data of the flat steel material of the channel section [142].	82
Figure 3.5. Distortional buckling mode obtained from the FE model for the channel section.....	84
Figure 3.6. Load-displacement curves of different initial imperfections used in the FEM for the channel section.....	85
Figure 3.7. Distortional buckling curve and modes for the channel section obtained from (a) CUFSM and (b) Distortional buckling mode obtained from the FE model after importing the buckling modes from CUFSM.....	87
Figure 3.8. Load-displacement curves of different initial imperfections used in the CUFSM-FEM for the channel section. ....	88
Figure 3.9. Stress-strain models for materials at different corners and stiffeners' bends used in FEM of (a) the channel section and (b) the zed section.....	91
Figure 3.10. Load-displacement curves for the channel sections from FEM, DSM and experimental results. ....	94
Figure 3.11. Deformed shapes at failure for the channel sections obtained by experimental tests (a), and FE modelling results isometric view (b), front view (c), back view (c), and un-deformed and deformed cross sections (e). Deformation values associated with colour contour ranged from green to blue with highest values in blue region.....	95
Figure 3.12. Load-displacement curves for the zed sections from FEM, DSM and experimental. ....	97
Figure 3.13. Deformed shapes at failure for the zed sections obtained by (a) experimental tests, and (b) FE modelling results. Deformation values associated with colour contour ranged from green to blue with highest values in blue region.....	97
Figure 3.14 (a) Cross-sections and geometries of column specimens and (b) overall view of testing setup Nguyen et al. [67] .....	101
Figure 3.15 FE model arrangement .....	102



Figure 3.16: Engineering stress-strain curves of the plain sheet steel materials [67].....	103
Figure 3.17 load-displacement curves of the FE models with and without cold-work compared with experiment .....	104
Figure 3.18: Buckling and failed mode shapes of the channel column (a) FE results and (b) experimental results. ....	105
Figure 4.1. Dimension parameters of the channel cross section (a) without flange stiffeners, and (b) with flange stiffeners. ....	108
Figure 4.2. Variation in the ultimate moment capacity for different positions of web stiffeners $h1/h$ without the cold work effect and with the cold work effect.....	110
Figure 4.3. Von Mises stress distribution at failure for different web stiffener positions (a) without the cold work effect and (b) with the cold work effect.....	111
Figure 4.4. Variation in the ultimate moment capacity for different shapes of web stiffeners $h2/h$ without and with the cold work effect. ....	113
Figure 4.5. Variation in the ultimate moment capacity for different positions of the web stiffener's peak in vertical direction $h3/h$ without the cold work effect and with the cold work effect. ....	115
Figure 4.6 Variation in ultimate moment capacity for different widths of the web stiffener $b1/b$ of web stiffeners without the cold work effect and with the cold work effect. FEM* is FEM results with bracing lengths the same with the critical distortional buckling half-wave length. ....	118
Figure 4.7. Comparison of the ultimate bending moment capacity for different widths of the web stiffeners (when $b1/b = 0.32$ and $0.39$ the sections failed in distortional-global interactive buckling modes).....	119
Figure 4.8. Variation in ultimate moment capacity for different positions of flange stiffeners $b2/b$ without the cold work effect and with the cold work effect.....	120
Figure 4.9. Variation in ultimate moment capacity for different sizes of flange stiffeners without the cold work effect and with the cold work effect. ....	122
Figure 4.10. Variation in ultimate moment capacity for different numbers of web and flange stiffeners for sections without and with the cold work effect. ....	124
Figure 4.11. The maximum % increase in the ultimate moment capacities without and with the cold work effect, of the channel sections with two web stiffeners and two flange stiffeners, against the geometric parameters.....	127

Figure 5.1. Dimension parameters of the zed cross section (a) without flange stiffeners, and (b) with flange stiffeners.....	132
Figure 5.2. Variation in the ultimate moment capacity for different positions of web stiffeners $h1/h$ without the cold work effect and with the cold work effect.....	134
Figure 5.3. Von Mises stress distribution at failure for different web stiffener positions (a) without the cold work effect and (b) with the cold work effect.....	135
Figure 5.4. Variation in the ultimate moment capacity for different shapes of web stiffeners $h2/h$ without and with the cold work effect. ....	137
Figure 5.5. Variation in the ultimate moment capacity for different positions of the web stiffener's peak in vertical direction $h3/h$ without the cold work effect and with the cold work effect. ....	139
Figure 5.6. Variation in ultimate moment capacity for different widths of the web stiffener $b1/b$ of web stiffeners without the cold work effect and with the cold work effect. ....	141
Figure 5.7. Comparison of the ultimate bending moment capacity for different widths of the web stiffeners (when $b1/b = 0.53$ and $0.63$ the sections failed in distortional-global interactive buckling modes).....	142
Figure 5.8. Variation in ultimate moment capacity for different positions of flange stiffeners $b2/b$ without the cold work effect and with the cold work effect.....	144
Figure 5.9. Variation in ultimate moment capacity for different sizes of flange stiffeners without the cold work effect and with the cold work effect. ....	146
Figure 5.10. Variation in ultimate moment capacity for different numbers of web and flange stiffeners for sections without and with the cold work effect. ....	148
Figure 5.11. The maximum % increase in the ultimate moment capacities without and with the cold work effect, of the zed sections with two web stiffeners and two flange stiffeners, against the geometric parameters. ....	151
Figure 6.1: Dimension parameters in (mm) and definition of design variables of the channel cross section (a) reference section, (b) without flange stiffeners, and (c) with flange stiffeners	158
Figure 6.2. The flowchart of the FE modelling and optimisation processes. ....	159
Figure 6.3: Normalized charts of the predicted vs observed values of section buckling and strength for DOE configuration. Square points are the DOE points and circular ones are the	

verification points. The black line shows the line in which the points could have a predicted value from response surface equal to the observed one in the design points. .... 164

Figure 6.4: Single parameter response for different positions of web stiffeners  $p1$  (a) buckling loads and (b) Developed stresses. .... 166

Figure 6.5: The local sensitivity bar chart of single parameters obtained for the channel section with flange stiffeners (a) buckling loads and (b) flexural developed stresses. .... 167

Figure 6.6: Double parameters response of the channel sections for different positions of web stiffeners  $p1$  and  $p2$  on (a) buckling loads and (b) flexural developed stresses, and for different sizes of edge and web stiffeners  $p3$  and  $p6$  on (c) buckling loads and (d) flexural developed stresses. .... 168

Figure 6.7. Strength results of standard, reference and optimised channel sections for (a) buckling and (b) ultimate moment capacity with the cold working effect included. .... 172

Figure 6.8. Load-displacement curves for the channel reference and design Candidate 6 sections. .... 173

Figure 6.9. Dimensions, deformed shapes and von Mises stress distribution for all design candidates of channel sections. .... 173

Figure 7.1. Dimension parameters in (mm) and definition of design variables of the zed cross section (a) reference section, (b) without flange stiffeners, and (c) with flange stiffeners. .... 187

Figure 7.2. Normalised charts of the predicted vs observed values of section buckling and strength for DOE configuration obtained for the zed section with flange and web stiffeners. Square points are the DOE points and circular ones are the verification points. The black line shows the line in which the points could have a predicted value from response surface equal to the observed one in the design points. .... 189

Figure 7.3. Single parameter response for different positions of web stiffeners  $p1$  (a) buckling loads and (b) Developed stresses. .... 191

Figure 7.4. Local sensitivity bar of single parameter obtained for the zed section with web and flange stiffeners (a) buckling and (b) developed stresses. .... 192

Figure 7.5. Double parameters response of the zed sections for different positions of web stiffeners  $p1$  and  $p2$  on (a) buckling loads and (b) flexural developed stresses, and for different web stiffeners through the angle parameters  $p6$  and  $p8$  on (c) buckling loads and (d) flexural developed stresses. .... 194

Figure 7.6. Strength results of standard, reference and optimised of the zed sections for (a) buckling and (b) ultimate moment capacities with the cold work effect included. ....	198
Figure 7.7. Load-displacement curves for the zed reference and design Candidate 6 sections. ....	199
Figure 7.8. Dimensions, deformed shapes and von Mises stress distribution for all design candidates of zed sections. ....	199
Figure 8.1. Locations of extracted tensile coupons (a) pre-cold rolled sheet coil, (b) longitudinal channel section, (c) channel cross-section, and (d) Zed cross-section. ....	208
Figure 8.2. Macro photograph of the cross section of a typical curved coupon. ....	209
Figure 8.3. Typical tensile test setup (a) flat coupon and (b) Curved coupons. ....	210
Figure 8.4. Typical curved coupons before and after testing attached with strain gauges for the cross-section Z-W200T2.0 (Extracted from curved location 1a, 1b, 1c and 1d). ....	211
Figure 8.5. The measured stress-strain curves of the flat and curved coupons carried out in this study, and used in the FEM (a) Z-W200T2.0 and (b) C-W200T2.0. ....	216
Figure 8.6. Dimension parameters in (mm) and definition of design variables of the channel cross section (a) reference section, (b) without flange stiffeners, and (c) with flange stiffeners. ....	218
Figure 8.7. Dimension parameters in (mm) and definition of design variables of the zed cross section (a) reference section, (b) without flange stiffeners, and (c) with flange stiffeners. ....	219
Figure 6.2. The flowchart of the FE modelling and optimisation processes [152]. ....	220
Figure 8.9. Engineering stress–strain relationships of the tensile tests for the cross-section Z-W200T2.0 (Typical flat and curved coupon test results). ....	227
Figure 8.10. Engineering stress–strain relationships of the tensile tests for the section (a) Z-W200T2.0, (b) Z-W145T1.2, (c) C-W200T2.0 and (d) C-W145T1.2. ....	229
Figure 8.11. Yield strength enhancement due to cold roll forming (a) channel cross-section C-W200T2.0, and (b) Zed cross-section Z-W200T2.0. ....	230
Figure 8.12. Ultimate strength enhancement due to cold roll forming (a) channel cross-section C-W200T2.0, and (b) Zed cross-section Z-W200T2.0. ....	231
Figure 8.13. Yield strength enhancement due to cold roll forming (a) channel cross-section C-W145T1.2, and (b) Zed cross-section Z-W145T1.2. ....	231

Figure 8.14. Ultimate strength enhancement due to cold roll forming (a) channel cross-section C-W145T1.2, and (b) Zed cross-section Z-W145T1.2.....	232
Figure 8.15. FE and experimental stress–strain curves of the typical flat and curved coupon specimens.....	235
Figure 8.16. Ultimate bending strength to yield ratio with the cold work effects and without the cold work effects for (a) the channel cross sections and (b) the Zed cross sections.....	240
Figure 8.17. Load-displacement curves for the reference section and design candidate 6 results for (a) the channel sections and (b) the zed sections. ....	241
Figure 8.18. Bending strength enhancement due to cold roll forming process obtained for different ratios of ultimate tensile strength to yield strength of the materials for the reference and optimised sections (a) channel sections and (b) zed sections. The material properties at flat parts obtained from [142] and the material properties at corners $f_{yc}$ was determined using the North the AISI Specification.....	243

## List of Tables

<b>Table 2.1:</b> Summary of previous research to evaluate influences of the manufacturing process on strength capacity of CFS column members based on experimental and numerical data for channel sections.....	45
<b>Table 2.2:</b> Summary of previous research to evaluate influences of the manufacturing process on strength capacity of CFS column members based on <i>experimental and numerical data</i> for other sections.....	46
<b>Table 2.3:</b> Summary of previous research to evaluate influences of the manufacturing process on strength capacity of thin-walled CFS column members based on <i>pure numerical data</i> for channel sections.....	47
<b>Table 2.4:</b> Summary of previous research to evaluate influences of the manufacturing process on strength capacity of thin-walled CFS column members based on <i>pure numerical data</i> for other sections.....	48
<b>Table 2.5:</b> Summary of previous research to evaluate influences of manufacturing process on strength capacity of thin-walled CFS structural beam members based on <i>experimental and numerical data</i> .....	53
<b>Table 3.1</b> Initial geometric imperfection values proposed by different studies. ....	84

<b>Table 3.2</b> Yield stresses and tensile strengths at corners and stiffener’s bends using the North American specification [3].	90
<b>Table 3.3</b> The average yield stresses of different cross sections obtained using the North American Specification.	92
<b>Table 4.1</b> Variation in ultimate bending moment capacity for different positions of web stiffeners. $M_u$ , $M_{uc}$ stand for ultimate moment capacity without and with the cold work effect, respectively. $f_{ya}$ is the average yield strength of the whole section.	111
<b>Table 4.2</b> Variation in ultimate bending moment capacity for different depths of the web stiffener.	113
<b>Table 4.3</b> Variation in ultimate bending moment capacity for different positions of the web stiffener’s peak in vertical direction.	115
<b>Table 4.4</b> Variation in ultimate bending moment capacity for different widths of the web stiffeners.	118
<b>Table 4.5</b> Variation in ultimate bending moment capacity for different positions of flange-intermediate stiffeners.	121
<b>Table 4.6</b> Variation in ultimate moment capacity for different sizes of flange stiffeners.	123
<b>Table 4.7</b> Variation in ultimate moment capacities for different numbers of web and flange stiffeners.	125
<b>Table 5.1</b> Variation in ultimate bending moment capacity for different positions of web stiffeners. $M_u$ , $M_{uc}$ stand for ultimate moment capacity without and with the cold work effect, respectively. $f_{ya}$ is the average yield strength of the whole section.	135
<b>Table 5.2</b> Variation in ultimate bending moment capacity for different depths of the web stiffener.	137
<b>Table 5.3</b> Variation in ultimate bending moment capacity for different positions of the web stiffener’s peak in vertical direction.	139
<b>Table 5.4</b> Variation in ultimate bending moment capacity for different widths of the web stiffeners.	142
<b>Table 5.5</b> Variation in ultimate bending moment capacity for different positions of flange-intermediate stiffeners.	144
<b>Table 5.6</b> Variation in ultimate moment capacity for different sizes of flange stiffeners.	146

<b>Table 5.7</b> Variation in ultimate moment capacities for different numbers of web and flange stiffeners.....	149
<b>Table 6.1:</b> Ranges of values considered for the optimisation in (mm for length parameters and degrees for angle parameters). .....	157
<b>Table 6.2:</b> Candidate design when the target objectives were maximizing buckling and minimizing flexural developed stresses (Candidate 6). .....	170
<b>Table 6.3:</b> The results of buckling load ( $P_b$ ), flexural developed stresses ( $\sigma$ ) and ultimate moment capacity of channel sections. $M_u$ , $M_{uc}$ stand for ultimate moment capacity without and with the cold working effect, respectively. ....	171
<b>Table 7.1</b> Range of values considered for the optimisation in (mm and degree).....	187
<b>Table 7.2</b> Candidate design when the target objectives were maximising buckling and minimising developed stresses (Candidate 6).....	196
<b>Table 7.3</b> The results of buckling load ( $P_b$ ), flexural developed stresses ( $\sigma$ ) and ultimate moment capacity of zed sections. $M_u$ , $M_{uc}$ stand for ultimate moment capacity without and with the cold working effect, respectively. ....	197
<b>Table 8.1</b> Cross-section dimensions of standard, reference and optimised CFS channel sections. ....	221
<b>Table 8.2</b> Cross-section dimensions of standard, reference and optimised CFS zed sections. ...	222
<b>Table 8.3</b> Measured material properties of tensile coupon for Z-W200T2.0.....	223
<b>Table 8.4</b> Measured material properties of tensile coupon for Z-W145T1.2.....	224
<b>Table 8.5</b> Measured material properties of tensile coupon for C-W200T2.0. ....	225
<b>Table 8.6</b> Measured material properties of tensile coupon for C-W145T1.2. ....	226
<b>Table 8.7</b> Comparison of the proposed predictive models and representative test data for the 0.2% proof strength of curved regions of cold-formed sections ( $f_{yc,pred} / f_{yc,test}$ ). The tensile tests conducted by the author in this study. ....	234
<b>Table 8.8</b> Ultimate moment capacity obtained from experimental tests [142] and FE models. $M_u$ , $M_{uc1}$ , $M_{uc2}$ stand for ultimate moment capacity without and with the cold work effect using both the measured material properties conducted by the author in this research and the AISI specification predicted values, respectively. ....	236

**Table 8.9** Buckling and ultimate moment capacity of standard and optimised CFS channel and zed sections.  $M_u$ ,  $M_{uc}$  stand for ultimate moment capacity without and with the cold work effect, respectively. The measured material properties carried out by the author was employed in the FE models to obtain buckling and ultimate moment capacities of the sections. .... 239

## Nomenclature

### English Symbols

CFS	Cold Formed Steel
FEM	Finite Element Modelling
DSM	Direct Strength Method
EWM	Effective Width Method
AISI	North American Specification
EC3	Eurocode 3
BS	British Standard
DOE	Design of Experiment
RS	Response Surface
MOGA	Multi-Objective Genetic Algorithm
LI	local imperfection
DI	distortional imperfection
GI	global imperfection
GBT	generalised beam theory
MRS	membrane residual stresses
FRS	flexural (bending) residual stresses
CR	cold roll forming
PB	press braking forming
$f_y$	material yield strength
$f_u$	material ultimate strength
$f_{yb}$	basic material yield strength
$f_{ya}$	average material yield strength



$f_{yf}$	average yield strength of the flat areas
$f_{yc}$	average yield strength of corners
$C$	ratio of corner area to total cross-section area
$f_{yv}$	yield strength of virgin material
$f_{uv}$	ultimate strength of the virgin material
$t$	plate thickness
$R$	inside bend radius
$A_g$	gross cross-section area
$M_{ne}$	nominal flexural strength for lateral-torsional buckling
$S_f$	gross section modulus referenced to the extreme fibre at first yield
$M_{cre}$	critical elastic lateral-torsional buckling moment
$M_{nl}$	nominal flexural strength for local buckling
$M_{nd}$	nominal flexural strength for distortional buckling
$E$	young's modulus of elasticity
$d_1$	maximum local buckling imperfection (Schafer and Peköz's)
$d_2$	maximum distortional buckling imperfection (Schafer and Peköz's)
$h$	section height
$c$	lip length
$h_1$	position of the web stiffener from the web-flange junction
$h_2$	depth of the web stiffener
$h_3$	position of the peak of the web stiffener in vertical direction from the web-flange junction
$b$	flange width
$b_1$	width of the web stiffener
$b_2$	position of the flange stiffener
$d$	width and depth of the flange stiffener (circular shape)
$S_{xx}$	major axis sectional modulus
$S_{zz}$	minor axis sectional modulus
$M_y$	yield bending moment
$M_u$	ultimate bending moment without the cold work effects

$M_{uc}$  ultimate bending moment with the cold work effects

### **Greek Symbols**

$\lambda_c$  global buckling slenderness

$\lambda_l$  local buckling slenderness

$\sigma_{crl}$  critical elastic local buckling stress

$\lambda_d$  distortional buckling slenderness

$\sigma_{crd}$  critical elastic distortional buckling stress

$\nu$  Poisson's ratio

$\sigma_{eng}$  engineering stress

$\varepsilon_{eng}$  engineering strain

$\sigma_{true}$  true stress

$\varepsilon_{true}^{pl}$  true plastic strain

$\varepsilon_f$  engineering strain at failure

## **Declaration**

I confirm that the work of this thesis is my own. I provide citations and references whenever I describe and quote from the published, or unpublished, work of others.

## Abstract

Cold-formed steel (CFS) materials are increasingly used in a wide range of applications in building construction. CFS structural members possess many advantages, most notably high load capacity-to-weight ratio and high speed of construction. To design CFS members accurately and gain optimal structural performance, the two factors, namely ‘geometry effect’ and ‘manufacturing effect’, must be included in design procedures. However, whilst the first has been widely investigated and implemented in design, the latter has not been much studied and considered in the current design practices. This research aims to develop and validate an optimal strength design approach that takes into consideration key ‘geometry’ and ‘manufacturing process’ effects on the material and structural properties into the design of CFS structural members. The cross-sectional shapes considered in this research were channel and zed sections as they are widely used in building construction applications. Numerical modelling and physical testing of the material during the manufacturing process were carried out and implemented to examine the behaviour and design of CFS structural members subjected to load in building applications.

Different Finite Element (FE) model arrangements and methods to predict the buckling and nonlinear buckling analyses were tested. The FE models were assessed and validated against experimental data from literature studies, with an excellent degree of comparability. The models were then utilised to perform comprehensive parametric studies and optimise CFS sections.

A comprehensive parametric study for longitudinally stiffened channel and zed beam sections under distortional bending was conducted to investigate the effects of a stiffener’s properties on the section strength including its position, shape, size and material properties by the cold work at bends. Limits for optimal design of the sections were suggested. The suitability of a design method, the Direct Strength Method (DSM), in predicting the ultimate moment capacity for CFS beam sections was assessed using the FE analyses results. The DSM predictions were found significantly cross-sectional dependent, especially in the sections where the tip of web stiffeners shifted away from the web in horizontal direction failed by distortional-global buckling (D-G), providing more accurate predictions for certain cross-sections than for others. Shortcomings were confirmed and suggestions for improvements were given, especially the inclusion of the D-

G in the DSM design guideline. This may confirm that the design methods previously used for optimisation are somewhat simplistic and the reported optimisation results not correct in their predictions.

A new, more sophisticated practical design approach has been developed by combining detailed nonlinear FE modelling and optimisation. It accounted for all possible buckling failures considering the effects of key ‘geometry’ and ‘manufacturing process’ factors, such as initial geometric imperfections and work-hardening introduced by the cold-rolling process. The validated FE model innovatively combined with the optimisation algorithms using integrated Design Of Experiment, response surface methodology and multi-objective genetic algorithm. The optimisation approach was devised to achieve the optimal design shape of the channel and zed sections under distortional bending. Some significant improvements have been obtained in distortional buckling and ultimate bending strength of the optimal cross-section shapes, compared to the original sections, without increasing the amount of the material used.

Experimental measurements and testing of the materials were carried out to investigate the change of material properties during the manufacturing process, and their results were used for the validation of numerical simulations. The experimental programme has been fully described within this research, including techniques implemented, data generated, and analysis methods adopted. The results of the current test programme were used to investigate the cold work effects on the corner and stiffener bend regions of CFS sections and the accuracy of existing predictive models was evaluated. The results were then used to accurately quantify the cold work effects on the bending strength of the CFS sections. It has been revealed that the optimised sections achieved were less prone to distortional buckling failure and have gained significant section strength benefit from the cold work effects. It was also shown that the effects of geometry and the manufacturing process had to be carefully considered to design CFS members accurately and gain optimal structural performance. Recommendations for further research are also proposed.

**Keywords:** Cold-formed steel (CFS); longitudinally stiffened section; distortional buckling; finite element modelling; optimisation; cold work effect; material testing.

## **Acknowledgements**

The research involved in this PhD thesis has come to end due to the advice and help of my friends and family whom I cannot name individually, but there are a few which I must name and thank specifically.

I am extremely grateful to my kind director of the study Ass. Professor Van Bac Nguyen for the excellent roles in guidance, insight knowledge, outstanding research, trust and support during the development of this work. It would be impossible to come to this point without his motivation, attitude, patient and kindness.

I am pleased to thank my supervisors Dr Boris Ceranic and Dr Eleni Tracada for the advice and support they provided me during my study.

I am also grateful to my external supervisor at the University of Sheffield Dr Iman Hajirasouliha for giving support, suggestion, explanation and help for everything I asked.

I would like to thank the University of Derby for providing the fund of the project [PGTA Studentship - E&T\_14\_PGTA\_0717] that helped me to conduct this work.

I am pleased to thank Hadley Industries plc. for the support provided during my PhD study, especially Dr. Martin English and Mr Brian Cartwright.

I am very grateful to Ass. Professor Dr Sirwan Kh.Rashid at the University of Sulaimani/ College of Engineering/ who encouraged me to do my PhD.

I am pleased to thank all my friends and relatives in Kurdistan and UK who encouraged me throughout my study.

The last but not the least I want to thank my wonderful mother, Maryam Hama, my father, Jamal Qadir, and my sisters Dilman, Dilan, Daron, Hezha and Darvin. I dedicate my thesis to them.

## **Publications**

The following publications are the results of this doctoral study including journal and conference paper as well as presentations.

### **Journal publication**

“**Qadir, S. J.**, et al. "Optimal design of cold roll formed steel channel sections under bending considering both geometry and cold work effects." *Thin-Walled Structures* 157 (2020):107020.”  
<https://doi.org/10.1016/j.tws.2020.107020>.

“**Qadir, S. J.**, et al. “Shape optimisation of cold roll formed sections considering effects of cold working”, *Thin-Walled Structures* 170 (2022) 108576. <https://doi.org/10.1016/j.tws.2021.108576>

“**Qadir, S. J., et al.** “The effects of cold working on tensile and flexural strengths of cold roll formed steel sections with complex stiffeners. To be submitted to *Journal of Constructional Steel Research*.

### **Conference publication**

“**Qadir, S. J.**, et al. "Optimisation of flexural strength for cold roll formed sections using design of experiments and response surface methodology." (2020).” URL:  
<http://jhir.library.jhu.edu/handle/1774.2/63190>.

### **Conference oral presentation**

**Qadir, S. J.**, et al. Optimisation of flexural strength for cold roll formed sections using design of experiments and response surface methodology, CFSRC Colloquium, United State, online 20-21 October 2020.

**Qadir, S. J.**, et al. Development of more efficient cold roll formed steel channel sections under bending using combined Finite Element modelling and optimisation, PGR Virtual Café, University of Derby, online 28 January 2021.

**Qadir, S. J.**, et al. Finite Element modelling Optimisation of cold roll formed UltraBeam and UltraZed beam sections under bending, Hadley Industry, online 17 February 2021.

# Chapter 1 Introduction

## 1.1 Background

Two families of structural metallic material are widely used in building construction such as steel and stainless steel. Both families can be hot-rolled shapes or cold-formed from a plane or strip sheet in press braking and cold roll forming process. The hot-rolled structural members are inevitably used in many structural applications, in particular, the primary structural members of a high-rise building. While the use of cold-formed steel (CFS) structural members begun in the 1850s in the United States and Great Britain in building applications, such steel members were not widely used in building construction. However, the use and the development of thin-walled cold-formed steel structural members have emerged in the world as primary framing components over the past years. The types of CFS members in building constructions are generally classified per their applications such as panel decking and individual structural framing members.

CFS members in the form of panels decking have gained widespread acceptance to be used for wall panels, floor decks and roof decks. The surface decking with applied concrete forms composite walls and composite slabs that have been used in multi-storey floors building. Composite walls and slabs are efficient in terms of strength and stiffness to carry loads. The steel sheets used in the composite slabs are thin enough to provide light-weight members, less than 2 mm. Thus, the CFS structural members can be effectively used to develop a composite system with impressed load carrying capabilities for walls and floor structures.

Another important form of CFS structural members used in building construction is individual structural sections as shown in Figure 1.1 for typical structural members. The most common CFS sections are channels (C-Section), Z-sections, hollow sections (circular, square and rectangular hollow sections), pallet rack, angles and hat sections. The first two types of cross-sections are often used for structural beam members and the other cross-sections are generally utilised for structural column members. The cold roll formed steel channel and zed beams, commonly used in industrial roof systems, were used in this study. They are thin-walled sections formed subsequently from the cold forming process. The thickness of the sections is generally less than



6mm and called light gauge sections. However, the thickness of less than 25mm has been cold-formed due to the new advanced technology of manufacturing process and the thickness of about 8mm has been successfully implemented in building applications. The depth of the individual structural sections usually ranges between 50 mm to 400 mm and the depth of 457 mm has been used, in some cases, with a thickness of about 13mm in transportations and building applications.

‘Content removed due to copyright reasons’

Figure 1.1: Photo of different cold rolled formed steel channel and zed beams, commonly used in industrial roof systems (Hadley Industries plc.).

Both the panels decking and the individual structural framing members with the hot-rolled steel shapes are used to supplement each other [1]. The hot-rolled shapes are the main structural members and CFS members are the secondary elements in high-rise buildings. However, CFS

members have been also used as primary structural components such as column and beam in building up to six floors height [2]. Two methods are often used in the manufacture of CFS sections such as press braking and cold roll forming.

In the press braking process, the profile shape is formed by pressing the steel sheet between shaped die to form cross-sections and each bend is often formed separately. It is an efficient and cost-effective method of cold-formed of the manufacturing process only for low volume production and shorter cross-section length. Hence, a wide range of cross-sectional areas can be produced by the press braking approach. However, this method of the manufacturing process has some limitations including the length of the members that are normally ranged to less than 5 metres to the maximum 8 metres and it is labour intensive as well as it is often difficult to obtain value-added features like holes or punched shapes and restriction on the profile geometry that can be formed, in particular, complex geometry with rip and stiffeners.

For more complex cross-sectional shapes, cold roll forming of the manufacturing process is generally used to obtain a more economical product. In this approach, a continuous steel strip is fed through a series of opposing rolls arranged in tandem to progressively form the strip into the desired shape of the cross-section (as illustrated in Figure 1.2). The machine used in the cold roll forming consists of a pair of rolls and each pair of opposing rolls is called a stage. In general, simple sections need less time and few numbers of stages to form the cross-section, whilst the more complex the cross-sectional shape is the more times (several days) and the number of stages (as many as 22 stages) required. An automatic cut-off tool is used to cut the structural members to the desired length without stopping the roll forming operation. Thus, there is no restriction on the length of the members in the cold roll forming process and also allows adding tooling to form any complex cross-sections. In this method, most advanced profile systems for almost every cross-section type have been produced and made construction faster and easier. This versatility on the manufacturing side has required the structural engineers seeking for optimal design solutions that minimize the initial steel strip of the cross-section to a minimum while maintaining the structural performance, hence reducing the major financial outlay in the process which is the material cost.

‘Content removed due to copyright reasons’

Figure 1.2: Typical cold roll formed steel sections for structural members: channel section with stiffeners (a), zed section with stiffeners (b), zed section with complex stiffeners (c), and photo of different cold rolled formed sections (d) (Hadley Industries plc.).

On the other hand, different levels of cold-work (plastic deformation) are generated during the section forming process, resulting in changes to the mechanical properties of the virgin coil material. The varying level of cold-work induced at different positions around the section shape is often seen in CFS sections especially in the sections having stiffener's and rib regions. The curved regions of the CFS sections experience large plastic deformation from the cold work effects compared to the flat counterpart regions, hence resulting in an increased material yield strength and, relatively lesser, an increased material ultimate strength, but reduced material ductility. The influence of cold work effects on mechanical properties of the material and structural behaviour of the members is an essential part of structural engineering and a key component of analytical, numerical and design models. Over the last few decades, multiple studies have been carried out to quantify the cold work effects in the highly cold-worked curved regions of metallic material and developed a number of models to predict the strength enhancement. A number of studies has investigated the cold formed sections, where the researchers quantified the cold work effects on mechanical properties of the material and studied their effects on structural behaviour of the sections. Some researchers measured the strength enhancement in the section corners and pointed out that it had negligible effect on load-carrying

capacity of structural column members. Other researchers, however, have shown the cold work effects to have significant influence on load carrying capacity of structural column and beam member.

The design of CFS structural members is different from hot-rolled shape since the former is greatly affected by manufacturing process and subjected to various types of buckling such as global, local, distortional and interaction between these buckling. Local and distortional buckling are particularly prevalent in CFS sections, which are characterised by the relatively short wavelength buckling of the individual plate and members. Therefore, special design standards have been developed for these structural members.

The American Iron and Steel Institute published the specification for the design of CFS structural members in the United States in 1946. The specifications have been regularly updated to the most recent 2016 edition so as to include the developments obtained from research [3]. The first edition of the unified North American Specification that was applicable to the United States, Canada and Mexico published in 2001. The specification was later revised to include supplement 2004, Appendix 1, Design of Cold-Formed Steel Structural Members Using Direct Strength Method (DSM). In the UK, British Standard BS5950-5: 1998 [4] provides recommendation for the design of structural cold formed sections, which is primarily intended for steel sections of thickness up to 8 mm. In Europe, supplementary rules for cold-formed thin gauge members and sheeting are the primary specification document. This document originally produced by the ECCS Committee TC7 to provide the European Design Recommendations for light gauge steel members in 1987. Later on, the document further updated and published in 2006 as the Eurocode 3 (EC3): Design of steel structures. Part 1-3: General Rules [5].

The design methods available in the design guidelines [3-5] have been widely used to optimise the relative dimensions of predefined orthodox CFS cross-sections including channel, zed and sigma sections. The majority of these design guidelines [3-5] uses the Effective Width Method for strength determination. This method is feasible for rather conventional sections for which a distinction between web, flanges and lips can be made and which fall within the dimensional limits of the design standard. It becomes problematic, however, when the aim is to generate novel, previously undiscovered shapes in a free-shape optimisation, as the conventional

standards are typically not applicable. In addition, the design of the channel and zed sections with complex folded-in stiffeners used in this thesis using this method is very complicated and impractical, especially the incorporation of computing buckling modes such as distortional buckling would be difficult for these sections. Therefore, it has not yet a suitable method to be used in this research.

The Finite Strip Method (FSM) and the DSM have been used as an alternative in some of the recent optimisation studies of CFS structural members. The DSM only needs the elastic critical local, distortional, and global buckling stresses calculated in order to predict the strength capacity and can therefore, in principle, be applied to any shape. The elastic buckling stresses can thereby be obtained from a Finite Strip (FSM) analysis. This method, however, has some shortcomings. The statistical correlation between a cross-sectional slenderness parameter and the ultimate strength capacity was used to develop the DSM equations. This might exhibit a significant coefficient of variation and make the DSM predictions significantly cross-sectional dependent, resulted in providing more accurate prediction for certain cross-sections than for others. The DSM ignores distortional-global or local-distortional interactions. This can be significantly problematic as reported optimisation results may not be correctly predicted.

It should be noted that, however, the majority of the previous studies were for columns under compression or hat sections under bending and there have been limited investigations on channel and zed sections with web stiffeners subjected to bending stresses. Regarding optimisation, there has been a limited study on the stiffener's geometric effects including shape and position of the stiffeners to the section strength under bending. In these numerical studies, it was all assumed that the material properties at corner and bends of the intermediate stiffeners were the same with those at flat sections. On the other words, the effect of the cold work by the cold roll forming manufacturing process in enhancing the material properties at the stiffener's corners was not considered. This meant that there have been not available any optimal design studies that took into account the effect of both the stiffeners' geometry and the cold work effect on the strength of the section. In addition, previous studies on the optimisation of CFS sections have been primarily limited to use analytical formulas or the methods available in the Codes and Specifications to calculate the elastic buckling and flexural strength of the structural members. Given the listed shortcomings of the current design methods provided in standards and

specifications, uncertainty surrounds the question whether the presented solutions were truly optimal. The knowledge gaps require thorough investigations toward an optimal strength design of CFS structural members.

## **1.2 Aim and objectives**

This research study aims to contribute towards development of an optimal strength design approach that takes into consideration key ‘geometry’ and ‘manufacturing process’ effects to the material and structural properties into the design of cold formed steel (CFS) structural members.

The major objectives of this research are to:

- Carry out an in-depth detailed study of subject-specific literature in order to assess, interrogate and inform current approaches to the optimal strength design of thin-walled cold roll-formed steel structural members.
- Develop a validated numerical model using FE models to replicate CFS structural members subjected to load in building applications, which the channel and zed sections were selected in this study as they are widely used in building construction applications.
- Conduct a comprehensive parametric study to investigate the effects of stiffeners’ shapes, sizes, positions and cold work induced from the cold roll forming process on the section’s buckling and ultimate strengths of channel and zed cross-sections.
- Develop a new practical design approach using integrated detailed nonlinear FE models with design of experiment and response surface methodology so as to optimise CFS sections with longitudinal intermediate stiffeners in the flanges and web under distortional bending considering the geometry and manufacturing process effects.
- Undertake experimental tests for thin-walled cold roll-formed steel members during the manufacturing process and investigate the structural performance of the final members in applications as well as quantify the work-hardening introduced by the cold-rolling process in the corner and stiffener bend regions of cold roll formed sections and analyse the applicability of existing predictive models for CFS structural sections.
- Propose optimal cross-sectional shape of the longitudinally stiffened channel and zed sections, and propose a design methodology considering the effects of geometry and manufacturing process in CFS structural members.

The knowledge generated and engineering optimisation tools developed in this research will advance structural optimisation procedure and support developments of more efficient CFS sections to be used in civil and structural applications.

### 1.3 Thesis layout

The thesis comprises 9 chapters and a brief summary of each chapter is presented below:

**Chapter 1** covers an introduction and background of the project, where an overview of the geometry and manufacturing effects on mechanical properties and strength of the cold formed sections by experimental testing and combined detailed (FE) models and optimisation, the design method available in current standard and specifications, and the complicated behaviour of CFS structural members are discussed. The aim, objectives and organisation of the thesis are also provided.

**Chapter 2** is a review of most relevant literature, which provides: an overview of cold roll forming of the manufacturing process and its typical shape defects, how manufacturing process influences the mechanical properties and the behaviour of cold formed structural members, the most widely design methods for cold formed steel structures and their shortcomings, and previous studies of optimisations for cold formed sections. It identifies the knowledge gaps led to the subject of this research based on the main findings from current published studies.

**Chapter 3** presents a numerical validation study of cold roll formed steel structural members compared to laboratory experimental results. Several different modelling configurations are considered including model arrangement, material properties, mesh sizes and boundary conditions. The validated model is then employed for parametric study and optimisation in the following described chapters.

**Chapter 4** includes numerical investigations of the effect of both the stiffeners' geometry and cold work on the buckling and ultimate bending strength of **channel sections** with longitudinal web and flange stiffeners. Limits for optimal shape of the channel section are proposed by taking single parameter response into account. It covers the investigations of suitability of current DSM design rules for CFS longitudinally stiffened channel sections.

**Chapter 5** is an extension of chapter 4 but investigated the behaviour of structural **zed sections**. Limits for the optimal shape of the zed section are proposed by considering single parameter response surface (The single parameter response surface is always used for conventional optimisation design since it is easily obtained by an orthogonal test). It covers the investigations of suitability of current DSM design rules for CFS longitudinally stiffened zed sections.

**Chapter 6** describes a new practical design optimisation method by combining detailed nonlinear FE models and optimisation using integrated Design of Experiment (DOE), Response Surface (RS) method and Multi-Objective Genetic Algorithm (MOGA). It includes the detailed optimisation of CFS channel sections under bending using the developed optimisation method. The optimal shape of the channel sections is achieved by considering multiple parameter response surfaces such as parameters related to the relative dimensions of the section, the stiffeners' geometry and the cold work effects.

**Chapter 7** presents the detailed optimisation of CFS zed sections under bending using the developed optimisation approach. It confirms the applicability of the optimisation method that can be applied for any cross-sectional shapes. It provides the optimal design shape of the zed sections.

**Chapter 8** includes study of the cold work effects on mechanical properties of the material and structural behaviour of the longitudinally stiffened cold roll formed steel beam sections under bending using experimental testing and numerical modelling. It describes a test programme of the materials during the manufacturing process which cover a wide range of cross-section geometries (longitudinally stiffened channel sections and longitudinally stiffened zed sections). The experimental programme is fully described including implemented techniques, data generated and analysis methods adopted. The results from the test programme are used to investigate the cold work effects in the corner and stiffener bend regions of cold roll formed sections and the accuracy of existing predictive models is evaluated. The results are then incorporated into detailed non-linear Finite Element (FE) modelling to obtain more efficient cold roll formed steel sections in bending.

**Chapter 9** provides the conclusions and outcomes of the research of previous chapters, and presents some recommendations needed for future works.



## **Chapter 2 Literature review**

The present research deals with the possibility of considering key ‘geometry’ and ‘manufacturing process’ effects to the material and structural properties into the design of cold formed steel (CFS) structural members. The most relevant studies including analytical, experimental and numerical investigations related to the subject is reviewed in this chapter. The reviews comprise several sections: the cold roll forming of the manufacturing process and its typical shape defects induced in cold roll formed steel members are introduced in Section 2.1; then, how the manufacturing process and the shape defects affect the material properties and the behaviour of structural members are reviewed in Section 2.2; next, the current design methods for cold formed structural members are critically reviewed and the shortcomings from each of the method are identified in Section 2.3; Section 2.4 concerns with some important findings in optimisation of cold formed sections, especially the optimisation of the relative dimensions of the sections; finally, Section 2.5 presents the knowledge gaps.

### **2.1 Cold roll forming of the manufacturing process and its typical shape defects**

Cold roll forming process has gained a renewed interest due to its capacity to form a rather complex geometry and ultra-high-strength steels. It is a continuous sheet forming process with multiple pairs of controlled rolls to form manufacturing products with an open or closed cross-section. The products are generally formed at room temperature without significant change in the material thickness. Sophisticated shapes and increasing demand to satisfy industry requirements for high-strength lightweight members have made cold roll forming process a noteworthy and successful comeback with respect to its competing forming method in the manufacturing industry including press braking process that the deformation of the panel is often performed in one step.

High-quality output and high-volume production are the key features that allow cold roll forming method to produce highly complex sections from high yield strength thin-gauge metals,

without the drawbacks such as (limited press power, sheet tearing, large spring-back, and limited formability) that may experience using the conventional press-braking forming method.

Even though the cold roll forming product provides high-quality output, some shape defects may still arise from the process due to induced undesirable strains as the strip of sheet metal moves through the rolls such as spring-back (elastic recovery after forming), bow (curving in the vertical direction), camber (curving in the horizontal direction), flare (change in the cross-section at the cut ends of a roll-formed product), twist, corner buckling, edge waving, edge cracking and splitting. These defects are often not observed unless the sheet strip is completely unloaded [6]. The fundamental relations between the shape defects and the roll forming process design have been investigated before both experimentally and numerically using Finite Element Analysis FEA as well as different approaches have been considered to reduce and minimise these defects. Some of these shape defects including longitudinal bow, spring-back and end flare are investigated and reviewed briefly here.

#### 2.1.1.1 Longitudinal strain and longitudinal bow

The longitudinal and shear strain is generally induced by cold roll forming of the manufacturing process. These strains are different in flange from the web of the section as the material fibres at the flange often move more than the material fibres at the web of the sheet before forming the section [7]. The relationships between longitudinal and shear strain were investigated and a combination of these two strains was observed by Panton et al. [8]. The study concluded that shape defects such as bow, camber and edge waviness will arise if the longitudinal strain reaches beyond the yield strain of the material. The authors also showed that the major shape defects can be avoided by keeping the material in the elastic range, while this is not a practical solution in the cold roll forming process. As the plain sheet undergoes the forming process and contacts with pair of rolls at the first stage, the longitudinal strain will be generated in some places of the cross-section and the peak longitudinal strain can be observed in some regions.

It was shown that the peak strain can be decreased by increasing the roll diameter Panton et al. [9]. Appropriate strategy can also be used to reduce the magnitude of longitudinal and its transversal strain distribution in cold roll forming process design such as an optimum number of

passes. For example, if the number of passes was too few then the amount of transversal bending induced due to each pair of rolls would be excessive, which will lead to uneven distribution of longitudinal strain in the transversal direction. However, if a significant number of passes is used, then the production costs will increase. Therefore, choosing an optimum number of passes for a cold roll forming process is crucial. This allows the manufacturing processes to achieve optimum design solution so that the shape defects induced to be minimised and the production costs are also to be reasonably decreased.

In addition, previous researchers have conducted experimental tests and numerical analysis using FEA to evaluate the effects of manufacturing process variables on the longitudinal strain and longitudinal bow [7, 10-15]. The results showed that bowing increases with an increasing bending angle increment at each stand, flange width, and strip thickness, whilst the effects of the inter-stand distance between successive stands, the radius of the bend, the friction coefficient and roller speed on the bow were negligible.

However, there was a debate on the effect of yield stress on the longitudinal peak strain. For instance, some researchers stated that the longitudinal peak strain was increased when the yield stress was decreased [16], whilst other showed opposite results [11]. Thus, many parameters can affect the longitudinal strain and bow defects during cold roll forming and solutions to minimize them have been presented.

Wiebenga et al. [17] attempted to reduce the longitudinal bow and the spring-back by setting the gap between the upper and the lower rolls at each stand, the horizontal distance between the stands and the downhill strategy. A study on twisting and bowing defects in roll-formed products made of high-strength steel were also conducted [18]. They reported that the reason of occurrences of the defects was mainly due to the difference of longitudinal strains between at the edge and in the web and proposed a method to decrease the mentioned difference by increasing the web's longitudinal strain using additional compression of the web.

The effect of increased yield stress on longitudinal peak strain, spring-back and deformation length was also studied by Lindgren [19]. He showed the inter-dependency between the longitudinal peak strain and the deformation length. The transversal non-uniformity of the longitudinal strain was observed as one of the fundamental causes of the longitudinal bow in

roll-formed products [15], which can be reduced with the use of levelling roll to the lab-scale flexible roll forming machine. This result corresponds with the results of the previous research of Bidabadi et al. [13] to reduce the bowing defect, controlling the forming angle by changing the number of forming stands was an effective solution.

#### 2.1.1.2 Spring-back

Springback is defined as undesired geometric modification occurred at each step of the cold roll forming process and it is a deviation of the required design geometry due to the release of the forces on the part of the forming tools. These deviations influence the dimensional accuracy of a roll-formed profile after the part is released of the tooling. It causes important shape defects in a cold roll forming process. The degree of spring-back shape defects is dependent on many different factors that the spring-back angle is generally increased with the increase of yield and tensile strength of the material [20], forming radius to thickness ratio  $R/t$  (Radius/thickness and roll gap [21], whereas it is reduced with decreasing of Young's Modulus of the material [22] and increasing the number of forming passes used [23]. Thus, the spring-back defects were investigated, and methods were also proposed to minimise its effects.

Weiss et al. [24] explored the potential use of different roll forming methods to reduce spring-back and part shape defects in the cold roll forming of high strength titanium sheet such as Ti-6Al-4V using experimental and numerical results. The study indicated that the constant radius forming method leads to fewer shape defects in the process and reduced spring-back.

#### 2.1.1.3 End Flare

The end deformation (front and rear) in the cross-sectional geometry of a cold roll forming part is called end flare that induces a change in the sectional shape compared to other sections along its length. The end flare is induced using different methods of cutting including pre-cut section, cut with flame, saw, and cut off with a die, whereas it is usually higher in pre-cut strips to form a required profile [7]. Both the front and the tail end can be 'flare in' or flare out' that depends on many parameters including yield and tensile strength of the material and spring-back of the strip.

Springback is often generated by residual shear stresses at the edges of the formed section. Thus, the release of residual shear stresses induces end flare in both pieces of the formed section after cut-off [7].

Saffe et al. [25] studied the influence of different components of stress in the formed section on end flare for a roll forming process. It was concluded that the end flare of the cold-formed section after cutting is due to the release of the bending and twisting moments as well as the release of residual shear stress in the longitudinal direction and in-plane shear stress at the edge. They paid attention to the flare after the cutting operation, whilst the flare before cutting was not explored.

#### 2.1.1.4 Summary

The cold roll forming of the manufacturing process is an efficient and very competitive method of forming, whereas the care needs to be taken during the manufacturing process since the deformation of roll forming is very complicated and shows obvious material and geometric nonlinearity. According to the previous studies on the cold roll forming process, it can be concluded that shape defects induced due to undesirable strains such as longitudinal bow, springback and end flare are the main source of uncertainty at the end formed sections. Therefore, previous researchers have attempted to adjust the tooling to significantly improve product quality by compensating for product defects and minimizing the deteriorating effects of scattering variables.

**It should be noted that there is an obvious link between the above-mentioned shape defects and material properties of the cross-section as well as the structural behaviour of the cold-formed members.** For instance, the longitudinal strain and longitudinal bow can induce plastic strain and residual stresses. In general, the plastic strain has positive effects on the strength capacity of the structural column and beam members, whereas the residual stresses have a negative impact on the load-carrying capacity. In additions, the shape defects such as springback and end flare can have significant effects on the imperfections of the end section. In particular, distortional imperfections which have been proven to have a significant influence on the ultimate strength capacity of cold-formed structural members.

Therefore, the question here is what effect does cold roll forming have on the behaviour of structural members? Load carrying capacity of the structural members plays an important role in reducing the cost of the members and obtaining an optimal design solution could improve the capability of the cross-section to resist high external applied load, so the influence of cold forming including press braking and roll forming on mechanical properties and structural performance, in particular, the stiffness and strength capacity of the structural members will be reviewed in the next few sections.

## **2.2 Manufacturing process effects in thin-walled cold formed structural members**

As the plain sheet undergoes a long process of cold roll forming to form the desired section, the material properties of the section are susceptible to modification compared to the virgin material. It is well known that the cold roll forming of the manufacturing process changes the stress-strain curve of the steel material at corners and heavy cold worked areas, which increases the yield strength of the material due to strain hardening and increases the tensile strength of the steel due to strain ageing at the same time decreases ductility that mainly depends on the types of the steel materials used [26-28]. The increase in yield strength is much bigger than the increase in tensile strength.

As the corners of the cross-section induced plastic strain due to the increase of yield strength, the flat regions of the section normally start to spread yielding when an external load is applied and any additional load applied to the section will then spread to the corners. It is noted that the modification in the basic steel material is taken into account by Eurocode 3 [5] through formulas to obtain the increase of the yield strength of cold-formed steel sections. However, not only does the cold roll forming process modify the yield and tensile strength of the material in the cross-section, but it also induces residual stresses and initial geometric imperfections.

Residual stresses in the cold-formed steel sections have shown to be different from the hot-rolled sections. In hot-rolled sections, the residual stresses are mainly of membrane-type caused by uneven cooling after hot rolling or welding. The membrane residual stresses have significant influence on the buckling strength and hence different buckling strength curves are used in the

European design codes (CEN, 2005a) to calculate the load-carrying capacity of the sections. However, the membrane residual stresses have shown to be less prevalent in cold-formed members compared to the flexural counterpart. Although the flexural residual stresses are proven to have a less detrimental influence on the buckling strength of the sections, the same buckling curves for hot-rolled sections are still used for cold-formed sections as well (CEN, 2005a and CEN, 2006a). The buckling curves assumed to account for all imperfections in real compressed members such as induced strain hardening, residual stresses and geometrical imperfections (initial global, local and distortional imperfections).

The deviation of an actual member from a 'perfect' geometry is generally called geometric imperfections that include the effects of real geometric imperfections, the possible eccentricity of the loads and the influence of cold work effects. The two former imperfection types may induce during shipping, storage and construction, whereas the latter is undoubtedly generated by the manufacturing process of the cold roll forming. These imperfections affect axial and flexural capacity that tends to reduce stiffness and ultimate strength capacity of the CFS structural members [29, 30].

Therefore, a series of structural section types, both cold-rolled and press-braked, and a range of structural materials, including various grades of stainless steel and steel, has been gathered. The previous experimental and numerical data include two types of structural members such as columns and beams. A total of 27 studies were collected for structural column specimens that 13 of them were experimental and 14 of them were numerical studies. However, only 7 studies were available for beam members, which two of them were experimental and five of them were numerical. The collected database has been used to investigate the effects of the manufacturing process on the material properties and structural behaviour of thin-walled cold-formed structural members. In particular, the influences of manufacturing process such as initial geometric imperfection (local and distortional), strain hardening and residual stresses on ultimate strength capacity and stiffness have been examined.

## 2.2.1 Manufacturing process effects in cold formed structural column members

Manufacturing process effects induce initial geometric imperfection, residual stresses and plastic strain in the structural column members. The stiffness and strength capacity of the members will be modified due to the fact that the mechanical properties of the structural members are significantly varied in those regions with high cold working from the manufacturing process. Hence, the experimental and numerical data collected from available literature, conducted by different researchers, will be used to evaluate the load-carrying capacity of structural column members. All the experimental and numerical specimens gathered were thin-walled cold-formed steel and stainless-steel sections. A number of structural section types collected is presented in Figure 2.1. The data of manufacturing process effects (imperfection, residual stresses and plastic strain) on load carrying capacity are summarised in the Tables, the channel sections are presented in Table 2.1 and 2.3 as well as the other section types are shown in the Table 2.2 and 2.4, and briefly reviewed in the following sub-sections.

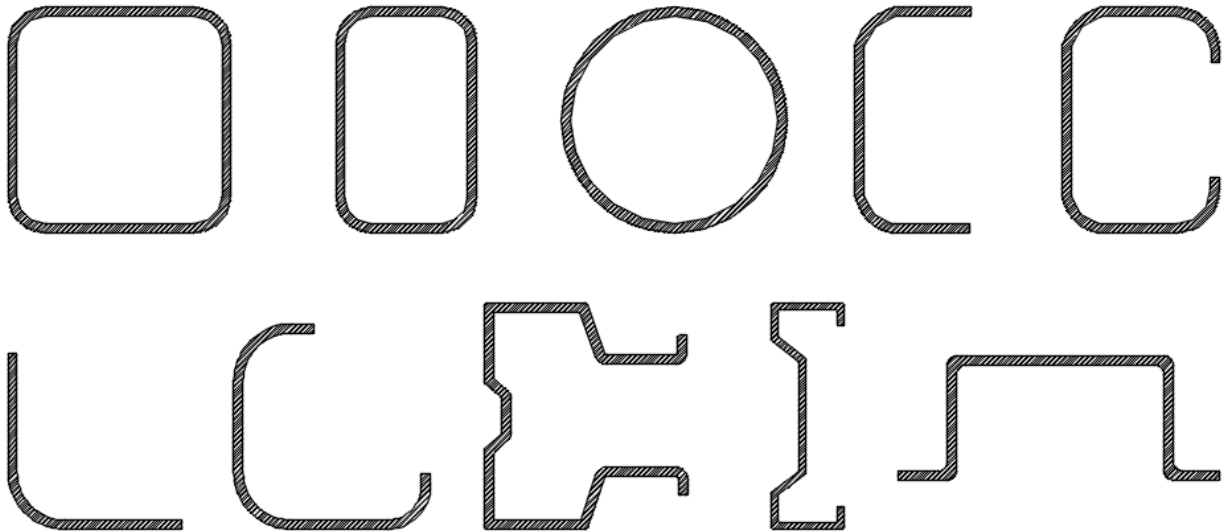


Figure 2.1: Example of cold-formed cross-sections gathered for column members

### 2.2.1.1 Initial geometric imperfection

Initial geometrical imperfection can be defined as a deviation of any plate of a cross-section from perfect geometry as shown in Figure 2.2. Imperfections of a section include local and distortional



deviation, which is a function of plate geometry (width, depth and thickness), forming process, transporting, installation and other unknown factors [31]. Local deviations are characterized by dents and regular undulation in the plate, whilst distortional deviations are the translation of one plate end with respect to the other end.

The influences of global geometric imperfections (GI) on load carry capacity of structural column members have been intensively studied that, in general, reduce the ultimate strength capacity of column members. The reduction of column strength caused by global geometrical imperfections is an experimentally verified and well-understood fact [32-34]. Therefore, only specimens with sectional imperfections, local imperfection (LI) and distortional imperfection (DI), were collected and evaluated in the current study. Thus, from now on the term imperfections refer to local and distortional imperfections.

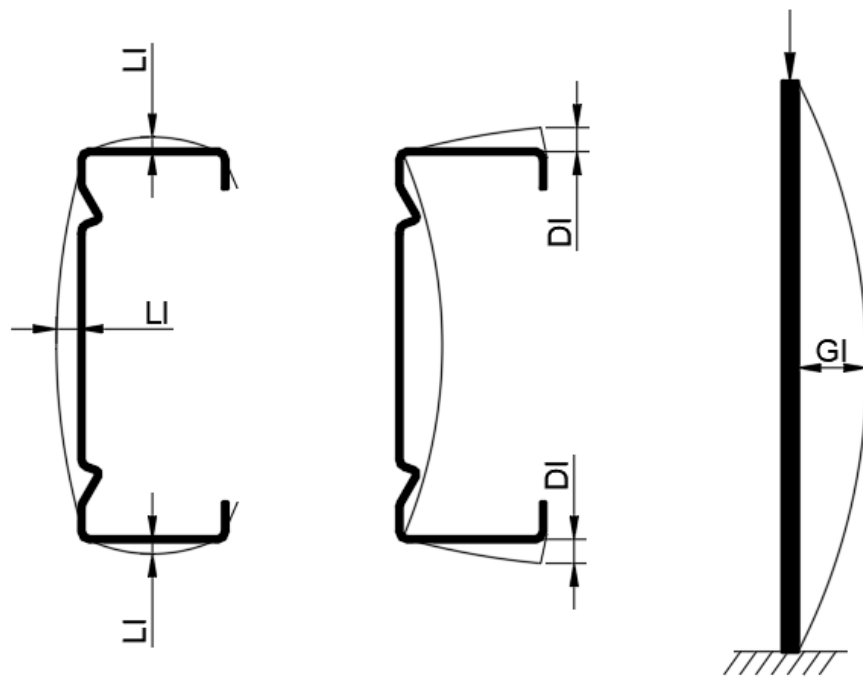


Figure 2.2: Local, distortional and global imperfections

Many studies have seen to investigate the magnitude and distribution of imperfections in cold-formed members. Previous researchers have measured geometric imperfections of cold-formed column members [35-45]. The measured data on geometric imperfections are generally sorted

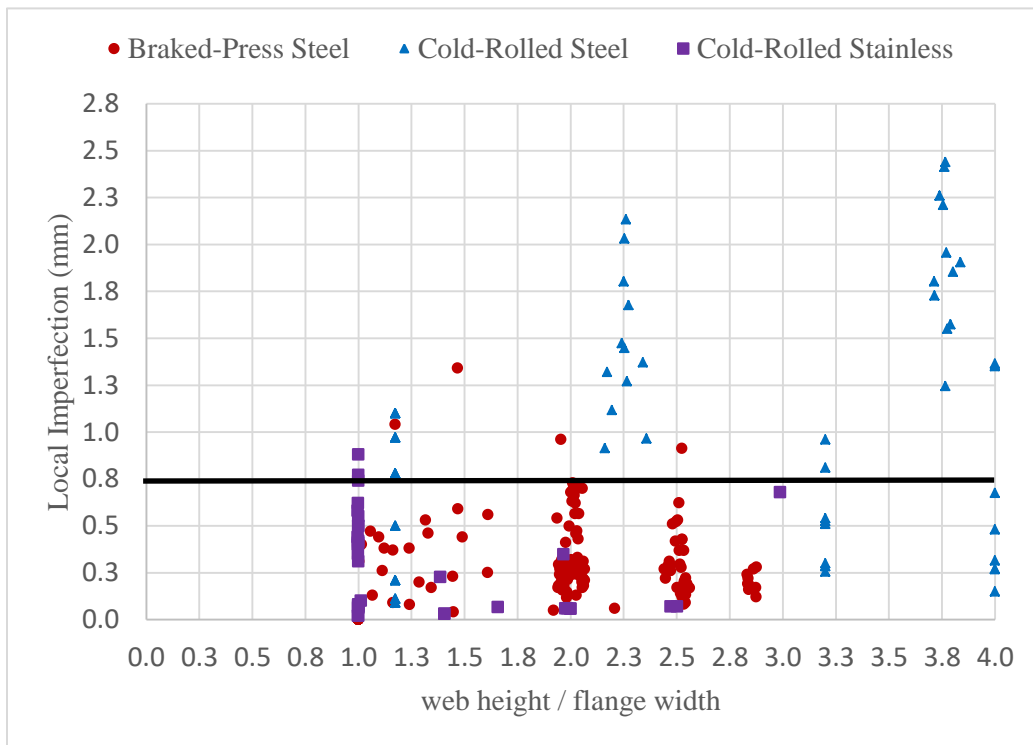
into two types as maximum local imperfections (LI) and distortional imperfections (DI). These two kinds of imperfections are quite sensitive to cold-formed column members, resulted in a relatively wide range of scattering when buckling and ultimate strength of cold-formed members are investigated experimentally as shown in the Figure 2.3 and Figure 2.4. One of the main reasons is that there is a lack of experimental works to assess the load-carrying capacity of column members with different imperfections but with the identical cross-section, material and column length. Thus, the attempt has been made to evaluate how imperfections affect ultimate strength capacity based on collected experimental results in the current study.

A total of 13 experimental studies have been gathered, which the researchers measured local or distortional imperfections or both of them. These studies were categorised into three types depending on the manufacturing process (press braking and cold roll forming) and material types (steel and stainless steel) as well as cross-section types (channel, sigma, pallet rack and hollow sections). The first type consisted of 6 studies (172 specimens) on steel material formed with press braking process. The second type consisted of 4 studies (36 specimens) on stainless steel material formed by the cold roll forming process. The third type consisted of 3 studies (61 specimens) on steel sections formed with the cold roll forming process. It is noted that most of the testes (172 out of 269) were conducted on the press braking of the manufacturing process. Figure 2.3 compares the local imperfection amplitudes (LI) of different ratio of web height to flange width of cross-sections for the 269 structural column specimens. Even though there are very limited tests carried out (61 out of 269) for steel material formed with cold roll forming, it can be seen that the LI is significantly larger for steel material formed with cold roll forming approximately 2.5 mm compared to both steel sections formed with press braking process and stainless-steel sections formed by cold roll forming process of about 0.8 mm. In addition, the LI seems to have a larger influence on a load-carrying capacity of carbon steel formed with cold roll forming process compared to two other types that the ultimate strength did not reach more than 70% of its squash load. It is also noted that most of the test specimens of stainless steel were hollow sections which these types of sections appear to be susceptible to lower level of imperfections. Figure. 2.4 compares the distortional imperfection amplitudes (DI) of different ratio of web heights to flange widths of cross-sections for the 168 structural column specimens. As shown, DI is generally higher for these specimens formed by cold roll forming process ranging from 4.0 to 5.0 mm with ratio of web height to flange width between 1.0 to 3.0 than

those specimens formed with press braking process ranging from 0.2 mm up to 4.0 mm. This is partly because as the strip sheet undergoes many rolling stages, it experiences the changes in material properties as well as induces shape defects such as longitudinal bow, longitudinal strain, spring-back and end flare (see section 2.1). Increasing web height to flange width has also a significant influence on the DI amplitude as the ratio of web height to flange width increase the DI reduces. This is due to the fact that the flange of the sections is more susceptible to change of mechanical properties compared to the web of the section. In the cold roll forming process, the strains induced different in the flange from the web of the section as the material fibres at the flange often move more than the material fibres at the web of the sheet before forming the section [7].

In addition, the DI seems to have the significant influence on strength of those specimens induced by cold roll forming as maximum ultimate strength did not reach 70% of its squash load, whereas the specimens formed with press braking can have an ultimate strength of more than its squash load. Thus, it is obvious that the cold roll forming process can have a significant influence on imperfection amplitude and load carrying capacity, while most of the studies were focused on press braking and test data for cold roll forming of the manufacturing process is limited (40 out of 168). Figure 2.5 show LI of four different cross-section types of namely channel, sigma, pallet rack and hollow section, whereas Figure 2.6 presents DI of two different cross-section types including channel and sigma sections. It can be observed that different geometries and cross-section types can have different imperfection amplitudes. In all four different geometries gathered, more imperfection amplitude (up to 2.5 mm for LI and 5.0 mm for DI) is observed in channel section compared to other cross-section types as shown in the Figure 2.5 and Figure 2.6. As it can be seen that there is no test data for Z-section to be used as structural column members. Another observation is that the maximum DI amplitude is larger than the maximum LI amplitude in most column sections. This seems to be due to the undesired spring back occurred during cold roll forming of the manufacturing processes as undesired geometric modification occurred at each step of the cold roll forming process. Based on the entire collected test data (13 studies), maximum LI magnitude was seen up to 2.5 mm and the maximum DI magnitude was about 5.0 mm. The influence of imperfections of various cross-section types on strength capacity of column member is not as obvious. *Thus, it was clear that*

*the effects of imperfections induced from cold roll forming on strength and stiffness of different cross-section types should be studied, in particular for channel and Z-sections.*



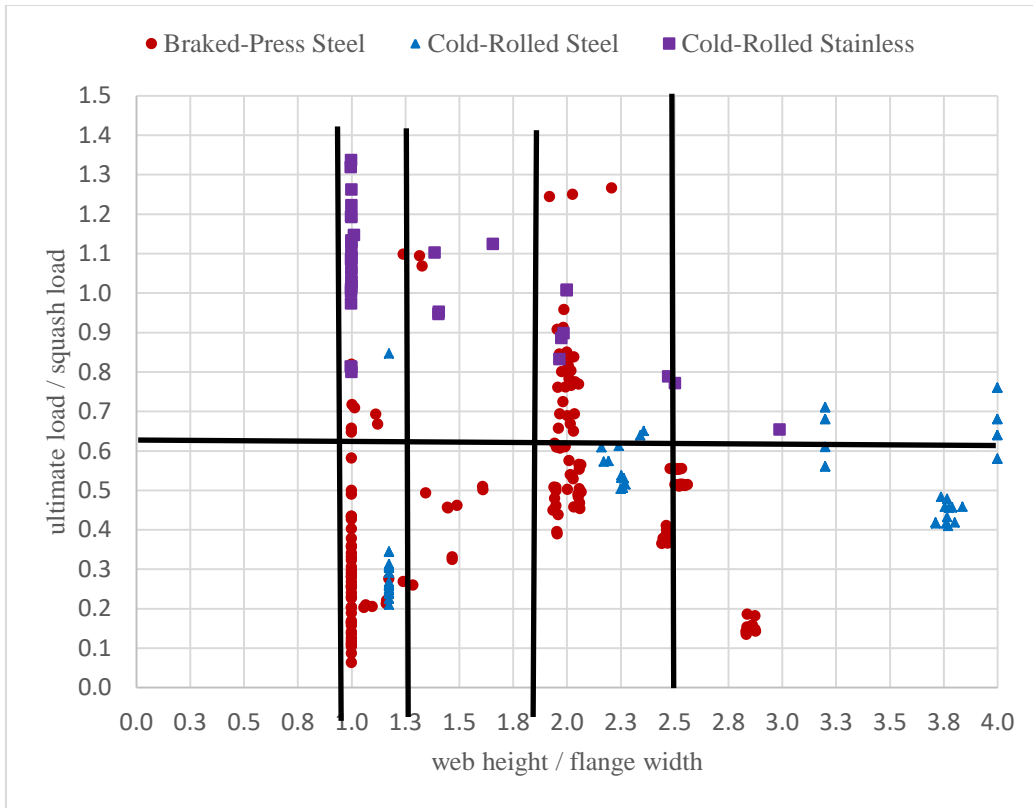
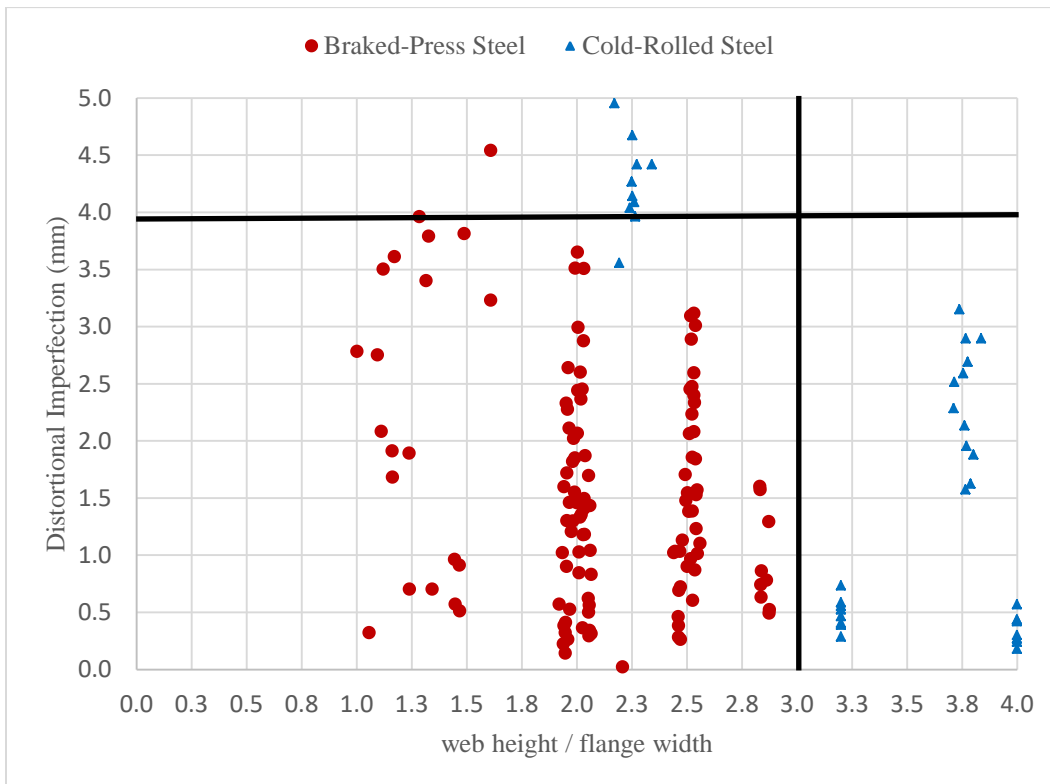


Figure 2.3: LI effects from two manufacturing process types on peak load [35-45]



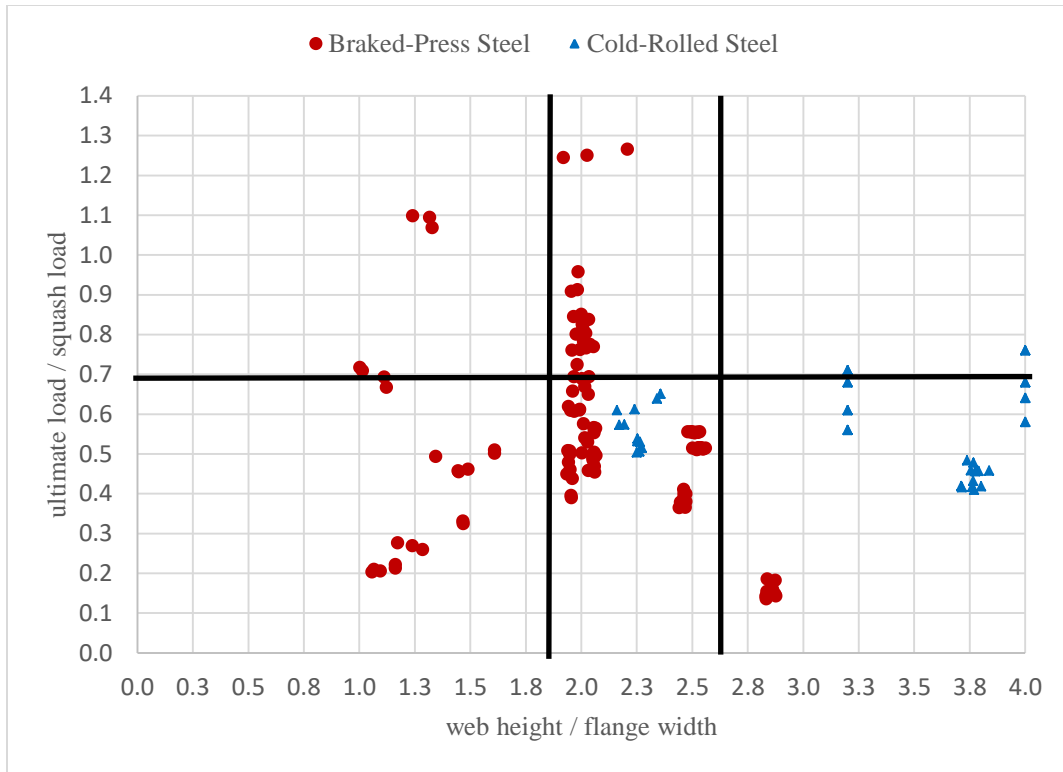
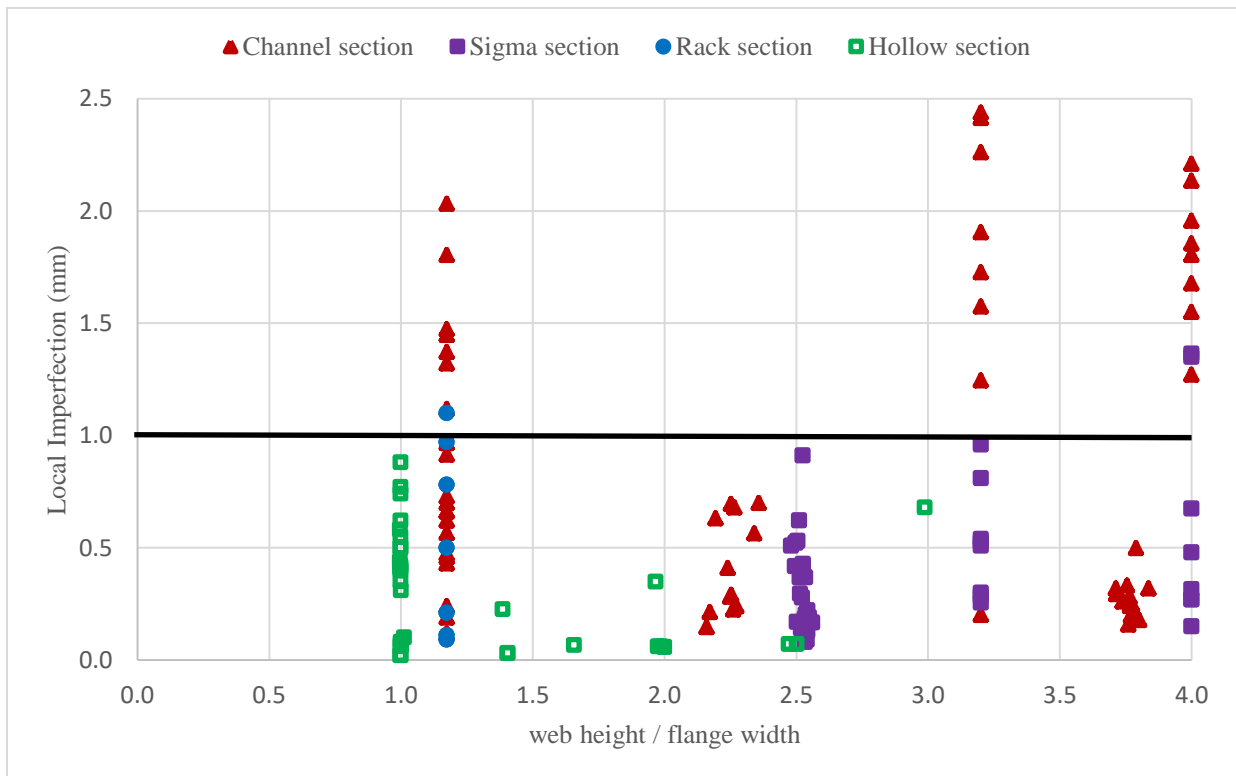


Figure 2.4: DI effects from two manufacturing process types on peak load [35-45]



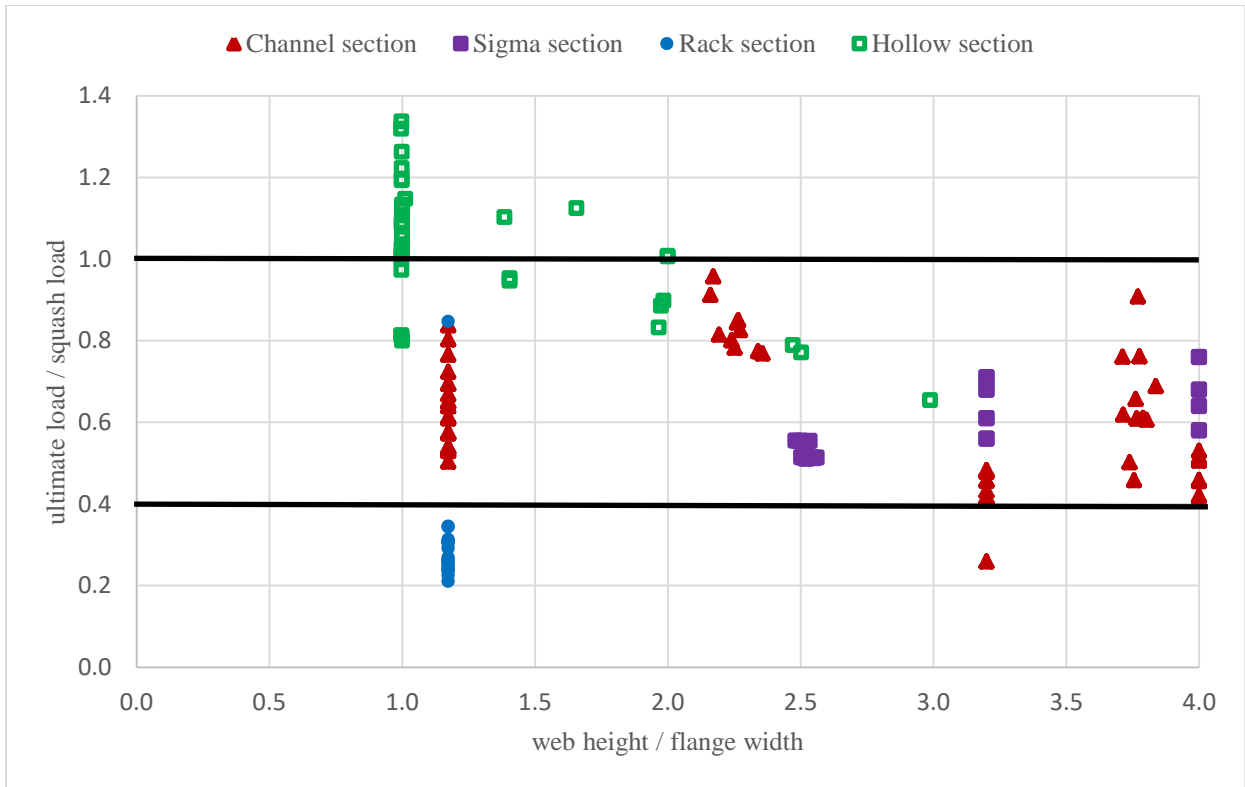


Figure 2.5: LI effects of different cross-sections on peak load [35-45]

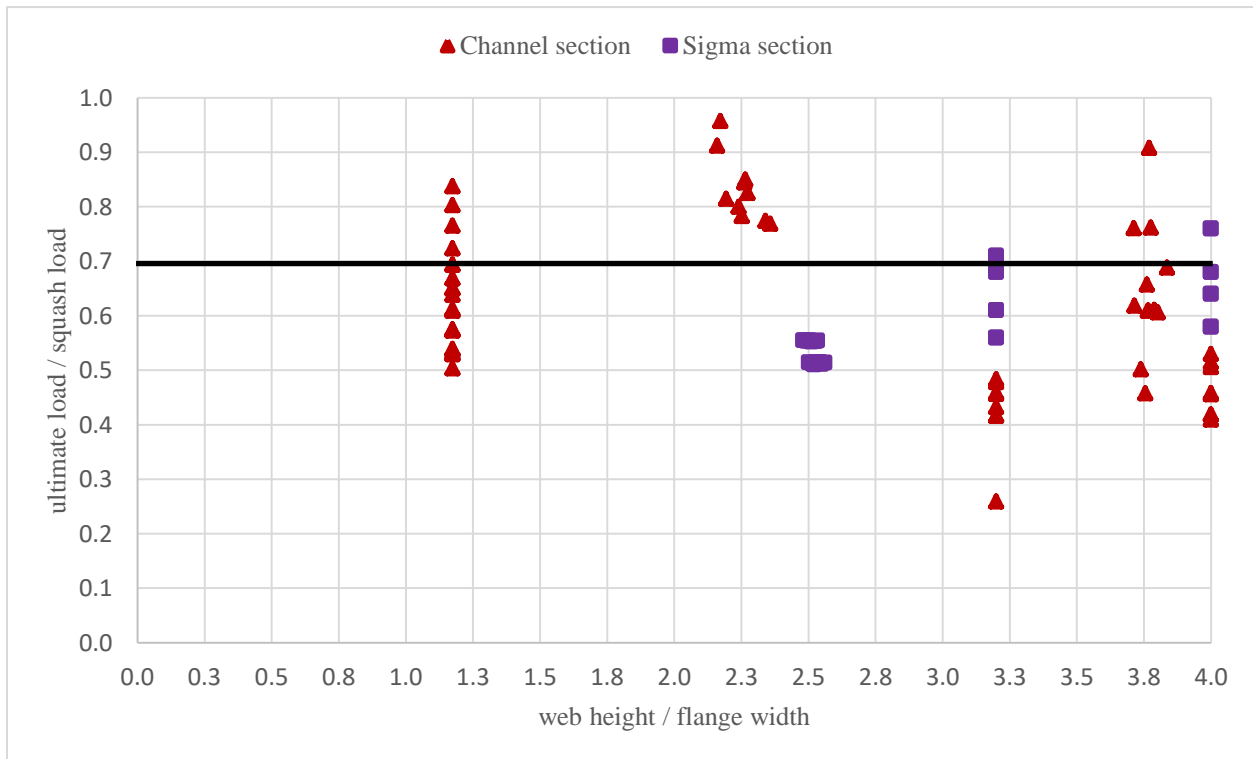
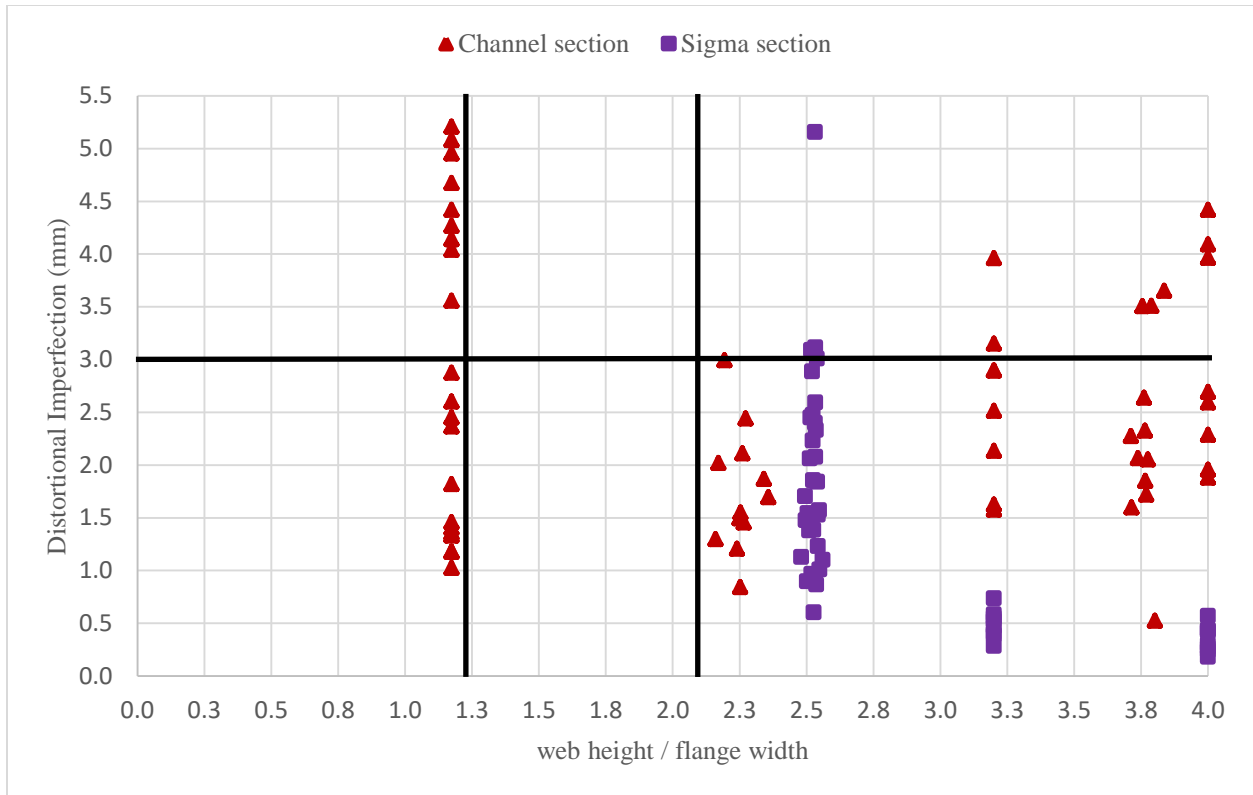


Figure 2.6: DI effects of different cross-sections on load-carrying capacity [35-45]



While there is a lack of study to investigate the influences of sectional imperfections (local and distortional) on strength and stiffness of thin-walled cold-formed structural columns experimentally, numerical analysis has been conducted before to evaluate the influences of initial imperfections on the behaviour of steel members and many researchers have attempted to assess the buckling and ultimate strength capacity of column members using the finite element numerical simulation [46-56].

Schafer and Pekoz [46] proposed numerical models to generate automatically geometrical imperfection modes into the non-linear analysis. As different buckling modes of members have various magnitudes of imperfections, they conducted the analysis results for the five different imperfection patterns (five seeds) and the four different imperfection magnitudes such as  $P(\Delta < d) = 0.25$ ,  $P(\Delta < d) = 0.50$ ,  $P(\Delta < d) = 0.75$  and  $P(\Delta < d) = 0.99$ . The conclusions from the results were more complicated and greater losses in ultimate strength were seen about 30% when different imperfection magnitudes were used. Hence, appropriate imperfection magnitudes ( $P(\Delta < d) = 25$  and 75%) were proposed for CFS members to be used based on numerous FE data.

Later on, numerical modelling using a nonlinear finite element analysis on the post-buckling behaviour of the thin-walled cold-formed lipped channel and hat-section stub columns under axial compression was carried out by Chou et al. [47] to model the carefully controlled stub column tests conducted by Zaras and Rhodes (1987). Four degrees of imperfections was used for non-linear post-buckling analysis to evaluate ultimate strength and it was found that the various imperfection amplitudes had insignificant effects, only 2%, on the load-carrying capacity of the columns.

Dubina and Ungureanu [48] also analysed the influence of imperfections on the behaviour of cold-formed steel column members. They pointed out that the different shapes of local-sectional imperfections had a different effect on the member buckling strength. For instance, the column ultimate strength was reduced by about 25% if distortional buckling (symmetric sine shape) was used instead of distortional buckling (asymmetric sine shape) with the same magnitude of initial imperfections.

Gardener and Nethercot [49] defined four different levels of local geometric imperfection amplitude for cold-rolled stainless steel circular hollow sections (CHS) stub column. They found

that the increase of local imperfection amplitude from  $0.1t$  to  $0.5t$  had a maximum influence of 10% on the ultimate strength of CHS.

The work was then extended by Ashraf et al. [50] that performed parametric studies of 32 stainless steel stub columns with 4 different cross-sections (angle, channel, lipped channel and I shape) types so as to investigate load-deformation behaviour of the stub columns. They used the first three Eigenmodes individually and two values for the amplitude were used in the imperfection distribution defined using Eigenmodes to investigate the effect of imperfection distribution on load-deformation response. They pointed out that, on average, using the first Eigenmodes reduced the ultimate strength of up to 5% compared to the third Eigenmodes and increasing imperfection amplitude decreased the ultimate strength of about 7%.

Crisan et al. [51] investigated the influence of imperfections on the erosion of critical bifurcation load in the coupling point, both for brut (RSB95 and RSB125) and perforated sections (RSN95 and RSN125), subjected to uniform compression using numerical analysis. They determined that the most significant primary erosion in RS125 is due to the distortion that reduced the capacity of the section by (22-27) %.

Bonada et al [52] presented three methodologies to examine the ultimate buckling strength of carbon steel rack column using the first buckling mode, an iterative methodology in which the shape that leads to the lowest ultimate load was used, and combines the finite element analysis with the generalised beam theory (GBT) to find the modal participation of the FEM buckling mode and generate a particular combined geometric imperfection. They chose column lengths in the range where the main failure was due to distortional buckling since this mode demonstrated to be more critical than local and global buckling mode. It was found that using the first method overestimated the result by about 15%, while the two other methods appeared to be more appropriate that overestimated the results by only 6%.

Later on, the study was extended by Pastor et al. [53] that carried out a numerical analysis to predict the behaviour of rack uprights (with and without perforations) under compression for different column lengths to reproduce a mainly local, distortional and global failure mode, so that coupled instabilities were not considered. They concluded that distortional mode was more

sensitive to the magnitude of initial imperfection. For the range of values tested, differences were detected up to 31% in the value of the ultimate load.

The same research group analysed the influence of residual stresses and strain hardening due to the cold roll-forming process on the load-carrying capacity of perforated rack columns under pure compression load [54]. They found that the effect of geometrical imperfection was not relevant for prediction of the ultimate load of the column when residual stresses were considered.

The same authors presented the influence of the bending moment on the load-bearing capacity of rack uprights subject to axial load together with bending moment considering residual stresses and strength enhancement induced during cold forming of sections [55]. Hence, they developed two methods to be used for five different eccentricities. The first methodology presented did not take into account the residual stresses and strength enhancement due to the manufacturing process. The results showed that an initial geometrical imperfection had to be included in the nonlinear analysis for all eccentricities to obtain accurate results when a distortional column length was analysed. Moreover, the shape of this initial geometrical perturbation was only relevant to obtain accurate results if the failure mode obtained was different from the experimental one. The residual stresses and the strength enhancement of corner areas were included in the second methodology developed. Good predictions of the ultimate loads were also obtained for all eccentricities. It was claimed that the main advantage of this second methodology was the lack of necessity to introduce an arbitrary geometrical imperfection as an initial state to obtain accurate results.

Recently, Ye et al. [56] studied the interaction of local and overall flexural buckling in cold-formed steel (CFS) lipped and plain channel columns under axial compression using detailed nonlinear FE models. They investigated the effects of the initial geometric imperfections on the ultimate strength of the column members. The study concluded that the initial geometric imperfections changed the load-carrying capacity by around 20% and 40%, respectively, for lipped and plain channel columns.

### 2.2.1.2 Residual stresses

Cold forming of the manufacturing process generally affects the strength and stiffness of cold-formed structural column members, which apply progressively cold work such as geometrical imperfections and modification to mechanical properties of the material. The effects of geometric imperfections including local and distortional imperfections on ultimate strength capacity of thin-walled cold-formed column members were reviewed in the preceding section. In this section, the changes of mechanical properties of the material induced from the manufacturing process, in particular, the influences of residual stresses on the ultimate strength capacity of thin-walled cold-formed structural column members are reviewed.

Residual stresses can be defined as self-equilibrated stresses retained in a finished section or member before applying any external load and often have significant influences on buckling and post-buckling strength as a result of premature yielding and loss of stiffness of steel members (European Convention for Constructional Steelwork (ECCS) Technical Committee 8 (TC8), 1976). The residual stresses are often induced due to uneven cooling of shapes after hot-rolling, welding or cutting operations in the hot-rolled sections, whilst the main source of those stresses in cold-formed members is plastic deformation caused by cold-forming, cold-straightening and cambering [57]. The existence of those stresses is decomposed into the longitudinal and transverse components. Each of these components is varied along with the wall thickness of a plate of the cross-section and often divided into membrane residual stresses (MRS) and bending (flexural) residual stresses (FRS) as shown in the Figure 2.7.

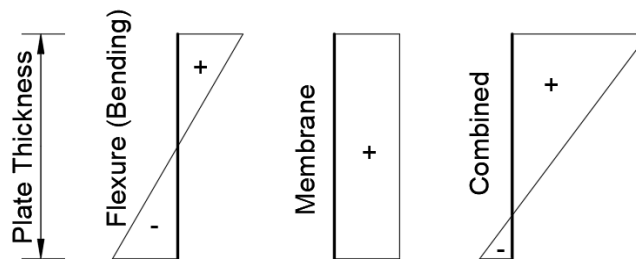


Figure 2.7: FRS and MRS through wall thickness of a plate [46]

The residual stresses from cold working in thin-walled cold-formed steel sections were generally idealized as a summation of two types: flexural and membrane (see Figure 2.7). Flexural residual

stresses, which is also called bending residual stresses, can be defined as the stresses that are variable through the thickness and cause curvature of the plate during cutting or sectioning method, whilst membrane residual stresses cause axial deformation of the plate and assumed to be constant through the thickness of the plate (at each layer of the thickness). The large magnitude of flexural residual stresses was often seen with a large degree of variation, while the membrane residual stresses were shown to be less prevalent in thin-walled cold-formed structural members as shown in the Figures 2.8 to 2.11.

Although it is clear that the available experimental data on residual stresses measurement is very limited, it is still some conclusions can be drawn based on previous experimental tests of the residual stresses measurement that have been gathered in this study and presented in the Figures 2.8 to 2.11. First of all, the amount of flexural residual stresses (FRS) is significantly larger than the amount of membrane residual stresses (MRS) in both flat and corner region. The magnitude of FRS is up to 40% and up to 60% of the material yield strength for flat and corner regions respectively, whereas the magnitude of MRS is about 25% and 30% of the material yield strength for flat regions and corner regions respectively. This is well agreed with most of the previous findings.

Secondly, the amount of both FRS and MRS are much bigger in those sections formed with stainless steel sections compared with steel sections which can be attributed to the mechanical properties of the materials.

Thirdly, the effect of manufacturing process types on the magnitude of residual stresses seems to be different in press braking and cold roll forming. As it can be seen in the Figure 2.8 to 2.11, the magnitude of residual stresses is generally higher in both cold rolled formed stainless steel and press braking formed steel compared to cold roll forming steel. This is clearly shown that both material properties and manufacturing process types can affect residual stresses distribution. However, the influence of residual stresses (FRS and MRS) on the load-carrying capacity of steel column members is not as obvious based on the experimental database.

Therefore, researchers have attempted to investigate the ultimate strength capacity of thin-walled cold-formed column members through the analytical solution and numerical simulations. In these studies, initial geometric imperfections were often characterised by the imperfection

measurement data or using the convenient modelling technique, while two different stress-strain curves were used in flat and corner region of thin-walled cold-formed steel sections to account for the cold work effects (residual stresses) induced from the manufacturing process.

To take into account the effects of residual stresses on strength capacity, both idealised residual stresses distribution and measured residual stresses were used in numerical modelling. Many researchers concluded that the effects of residual stresses on load-carrying capacity of thin-walled cold-formed steel column members were negligible [35, 41, 44, 46, 49-51, 55, 58], whilst some other researchers found that the influences of residual stresses on ultimate strength capacity of steel column members were significant [38, 54, 59-63]. These different findings are briefly reviewed here.

The researchers observed that the effect of residual stresses on the ultimate strength capacity of column members was very small [35, 41, 44, 46, 49-51, 55, 58], they generally ignored membrane residual stresses in the corner areas and pointed out that the increasing yield strength benefit is going in the opposite sense compared with the negative effects of residual stresses in the corner regions. This is partly because the amount of strain hardening, and residual stresses were not clearly known due to the inherent uncertainty associated with residual stress magnitudes and distributions. Therefore, further study is needed in order to quantify the effects of each of them and how much they counteract in cold bending areas.

However, the influences of flexural residual stresses have been implicitly taken into account through the stress-strain curve and it was observed that the tension and compression coupons cut from finished sections curved longitudinally as a result of the through-thickness bending residual stresses [62]. While elastic straightening of the coupons as part of the testing procedure approximately re-introduces the bending residual stresses, the effects were assumed to be present in the material properties that cut from within the cross-section [49]. This assumption might have led to the conclusion that flexural residual stresses had a less detrimental influence on the ultimate strength capacity.

Despite substantial studies in the effects of residual stresses on strength capacity of thin-walled cold-formed steel column members, there were some limited studies that were shown the

significant effects of residual stresses on buckling and post-buckling strength of column members [38, 54, 59-62].

The theoretical and experimental studies of residual stresses effect induced from cold working on strength capacity have been conducted over past years. In 1975, Ingvarsson investigated box columns built up by two cold-formed channel members welded together [63]. Based on theory and tests, he concluded that the combined effects of residual stresses and strain hardening at the cold-formed corner had a positive effect on ultimate strength resistance due to the strain-hardening caused by cold-forming results in an increase of the yield stress.

Later on, Dat conducted a study on the stiffened channel and the hat sections to investigate residual stresses due to cold-forming, both press braking and cold roll forming considered [59]. In addition, he developed a computer program to account for variations in yield strength over the cross-section and the presence of residual stresses, which assumed three distributions of residual stresses across the thickness: uniform, linear and "rectangular". He noticed that the influence of residual stresses decreases as initial out-of-straightness increases and residual stresses result in earlier initiation of yield in a column, causing a loss of stiffness, and thus a lower strength as compared to residual stress-free columns. The lowering of strength (up to 30%) was greatest at slenderness ratios corresponding to a critical Euler stress about equal to the yield stress of the material. He also examined another distribution consisting of residual stresses at only corners and concluded that since the residual stresses affect only a small proportion of the cross-sectional area, there was no reduction in strength.

Davison and Birkemoe also presented a theoretical model describing the column behaviour of cold-formed hollow structural steel shapes [60]. They made a parametric study to determine the effects of the yield strength and residual stresses gradients on column strength. The study concluded that the residual stress gradient through the tube wall thickness was the most dominant cross-sectional parameter that affected both tangent modulus and maximum strength capacity of structural steel shape, which decreases in through-thickness residual stress gradient of 60% produced an increase in column strength of roughly 13% at slenderness ratio of approximately equal to the unity. In addition, Davison and Birkemoe noticed the same phenomena that were

observed by Dat, that the member crookedness reduced the effect of the cross-sectional yield strength and residual stress parameters on the column behaviour.

Ten years later, Key and Hancock published a detailed study using a large deflection elastic-plastic finite strip analysis including the measured distributions of yield stress and residual stress to investigate the influence of the measured through-thickness residual stress components on the ultimate load and behaviour of the cold-formed steel square hollow section stub and pin-ended columns [62]. They concluded that the membrane and layering components of the residual stress analytical models produce no net force or moment imbalance on the section either considered as a whole or locally through the plate thickness. The bending component of residual stress, however, results in a net moment through the plate thickness in both the longitudinal and transverse directions, which caused the reduction of the ultimate load-carrying capacity of up to 5.4% and 15.8% for stub and pin-ended column respectively.

Jandera et al. [38] also measured through-thickness residual stresses in cold-rolled stainless steel box sections directly by means of X-ray diffraction and their effect on structural behaviour were carefully assessed through detailed non-linear numerical modelling. From the X-ray diffraction measurements, it was concluded that the influence of through-thickness (bending) residual stresses in cold-rolled stainless steel box sections could be effectively represented by a rectangular stress block distribution. The bending residual stresses had a significant effect on the non-linear stress-strain curve and secant modulus was always lower due to the fact that the material stress-strain curve containing residual stresses consistently below the residual stress-free curve, while the influence of membrane residual stresses was found to be insignificant in comparison to the influence of the bending component. In addition, the tangent modulus of the stress-free curve was higher than that of the residual stresses containing curve below strains of approximately 0.12%. Beyond this strain, however, the reverse was seen. The higher tangent modulus generally led to an increase in load-carrying capacity when column failure strains coincide with the region of increased tangent modulus of the stress-strain curve. Moreover, a variation between -2% and +10% was observed in global buckling strength resistance for column non-dimensional slenderness, which was the square root of the ratio between yield load and elastic column buckling load, ranging from 1.8 and 0.9 accordingly. It was also concluded that the bending residual stresses were not required to be explicitly re-introduced into numerical



models since these stresses were inherently present in the stress-strain behaviour of material extracted from structural sections during the physical test of the material.

The same authors in 2014, Jandera and Machacek [61] also studied the influence of forming-induced residual stresses in stainless steel SHS (Square Hollow Sections) on the behaviour of compressed members. While they confirmed the results of the aforesaid study by Jandera et al. [38], they concluded that the influence of residual stresses was between +10% to -16% for global buckling and up to +9% for local buckling of SHS members using the FE model based on measured material characteristics. The influence of residual membrane stresses in the analyses was usually very low and was neglected in most cases. Thus, no negative influence of residual stresses occurred for local buckling due to the post-buckling behaviour which increases the failure strain for very slender webs. In opposite to the post-buckling behaviour of columns, the local buckling failure strain was always greater than 0.12%, where residual stresses had a positive influence on the tangential modulus.

The above investigations were often used different stress-strain curves for different parts of a cold-formed section, which was generally obtained from the testing of coupons cut from the section member. The analytical solution was then introduced to model the cold work effect of the manufacturing process on the structural performance using residual stresses and equivalent plastic strains by Quach et al. [64]. Both steel and stainless-steel press-braked thin-walled columns were considered in the proposed approach. They noticed that the combined effects of residual stresses and strain hardening in corner regions always enhance the column strength (by up to 6% for the steel and 9% for the stainless-steel stub column), which the effect of material strain hardening dominates over the effect of residual stresses in a cold-bent corner of small curvature. This positive effect was seen to be reduced with column length and became negligible for sufficiently long columns.

On the other hand, they observed the cold work in flat portions may either increase or decrease the column strength. The detrimental effect of cold work in flat portions on long columns was seen to be more obvious, the largest reduction of 16% was a quite significant reduction than the beneficial effect on short columns. Hence, it was concluded that by considering the combined effect of cold work in both flat portions and corner regions, the stub column strength was

increased by 11% and 10% for steel and stainless steel, respectively. The longer stainless steel columns strength was also increased by 4%, whereas the strength of longer steel column was reduced by up to 16%.

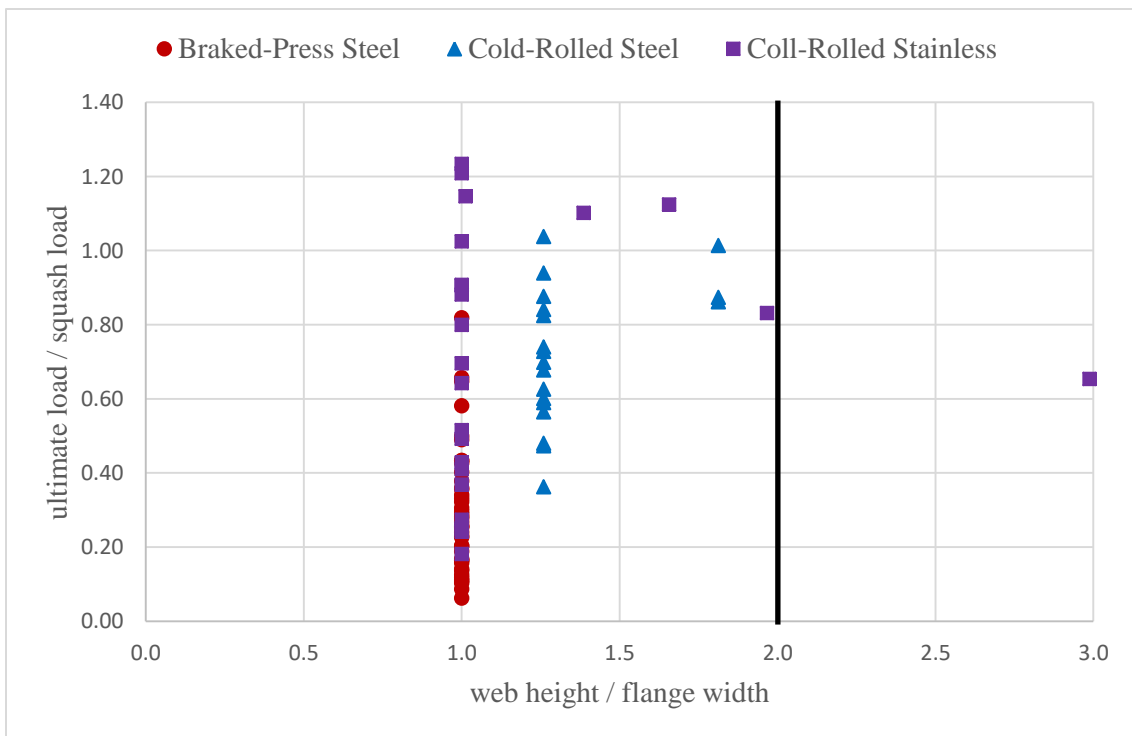
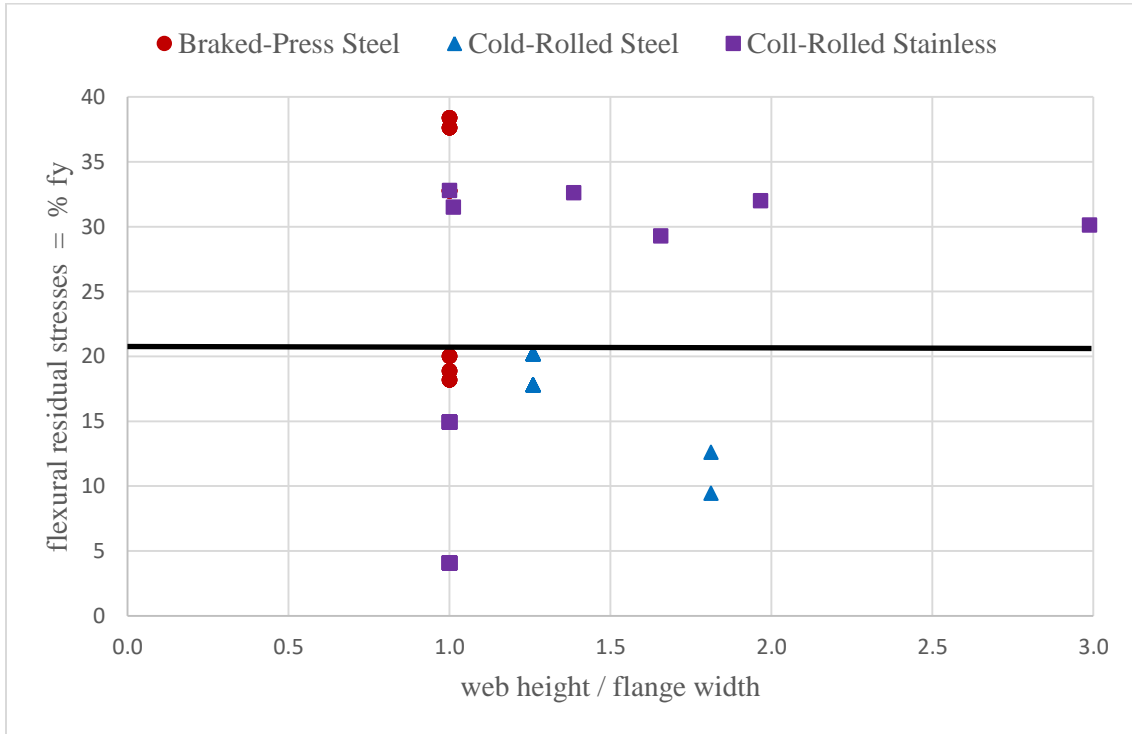


Figure 2.8: Flat regions FRS effects from CR & PB on peak load [35, 36, 38, 41, 59]

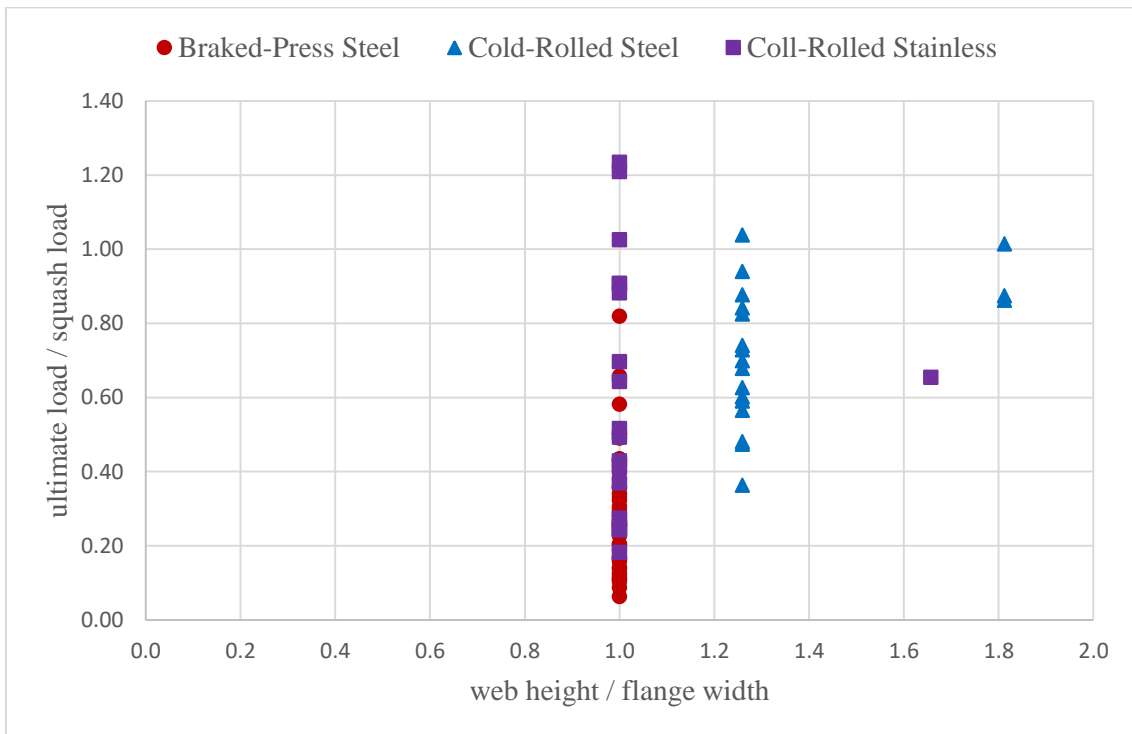
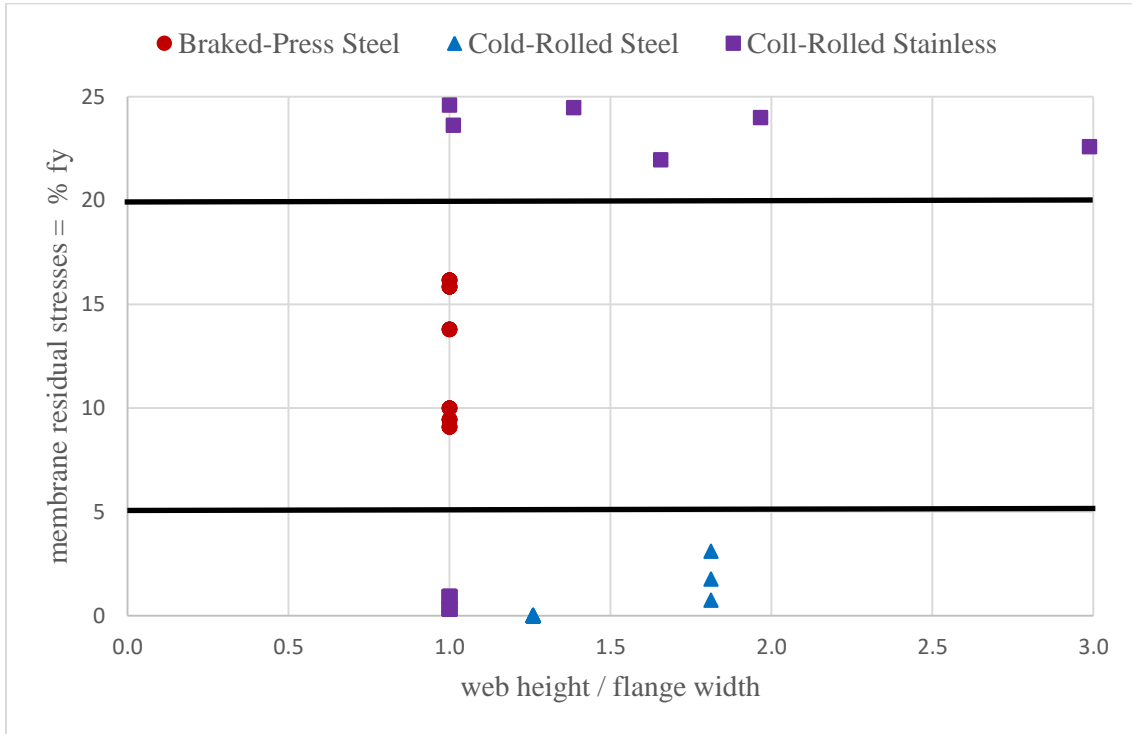


Figure 2.9: Flat regions MRS effects from CR & PB on peak load [35, 36, 38, 41, 59]

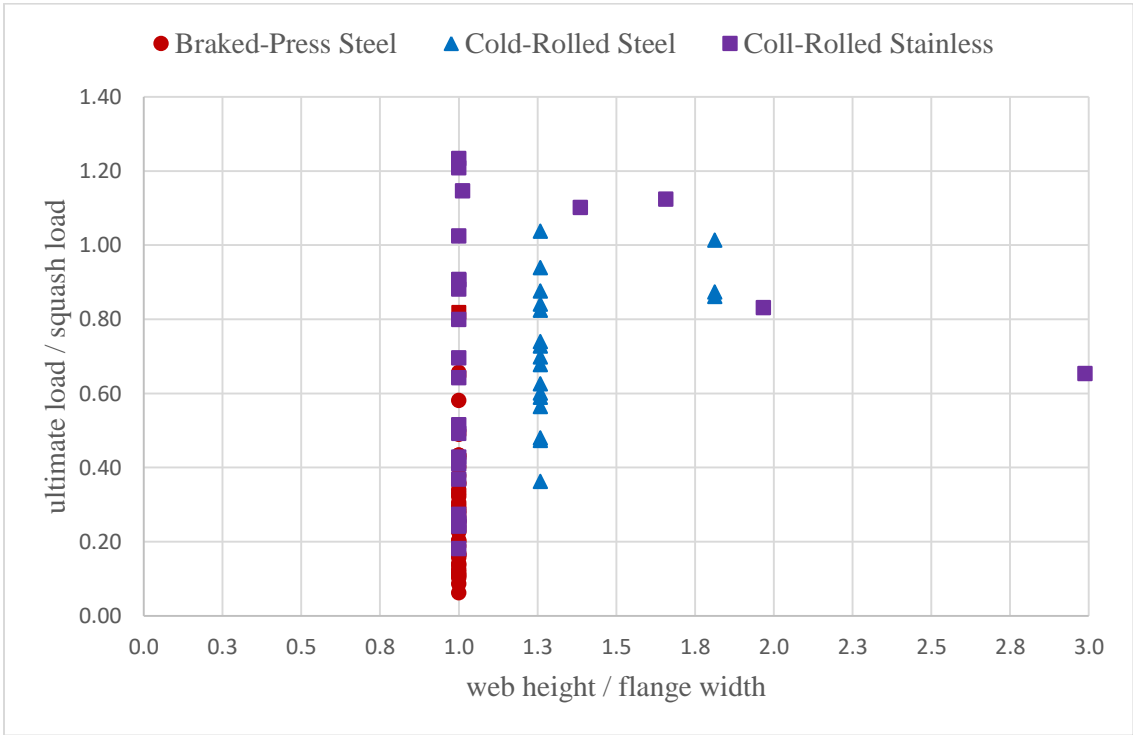
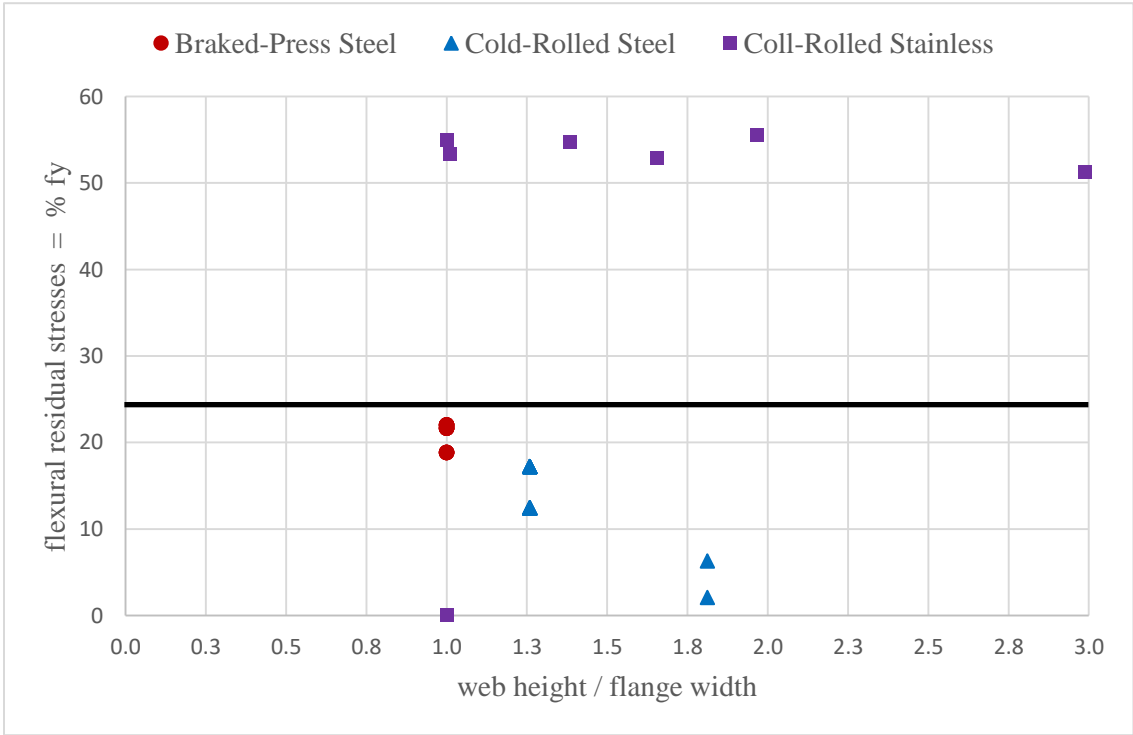


Figure 2.10: Corner regions FRS effects from CR & PB on peak load [35, 36, 38, 41, 59]

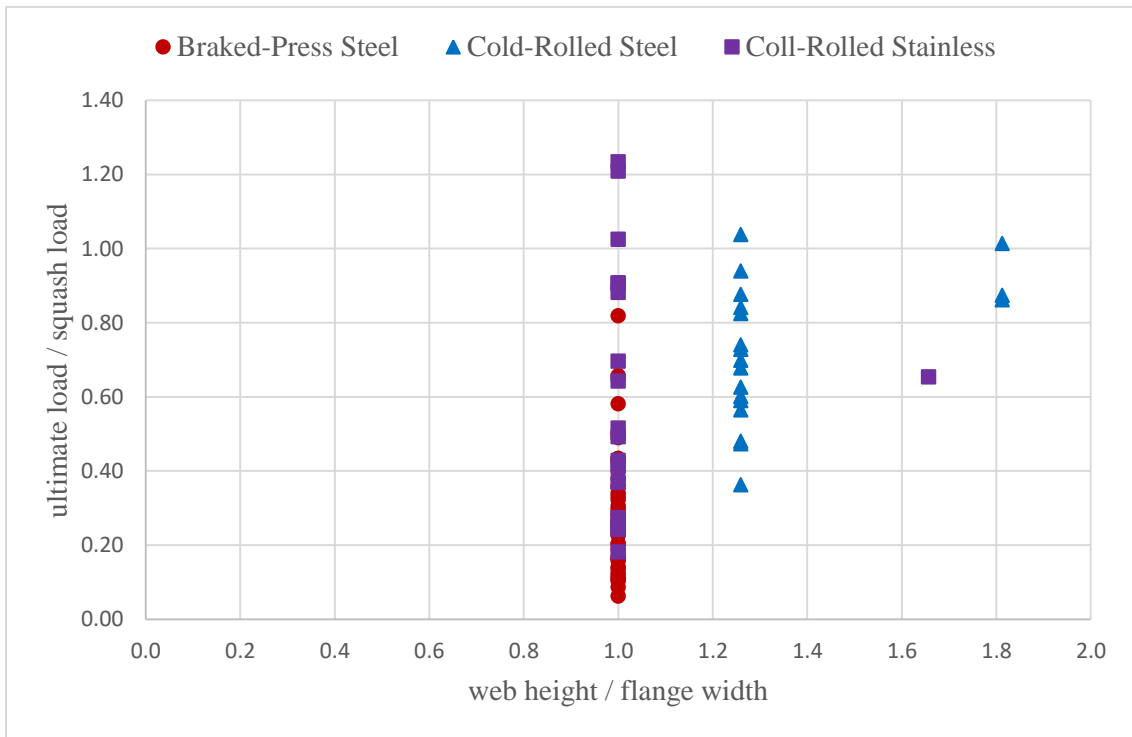
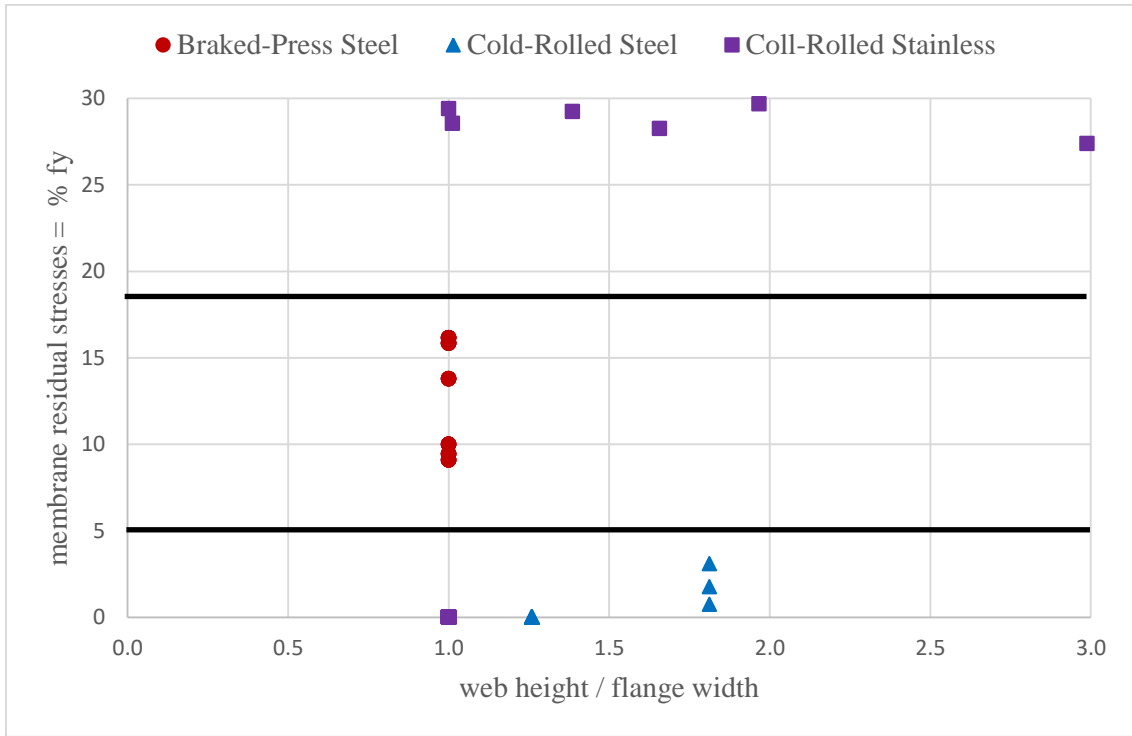


Figure 2.11: Corner regions MRS effects from CR & PB on peak load [35, 36, 38, 41, 59]

### 2.2.1.3 Plastic strain (Strain hardening SH)

Plastic strain is characterised by non-recoverable deformation and induced when stresses exceed the material yield strength. The high residual stresses reported in the previous subsection are indicative of large plastic strain during production; in this subsection, the associated strength enhancements due to cold-work are assessed through tensile material testing. The previous research on the measurement of strain-hardening of thin-walled cold-formed members is generally classified into two categories: (1) in bend or corner regions, and (2) in flat regions (as shown in Figure 2.12). The main aim of the research work was to quantify the amount of cold working from manufacturing, which was conventionally obtained from coupon tests. The cold work generally includes effects of residual stresses, which was reviewed in the preceding section, and strain hardening on ultimate strength capacity of structural members. Hence, the influences of plastic strain in bend or corner and flat regions on the load-carrying capacity of column members are briefly reviewed below.

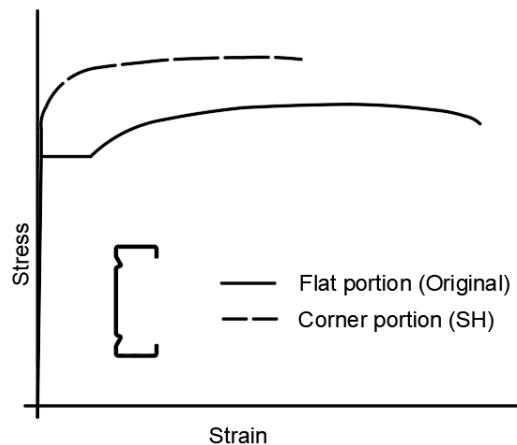


Figure 2.12: Stress-strain diagram for flat and corner region of a section

As discussed in the previous subsection, several experimental tests have been carried out to evaluate the strength and stiffness of thin-walled cold-formed structural members. This subsection compiles an experimental database by reviewing these tests. A total of 13 studies (152 column specimens) of CFS structural members were included in the database. These specimens were categorized into four types depending on cross-section geometries namely channel, angle, pallet rack and hollow sections as well as the method of the manufacturing process and material properties as shown in the Figure 2.13 and Figure 2.14. The first type comprised 4 carbon steel

channel column specimens manufactured with cold roll forming and 12 channel column specimens manufactured with press braking. The second type comprised 23 steel angle column specimens manufactured with press braking. The third type comprised 37 carbon steel rack column specimens manufactured with cold roll forming. The fourth type comprised 76 stainless steel hollow section column specimens manufactured with cold roll forming. As shown, most of the tests (76 out of 152) were conducted on the hollow sections formed with cold roll forming, while the test data for channel section manufactured with cold roll forming is limited and no test data is carried out for Z-section.

Figure 2.13 compares the ratio of yield strength increase of corner to flat regions of different web height to flange width of cross-section types for the 152 structural column specimens. It can be seen that both press braking and cold roll forming can induce approximately the same amount of plastic strain in the corners up to 30% for steel, whilst the cold roll forming can generate yield strength increase of about 80% for stainless steel. However, while the increase in ultimate strength capacity of column specimens is not as an obvious, the strength capacity increases of the structural members due to plastic strain is generally less than the increase of yield strength in the material properties.

Figure 2.14 compares the yield strength increase of corner to flat regions of different web height to flange width of cross-section types for the 152 structural column specimens. It can be seen that yield strength increases in all three sections namely angle, pallet rack and channel sections are very similar not more than 30%, the strength increase in stainless steel hollow sections are very significant up to 80%. In addition, the plastic strain seems to have a larger influence on a load-carrying capacity of stainless steel formed with cold roll forming process, that the ultimate strength could reach more than its squash load, compared to two other types that the ultimate strength did not reach its squash load. However, while the existing test data gives inside to the effects of plastic strain from the manufacturing process on the load-carrying capacity of structural column members, it cannot provide precise answer how plastic strain affect strength capacity of column members.

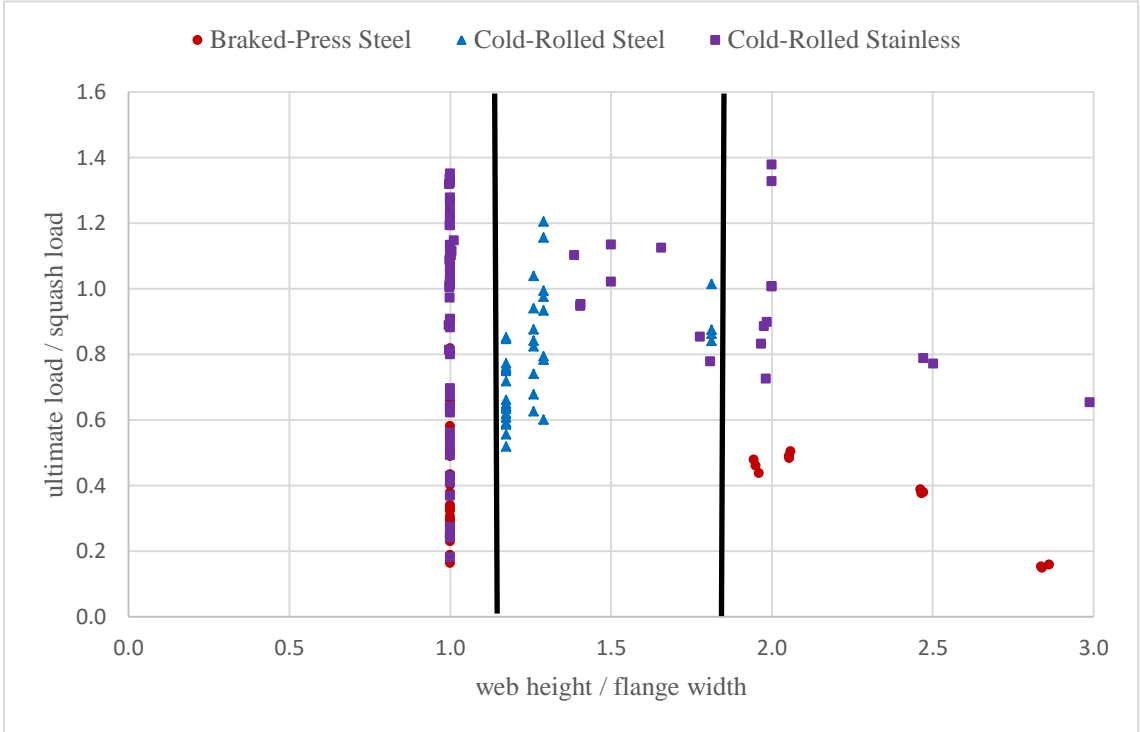
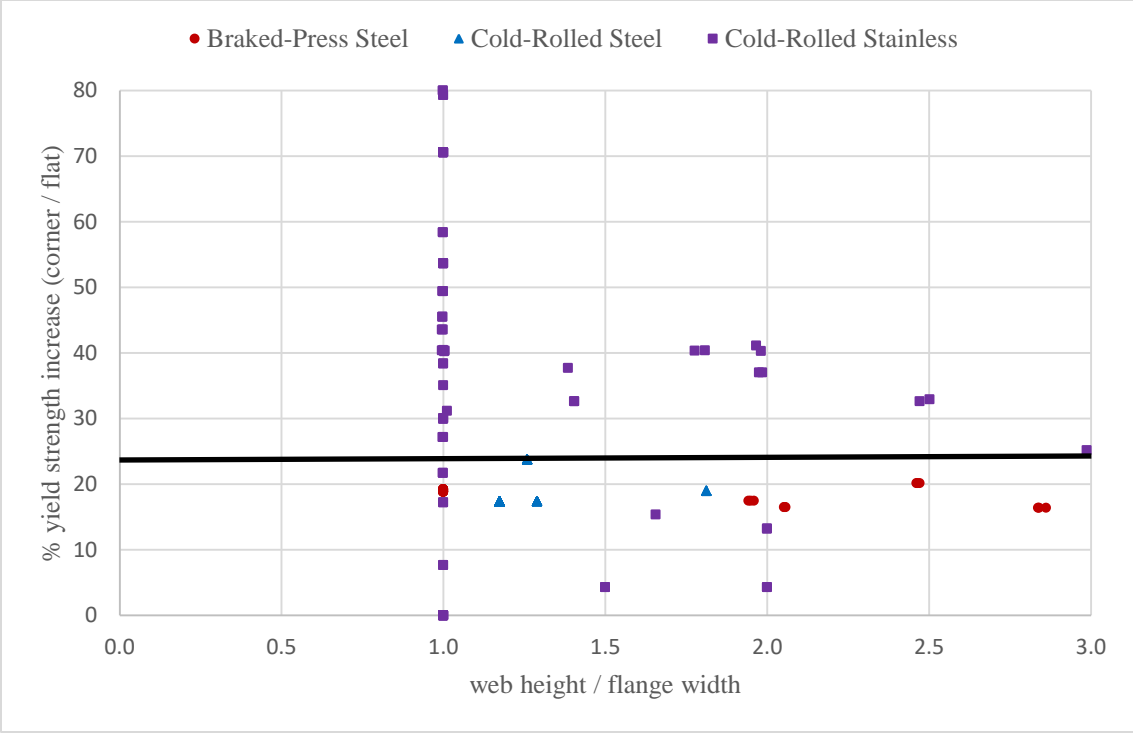


Figure 2.13: % yield strength increases effects from CR & PB on peak load [35, 36, 38, 41, 56, 58, 59]



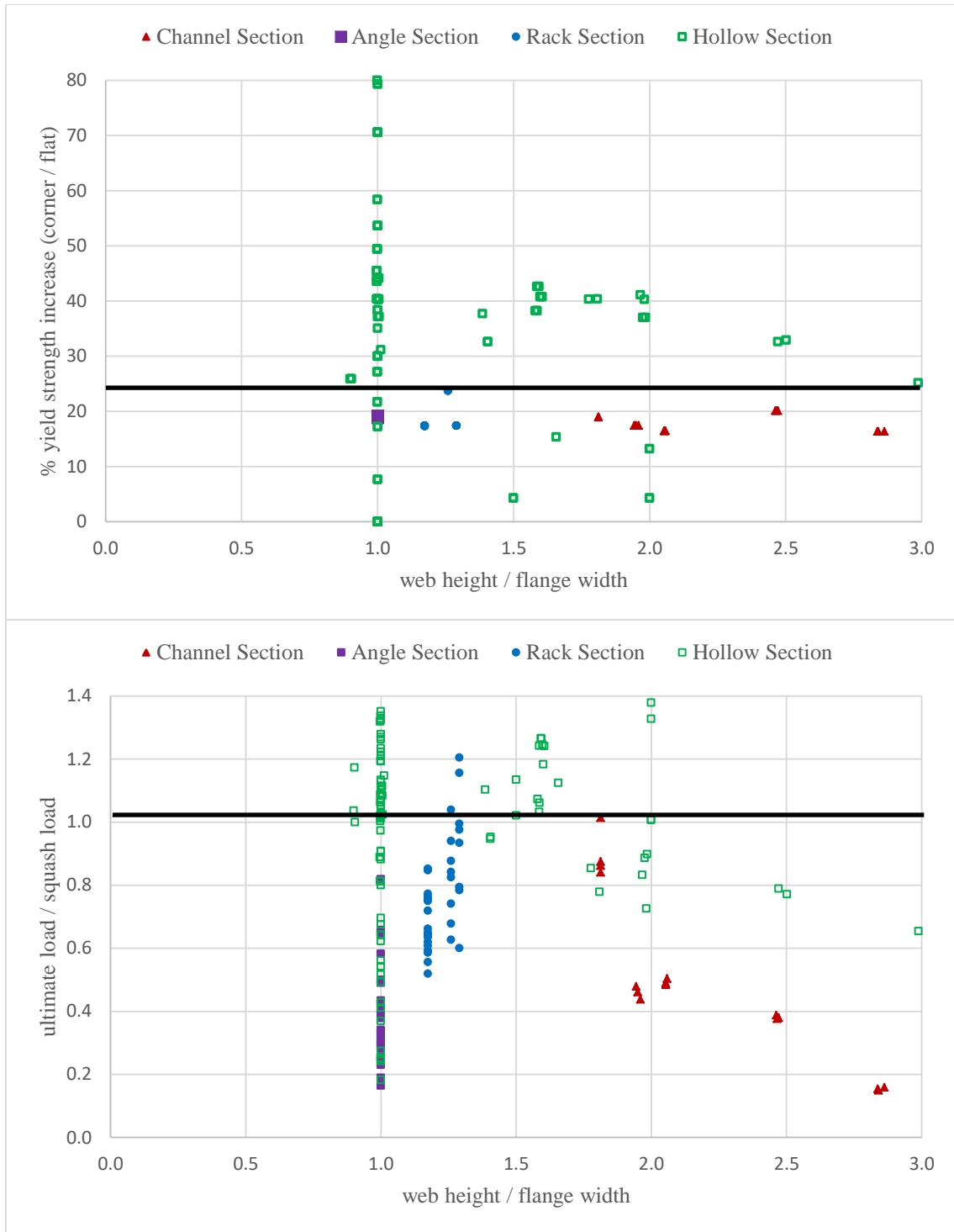


Figure 2.14: % yield strength increases effects of different sections on peak load [35, 36, 38, 41, 56, 58, 59]

Therefore, much research has been conducted to evaluate the influence of plastic strain on ultimate strength capacity in cold-formed column members based on finite element analysis.

Some researchers ignored the strain hardening experienced along the section induced from manufacturing and used elastic perfectly plastic stress-strain curve [47, 48, 62], while many researchers have measured the strain hardening and some of them pointed out that it had negligible effect on load-carrying capacity of column members [54, 56, 65]. However, some other researchers have shown plastic strain to have significant influence on ultimate strength of structural column members [38, 49, 61, 66-69].

Gardner and Nethercot [49] carried out the FEA of stainless steel CHS, SHS and RHS members to develop a consistent approach to the modeling of stainless-steel structures. They noticed the influence of the corner properties on ultimate strength resistance and concluded that FEA (using measured initial geometric imperfection amplitudes) with corner properties extended to  $2t$  beyond the curved portions of the cross-sections yield better agreement with test results than FE models with corner properties extended only to a distance  $t$ . Hence, it was found that FE models with no allowance for corner strength enhancements produce average under-predictions of the strength of around 8%.

Jandera et al. [38] also examined the influence of plastic strain and residual stresses in cold-rolled stainless steel box sections using experimental and numerical techniques. They assessed the generation of large plastic strain during production through tensile material testing which enhanced the associated strength due to cold-work. The stress-strain curve was obtained from tensile coupon extracted from the flat and corner regions of the tested section sizes. The study concluded that the combined effect of plastic strain and residual stresses in terms of load-carrying capacity was variable due to varying local plate slenderness, which was the square root of the yield load to the elastic local buckling load of the plate elements), and the maximum influence was a 5.3% increase in the local buckling strength.







The study was then extended by Jandera and Machacek [61] by conducting an extensive numerical parametric study using geometrically and materially non-linear FE analysis. They noticed even larger enhancement due to combined influences of plastic strain and residual stresses between 10% for global buckling and up to 9% for local buckling of SHS members using the FE model based on measured material characteristics. While there was no reduction in

local buckling strength due to the fact that the positive effect of plastic strain always dominated the negative effect of residual stresses, the reduction of 16% was seen for global buckling.








As clarified in the previous section, Quch et al. [64] investigated the combined effects of plastic strain and residual stresses on the ultimate strength of press braking steel and stainless-steel lipped channel sections. They noticed that the combined effects depend on the following parameters: the diameter of the original sheet coil, the radius of the bent corners, the material properties of the virgin sheet material, and the column length. The study also showed that the cold work in the corner regions of the stainless-steel section enhanced the column strength (within the range of 1% to 9%) and the degree of enhancement generally decreased as the column became longer. The cold work in corner regions leads to a 9% increase in the strength of the stub column for stainless steel, while the increase of 6% achieved for the carbon steel stub column. This greater enhancement is due to the greater extent of strain hardening experienced by the stainless-steel section than the carbon steel section during fabrication as a result of their different stress-strain responses.

Tension, bending and compression tests were also carried out to investigate the effect of cold working during the UltraSTEEL® dimpling process on the mechanical and structural properties of the steel material [66, 67, 70]. They observed the increase in the yield strength and the ultimate strength in the same time decrease in the ductility of metals through tensile and plate bending tests. They also concluded that even though significant enhancement was achieved in improving mechanical properties of the dimpled specimens compared to plain metals due to large induced plastic strain, the same enhancement in the structural performance of the compression and bending strength capacity of the structural members were not obtained as well. For instance, while the increase in the yield strength and ultimate strength of the material obtained for the dimpled specimens were obtained 14–51% and 9–34%, respectively, compared to plain specimens, the buckling and ultimate strengths capacity of dimpled steel columns were up to 33% and 26%, respectively. This may be due to the fact that when metals generate large plastic deformation during the manufacturing process, the large residual stresses are inevitably induced deemed to be the reason for the reduction of the strength capacity of the structural members.


**Table 2.1:** Summary of previous research to evaluate influences of the manufacturing process on strength capacity of CFS column members based on experimental and numerical data for channel sections

Researcher	Manufacture/ Material	Effect on Peak Load		
	& cross-section type	Imperfection	Residual stresses	Plastic strain
Ingvarsson 1975 [63]	Brake-pressed steel channel section 	Positive effects	Positive effects	Not studied
Dat 1980 [59]	Roll-formed and brake-pressed steel channel section 	Not studied	-5.4 to -15% Up to -30%	Not studied
Kwon and Hancock 1992 [65]	Roll-formed steel channel section 	Not studied	Not studied	insignificant
Becque 2008 [71]	Roll-formed stainless steel channel section 	Not studied	-0.4%	Not studied
El Aghoury et al. 2017 [44]	Roll-formed steel sigma section 	No remarkable effect	-4%	Not measured
Ye et al. 2018 [56]	Brake-pressed steel channel section 	20 to 40%	Not measured	Less than 1%









**Table 2.2:** Summary of previous research to evaluate influences of the manufacturing process on strength capacity of CFS column members based on *experimental and numerical data* for other sections

Researcher	Manufacture/ Material	Effect on Peak Load		
	& Cross-section type	Imperfection	Residual stresses	Plastic strain
Key and Hancock 1993 [62]	Roll-formed steel hollow section 	Not studied	-1.9 to -5.4% up to -15.8%	Not studied
Abdel-Rahman and Sivakumaran 1997 [58]	Roll-formed stainless steel hollow section 	Not studied	Less than -2%	Not studied
Gardner and Nethercot 2004 [49]	Roll-formed stainless steel hollow section 	10%	Little influence	8%
Ellobody and Young 2005 [35]	Brake-pressed steel angle section 	Not studied	Negligible effect	Not studied
Young and Ellobody 2005 [36]	Brake-pressed steel angle section 	Not studied	Negligible effect	Not studied
Jandera et al. 2008 [38]	Roll-formed stainless steel hollow section 	Not studied	-2%	10%
Huang et al. 2012 [41]	Roll-formed steel pallet rack 	Not studied	-1%	Not studied

**Table 2.3:** Summary of previous research to evaluate influences of the manufacturing process on strength capacity of thin-walled CFS column members based on *pure numerical data* for channel sections

Researcher	Manufacture/ Material	Effect on Peak Load		
	& Cross-section type	Imperfection	Residual stresses	Plastic strain
Schafer and Pekoz 1998 [46]	Roll-formed and brake-pressed steel channel section 	30%	Small net effect	Not studied
Chou et al. 2000 [47]	Roll-formed channel and hat section 	2%	Ignored	Ignored
Dubina and Ungureanu 2002 [48]	Cold-formed steel channel section 	25%	Ignored	Ignored
Ashraf et al. 2006 [50]	Brake-pressed stainless steel angle, Channel, Lipped channel and I sections	7%	Little influence	Not studied
Quach et al. 2010 [64]	Brake-pressed steel channel section 	Not studied	-16%	11%
Quach et al. 2010 [64]	Brake-pressed stainless steel channel section 	Not studied	+4%	1 to 9%

**Table 2.4:** Summary of previous research to evaluate influences of the manufacturing process on strength capacity of thin-walled CFS column members based on *pure numerical data* for other sections

Researcher	Manufacture/ Material	Effect on Peak Load		
	& Cross-section type	Imperfection	Residual stresses	Plastic strain
Davison and Birkemoe 1983 [60]	Roll-formed steel hollow section 	Not studied	13%	Not studied
Crisan et al. 2012 [51]	Roll-formed steel pallet rack 	22 to 27%	Less than -3%	Not studied
Bonada et al. 2012 [52]	Roll-formed steel rack sections 	Up to 15%	Ignored	Ignored
Pastor et al. 2013 [53]	Roll-formed steel rack sections 	Not studied	- 24%	Not studied
Jandera and Machacek 2014 [61]	Brake-pressed stainless steel hollow sections 	Not studied	-16%	10%
Pastor et al. 2014 [72]	Roll-formed steel rack sections 	Up to 31%	Ignored	Ignored
Bonada et al. 2015 [54]	Roll-formed steel pallet rack 	No effect	Increase only short column	Insignificant
Bonada et al. 2016 [55]	Roll-formed steel rack sections 	2 to 18%	Insignificant	Insignificant

## 2.2.2 Manufacturing process effects in thin-walled structural beam members

In this section, existing studies on the effect of cold work of the manufacturing process such as initial geometrical imperfection and residual stresses on the structural behaviour of cold-formed beam members are reviewed. In total 7 studies that are available in the literature have been gathered and the cross-section shapes investigated are shown in Figure 2.15. Two of them were experimental studies for hollow sections and one of them was experimental studies for the new mono-symmetric LiteSteel beams (LSB), as well as four of them, were numerically studied for channel and Z-sections. But up until now, the effect of cold work of the manufacturing process on the ultimate strength of beam members has not been investigated explicitly.

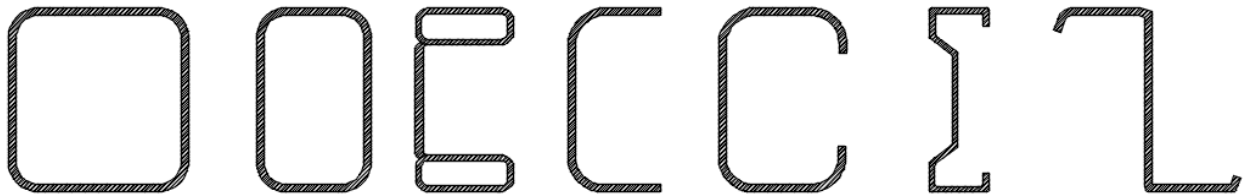


Figure 2.15: Example of cold-formed cross-sections collected for beam member

### 2.2.2.1 Imperfection

Only a limited amount of work has been conducted in order to evaluate the influence of initial geometric imperfection on the strength capacity of thin-walled cold-formed beam members [73-75] (and these studies are summarised in Table 2.5. Although less attention was paid to investigate the effect of local and distortional imperfections on the ultimate strength of beam members, the effect of global imperfection on load-carrying capacity was shown to be significant. It has been observed that the interaction between sectional modes (local and distortional) and global mode is not significant in beams compared to columns and the sectional imperfection has little influence on lateral-torsional buckling strength [48].

Seo et al. [73] studied the initial imperfection characteristics of the new mono-symmetric LiteSteel beams (LSB) and their effects on the moment capacity. They realized that the initial imperfections depend on the aspect ratio of the web, flange width as well as other factors such as



material properties, welding condition, and rolling process. The moment capacity loss due to the cross-section or plate imperfections was considerably less than that due to the use of overall member imperfection, which was predominant in the longitudinal direction.

Theofanous and Gardner [74] carried out 3-point bending tests on lean duplex stainless steel hollow sections and extended the study by parametric study using finite element (FE) analysis. They found that the incorporated imperfection amplitude can be seen to have only a modest effect (5%) on the ultimate moment capacity.

Kankanamge and Mahendran [75] conducted a numerical study to investigate the lateral-torsional buckling behaviour of simply supported cold-formed steel lipped channel beams subjected to uniform bending. They observed that for G250 steel sections the maximum percentage of reduction in moment capacity was only about 7% when the beam slenderness was about 1.0 as the imperfection magnitude was increased from  $L/3000$  to  $L/1000$ , whereas no clear trend for some G450 sections was seen.

#### 2.2.2.2 Residual stresses and strain hardening

In comparison to the initial geometrical imperfection, there have been some studies to investigate the effect of cold work of the manufacturing process on ultimate strength of structural beam members [69, 73, 75-78], which are summarised in the Table 2.5 and briefly reviewed here.

Pi et al. [76-78] performed a series of study to investigate the lateral buckling strengths of the cold-formed hollow flange (HFBs), channel section (CFC) and Z-section (CFZ) beams with residual stresses, respectively. They adapted the residual stresses measured by Key and Hancock [62] for a 254SHS with  $f_y = 350$  MPa for (HFBs) and the longitudinal normal residual stresses recommended by Weng and Pekoz [79] for CFC sections. However, they modified the longitudinal normal residual stresses recommended by Weng and Pekoz [79] for CF channel sections and used for the CFZ-sections, because they claimed that no measurements for the residual stresses in CFZ beams were found and the method of cold-forming a CFZ-section is similar to that of a CF channel section. The investigations showed that the strengths of the beams with residual stresses were significantly lower, except at high and lower slenderness than those

without residual stresses about 9% for (HFBs), whereas the residual stresses had little influence on the strength of (CFZ) and (CFC) less than 5%.

Seo et al. [73] presented a sensitivity study of residual stress on the ultimate strength of LSBs under pure bending. They observed that when both membrane and residual stresses were included, the strength ratio was reduced by up to 14.5%. The other interesting results were also noted that the ultimate strength reduction characteristic due to residual stresses was different as a function of span length for all sections and the effect was minimal for longer spans. The study also concluded that although the use of flexural residual stresses alone in the numerical studies of LSBs can give a reasonable estimation of their moment capacity, accurate estimates were obtained when membrane residual stresses were also included in the analyses.

Kankanamge and Mahendran [75] also conducted a numerical study to investigate the lateral-torsional buckling behaviour of simply supported cold-formed steel lipped channel beams subjected to uniform bending. Effects of residual stresses were investigated by comparing the moment capacity results with and without residual stresses. Hence, it was observed that the influence of residual stresses on the ultimate moment capacity was insignificant.









Recently, Wang [69] established numerical models based on the bending test of roll-formed sigma section conducted by Liu et al. [80] to investigate the distribution and effect of cold working and welding residual stress on CFS sigma beams. He performed comparisons between the virgin model without cold work effects and modified model incorporated the effect of residual stress and strain hardening. The study concluded some interesting points that are briefly reviewed here.

During the coiling-uncoiling process, the residual stresses in both longitudinal and transverse directions decreased as the yield strength and sheet thickness increased as well as the residual stresses and plastic strain closed to zero as the roll radius to thickness ratio approach to 1000. It was found that the roll diameter was a dominant factor and followed by the effect of sheet thickness, and the change of yield strength has the least impact on the final residual stress. After the coiling process, the tensile stress was found on the outside surface and compression on the inside surface.

In the roll forming process, nonlinear residual stresses distribution along the thickness was observed in both corner and flat portions and the curve was anti-symmetrical about the neutral axis. Although, the maximum longitudinal residual stresses, which located on  $\pm 0.25$  of normalized thickness, was noted exceed the transverse counterpart at the flat portion, the peak value of longitudinal residual stresses was lower than the transverse residual stresses at corner portion as the deformation was mainly found in the transverse direction.

After the roll forming process, the equivalent plastic strain was mainly occurred on the bending zone between the inner web and outer web, whereas the plastic strain in the rest part of the cross section was insignificant. Thus, the combined effect of residual stresses and plastic strain in the corner areas increased the ultimate strength of sigma beams as the enhancement induced by strain hardening was the dominant factor, while the residual stresses reduced the stiffness of the beam.

**Table 2.5:** Summary of previous research to evaluate influences of manufacturing process on strength capacity of thin-walled CFS structural beam members based on *experimental and numerical data*

Researcher	Manufacture		Effect on Peak Load		
	Structural type		Imperfection	Residual stresses	Plastic strain
Pi and Trahair 1997 [78]	Cold-formed steel hollow flange beams		Not studied	9%	Not studied
Pi et al. 1998 [76]	Cold-formed steel channel section		Not studied	5%	Not studied
Pi et al. 1999 [77]	Cold-formed steel Z-section		Not studied	5%	Not studied
Seo et al. 2008 [73]	Roll-formed steel LSBs		Not studied	Up to 14.5%	Not studied
Theofanous and Gardner 2010 [74]	Roll-formed stainless steel hollow section		5%	Not studied	Not studied
Liu 2011 & Wang 2015 [69, 80]	Roll-formed steel sigma section		5%	1 to 4%	2 to 12%
Kankanamge and Mahendran 2012 [75]	Roll-formed steel channel section		5 to 7%	insignificant	Not studied
Ye et al. 2018 [81]	CFS back-to-back channel section		7%	insignificant	5%

### 2.2.3 Summary

Manufacturing process effects in thin-walled CFS structural members reported in the previous subsections are briefly recapped. Based on the previous findings and discussions, the following observations can be made.

1. While there is only limited study showed sectional imperfection (local and distortional) had insignificant effects on ultimate buckling strength, most researchers concluded that the initial geometric imperfections could have significant influence, up to 40% as presented in Tables 2.1 to 2.4, on a load-carrying capacity of column members.
2. The imperfection influences depend on many factors including types of failure (local or distortional buckling failure), length of the column, the shape of imperfection (symmetric or asymmetric), and the imperfection amplitude.
3. The influence of residual membrane stresses on ultimate buckling strength was usually very low, maximum 4% as depicted in Table 2.1, and was neglected in most cases.
4. The combined influences of flexural (bending) residual stresses and strain hardening were varied that can be beneficial or detrimental on ultimate strength capacity depending on some parameters such as steel grade, material types (steel or stainless steel), corner or bend radius, column length, and thickness of the sheet.
5. The maximum detrimental combined effects of residual stresses and strain hardening were seen up to 30% reduction, while the maximum positive effect was the increase of 11% in load-carrying capacity.
6. Taking flats and corner portions of the cross-section of beam members into account, the effect of residual stresses decreased the peak load by only 2%, whilst the strain hardening increased the failure load about 6% and the combined effect of residual stresses and plastic strain increased the ultimate strength by about 4%.
7. The cumulative distribution function (CDF) values for the maximum imperfections suggested by Schafer [46] are more universally applicable and is thus recommended to be used for type 1 (local buckling  $d_1$ ) and type 2 (distortional buckling  $d_2$ ) in the Finite Element modelling.
8. Residual stresses could be indirectly considered in the FE models through the stress-strain data obtained from the material tests. In particular, the membrane residual stresses could be

safely ignored in the open sections [30, 46], whereas the longitudinal flexural residual stresses reported being implicitly presented in the stress-strain behaviour of the coupon tensile test results as long as the coupons were cut from the final sections. Cutting a coupon might release the flexural residual stresses that caused the coupon to curl [38], whilst these stresses were re-introduced when the coupon is straightened during the initial stages of tensile loading.

## 2.3 Current design methods for thin-walled (CFS) members

Two design methods for cold-formed structural members are formally available in the design specifications and widely used nearly worldwide the traditional Effective Width Method (EWM) and the Direct Strength Method (DSM). The EWM is available in the most of the standard and specifications such as North America specification AISI-S100 Specification [3], British Standard BS5950 [4], and Eurocode 3 (EC3) [5], whereas the DSM is used in North America specification [3]. Both design methods EWM in the EC3 and the DSM in AISI-S100 are reviewed and the shortcomings from each method are identified.

### 2.3.1 Design of CFS members based on EWM in Eurocode 3

Different modes of failure including local (L), distortional (D), local/distortional (LD) and global buckling have to be considered in order to carefully design thin-walled CFS structural members according to Eurocode EN1993-1-3. The mechanism to design these modes of failure is briefly discussed in this section.

#### 2.3.1.1 Local buckling

Local buckling may occur in the pure elastic region or close to the yield load. Large strength reserve is generally obtained when the local buckling occurs below the yield load region. The primary design method for CFS structural members to take the influence of local buckling into consideration is the effective width method (EWM), introduced by von Karman [82] and subsequently modified by Winter [26], adopted in the European Codes EN1993-1-3 [5]. The basic notion of the EWM to account for local buckling is that the effectiveness of the plates which constitute the cross-section is reduced due to local plate buckling. This reduction can be accounted for a simplified stress distribution as opposed to the actual nonlinear stress distribution generated due to buckling as shown in Figure 2.16. Local buckling of each plate in the cross-section has the ability to shift the carrying load toward the end of the plate and the material at the central part of the plate is ineffective in carrying the load.

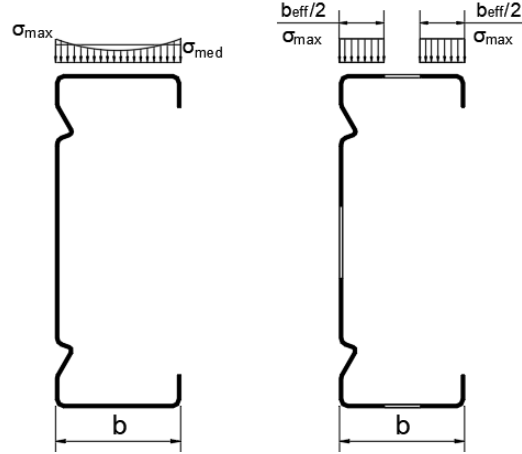


Figure 2.16: EWM simplified stress distribution

$$\frac{b_{eff}}{b} = \frac{1}{\lambda_p} x \left( 1 - \frac{0.22}{\lambda_p} \right) \leq 1.0 \quad \lambda_p = \sqrt{\frac{\sigma_{max}}{\sigma_{cr}}} \quad (2.3)$$

$b$  and  $b_{eff}$  are the width and effective width of the plate while  $\lambda_p$  is relative plate slenderness against local buckling. The relative plate slenderness is calculated based on the critical buckling stress  $\sigma_{cr}$  and maximum stress  $\sigma_{max}$  which depend on the material yield stress ( $f_y$ ). It is noted that the plate is fully effective if  $\lambda_p \leq 0.673$  which depend mainly on thickness-to-width ratio and material yield stress. It is worth to note that the EWM is a simple design rule and can give inside into the behaviour of the plate while reaching the ultimate condition. This method is proven to provide satisfactory strength and stiffness results.

However, the EWM is often not adequate to predict the accurate design results due to some approximations in the developed method. It accounts for only membrane stress conditions in width of a plate and ignores the stresses through the thickness as well as the variation of stresses along the plate length. In addition, while any relation between the flange and the web plate of a cross-section is ignored when the elastic local buckling is calculated using the EWM, for the calculation of local buckling in a single plate with stiffeners, the method assumes that each part of the plate is to be treated separately. Finally, the EWM is unable to predict the distortional buckling of a plate. Hence, the approximation of two-dimensional non-linear stresses distribution which has shown as the base of EWM of a plate is not as efficient due to the simplified nature of the method.



### 2.3.1.2 Distortional buckling

It is well known that sufficient design procedure is not provided for predicting the distortional buckling (D) strength by EWM. Although researchers proposed design methods, based on the EWM, for determining the nominal distortional buckling strength of typical cold-formed C and Z sections subjected to bending [83, 84], the proposed methods have not been included in the European Codes. Instead, an interpretation of the rules provided in the Eurocode is generally used to calculate distortional buckling strength. The distortional failures often occur in the lipped zed sections and lipped channel sections. These sections are more susceptible to distortional failure as the constituted plates in these cross-sections have ability to rotate in plane and out of plane about the region of the connecting plates which are the connection regions between the flange and the web plate (web/flange juncture) as well as the connection regions between the stiffeners and the flange (stiffener/flange juncture) or the web plates (stiffener/web juncture).

The web plate width to flange plate width plays an important role to provide sufficient strength and stiffness to the juncture. As the width of the web increases with the constant flange width, the connection region becomes more flexible and thereby the distortional buckling controls the failure behaviour of the cross-section. However, if the width of the web plate assumes to be constant and varying the flange plate width, take narrow flange width for instance, distortional failure is not critical as distortional buckling stress will be lower than local buckling stress, while for excessively wide flange width the local buckling is not critical and the distortional buckling failure depends mainly on the length of the provided end stiffeners. The increase in the length of the end stiffeners is often beneficial for preventing distortional buckling, while this might lead to a detrimental effect on local buckling strength.

The EC3 approach uses a combination of effective width and reduced thickness methods to determine the distortional buckling strength, it requires the elastic distortional buckling stress to be obtained from Eq. 2.2. This is an extension of the elastic model and the assumption that the stiffeners need to follow a basic column curve for strength calculation. Hence, ignoring the post-buckling capacity.

$$\sigma_{cr,s} = \frac{2 \cdot \sqrt{K \cdot E \cdot I_s}}{A_s} \quad (2.4)$$

Where  $E$  is the modulus of elasticity,  $I_s$  is the second moment of area of the stiffener about an axis through its centroid parallel to the plate,  $K$  is the spring stiffness per unit length and  $A_s$  is the stiffener area. The spring stiffness  $K$  is determined by applying a unit load  $f = 1$  (per unit length) to the full cross-section at the centroid of the stiffener assembly and by calculating the corresponding displacement.

### 2.3.1.3 Modal interaction

Experimental and numerical studies have shown the strong interaction of local-global buckling. The current design standard can handle local-global interaction that is one of the fundamental steps toward making thin-walled structural steel sections practical. The Eurocode adapted the effective width method to account for the local-global interaction as well as the distortional-global interaction. However, proper inclusion of local-distortional interaction is far more difficult to be treated with the traditional effective width method as local buckling and distortional buckling strength have to be calculated for the same element. Thus, the combination of traditional effective width method with reduced thickness method is used by the Eurocode to account for the local-distortional interaction.

### 2.3.1.4 Cold work effects in CFS structural members

In EC3, the average yield strength  $f_{ya}$  of a cross-section due to cold working is calculated by the following equations:

$$f_{ya} = f_{yb} + (f_u - f_{yb}) \frac{kn t^2}{A_g} \quad \text{and} \quad f_{ya} \leq \frac{f_u + f_{yb}}{2} \quad (2.1)$$

$f_{yb}$  is the basic yield strength and  $A_g$  is the gross cross-section area.  $K$  depends on the type of the manufacturing process and it is equal to 7 for cold roll forming as well as  $t$  is the thickness of the steel material before cold forming. It is noted that only the bends of  $90^\circ$  in the cross-section with an internal radius of equal and less than  $5t$  is considered in the calculation of the number of

bends (n) which seems to be conservative in some cross-sections with complex shapes having ribs and stiffeners such as newly developed channel and Z-Sections.

### 2.3.2 Design of CFS members based on DSM in AISI S100

A more recently developed design method for thin-walled CFS members is the Direct Strength Method (DSM). It is based on the original idea of Hancock et al. [65, 85, 86] at the University of Sydney and first proposed by Schafer and Peköz [87]. The method has been shown to provide more efficient estimates to obtain accurate results of the ultimate strength capacity of column and beam members compared to the EWM and hence can overcome some of the shortcomings of the conventional EWM. The ultimate strength capacity is calculated based on yield stress and member elastic critical buckling stresses (local, distortional and global buckling stresses). These stresses are linked to the buckling stability modes of the member (local, distortional and global buckling mode), as well as the interactions between these modes. The design procedure of, and continued research into, the DSM is explored further in this section.

#### 2.3.2.1 Global buckling

##### **Columns**

The global buckling strength for columns and beams are provided following DSM. The nominal axial strength  $P_{ne}$  for flexural, torsional or torsional- flexural buckling is calculated in accordance with the following:

$$\text{For } \lambda_c \leq 1.5 \quad P_{ne} = (0.658^{\lambda_c}) P_y \quad (2.2)$$

$$\text{For } \lambda_c > 1.5 \quad P_{ne} = \left( \frac{0.877}{\lambda_c^2} \right) P_y \quad (2.3)$$

Where 
$$\lambda_c = \sqrt{\frac{P_y}{P_{cre}}} \quad \text{and} \quad P_y = A_g f_y$$

$\lambda_c$ : the slenderness ratio

$f_y$ : yield stress which is the 0.2% proof stress ( $\sigma_{0.2}$ ) obtained from tensile coupon tests

$A_g$ : gross area of the cross – sction

$P_{cre}$ : the minimum of the critical elastic column buckling load in flexural, torsional, or torsional – flexural buckling

### Beams

The nominal flexural strength  $M_{ne}$  for lateral-torsional buckling is calculated in accordance with the following:

$$\text{For } M_{cre} < 0.56M_y \quad M_{ne} = M_{cre} \quad (2.4)$$

$$\text{For } 2.78M_y \geq M_{cre} \geq 0.56M_y \quad M_{ne} = \frac{10}{9} M_y \left( 1 - \frac{10M_y}{36M_{cre}} \right) \quad (2.5)$$

$$\text{For } M_{cre} > 2.78M_y \quad M_{ne} = M_y \quad (2.6)$$

Where  $M_y = S_f f_y$

$S_f$ : gross section moduls referenced to the exterme fiber at firt yield

$M_{cre}$ : critical elastic lateral – torsional buckling moment

### 2.3.2.2 Local buckling

#### Columns

The nominal axial strength  $P_{nl}$  for local buckling is calculated in accordance with the following:

$$\text{For } \lambda_l \leq 0.776 \quad P_{nl} = P_{ne} \quad (2.7)$$

$$\text{For } \lambda_l > 0.776 \quad P_{nl} = \left[ 1 - 0.15 \left( \frac{P_{crl}}{P_{ne}} \right)^{0.4} \right] \left( \frac{P_{crl}}{P_{ne}} \right)^{0.4} P_{ne} \quad (2.8)$$

Where 
$$\lambda_l = \sqrt{\frac{P_{ne}}{P_{crl}}} \quad \text{and} \quad P_y = A_g f_y$$

$P_{crl}$ : critical elastic local buckling load

$P_{ne}$ : the predicted ultimate global buckling load obtained from Eq. (2.2) and Eq. (2.3)

### Beams

The nominal flexural strength  $M_{nl}$  for local buckling is calculated in accordance with the following:

For  $\lambda_l \leq 0.776$  
$$M_{nl} = M_{ne} \quad (2.9)$$

For  $\lambda_l > 0.776$  
$$M_{nl} = \left[ 1 - 0.15 \left( \frac{M_{crl}}{M_{ne}} \right)^{0.4} \right] \left( \frac{M_{crl}}{M_{ne}} \right)^{0.4} M_{ne} \quad (2.10)$$

Where 
$$\lambda_l = \sqrt{\frac{M_{ne}}{M_{crl}}}, \quad \text{and} \quad M_{crl} = S_f \sigma_{crl}$$

$S_f$ : gross section modulus referenced to the extreme fiber at first yield

$\sigma_{crl}$ : critical elastic local buckling stress

$M_{ne}$ : as defined in section 2.3.2.1

### 2.3.2.3 Distortional buckling

#### Columns

It is noted that the open cross-sections such as C-channel and Z-section encounter the distortional buckling that the nominal axial strength  $P_{nd}$  for distortional buckling is calculated in accordance with the following:

$$\text{For } \lambda_d \leq 0.561 \quad P_{nd} = P_y \quad (2.14)$$

$$\text{For } \lambda_d > 0.561 \quad P_{nd} = \left[ 1 - 0.25 \left( \frac{P_{crd}}{P_y} \right)^{0.6} \right] \left( \frac{P_{crd}}{P_{ne}} \right)^{0.6} P_y \quad (2.15)$$

$$\text{Where} \quad \lambda_d = \sqrt{\frac{P_y}{P_{crd}}} \quad \text{and} \quad P_y = A_g f_y$$

$P_{crd}$ : critical elastic distortional buckling load

### Beams

The nominal flexural strength  $M_{nd}$  for distortional buckling is calculated in accordance with the following:

$$\text{For } \lambda_d \leq 0.673 \quad M_{nd} = M_{ny} \quad (2.16)$$

$$\text{For } \lambda_d > 0.673 \quad M_{nd} = \left[ 1 - 0.22 \left( \frac{M_{crd}}{M_y} \right)^{0.5} \right] \left( \frac{M_{crd}}{M_y} \right)^{0.5} M_y \quad (2.17)$$

$$\text{Where} \quad \lambda_d = \sqrt{\frac{M_y}{M_{crd}}} \quad , \quad M_y = S_f f_y \quad \text{and} \quad M_{crd} = S_f \sigma_{crd}$$

$S_f$ : gross section modulus referenced to the extreme fiber at first yield

$\sigma_{crd}$ : critical elastic distortional buckling stress

#### 2.3.2.4 Local-global interaction buckling (NLG)

The current codified DSM is taken local-global interaction buckling of columns into account by substituting the yield load  $P_y$  by the predicted ultimate load of global buckling ( $P_{ne}$ ). Similarly, for beam, replacing yield moment ( $M_y$ ) by the predicted ultimate flexural buckling moment ( $M_{ne}$ ).

### 2.3.2.5 Continued research on modal interaction

The current codified DSM ignores the local-distortional and global-distortional interactions [88]. This is partly because there are conflicting data that have shown including such interactions to determine the load-carrying capacity of the thin-walled members may result in inconsistent results with the observation. Previous studies were also shown the weak interaction between distortional buckling with another buckling mode (local or global). Experimental tests were conducted to investigate the modal interaction, in particular, the interaction of other buckling modes with distortion buckling [65, 89-92]. They confirmed the weak interaction of distortional buckling with other local or global buckling. It was noted by Schafer [89, 90] that replacing ( $P_{ne}$ ) with ( $P_{nd}$ ) to account for local-distortional interactive strength resulted in overly conservative prediction. Based on 169 of the 187 tests that were identified to fail in local-distortional interaction, the average tests to predict ratio was 1.35 [89, 90]. Hence, he claimed that due to the lack of agreement between tests and observation, it was not recommended to include local-distortional interaction in current codified DSM.

However, experimental and analytical studies were conducted for high strength steel sections such as lipped channel with intermediate stiffeners and optimised open cross-sections with multiple distortional buckling modes at university of Sydney [91, 93]. They found that the reduction of post-buckling strength in those sections compared with the current distortional strength curve of the Direct Strength Method and local-distortional interaction was clearly observed in the testing. Although ignoring the local-distortional interaction provided the best agreement in the calculation, distortional-global interaction was still required to be considered by substituting ( $P_y$ ) in Eq. (2.14 to 2.15) with ( $P_{ne}$ ). Hence, these studies have left the current codified DSM somewhat in question with regard to distortional buckling interaction with other buckling modes (local or global).

In additions, the research team led by Camotim has also been studying local-distortional, global-distortional and local-distortional-global interaction [92, 94-98]. They followed the procedure adopted to handle local-global (LG) interactive strength method and local-distortional interaction (NLD) that were first proposed by Schafer [89], by replacing yield load ( $P_y$ ) or yield moment

( $M_y$ ) by the predicted ultimate distortional buckling load ( $P_{nd}$ ) in the ( $P_{nl}$ ) equations or ultimate distortional buckling moment ( $M_{nd}$ ) in the ( $M_{nl}$ ) equations to take local-distortional interaction into account. Furthermore, replacing yield load or yield moment by the predicted ultimate global buckling load ( $P_{ne}$ ) in the ( $P_{nd}$ ) equations and predicted ultimate global buckling moment ( $M_{ne}$ ) in the ( $M_{nd}$ ) equations. It has been again confirmed that the methods give unduly conservative predictions of strength capacity at a high level of slenderness.

Therefore, the methods were modified by Silvestre et al. [94] for lipped channel column undergoing local-distortional interaction so as to be accurate and safe over the whole range of slenderness, and later it was further extended to validate over different geometry cross-sections including hat-section, Z-section, and Rack-section. The refined methods were shown to provide rather efficient (safe and accurate) and expected to be codified in the near future. Moreover, the distortional-global and local-distortional-global interaction had been also investigated and methods to predict ultimate strength capacity was proposed for lipped channel column with intermediate stiffeners [99]. Thus, they claimed that the modified methods provide more accurate prediction with experimental results compared to the current codified DSM.

### 2.3.2.6 The cold work effects in CFS structural members

The North America specification AISI-S100 Specification [3] for CFS structural members is also taken the increase in yield strength into account. The specification was originally allowed the use of cold work of forming based on full section tests in 1962. Later in 1968, the specification has permitted the utilization of the increased average yield strength of the section,  $f_{ya}$ , to be found by the full section tensile tests, stub column tests or calculated in accordance with the equation (2.18) which was originally developed by Karren [28]. However, the specification has limited the use of such increase only to relatively compact sections designed according to the specification including tension members, bending strength excluding the utilization of plastic reserve capacity, concentrically loaded compression members, combined axial load and bending, cold-formed steel lightweight construction and purlins/ grills.

$$f_{ya} = C f_{yc} + (1 - C) f_{yf} \quad (2.18)$$



Where

$f_{ya}$  : The average yield strength of the cross-section

$f_{yf}$  : The average yield strength of the flat areas

C: Ratio of corner area to total cross-section area

$f_{yc}$  : Average yield strength of corners =  $\frac{B_c F_{yv}}{\left(\frac{R}{t}\right)^m}$

$$m = 0.192 \frac{F_{uv}}{F_{yv}} - 0.068$$

$$B_c = 3.69 \frac{f_{uv}}{f_{yv}} - 0.819 \left( \frac{f_{uv}}{f_{yv}} \right)^2 - 1.79$$

$f_{yv}$  : Yield strength of virgin material

$f_{uv}$  : Ultimate strength of the virgin material

R: Inside bend radius

t: Plate thickness

It is noted that the use of strength increase from cold working was permitted to the Effective width method of the specification prior to 2016. The utilization of strength increase was revised and also permitted to be used for the DSM in 2016. However, according to the specification, the increase in yield strength is allowed only for these sections that are not subjected to strength reduction due to local buckling. The limitation requires the cross-section to be fully effective,  $\tau_l \leq 0.776$  when using the DSM. The adopted design procedure is described briefly here for both the European and the American design approaches.

## 2.4 Optimisation of CFS section

Optimisation of CFS section is a design process of selecting alternative forms to obtain its maximum strength while maintaining the same weight, leading to the most economical and efficient cross-section. Amongst steel structures, cold rolled steel ones can effectively gain this requirement as they are thin-walled structures that offer the high ratio of strength over weight. However, the design is very challenging as these members are prone to buckling and failure at low loads. There have been different solutions to increase the strength of cold-formed sections including buckling and ultimate strengths. This could be done through applying the mechanical work (or cold work) to enhance the material strength by imparting a dimpled surface deformation to the whole steel strip prior to the forming process [100]. However, the most popular development has been the inclusion of additional bends in the cross-section such as intermediate stiffeners [101-105]. These stiffeners subdivide the plate elements into smaller sub-elements and hence can considerably increase the local buckling of cold-formed sections subjected to compressive stresses due to the smaller width-to-thickness ratio of the sub-elements.

Many researchers have previously carried out the optimisation of predefined orthodox CFS cross-sections including channel, zed and sigma sections so as to optimise the relative dimensions of the sections. A neural network methodology for the optimal cross-sectional design of CFS steel beam members was developed for the hat- and I-sections [106]. Other studies [107, 108] also optimised the geometry of CFS channel beams subjected to uniformly distributed load and columns under a compressive axial load using Micro Genetic Algorithms, respectively. Various load levels were considered in the studies to obtain an optimum design curve from numerical results. A theoretical study on the optimisation of lipped channel beams under uniformly distributed transverse load was presented to maintain the local, distortional, and global buckling strength as well as yielding, in combination with allowable deflection limits while minimising the coil width [109]. The shape optimisation of CFS channel beams with closed drop flange and open flange was also described in [110]. They observed that the closed drop flanges can provide better structural performance compared to standard lips or open drop flanges. However, the efficiency of the optimised sections may not provide significant improvements of the ultimate strength of the members due to the fact that CFS sections are highly susceptible to local, distortional, global, and the interaction between these buckling modes. Several

investigations have been conducted which aimed at enhancing the buckling load by including ribs and stiffeners to the web and flanges of the predefined cross-sections [101-105].

The development of zed section with longitudinal stiffeners in the web, introduced during the cold roll forming using an analytical method [111] suggested that when the stiffeners were placed about one fifth of the web width from each flange, the problem of local buckling in the web was eliminated. The channel section with longitudinal stiffeners in the web was later developed in an attempt to incorporate the innovative web stiffener configuration used in the new zed, into a channel shape [112]. These new sections have a considerably improved bending strength to weight ratio considerably by using the web stiffener types. Additional stiffeners in channel and zed sections that have large width-to-thickness ratios were added to introduce a greater degree of work hardening, which raised the material yield strength in these regions, increased further advantage of eliminating the local and distortional buckling. In addition to bending strength, comprehensive experimental studies [113, 114] were conducted to provide test data on complex C-sections and stiffened web channels with various stiffener sizes subjected to pure bending, shear and combined bending and shear. The results of their studies showed that the longitudinal intermediate stiffeners in the web could considerably improve the bending and the shear strength of the channel sections. Recent investigations by Nguyen et al. [115, 116] using Finite Element analysis and optimisation techniques have proved that when the two symmetrical stiffeners on the web were placed as much closely as possible to each flange, maximum buckling and ultimate strengths for the section were achieved. The effects of both edge and intermediate stiffeners in the compression and tension flange of the cold-formed steel zed sections were investigated [117]. They found out that the flexural strength capacity increased when the intermediate stiffeners moved towards the web and flange junction.

A study using Particle Swarm Optimisation method to enhance the maximum bending capacity of different cross-sectional prototypes was also carried out [118]. It was observed that using two stiffeners in a symmetrical arrangement reduced the strength capacity of the section compared to other optimised sections. Mojtabaei et al. [119] developed an optimum CFS beam using Big Bang-Big Crunch optimisation. The study concluded that using intermediate stiffeners at web did not increase the bending strength capacity and stiffness of the section, which confirmed the study carried out by the previous study results [118]. Most recently, a new approach was developed by

Nguyen et al. [120] for optimal design of structural profiles by cold roll forming using a combined approach of Finite Element modelling and optimisation utilising Design Of Experiment method. In this approach, the dimensions of the product were defined as geometric parameters in the Finite Element modelling; in the design of experiments, these parameters were automatically assigned a range of values and a response surface model was used to determine parameter values that achieved the target optimised performance. This was used for the development of a channel section with longitudinal stiffeners in the web, considering the maximum buckling load as the target for the optimisation.

The majority of previous studies on the Optimisation of CFS sections have primarily been limited to using analytical formulas or the methods available in the Codes and Specifications such as AISI-S100 Specification [3], British Standard BS5950 [4], and Eurocode 3 (EC3) [5] (i.e. the Effective Width Method (EWM) and the Direct Strength Method (DSM)) to calculate the elastic buckling, compression and flexural strength of the structural members.

Analytical formulas were developed to calculate local and global buckling strengths of CFS cross-section beams such as mono-symmetrical open cross-sections and cosinusoidally corrugated flanges, I-sections with mono and anti-symmetrical I-shapes, and channel beams with closed hollow flanges [110, 121-123]. In these studies, the flexural strengths were Optimised in a process to achieve practical solutions in a design space constrained by geometric conditions. The results indicated that the global and local buckling strengths of the Optimised sections could be enhanced compared to the standard plain and lipped channel sections.

Previous researchers used the analytical equations only to maximize the second moment of area and minimize the cross-sectional area of CFS beams [124, 125] The results provided an optimal shape obtained from arbitrary selected cross-sections. Other researchers performed global Optimisation of CFS channel beams using the trust-region method and the results of Optimised sections were compared with those obtained from the application of BS5950 [4] and EC3 [5]. It was found that these two design guidelines provided almost the same Optimised section area. The EWM in AISI specification [3] was used to develop an optimal design of predefined orthodox CFS cross-sections including hat, I-, and Zed- beams [106], lipped channel beams

[108], hat-shape beams and channel columns with and without the edge stiffeners [107]. Thus, the study results proposed optimal design curves for various load levels.

The Effective width/Effective thickness methods available in EC3 were used to calculate local, distortional, and global buckling strengths of compression [126] and flexural [118, 127] structural members. The strength capacities of different cross-sectional prototypes were Optimised using Genetic Algorithms and Particle Swarm Optimisation. The researchers also evaluated the adequacy of EC3 in predicting the changes in strength capacity as a result of increasing/decreasing geometric parameters using detailed nonlinear FE modelling. While this led to some innovative new geometries, the only optimal design sections were verified by using FE models accounting for material and geometric nonlinearities and imperfections; hence casting some doubt on the Optimisation approaches.

The majority of these design methods available in the design guidelines [3-5] uses the Effective Width Method for strength determination. This method is feasible for rather conventional sections for which a distinction between web, flanges and lips can be made and which fall within the dimensional limits of the design standard. It becomes problematic, however, when the aim is to generate novel, previously undiscovered shapes in a free-shape optimisation, as the conventional standards are typically not applicable.

The Finite Strip Method (FSM) and the DSM were used as an alternative in some of the recent optimisation studies of CFS structural members [128-138]. The DSM only needs the elastic critical local, distortional, and global buckling stresses calculated in order to predict the strength capacity and can therefore, in principle, be applied to any shape. The elastic buckling stresses can thereby be obtained from a Finite Strip (FSM) analysis.

The method employed in the majority of these studies was solely restricted to columns with unconstrained (where the Optimisations are free to obtain any cross-sectional shapes results in impractical irregular or curved shapes which are expensive or impossible to manufacture) [128-132] and constrained (where the sections can be practicably manufactured and assembled onsite) [133-135]. Other very few limited Optimisation studies of CFS beam and beam-column have also been found [136-138] where the optimisation was carried out using the DSM. This method, however, does incur some shortcomings. The statistical correlation between a cross-sectional

slenderness parameter and the ultimate strength capacity was used to develop the DSM equations. This may exhibit a significant coefficient of variation and make the DSM predictions significantly cross-sectional dependent, resulted in providing more accurate prediction for certain cross-sections than for others. The DSM ignores distortional-global or local-distortional interactions [88]. This can be significantly problematic as reported Optimisation results may not be correctly predicted.

Only few Optimisation studies have been found [139, 140], focusing on maximizing energy dissipation in a cantilever beam under monotonic and cyclic loads, where the Optimisation was performed using the general purpose finite element program accounting for geometric and material non-linearity and initial imperfections (GMNIA). A Simulated Annealing algorithm was combined with detailed nonlinear FE models to obtain hot-rolled H-beams with optimal flange shapes that the energy dissipation capacity was significantly improved [139]. A Particle Swarm Optimisation (PSO) algorithm was combined with detailed FE models to perform size Optimisation of 15 CFS cross-sectional prototypes [140]. The Optimised cross-sectional shapes were dissipated up to 60% more energy compared to commercially available lipped channel. While these two studies could be considered as an essential step toward a robust and an efficient Optimisation procedure, some shortcomings were reported and could be observed from the studies. They were reported to be substantially computationally expensive, and they were performed on the high-performance computing system. The FE models were not validated against experimental testing before using them for the Optimisation studies. The later study [140] validated against four-point beam bending tests, whereas it was used for the Optimisation of a cantilever beam. While the later study [140] focused on CFS members, the effect of cold work in the corners and stiffeners' bends induced from the manufacturing process was ignored.

## **2.5 Knowledge gap**

Despite substantial findings were presented in the study of manufacturing effects (initial geometric imperfection and the cold work effect) and geometry effects (optimising the relative dimensions of the cross-section) on mechanical properties and behaviour of structural members,

some issues are still not fully understood and require further investigations. The following knowledge gaps are identified based on the literature reviews.

1. The majority of previous studies were for columns under compression or hat sections under bending and there have been limited investigations on channel and zed sections with web stiffeners subjected to bending stresses. Regarding previous numerical investigations, there has been a limited study on the stiffener's geometric effects including shape and position of the stiffeners to the section strength under bending. In these numerical studies, it was all assumed that the material properties at corner and bends of the intermediate stiffeners were the same with those at flat sections. On the other words, the effect of the cold work by the cold roll forming manufacturing process in enhancing the material properties at the stiffener's corners was not considered. This meant that there have been not available any optimal design studies that took into account the effect of both the stiffeners' geometry and the cold work effect on the strength of the section.
2. Prior studies were mainly focused on the optimisation of predefined orthodox CFS cross-sections including channel, zed and sigma sections so as to optimise the relative dimensions of the sections. The optimisation of unorthodox cross-sectional shapes (channel and zed sections contain complex folded-in stiffeners) is still rarely. The majority of the cross-sectional shape investigated previously rather conventional sections for which a distinction between web, flanges and lips can be made and which fall within the dimensional limits of the design standard. Other very few limited studies on optimisation were solely restricted to structural columns with unconstrained shapes, where the optimisations were free to obtain any cross-sectional shapes resulted in impractical irregular or curved shapes which were expensive or impossible to manufacture. Therefore, it was essential to optimise the unorthodox cross-sectional shapes so as to obtain innovative nonstandard sections and the sections could be practicably manufactured and assembled onsite.
3. Previous studies on the optimisation of CFS sections have primarily limited to use analytical formulas or the methods available in the Codes and Specifications such as AISI-S100 Specification [3], British Standard BS5950 [4], and Eurocode 3 (EC3) [5] (i.e. the Effective Width Method (EWM) and the Direct Strength Method (DSM)) to calculate the elastic

buckling, compression and flexural strength of the structural members. This is due to the fact that the prior studies mainly optimised the standard CFS cross-sections. However, the analytical formula is often unable to account for nonlinear behaviour of the structural members and the majority of these design methods available in the design guidelines [3-5] uses the traditional Effective Width Method for strength determination. This method is feasible for rather conventional sections, and it becomes problematic, when the aim is to generate novel, previously undiscovered shapes in a free-shape optimisation, as the conventional method is typically not applicable. The Finite Strip Method (FSM) and the DSM were used as an alternative in some of the recent optimisation studies of CFS structural members. This method, however, has some shortcomings. The statistical correlation between a cross-sectional slenderness parameter and the ultimate strength capacity was used to develop the DSM equations. This might exhibit a significant coefficient of variation and make the DSM predictions significantly cross-sectional dependent, resulted in providing more accurate prediction for certain cross-sections than for others. The DSM ignores distortional-global or local-distortional interactions [88]. This can be significantly problematic as reported optimisation results may not be correctly predicted.

4. Only few optimisation studies were available to use the general-purpose finite element program accounting for geometric and material non-linearity and initial geometric imperfections (GMNIA). While these studies could be considered as an essential step toward a robust and an efficient optimisation procedure, some shortcomings were reported and could be observed from the studies. They were reported to be substantially computationally expensive, and they were performed on the high-performance computing system. The FE models were not validated against experimental testing before using them for the optimisation studies and the effect of cold work in the corners and stiffeners' bends induced from the manufacturing process was ignored. Thus, a new practical optimisation approach developed using combined nonlinear Finite Element modelling and optimisations by combining Design of Experiment (DOE), Response Surface (RS) methodology and Multi-Objective Genetic Algorithm (MOGA). It considered the key geometric and material non-linearity, initial geometric imperfections, and the cold work effects (GMNIA).



5. Most of the previous experimental tests were focused on press-braked forming for structural steel sections and cold roll forming for structural stainless-steel sections. Although the effect of cold roll forming of the manufacturing process is more significant than press-braked forming on mechanical properties and structural behaviour of CFS structural members, only very few limited data were available to investigate the effects of cold roll forming for steel sections. In addition, there was a lack of experimental data for cold-formed newly channel and zed sections with folded in stiffeners. Thus, experimental tests were carried out to quantify the cold work from the manufacturing process of cold roll forming of new steel channel and zed sections, and the results were used to explore the influence of cold work effects on mechanical properties and flexural strength of the cold roll formed sections by experimental testing and detailed (FE) modelling.

The present study addressed the above-mentioned gaps by using experimental tests and combined nonlinear Finite Element analysis and Optimisations. The tensile tests were carried out in virgin material (pre-cold rolled), flat parts, corner and bend regions of the sections to quantify cold work from cold roll forming of the manufacturing process. The test results were employed in simulation of structural beam bending tests to obtain the load-carrying capacity of newly developed UltraBEAM<sup>TM2</sup> and UltraZED<sup>TM2</sup> sections and compared with the optimised sections achieved in this study. The experimental tests were further used for validation purpose.

## **2.6 Conclusions**

This chapter summarises the research area of the present study based on the literature reviews performed in this thesis, especially the methods that have been widely used to strength design and optimise cold roll formed steel structural members. None of the current design approaches available are ideal for the design and optimisation of cold roll formed steel channel and zed sections with complex intermediate stiffeners. Therefore, the present studies in this thesis will contribute towards development of an optimal strength design approach that takes into consideration key ‘geometry’ and ‘manufacturing process’ effects to the material and structural properties into the design of cold formed steel (CFS) structural members. The detailed numerical validation of cold roll formed steel structural members will be presented. A comprehensive parametric study will be carried out to investigate the influence of both the web and flange

intermediate stiffeners' positions, shapes, sizes, and enhanced material properties at corners and stiffeners' bends on the section's buckling and ultimate strengths of the new channel and zed sections. A new practical approach to optimise CFS channel and zed sections with longitudinal intermediate stiffeners in the flanges and web under bending while considering both the stiffeners' geometry and cold work influences on the buckling and ultimate bending strength of the sections will be provided. Experimental testing and Finite Element modelling approaches will be further proposed for validation purpose and to study the cold working effects on mechanical properties of the material and structural behaviour of the cold roll formed steel sections with complex longitudinally stiffeners under bending.

## **Chapter 3 Numerical validation of cold roll formed steel structural members**

### **3.1 Numerical Validation of cold formed steel beam member**

This section covers the validated numerical model using FE modelling that capable of simulating the buckling and ultimate bending strength of cold rolled steel beam sections. The FE models, which were developed in ANSYS (ANSYS, Inc.) [141] and verified against earlier experimental testing [142], were used to calculate buckling, developed stresses and ultimate bending strength to understand and achieve robust validated FE model.

*This work is based on the journal publication "Optimal design of cold roll formed steel channel sections under bending considering both geometry and cold work effects." Thin-Walled Structures 157 (2020):107020." by Qadir et al [149].*

### 3.1.1 Reference test programme

This section summarises the key information of the reference testing programme reported previously [142] and the data which was used to validate the FE simulations. The cold roll formed steel channel and zed beams, commonly used in industrial roof systems, were used in this study. The beam specimens were channel and zed sections which were the industrial UltraBEAM™2 and UltraZED™2 sections (Hadley Industries plc.), respectively; they were cold roll formed along the rolling direction on steel coils. Figure 3.1 shows the overall view of the test setup which replicated the configuration of a four-point bending test. Cleats were bolted to the web of the specimens at the loading points and the end supports which were fixed to the beam webs to avoid web crippling problems at these locations. Half round blocks were used to ensure that the load applied to cleats was a point load. A rotating end station was provided to model the pin end condition of the beams at the end supports. Small steel angles 45x45 mm were periodically attached to the top and bottom flanges of two specimens.

The tests were carried out using a calibrated 220-kN capacity load cell and an electric machine screw jack. Four electrical strain gauges were used (one in the top flange, two in the large part of the web, and one in the bottom flange) to measure the axial strains along with the web and flanges of the cross-section of the beam specimens. The vertical displacements from the top and bottom of the beam specimens were also determined using LVDTs or displacement transducers. A downward load was symmetrically applied via the load cell which moved vertically down at two support cleats at the position of one-third of the main span. The specimens were loaded using the electric screw jack and the displacement control used to reach the load cell actuator at a constant rate of 2.5 mm/min. The specimens were loaded to failure and the test stopped at a load about 90% of the ultimate load. The test data including load, displacement and strain gauge readings provided the user plots load-displacement curve was recorded by the DASyLab data acquisition software. Failure modes were also recorded by photos and deformations and

locations were measured. Four duplicated tests were performed for each section referenced to take into consideration the testing conditions and variation in samples. A total of 20 different sections of UltraBEAM™2 and UltraZED™2 sections were investigated. Each section with the same depth had three different thicknesses that ranged from 1.20 mm to 3.05 mm in order to cover a wide popular range of section slenderness used in building construction. Four duplicated tests were carried out for each section so there were 116 tests in total for both sections.

The tested UltraBEAM™2 and UltraZED™2 sections was used for validation and later referred as the reference section for the parametric study of the Finite Element models and the Direct Strength Method and optimisations. It had cross section and general dimensions as shown in Figure 3.2. The test configuration for these sections consisted of a pair of 2920 mm long channel or zed sections placing in parallel with a central span of 2691 mm. The four-point bending testing setup including the lateral braces was conducted approximately reflecting their configurations in real applications. The steel angles 45x45 mm were attached to the top and bottom flanges of two specimens symmetrical to the mid-span. The practical bracing length was about 900 mm as shown in the test setup in Figure 3.1. This length was also examined in the FE model and showed that in general it was sufficient to determine the minimum length required to generate distortional buckling results that were not boundary condition dependent. Hence, the FE model developed and validated against this four-point bending testing setup as presented in this chapter, was utilized for the parametric study and optimisation.



Figure 3.1. A typical four-point bending test setup with channel sections.

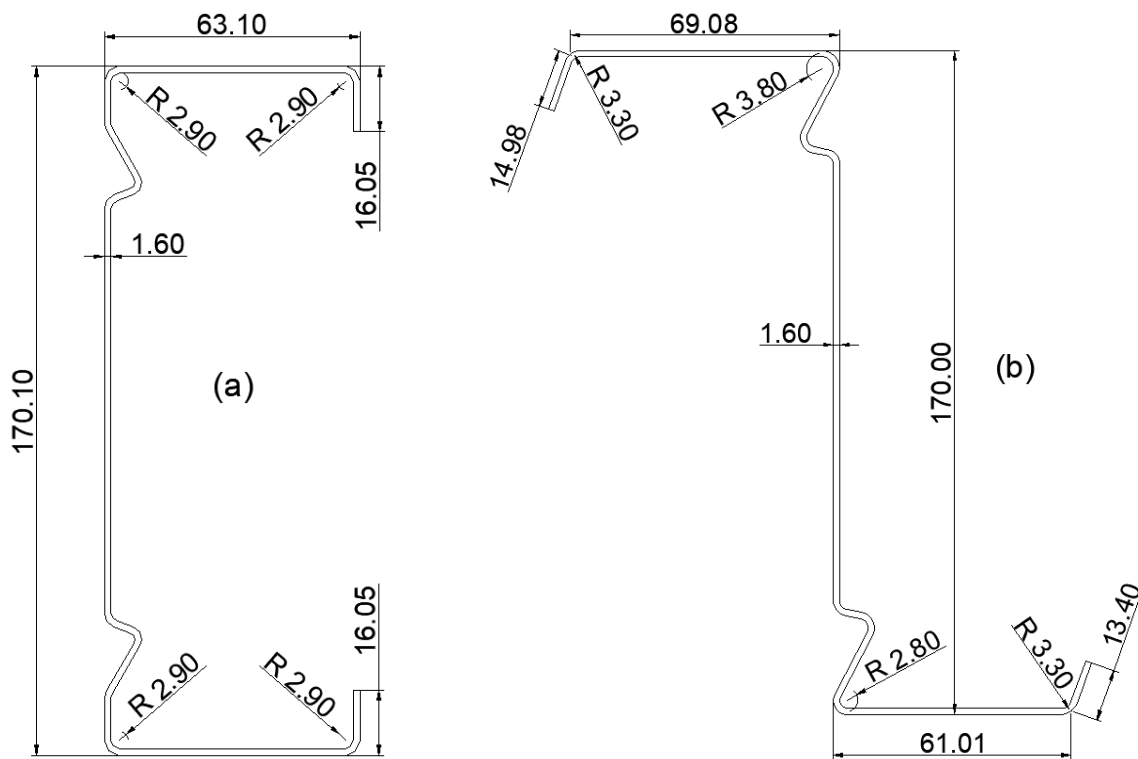


Figure 3.2. Cross section and dimensions (in mm) of the beam specimens used in experimental tests: (a) channel section, and (b) zed section.

### 3.1.2 Finite Element modelling

#### 3.1.2.1 General modelling setup

Finite Element (FE) model was conducted using ANSYS (ANSYS, Inc.) [141] to simulate the four-point bending test of the beams. In the simulation validation, the channel section had a total length of 2920 mm, a span of 2691 mm, a load centre of 897 mm, thickness of 1.60 mm, flange width of 63 mm, web width of 170 mm, and lip length of 16 mm. The zed section had a total length of 2920 mm, a span of 2691 mm, a load centre of 897 mm, thickness of 1.60 mm, top flange width of 69 mm and bottom flange width 61 mm, web width of 170 mm and lip length of 15 mm.

In the FE models, two different arrangements were considered for the purpose of validation: (1) a full model in which the two beam specimens were modelled similar to the actual setup in the experimental test, and (2) a half model in which only one beam specimen was modelled and appropriate boundary conditions were used to model the symmetry about the longitudinal axis of the full system. The full model had the same arrangement with the laboratory test setup. The two channel specimens (flanges faced inwards) were modelled with 180 mm distance between their webs. The 45x45 mm angle braces connecting the top and bottom flanges were modelled using shell element, which only provide lateral restraints. The results obtained from full models were compared to those of the half model with symmetry conditions for verification purpose (results not shown). It was found that the difference in maximum load capacity was very small, 0.07%, which could be negligible. However, the full model required considerable computational time (3 times in comparison to the half model). Therefore, the half model setup was used to conduct all numerical investigations in this study.

Figure 3.3 displays the overall arrangement for the half model with symmetry conditions. To model the lateral braces corresponding to the connection positions of the angle-to-beam screws in the actual test, tie nodes at the central of the connection were used to rigidly connected to three nodes from the compression / tension flanges and these tie nodes were restricted against the transverse direction. Similarly, sets of nodes at supports and loading points were tied together by reference points at the centre of the nodes using rigid connections to model the connections of cleats attached to the web of the section (by bolted connections). These reference points were

restricted against the transverse and vertical movement as well as out-of-plane movements including torsional rotations. The beams were also restricted against the longitudinal movement by adding additional longitudinal restraints at nodes in their tension flanges at the mid-span line. The vertical loads were applied at the reference points at one-third of the beams.

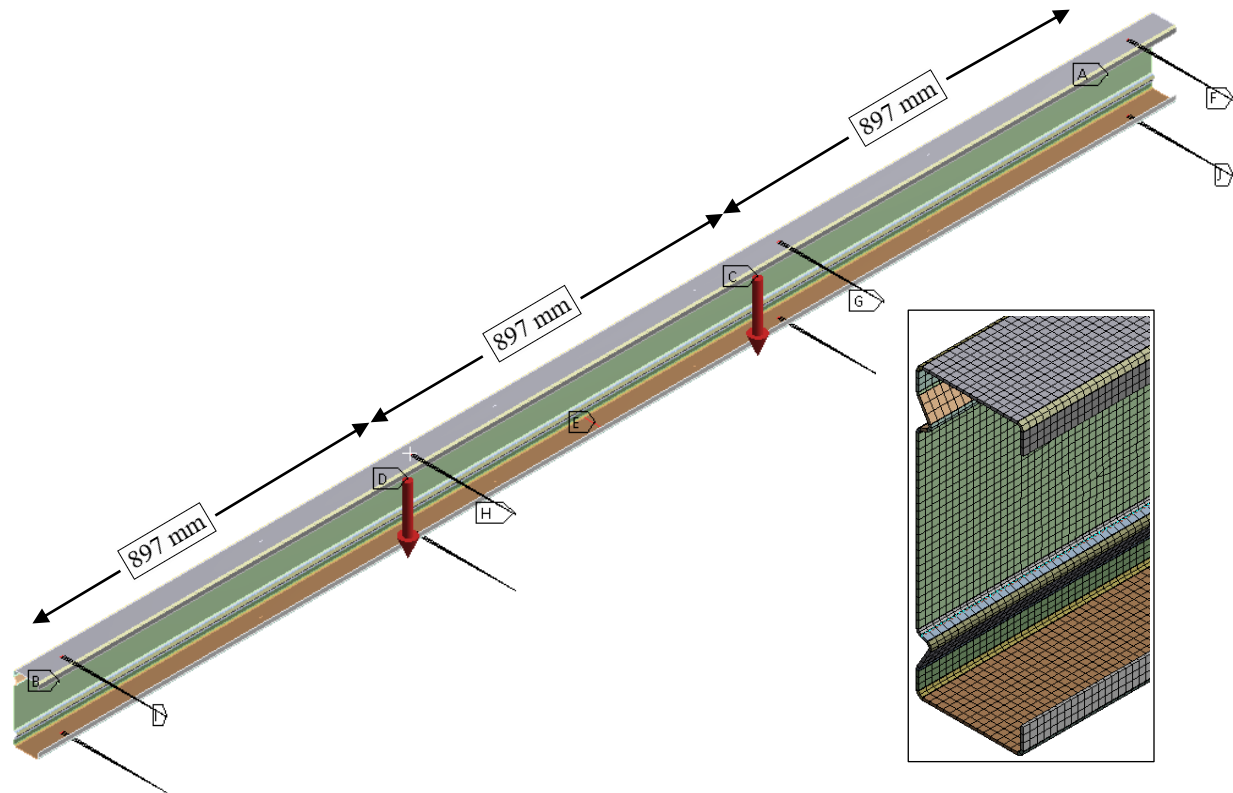


Figure 3.3. Finite Element symmetry model with boundary conditions and closer view of the mesh of the channel section (in the box).

Different methods and algorithms could be selected for the meshing purpose of the FE modelling. The methods included Tetrahedral meshing, Hex meshing and 2D meshing. For the Tetrahedral meshing, two algorithms were available such as Patch conforming, which could be used for clean CAD and accurate surface mesh, and Patch independent, which would be adopted for dirty geometry and defeatured surface mesh. For the Hex meshing, three methods were available including Sweep, Multizone and Hex dominant. The Hex meshing could reduce element count (run time) and reduce numerical error, but it required clean geometry and geometric decomposition. Sweep meshing involves a geometry discretization technique used for

specific sorts of geometries, such as thin geometries, geometries with bends, and models with little or no variation in a specific direction. Multizone meshing could provide automatic decomposition of geometry into mapped (structured/sweepable) regions and free (unstructured) regions. For the 2D meshing, three methods were also available including Quadrilateral mapped mesh, Traingles and Multizone Quad/Tri. A comprehensive literature review was carried out to select the most suitable method and algorithm in this research. It was found that the majority of the previous researchers in the field of cold formed steel structures have used shell elements in the Finite Element modelling [46, 48, 69, 71, 117, 143].

Therefore, the general-purpose 4-noded quadrilateral mapped mesh, shell elements with reduced integration namely SHELL181, were selected. The shell element SHELL181 was defined with two layers through the thickness of the section. Each layer had three integration points. There were 6 integration points through the thickness of the section. These elements had three translational and three rotational degrees of freedom at each node that take finite membrane and large rotations into account that are suitable for large-deformation and geometrically non-linear issues in this study.

Four different mesh sizes were used to study the influence of the mesh parameter on the accuracy of the simulation results. They included sizes of 20x20 mm, 8x8 mm, 4x4 mm, and 2x2 mm, these corresponded to a total number of elements of 5694, 21900, 70810 and 233600, respectively. The results showed that maximum difference between the ultimate loads of the 20x20 mm and the 2x2 mm was less than 5%, and when the mesh size was smaller than 4x4 mm the difference in slopes and ultimate loads was so small that could be neglected. The difference in ultimate load was less than 0.5% compared to the 2x2 mm mesh, whereas it was substantially more computationally efficient. Therefore, the 4x4 mm mesh was selected in this study as it could guarantee that the simulation results agreed well with the experimental ones as well as it was small enough to accurately model the corners and stiffener's bends of the section.

The measured material properties obtained in Nguyen et al. [142] were used for flat regions in the FE models. An elastic plastic material model was used as input material for steel for FE modelling. The material had Young's modulus (E) of 205 GPa and Poisson's ratio ( $\nu$ ) of 0.3. The FE model requires the input of the material stress-strain data in the form of the true stress  $\sigma_{\text{true}}$



and the plastic strain  $\varepsilon_{true}^{pl}$  obtained from the engineering stress-strain data ( $\sigma_{eng}$ ,  $\varepsilon_{eng}$ ) as follows:

$$\sigma_{true} = \sigma_{eng} (1 + \varepsilon_{eng}) \quad (3.1)$$

$$\varepsilon_{true}^{pl} = \ln(1 + \varepsilon_{eng}) - \frac{\sigma_{eng}}{E} \quad (3.2)$$

The engineering stress and strain data of the steel material from the flat parts of the channel section were obtained from the tensile tests and shown in Figure 3.4.

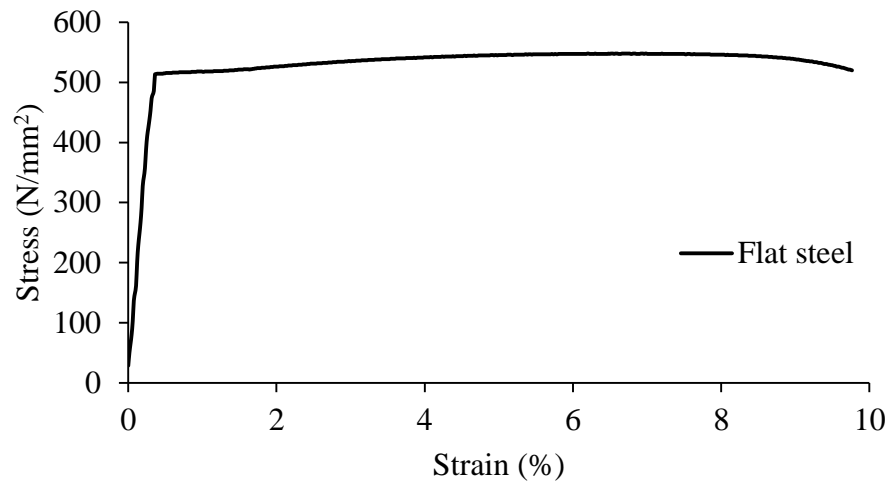


Figure 3.4. Engineering stress-strain data of the flat steel material of the channel section [142].

The material properties of steel material at the section bends (corners and intermediate stiffeners) had significantly higher yield stress and tensile strength than the flat parts of the section since the material in the bends was cold worked to a considerably higher degree than the material in the flat parts. In this study, the material properties of steel material at the section bends influenced by the cold work were obtained by using formulae from the North America specification [3] for cold formed structural members. The specification permits the utilization of the increased yield strength at corner and bend regions of the section,  $f_{yc}$ , which was originally developed by Karren [28]. In addition, for the plastic region of stress-strain curve, the equation developed by Hadarali and Nethercot [143] was used to model the slope of the inelastic region, which was  $E/50$ .

Geometric and material nonlinearity that occurred within the model were taken into account, thereby effectively modelling large strains and rotations. The displacement was increased in successive increments until the beams failed. In the nonlinear analysis, a full Newton-Raphson method was used for the iterative procedure and an implicit, static analysis was employed. The following values and criteria ranges were set for the force convergence (values = 2024 to 0.4272E+05 and criterion = 28.10 to 139.8), moment convergence (values = 0.9254 to 11.99 and criterion = 0.3074E-01 to 0.5385) and displacement convergence (values = 0.9592E-04 to 0.3157E-03 and criterion = 0.1265E-03 to 0.2688E-03). The line search was activated in order to select constant stabilization. The energy method was selected with energy dissipation ratio of  $1e^{-004}$  and stabilization force limit of 0.2. This allowed to accurately model the load displacement response.

### 3.1.2.2 Determination of buckling modes and geometric imperfections

Two different methods were used to model the first step, elastic buckling step, of the analysis in order to take the shape and distribution of initial imperfections for FE models of beam bending tests: (1) conducting elastic buckling analysis with the conventional Finite Element Model (FEM) via ANSYS, and (2) conducting elastic buckling analysis with Finite Strip Method (FSM) using CUFSM [144]. A linear elastic buckling analysis was carried out with FEM to obtain appropriate buckling modes (Eigenmodes) including distortional buckling modes for this study. These buckling modes were fed into the nonlinear analysis to include the shape and distribution of initial imperfections. Figure 3.5 shows the distortional buckling mode obtained from the elastic buckling analysis in FEM. This distortional buckling mode was the first mode with two half-waves along the constant moment span. The FEM first buckling mode was compared to experimental ones and the mode shape deemed to be similar to the mode observed in the tests. Therefore, the first buckling mode shape was selected to generate imperfections. The maximum amplitude of the buckling mode shape was generally used as a degree of initial imperfection. Using the first buckling mode shape derived from the elastic buckling analysis for the nonlinear analysis, together with appropriate initial geometric imperfections could result in an accurate failure mode and strength capacity for the FE model. There have been several methods proposed to determine appropriate magnitudes for initial geometric imperfections. Schafer and Peköz [46] suggested the cumulative distribution function (CDF) values for the maximum imperfections be

used for type 1 (local buckling  $d_1$ ) and type 2 (distortional buckling  $d_2$ ). Other researchers also defined the imperfection values in term of the plate thickness  $t$  [47]. Table 3.1 displays the initial geometric imperfection values considered in the FE models and the results were compared with the test result as shown in Figure 3.6.

**Table 3.1** Initial geometric imperfection values proposed by different studies.

Studies	Local buckling	Distortional buckling
Schafer and Peköz [46]	25% CDF magnitude = $d_1/t = 0.14$	25% CDF magnitude = $d_2/t = 0.64$
	50% CDF magnitude = $d_1/t = 0.34$	50% CDF magnitude = $d_2/t = 0.94$
	75% CDF magnitude = $d_1/t = 0.66$	75% CDF magnitude = $d_2/t = 1.55$
Chou et al. [47]	0.1t, 0.5t, and 1t	0.1t, 0.5t, and 1t

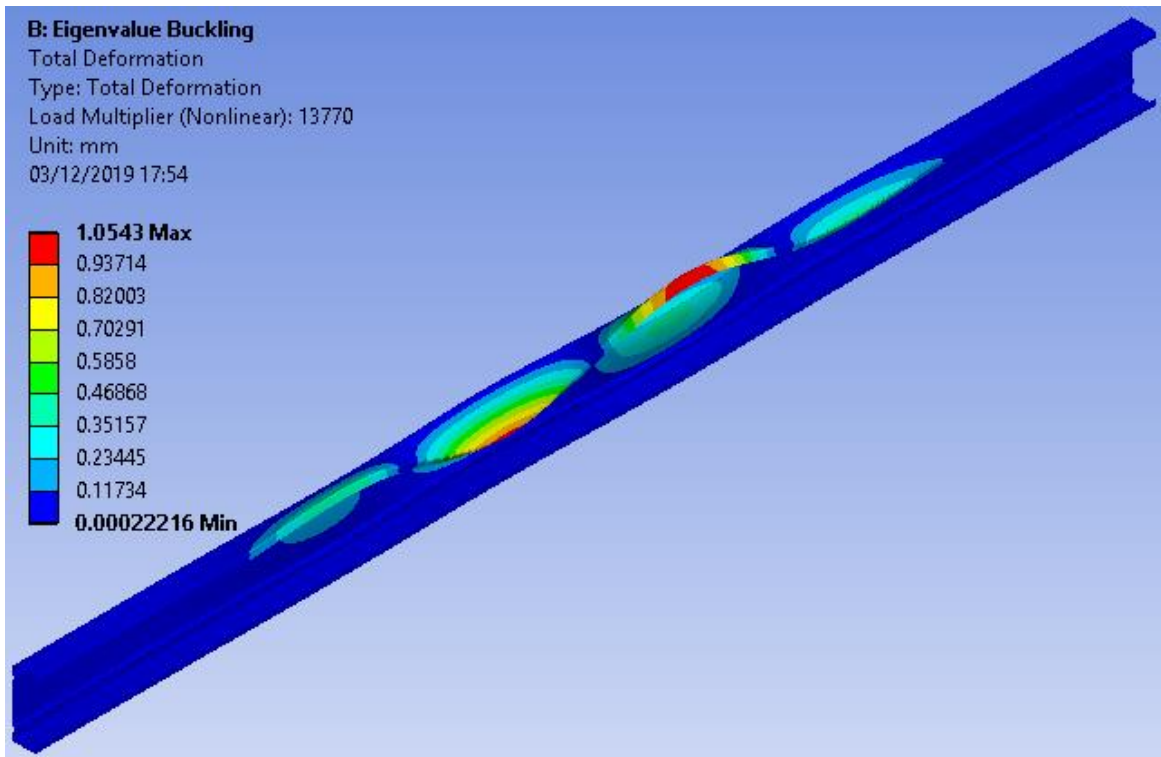


Figure 3.5. Distortional buckling mode obtained from the FE model for the channel section.

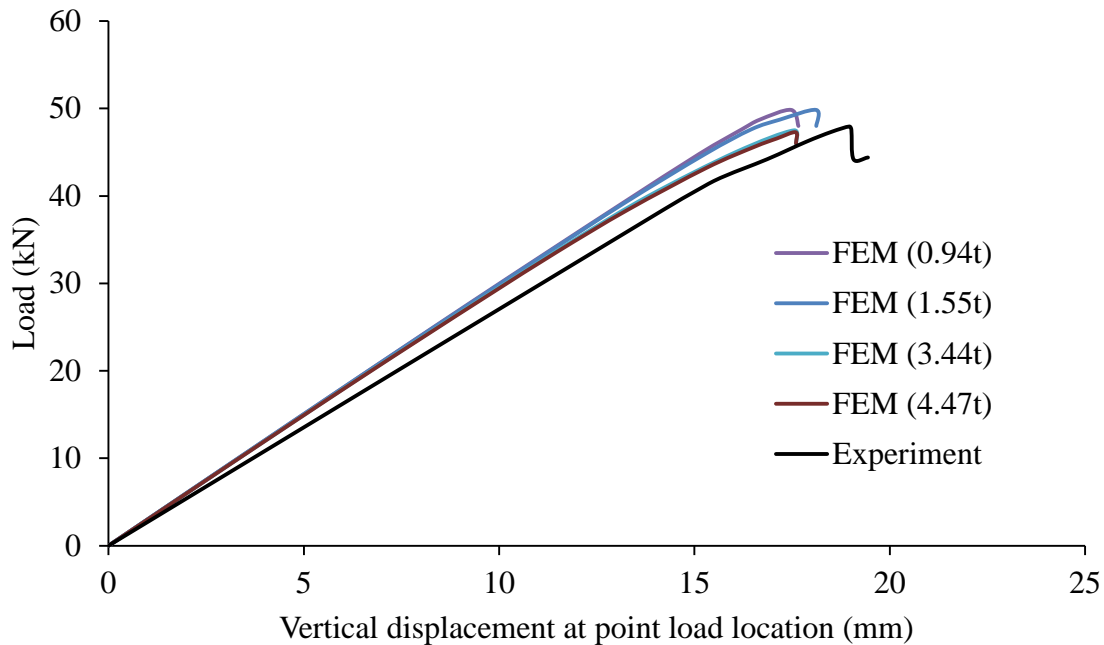
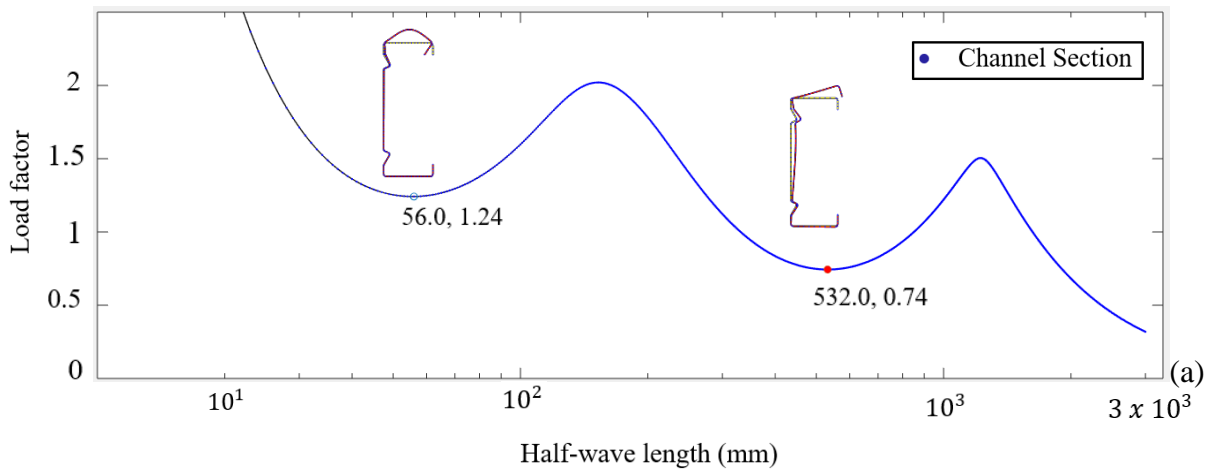


Figure 3.6. Load-displacement curves of different initial imperfections used in the FEM for the channel section.

The use of buckling modes from linear buckling analysis conducted with the conventional method, FEM, has some challenging issues. First of all, it was time consuming and computationally expensive to obtain the required pure buckling modes: local, distortional or global buckling modes as the derived buckling modes by FEM were often a combination of different buckling modes [143]. It was also very subjective as the controlling buckling mode needs to be selected by visual inspection; as the mode has to be identified through mode by mode visual inspection, it is difficult to select pure local, distortional and global buckling modes among many mixed buckling modes. Alternatively, the desired linear buckling mode obtained from FSM using CUFSM were then transferred to the FEM via the software ANSYS to conduct the nonlinear buckling analysis. This method has been already implemented by other researchers [143]. The entire elastic buckling modes of simply supported members were calculated using the Finite Strip software CUFSM, which used polynomial functions for the deformed shape in the transverse direction and a single half sine-wave for the longitudinal shape function. The same material properties, nodes, elements of the section were used in both CUFSM and ANSYS. The buckling curve obtained in CUFSM for the channel section is shown in Figure 3.7(a). The

minima of the buckling curve were representative of the critical half-wavelengths and load factors. The second minimum was associated with the distortional buckling mode and half-wave length for the channel section, as shown in Figure 3.7(b). The buckling mode shape was similar to that of FEM as obtained in Figure 3.5. It was for simplicity, therefore, decided that the linear elastic buckling analysis was used with CUFSM to generate the shape and then applied the distribution of initial imperfections. The results showed that the channel beams failed in distortional buckling modes so the use of local buckling and global buckling initial imperfections might not affect the results. Therefore, it deemed that it was reasonable to consider only distortional buckling initial imperfections for the sections used in this study. The magnitude of initial imperfections was applied fully to the whole section including the intermediate web and flange stiffeners as shown in Figure 3.7, using different CDF values proposed for imperfection amplitudes as shown in Table 1.



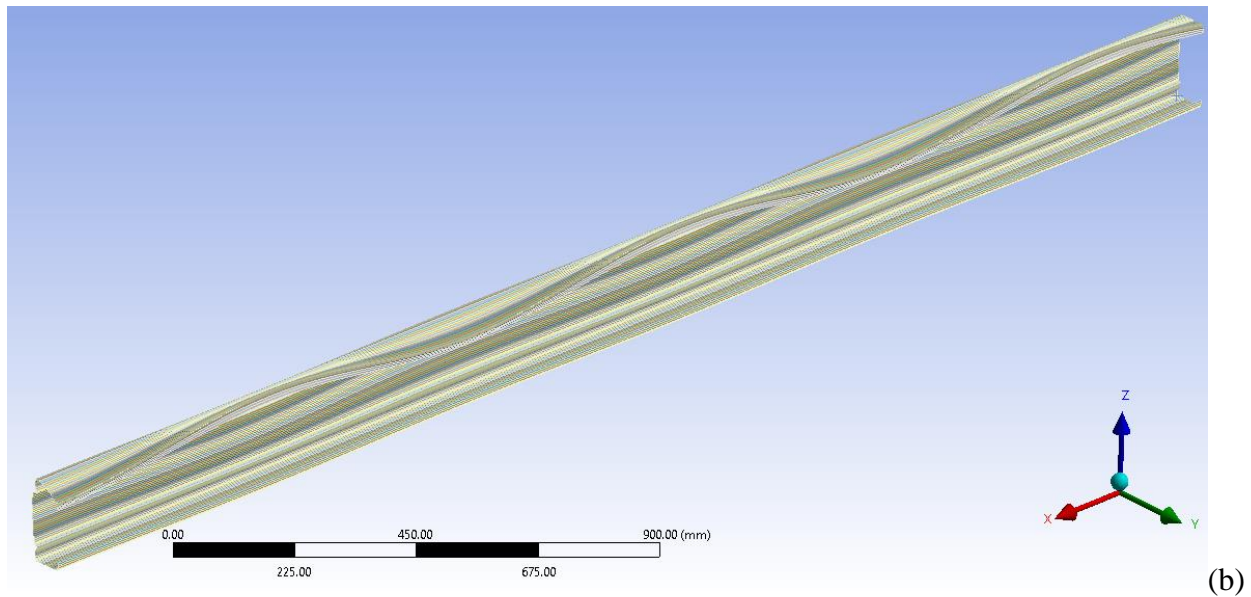


Figure 3.7. Distortional buckling curve and modes for the channel section obtained from (a) CUFSM and (b) Distortional buckling mode obtained from the FE model after importing the buckling modes from CUFSM.

Figure 3.8 shows the load-displacement curves of the channel sections obtained by this method with different imperfection amplitudes; it also includes the experimental result for comparison. The slope of the load-displacement curve and ultimate strength of the channel beams were found to be quite sensitive to the magnitude of initial imperfections; this reflected through significant differences between the slopes and ultimate loads of the FE model for different cases: with zero imperfection (amplitude of 0.0t) and with significant imperfections (amplitudes in the range of 0.64t to 4.47t). Overall, the ultimate load obtained from the FE model with zero imperfection 0.00t was 5% greater than the experimental result while those with 4.47t imperfection was 8% smaller than the experimental one. Other FE simulations with two different imperfections in between these extreme values, one with 0.64t and one with 1.55t imperfection amplitudes to cover the middle of 0.94t, were also studied. It was observed that the FE results with the imperfection value of 1.55t were the closest in agreement with the experimental results with less than 1% difference in the slope and strength values. The 75% CDF amplitude corresponded to an initial imperfection amplitude of 1.55t was, therefore, adopted for the parametric study and optimisation in this research.

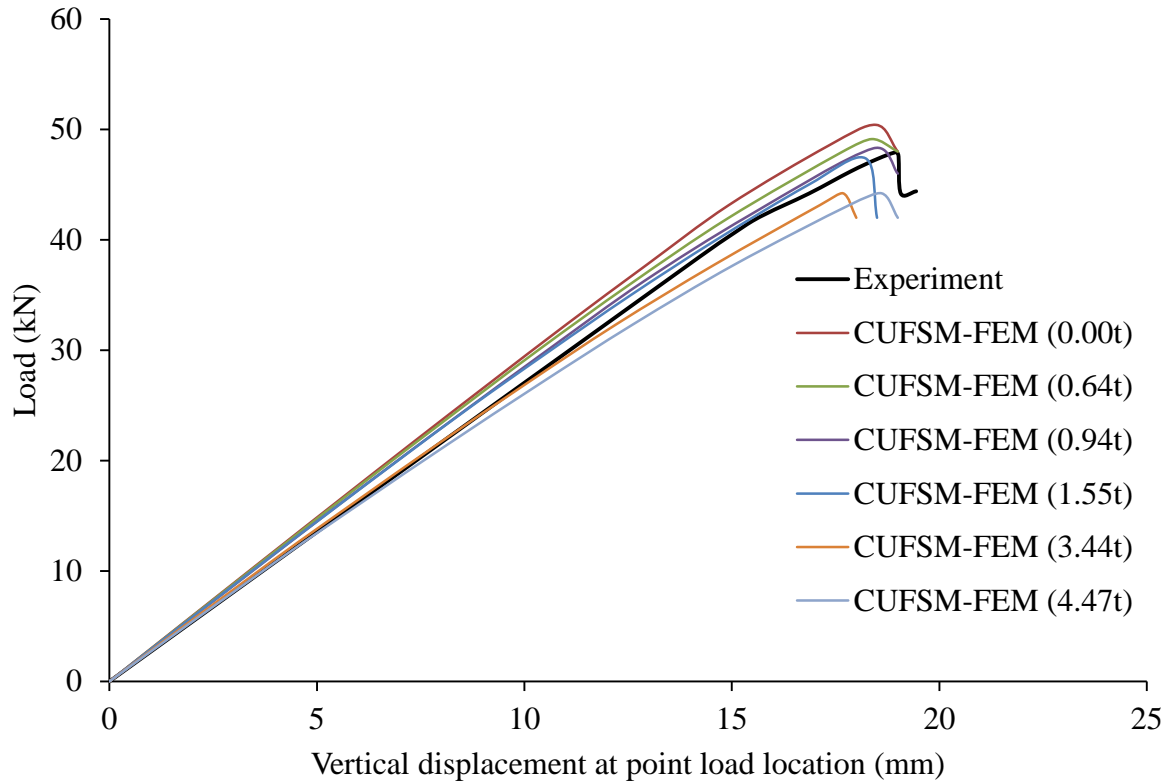


Figure 3.8. Load-displacement curves of different initial imperfections used in the CUFSM-FEM for the channel section.

### 3.1.2.3 Determination of cold work effect to the material properties at corners and stiffeners

The cold rolling process of the channel sections resulted in an enhancement of the yield strength and ultimate tensile strength in the corners and in the bends of the stiffeners in comparison to those in the flat regions of the section. While the material properties of flat regions were obtained from tensile tests [142], the material properties of corners and bends were not available from the tests for this section. However, the current study focused upon the effect of geometric shape and cold work by the cold roll forming manufacturing process on the buckling and ultimate strengths of channel sections to search for the optimal design shapes. Previous studies by Mojtabaei et al. [119] and Ye et al. [56] indicated that the measured imperfections and enhanced material properties of the corners obtained from coupon tests did not considerably affect the optimum

shape of the sections. Therefore, in the current study, other widely accepted methods were used to estimate the geometric imperfections and the enhanced material properties of the corners and stiffeners' bends, without loss of generality. In particular, the material properties at corners and stiffener's bends affected by the cold work could be obtained from the material properties of flat regions by using formulae from the North American specification [3] for Cold-formed steel structural members. The equation for determining the tensile yield strength,  $f_{yc}$ , of the corner was based on the Equation (3.3) which was empirically derived from tests by Karren [28].

$$F_{yc} = \frac{B_c F_{yv}}{\left(\frac{R}{t}\right)^m} \quad (3.3)$$

In which

$$m = 0.192 \frac{F_{uv}}{F_{yv}} - 0.068 \text{ and } B_c = 3.69 \frac{F_{uv}}{F_{yv}} - 0.819 \left(\frac{F_{uv}}{F_{yv}}\right)^2 - 1.79$$

Where:  $F_{yv}$  and  $F_{uv}$  are yield stress and ultimate strength of the flat region material, R is inside corner/bend radius and t is the plate thickness. For cold roll formed sections, modest levels of strength enhancement of around 2.5% over the virgin coil material were observed in samples taken from web and flange elements [67]. These were consistent with other studies [145, 146] despite that these were developed for stainless steel. Therefore, the changes of the mechanical properties of the material in the flat parts of the cold roll formed sections were considered to be negligible in this study. In addition, Bonada et al. [54] compared the yield strength increase for corner material predicted from different methods namely EC3 and Karren' theoretical model (used in the North American specification [3]) and found out that the Karren' theoretical model provides the best agreement with the experimental results. Therefore, this model is adopted in the current study (Equation (3.3)) to investigate the effect of geometric shape and cold work by the cold roll forming manufacturing process on the buckling and ultimate strengths of channel sections and search for the optimal design shapes.

The flat region material of the channel section had a Young's modulus (E) of 205 Gpa, Poison's ratio ( $\nu$ ) of 0.3 and yield stress and ultimate strength of  $519.4 \text{ N/mm}^2$  and  $550.0 \text{ N/mm}^2$ , respectively. The channel section was defined with 12 corners and bends, as shown in Figure 3.9, but only material properties at six corners and bends in the upper part of the section were



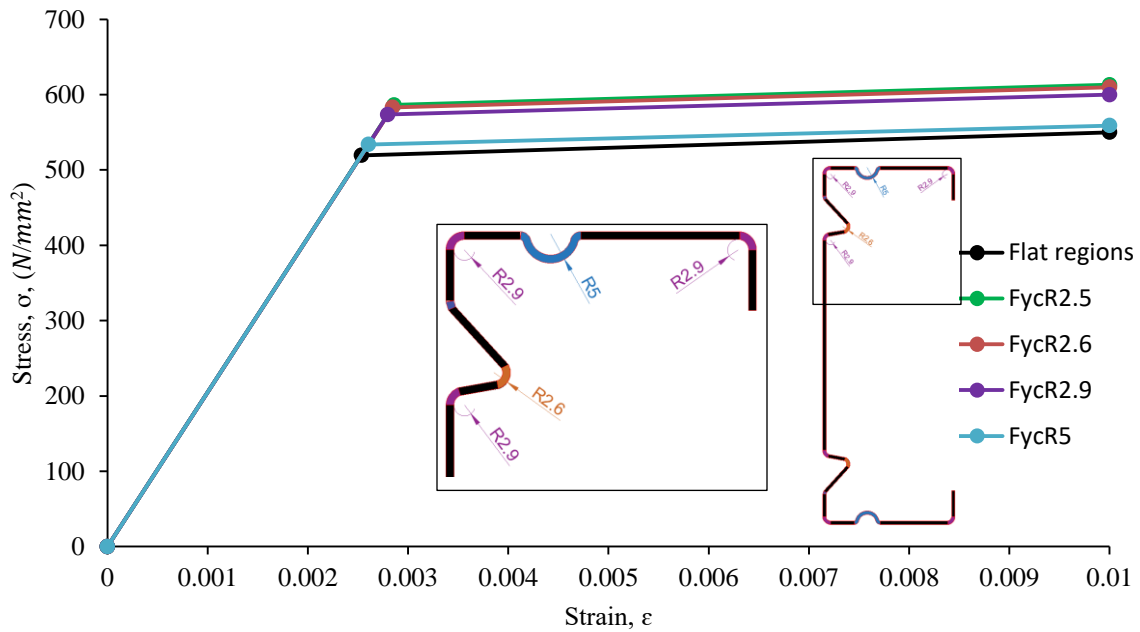
considered as the others in the lower part were assumed to be the same due to symmetry. Six increased yield stresses were calculated as the sections had a different radius at corners and bends and results were shown in Table 3.2, which also shows the calculated  $m, B_c, F_{yv}$  and various corners radius yield strength  $F_{ycR}$ .

**Table 3.2** Yield stresses and tensile strengths at corners and stiffener's bends using the North American specification [3].

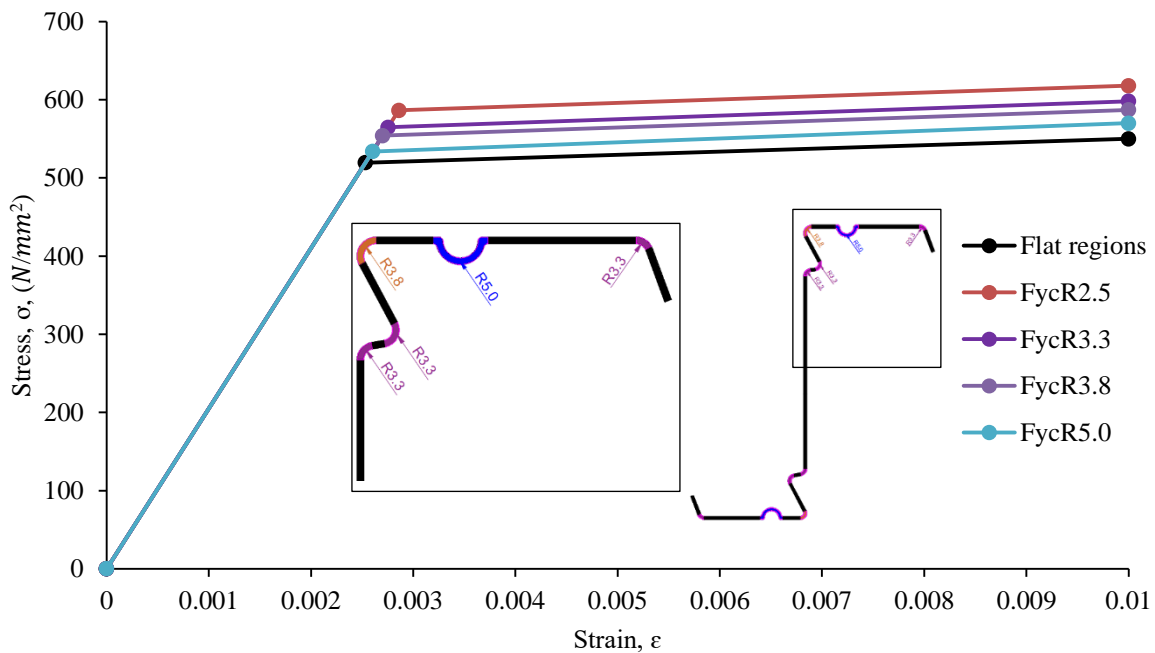
$m$	$B_c$	$F_{yv}$ ( $N/mm^2$ )	$F_{ycR}$ ( $N/mm^2$ )	$F_{ycR}$ ( $N/mm^2$ )	$F_{ycR}$ ( $N/mm^2$ )	$F_{ycR}$ ( $N/mm^2$ )	$F_{ycR}$ ( $N/mm^2$ )
			$R = 2.5$ mm	$R = 2.6$ mm	$R = 2.9$ mm	$R = 5$ mm	$R = 7.5$ mm
0.14	1.20	519.4	586.29	583.19	573.57	533.8	519.40

The constitutive stress-strain model proposed by Hadarali and Nethercot [143] was employed, in which the plastic region of the stress-strain curve was modelled with a straight line with a constant slope of  $E/50$ , where  $E$  is the elastic modulus obtained from material tests. Therefore, different stress-strain models of corners and stiffeners' bends were used for the cross-section in the FE simulations, as illustrated in Figure 3.9. FE simulations were carried out with stress-strain data obtained from the tensile test [142] and with the proposed stress-strain models and the results revealed that the maximum differences in the slope and ultimate load capacity was very small 0.8% and 0.0%, respectively, indicating the validation of the proposed stress-strain model. Therefore, the stress-strain model proposed in Figure 3.9 was used in this study for the parametric study.

Residual stresses could be indirectly considered in the FE models through the stress-strain data obtained from the material tests. In particular, the membrane residual stresses could be safely ignored in the open sections [30, 46], whereas the longitudinal flexural residual stresses reported being implicitly presented in the stress-strain behaviour of the coupon tensile test results as long as the coupons were cut from the final sections. Cutting a coupon might release the flexural residual stresses that caused the coupon to curl [38], whilst these stresses were re-introduced when the coupon is straightened during the initial stages of tensile loading. Thus, the effects of residual stresses were not separately implemented into the FE models but assumed to be included with the stress-strain data.



(a)



(b)

Figure 3.9. Stress-strain models for materials at different corners and stiffeners' bends used in FEM of (a) the channel section and (b) the zed section.



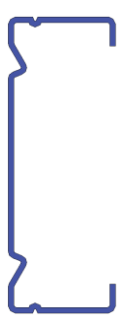
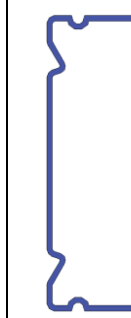
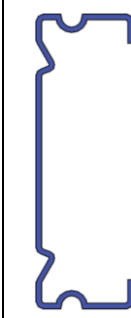
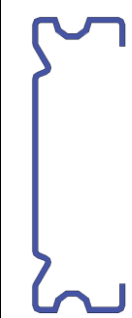


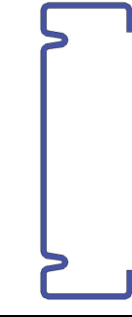
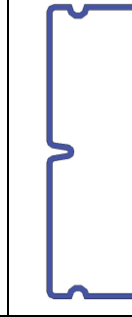
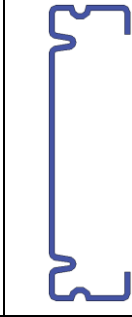
It should be noted that the term “cold-working” in this study is used to represent the effect of the cold roll forming manufacturing process in enhancing the material properties at the section


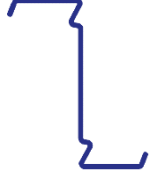
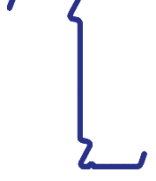
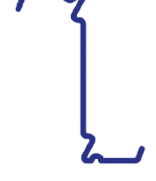
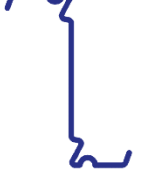


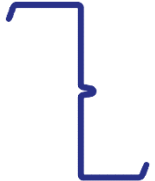
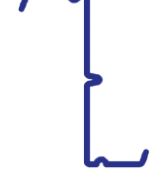
corners and the stiffeners' bends [147, 148]. Therefore, from now on in this study, it is called as “the cold work effect” in short.

### 3.1.3 Direct Strength Method

The Direct Strength Method specified in the North American Specification [3] was used in this study to determine the bending moment capacities of the channel sections. In this method, elastic buckling loads could be identified from a numerical analysis. In this study, the Finite Strip software CUFSM was used to identify the elastic buckling values for the channel and zed sections. They were performed for systematically increasing half-wavelengths to obtain the shapes and load factors for the buckling modes of the sections. The ultimate strength capacity was calculated based on the section yield stress and elastic critical buckling stresses (local, distortional and global buckling stresses). The effect of cold work to material properties of the channel section was also calculated to be used in the DSM following the North American Specification, which approximated the yield strength of the whole sections using the weighted average as shown in Table 3.3:

**Table 3.3** The average yield stresses of different cross sections obtained using the North American Specification.

Cross-Sections						
$f_{ya} (N/mm^2)$	522.74	526.40	529.37	527.76	527.08	526.40
Cross-Sections						

$f_{ya} (N/mm^2)$	524.09	525.30	527.85	526.65	529.21	
Cross-Sections						
$f_{ya} (N/mm^2)$	521.36	525.05	528.19	526.40	525.05	524.40
Cross-Sections						
$f_{ya} (N/mm^2)$	522.56	524.44	524.71			

These yield stress values obtained from Table 3.3 were used in the Direct Strength Method for the calculation of ultimate moment capacity of the sections to include the effect of cold work from cold roll forming of the manufacturing process on material properties of the sections.

In this study, the influence of the cold work on material properties to the section strength was considered with the Direct Strength Method. Therefore, the yield stress of the virgin material ( $f_y$ ) was replaced by a new yield stress enhanced by the cold work. This yield stress could be reasonably approximated as the average yield stress of the whole cross section  $f_{ya}$ , as shown in Table 3.3.

### 3.1.4 FE and DSM result validation

The four-point bending simulation showed that the channel sections had distortional buckling mode. However, for this particular setup the test did not clearly show elastic buckling prior to failure, but around the failure point. It was noted that the buckling load obtained from the FE analysis was even greater than the ultimate load. The main reason for this could be the fact that the tested channels deformed in plastic region while the FE buckling loads were evaluated by

means of linear elastic analysis. Figure 3.10 shows the load-displacement curves for both experimental test and FE model of the channel section. It can be seen that the slope (stiffness) and ultimate strength of the sections obtained by the FE model agreed very well with those of the experimental test. Overall, the FE model showed a slightly higher stiffness in comparison to the experimental one before peak load. The maximum load carrying capacity and the maximum displacement of the beam at peak load of the section, however, displayed slightly lower strength and displacement compared with the experimental one. The maximum difference in the peak load was 1% conservative while in the displacement was 4% unconservative. It was found that cold work influence on stiffness and strength of the channel beam was insignificant due to the fact that the distortional buckling slenderness in the section was very high and the beam failed by distortional buckling stress before it reached its yield strength capacity. If the failure stresses reached the yield and ultimate strength region then the cold work would be significant.

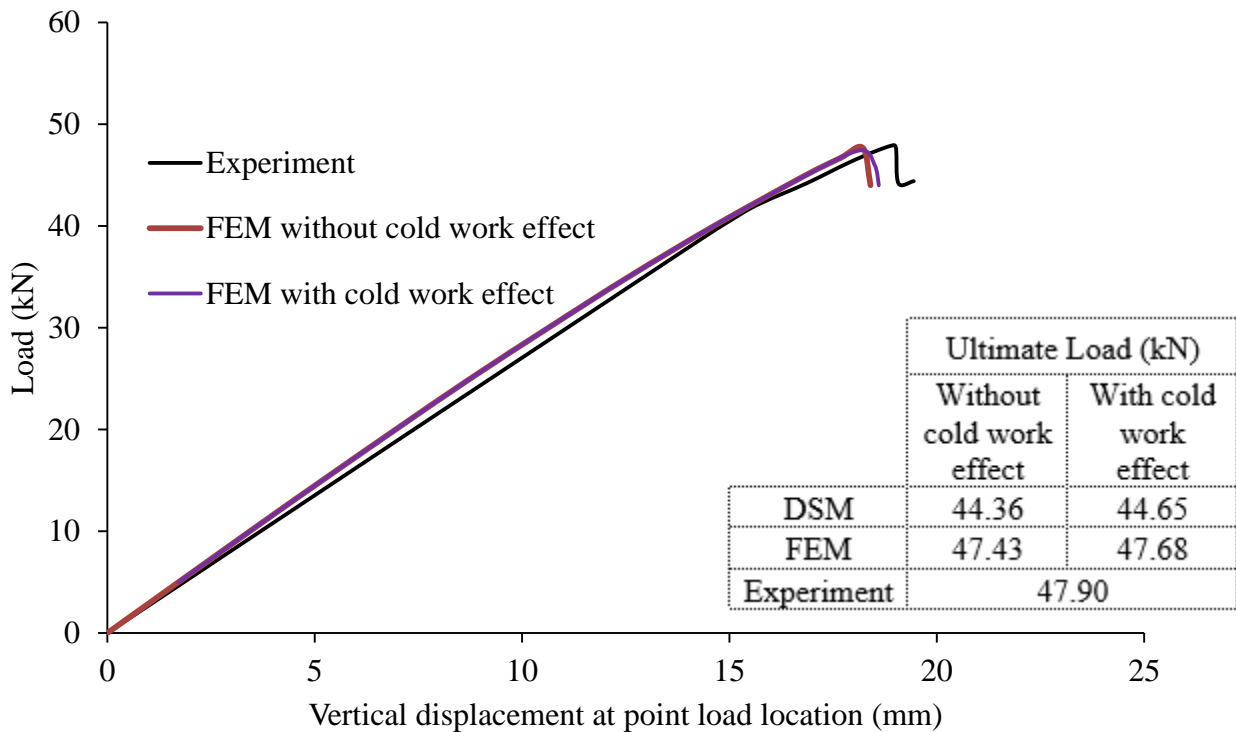


Figure 3.10. Load-displacement curves for the channel sections from FEM, DSM and experimental results.

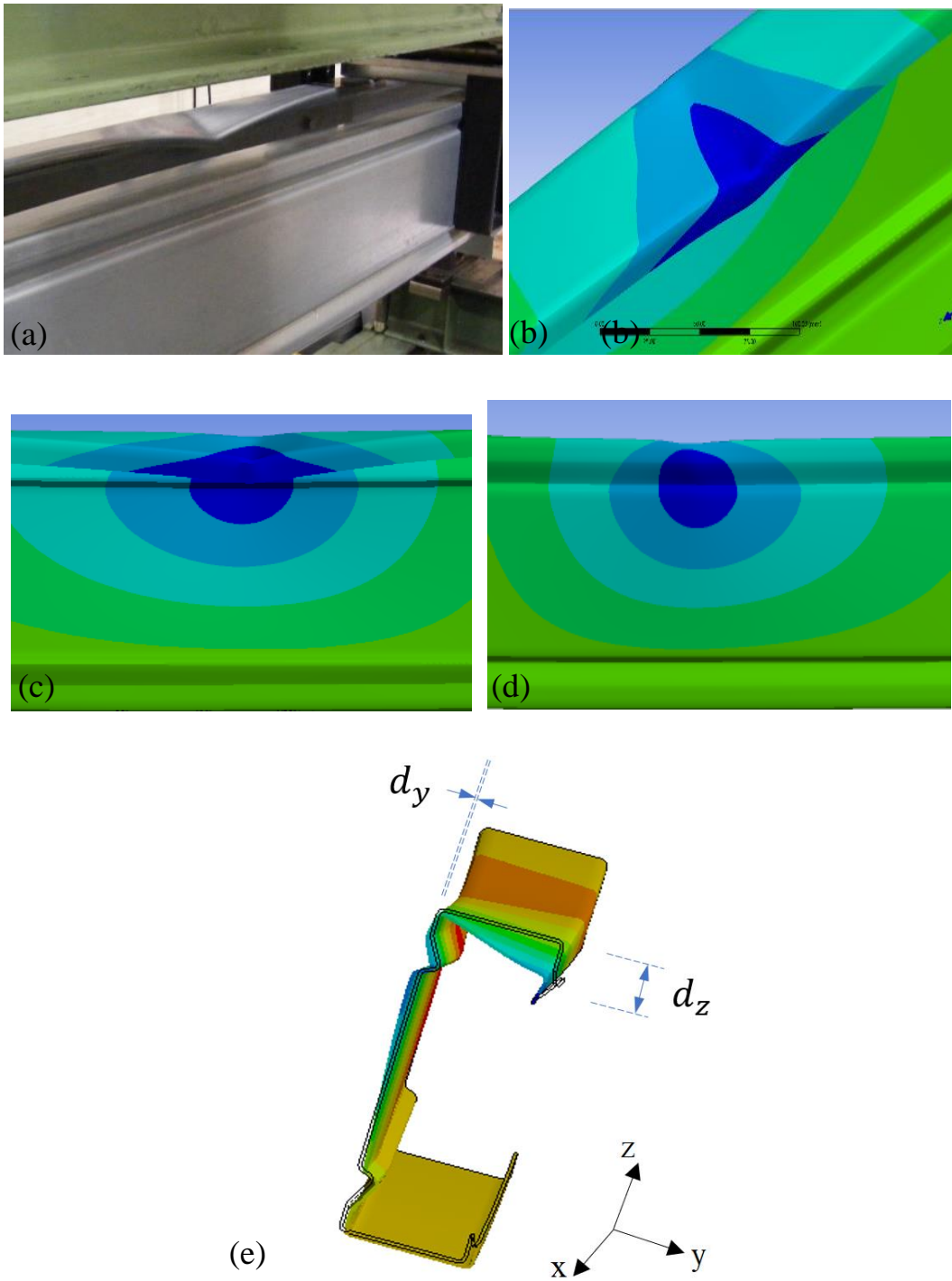


Figure 3.11. Deformed shapes at failure for the channel sections obtained by experimental tests (a), and FE modelling results isometric view (b), front view (c), back view (c), and un-deformed and deformed cross sections (e). Deformation values associated with colour contour ranged from green to blue with highest values in blue region.

It was observed that the zed beams failed with full strength capacity of the sections. The load-displacement curves of the zed sections under the four-point bending tests obtained by FE simulation and experiment are shown in Figure 3.12. It can be seen that both the stiffness and strength of the sections obtained by the FE model were in excellent agreement with experimental results, especially for the FE results when the cold work effect was included. The maximum difference in the peak load was 2% conservative whilst in the stiffness was 2% unconservative. However, the maximum difference in the peak load was 5% when the cold work effect was not taken into account in the FE model. As the sections gained their full strength, the generated stresses were in the inelastic region, the cold work effect was significant for the zed sections.

Figure 3.11 and Figure 3.13 illustrate the experimental and FE failure shapes of the channel and zed sections, respectively, for comparison. It was observed that the distortional buckling mode shape of the failed specimens was well represented by the FE models. In particular, the horizontal movement of the compressed web-flange corner  $d_y$  and the inward compressed flange-lip motion  $d_z$  in post buckling state of the channel cross section were 0 mm and 11 mm at failure, respectively; this clearly indicated the distortional buckling mode of failure of the section. The contours represented the displacement occurred in the beam and noted that the dark blue colour represented the maximum displacement, whereas as the colour became lighter the displacement became smaller values.

It was concluded that the developed FE model was an efficient way of representing the experimental tests and the FE results were in an excellent agreement with the experimental results in achieving accurate load-displacement curves and deformed shapes as well.

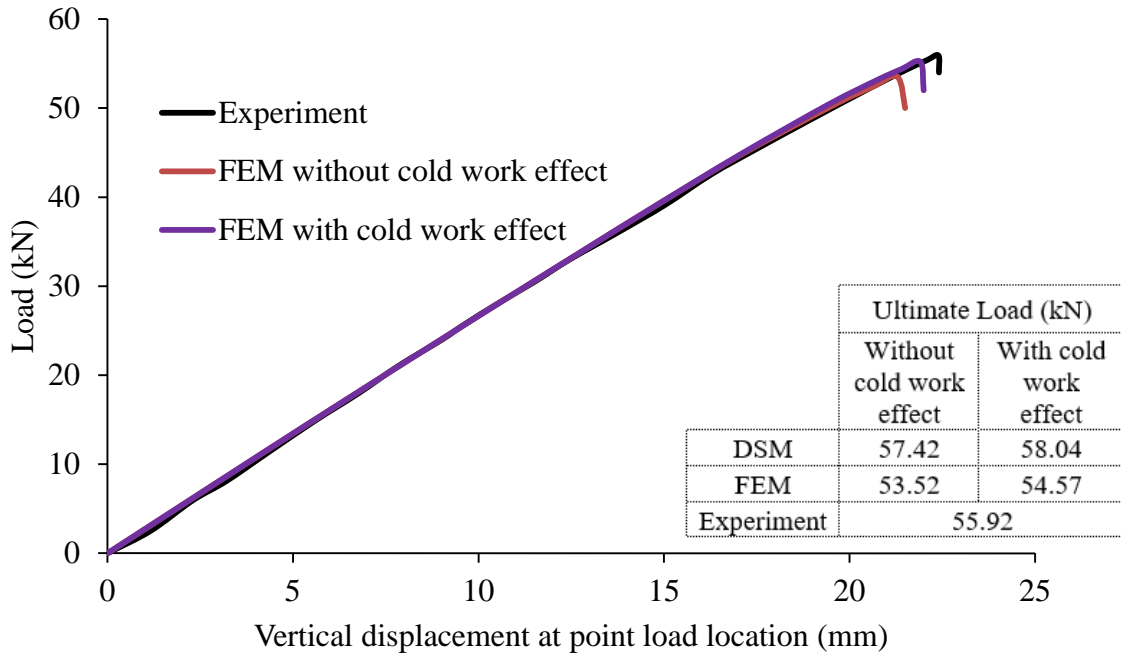


Figure 3.12. Load-displacement curves for the zed sections from FEM, DSM and experimental.

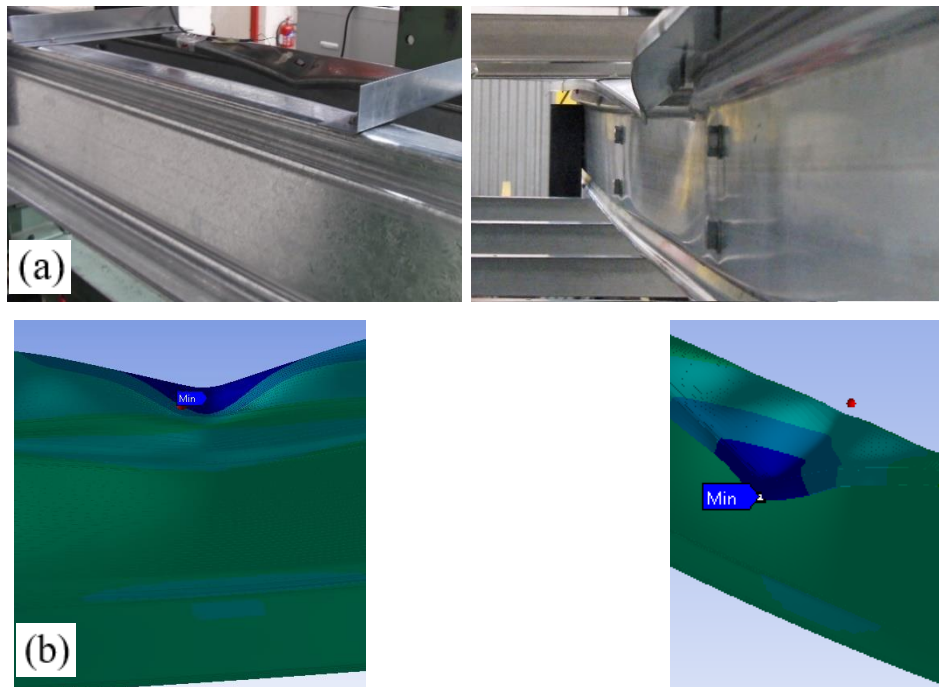


Figure 3.13. Deformed shapes at failure for the zed sections obtained by (a) experimental tests, and (b) FE modelling results. Deformation values associated with colour contour ranged from green to blue with highest values in blue region.



### 3.1.5 Conclusions

Numerical simulations using Finite Element (FE) analysis and design calculations using the Direct Strength Method (DSM) were developed to replicate four-point bending tests of the channel and zed sections. Two different arrangements were considered for the purpose of validation in the FE models: (1) a full model in which the two beam specimens were modelled similar to the actual setup in the experimental test, and (2) a half model in which only one beam specimen was modelled and appropriate boundary conditions were used to model the symmetry about the longitudinal axis of the full system. The results obtained from full models were compared to those of the half model with symmetry conditions for verification purpose and found that the difference in maximum load capacity was very small, 0.07%, which could be negligible. Therefore, the half model setup was used to conduct all numerical investigations in this study.

Two different methods were used to model the elastic buckling analysis in order to take the shape and distribution of initial imperfections for FE models of beam bending tests: (1) conducting elastic buckling analysis with the conventional Finite Element Model (FEM) via ANSYS, and (2) conducting elastic buckling analysis with Finite Strip Method (FSM) using CUFSM. The FEM first buckling mode is often the smallest buckling mode and could be selected for nonlinear buckling analysis. Therefore, the first buckling mode shape was selected to generate imperfections. In the second method, the first linear buckling mode obtained from FSM using CUFSM were then transferred to the FEM via the software ANSYS to conduct the nonlinear buckling analysis. Schafer and Peköz suggested the cumulative distribution function (CDF) values for the maximum imperfections be used for type 1 (local buckling  $d_1$ ) and type 2 (distortional buckling  $d_2$ ). It was observed that the FE results with the imperfection value of 1.55t were the closest in agreement with the experimental results with less than 1% difference in the slope and strength values. The 75% CDF amplitude corresponded to an initial imperfection amplitude of 1.55t was, therefore, adopted for the parametric study and optimisation in this research.

The material properties of flat regions were obtained from previous experimental tensile tests and the material properties at corners and stiffener's bends affected by the cold work were obtained from the material properties of flat regions by using formulae from the North American

specification for Cold-formed steel structural members. The constitutive stress-strain model proposed by Hadarali and Nethercot was employed, in which the plastic region of the stress-strain curve was modelled with a straight line with a constant slope of  $E/50$ , where  $E$  is the elastic modulus obtained from material tests. Therefore, different stress-strain models of corners and stiffeners' bends were used for the channel and zed sections in the FE simulations.

It was concluded that the FE results of four-points bending tests of the channel and zed sections were in excellent agreement with the experimental and DSM results, indicating that the buckling and nonlinear buckling behaviour of cold roll formed sections, considering the imperfections and the cold work effect, was accurately represented by the FE models.

## **3.2 Numerical validation of cold-roll formed steel column member**

### **3.2.1 Introduction**

In this section, the axial compression tests carried out by Nguyen et al. [67] were used as a basis for developing finite element analysis allowing for capturing local buckling as well as inclusion of geometrical and material nonlinearities. The FE models developed in Section 3.1.2 were used including the analysis type and solution control, element type and mesh, initial geometric imperfection and the cold work effect, whereas the material properties used obtained from Nguyen et al. [67]. The primary aim of this exercise was to further validate the FE models developed in Section 3.1.2.

### **3.2.2 Experimental investigation**

The numerical investigation conducted in this section to study the axial compression behaviour of cold roll-formed channel sections was based on the pure axial compression tests performed by Nguyen et al. [67]. The physical tests were carried out using a calibrated 200-kN capacity rig for column compression tests. The channel column specimens were designed to have a length of 500 mm, web width of 101.06 mm, flange width of 50.8 mm, corner radius of 1.30 mm and thickness of 0.90 mm. Other column specimens had dimensions and material properties as presented in Nguyen et al. [67]. Figure 3.14 (b) shows the basic arrangement of axial compression physical tests and the overall view of the test setup. The bottom support was fixed while the top support was movable to allow tests to be carried out for different lengths of the specimen. Two steel

endplates were used to compress the column specimen and each of them was bolted to a rigid flat bearing plate of the rig crosshead and the rigid bottom support. The top and bottom high-density polyethylene discs were circular; cut with the specimen's cross-sectional profile to support the specimen around its perimeter preventing the movement of the column ends hence, maintaining fixed-end conditions. The column ends passed through the discs and contacted the steel endplates.

The vertical load was applied through the electric screw jack. Seven simultaneously sampling input channels were used to set the data acquisition system. Three channels were attached to strain gage so as to record the strain gage outputs, one channel was attached to the test machine to measure loads and three channels were also attached to the LVDTs to measure displacements during each test. LVDTs or displacement transducers (LD620 model,  $\pm 5$  mm LVDT with 5 Vdc output) were used for determining the axial shortening and out-of-plane displacements of the specimens. The out-of-plane displacements were utilized to determine the critical buckling load. Three LVDTs were mounted at the specimen mid-height, outside the specimen section, at the centers of the web and two flanges. The arrangement of strain gauges and LVDTs is shown in Figure 3.14 (a) and 3.14 (b).

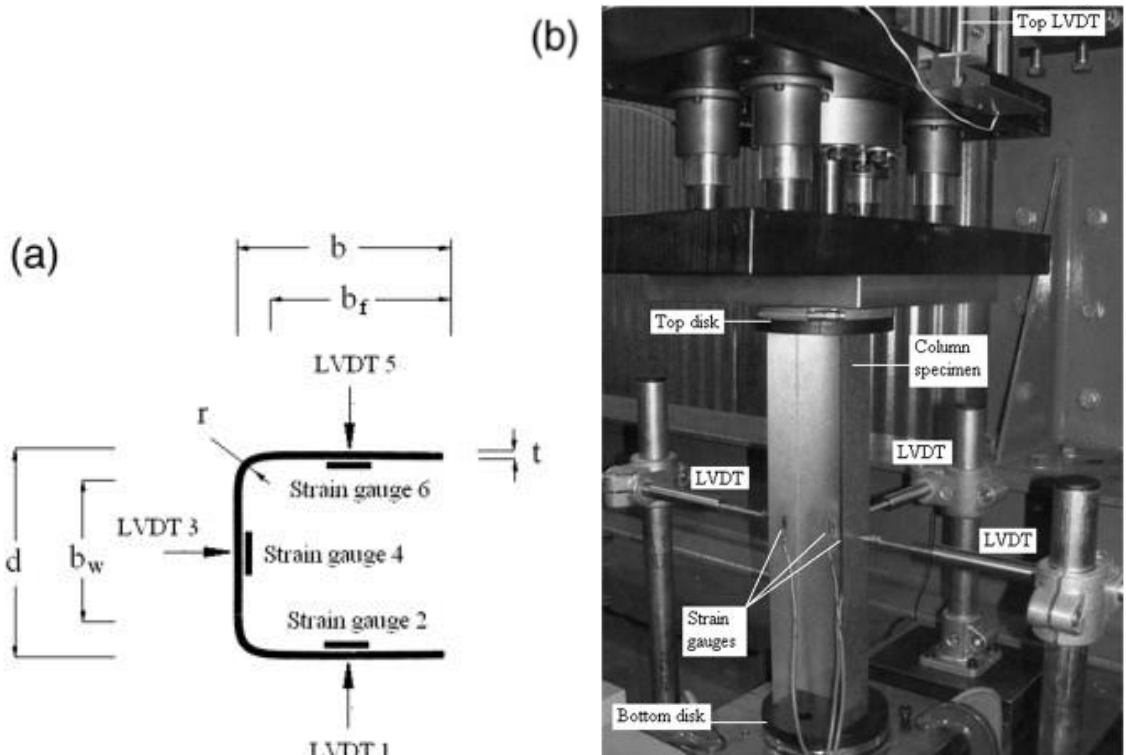


Figure 3.14 (a) Cross-sections and geometries of column specimens and (b) overall view of testing setup Nguyen et al. [67]

### 3.2.3 Development of FE models

The general-purpose finite element (FE) package ANSYS [141] was used to generate the numerical models which allow for both geometrical and material nonlinearities to be included. The local buckling, pure axial column compression, physical tests carried out by Nguyen et al. [67] was used to validate the numerical models.

### 3.2.4 Column member FE model's arrangement

The laboratory specimens were tested between fixed ends. The bottom support was fixed whilst the top support was movable to allow tests to be conducted for various lengths of the specimen. Two steel endplates were employed to compress the column specimen; each was bolted to a rigid flat bearing plate of the rig crosshead and the rigid bottom support. The top and bottom high-density polyethylene discs were circular; cut with the specimen's cross-sectional profile to support the specimen around its perimeter preventing the movement of the column ends hence, maintaining fixed-end conditions. The column ends with a depth of 30 mm passed through the discs and contacted the steel endplates.

To model the experimental program test specimens, two reference points were therefore established at the ends (at top and bottom) of FE models in order to apply boundary conditions of the experimental program as shown in Figure 3.14. The set of nodes at the ends of the model were linked to the related reference point using a rigid connection as indicated in Figure 3.15. The bottom reference point was restrained in all degree of freedoms, whereas the top reference point was allowed to move vertically (in the loading direction). The axial load was then applied through experimental displacements in the axial direction on the top reference node of the specimen.

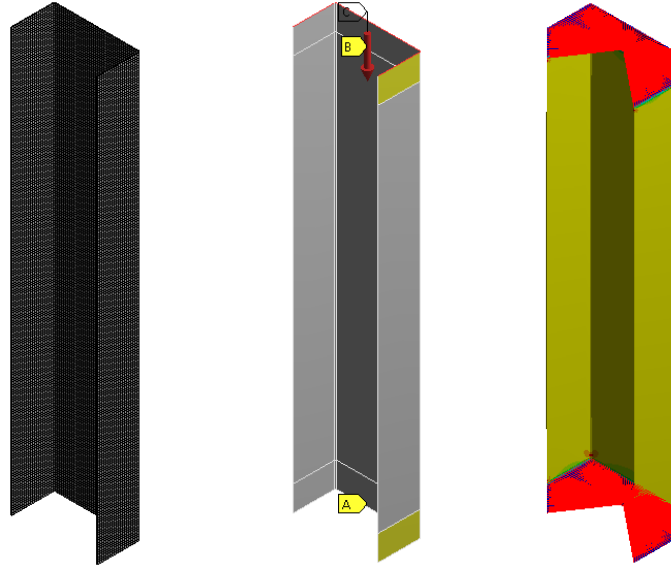


Figure 3.15 FE models arrangement

### 3.2.5 Material model

The measured material properties obtained in Nguyen et al. [67] were used for flat regions in the FE models. Both linear and nonlinear material properties (elastic and plastic material model) were employed as input in the FE model. The material had Young's modulus ( $E$ ) of 205 GPa and poisson's ratio of 0.3. FE models require the input of the material stress-strain data in the form of the true stress  $\sigma_{true}$  and the logarithmic plastic strain  $\epsilon_{ln}^{pl}$  obtained from the engineering stress-strain ( $\sigma_{eng.}$ ,  $\epsilon_{eng.}$ ) as follows:

$$\sigma_{true} = \sigma_{eng.} (1 + \epsilon_{eng.}) \quad (3-4)$$

$$\epsilon_{true} = \ln(1 + \epsilon_{eng.}) - \frac{\sigma_{true}}{E} \quad (3-5)$$

The engineering stress and strain data of sheet material was obtained from the tensile tests and shown in Figure 3.16.

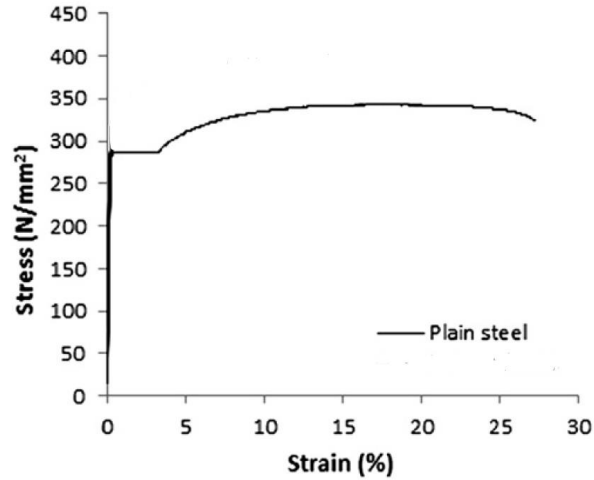


Figure 3.16: Engineering stress-strain curves of the plain sheet steel materials [67].

### 3.2.6 FE model result validation

Figure 3.17 shows the load-displacement curves for both experimental test and FE model of the channel section with the cold work effect and without the cold work effect consideration. It was observed that the effect of cold work was very small due to the small region of the bends in the section. It was seen that the slope (stiffness) and ultimate compression strength of the structural columns obtained by the FE model agreed very well with those of the experimental test.

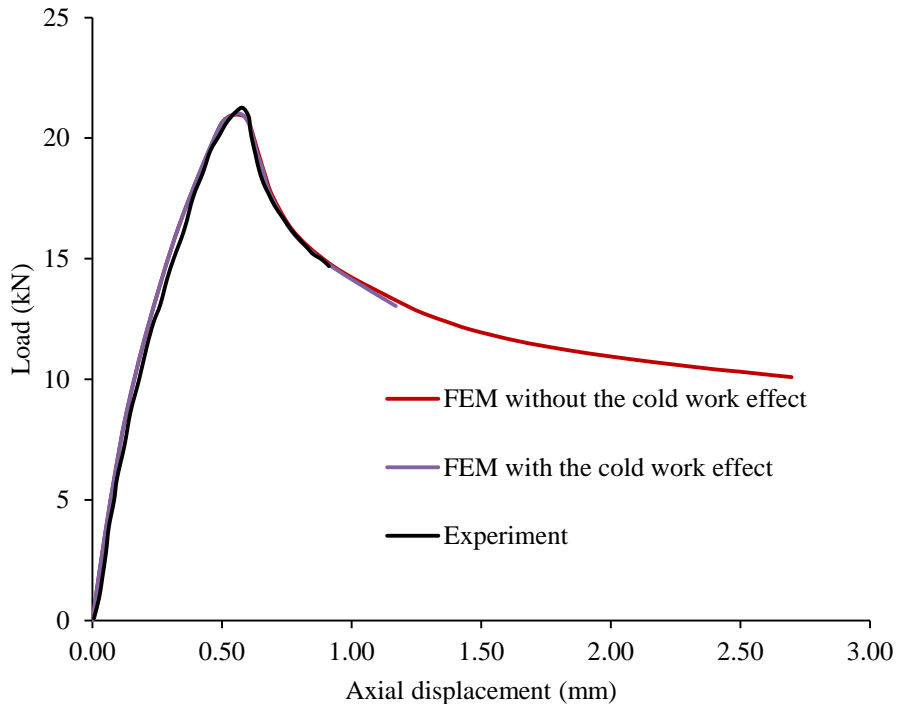


Figure 3.17 load-displacement curves of the FE models with and without cold-work compared with experiment

The column channel section tested by Nguyen et al. [67] was reported to have failed by local buckling. Figure 3.18 shows the typical buckling and failure modes of the column channel section. Both buckling and failure modes of FE models provided an excellent prediction of the experimental test.

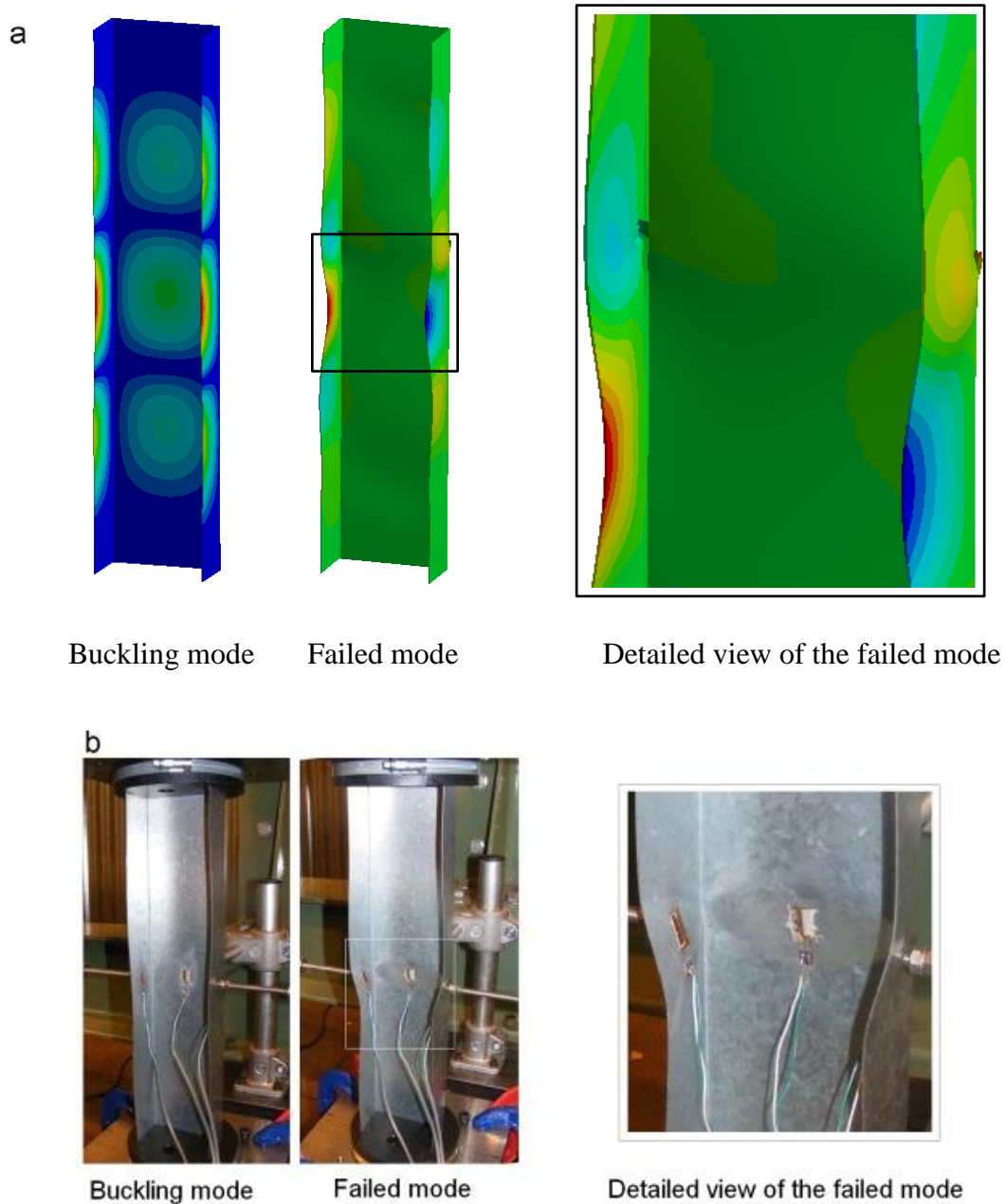


Figure 3.18: Buckling and failed mode shapes of the channel column (a) FE results and (b) experimental results.

### 3.2.7 Conclusions

The FE models were used to develop axial compression of channel columns, capable of producing solutions for non-linear problems, taking all geometrical and material nonlinearities into account. The FE models were verified against an axial compression column physical test conducted by Nguyen et al. [67]. The entire test was simulated including loadings, boundary conditions, material properties, and appropriate imperfection amplitude.

The geometric imperfections were incorporated in the FE model as a distortional mode scaled to an appropriate imperfection magnitude. The FE model was used to conduct a linear buckling analysis (an Eigenvalue analysis) to obtain the shape of initial imperfections along the cross-section as well as the length of the column. The first buckling mode was selected to feed into the nonlinear buckling analysis. It was found that the ultimate strength of FE models was particularly sensitive to the amplitude of initial imperfections. Hence, different initial geometric imperfection amplitudes were tested ranging from 0.1t up to 4.77t. It was found that the 1.55t provided accurate results compared to physical test results in term of strength and stiffness.

The equations proposed by Karin [28] included in the North American Specification used to calculate strength enhancement induced due to the cold work effect in the section corners, based on the flat tensile coupon tests performed by Nguyen et al. [67]. The cold work was found to have little effect on the axial compression resistance of cold-formed steel channel section since the corner regions were very small in the section and the section was very slender (the buckling slenderness was very high).

It was concluded that the FE models produced an excellent prediction of stiffness, ultimate strength capacities and failure modes of physical test.



## **Chapter 4 Parametric study of CFS longitudinally stiffened channel sections under bending**

*This work is based on the journal publication "Optimal design of cold roll formed steel channel sections under bending considering both geometry and cold work effects." Thin-Walled Structures 157 (2020):107020." by Qadir et al [149].*

### **4.1 Introduction**

This chapter presents a comprehensive parametric study carried out to investigate the influence of both the web and flange stiffeners' positions, shapes, sizes, and enhanced material properties at corners and stiffeners' bends on the section's buckling and ultimate strengths. The FE model developed and validated in chapter 3 was utilised for the parametric study. The number of the parametric studies and their results were arranged in orders so that all the maximum positive effects on the section strengths when changing parameter values were obtained. The channel sections together with its bending setup used in the experimental testing in chapter 3 were defined as "reference section". The section height  $h$ , thickness  $t$ , internal radius  $R$  and lip length  $c$  were fixed in the parametric study. The total length of the channel cross section was kept unchanged for the optimisation target, that was "obtaining maximum strength of the section while maintaining the same weight". Changes in parameters relating to the stiffeners' shapes, sizes, positions while considering enhanced material properties at corners and bends by the cold work effect resulted in new channel sections. The material properties at the flat regions, corners and at the stiffeners' bends were assumed to be the same in these new sections. In summary, the reference section had an initial imperfection of  $1.55t$ , an elastic modulus  $E$  of 205 GPa, a Poisson's ratio  $\nu$  of 0.3 and the stress-strain data determined in chapter 3 for the flat, corners and stiffener's bends.

## 4.2 Description of investigated section dimensions and parameters

The section without flange stiffeners is shown in Figure 4.1(a), in which all dimension parameters are also shown and the section with flange stiffeners is shown in Figure 4.1(b). The values for  $h$ ,  $t$ ,  $R$ , and  $c$  were taken of the reference section as 170.10 mm, 1.60 mm, 2.00 mm and 16.05 mm, respectively.  $h_1$  is the position of the web stiffener from the web-flange junction,  $h_2$  is the depth of the web stiffener,  $h_3$  is the position of the peak of the web stiffener in vertical direction from the web-flange junction,  $b_1$  is the width of the web stiffener,  $b_2$  is the position of the flange stiffener,  $d$  is the width and depth of the flange stiffener (assuming the flange stiffener had a circular shape),  $R$  is the radius of the section corners and it was assumed that they had the same radius. For the channel section shown in Figure 4.1(a), a total of 50 combinations with and without cold work between  $h_1/h$ ,  $h_2/h$ ,  $h_3/h$  and  $b_1/b$  were considered with  $h_1/h$  varying from 0.00 to 0.17,  $h_2/h$  varying from 0.07 to 0.24,  $h_3/h$  varying from 0.11 to 0.19 and  $b_1/b$  varying from 0.00 to 0.39. The reference section had  $h_1/h = 0.08$ ,  $h_2/h = 0.13$ ,  $h_3/h = 0.17$ , and  $b_1/b = 0.12$ . Hence, the buckling, ultimate moment capacity with and without cold work for each change were obtained and compared.

For the channel section shown in Figure 4.1(b), the position of flange intermediate stiffener  $b_2$ , size of flange intermediate stiffener  $d$  and flange width  $b$  were changed. A total of 22 combinations with and without cold work between  $b_2/b$  and  $d/b$  were considered with  $b_2/b$  varying from 0.06 to 0.63 and  $d/b$  varying from 0.08 to 0.40. In total, 72 combinations with and without cold work effect were generated through FE models, for different positions  $h_1/h$ , different shapes  $h_2/h$  and  $h_3/h$ , and different sizes  $b_1/b$  of the web stiffeners as well as different positions  $b_2/b$  and different sizes  $d/b$  of the flange stiffeners. Hence, the buckling, ultimate moment capacity with and without cold work for each change were obtained and compared to evaluate the effect of these changes.

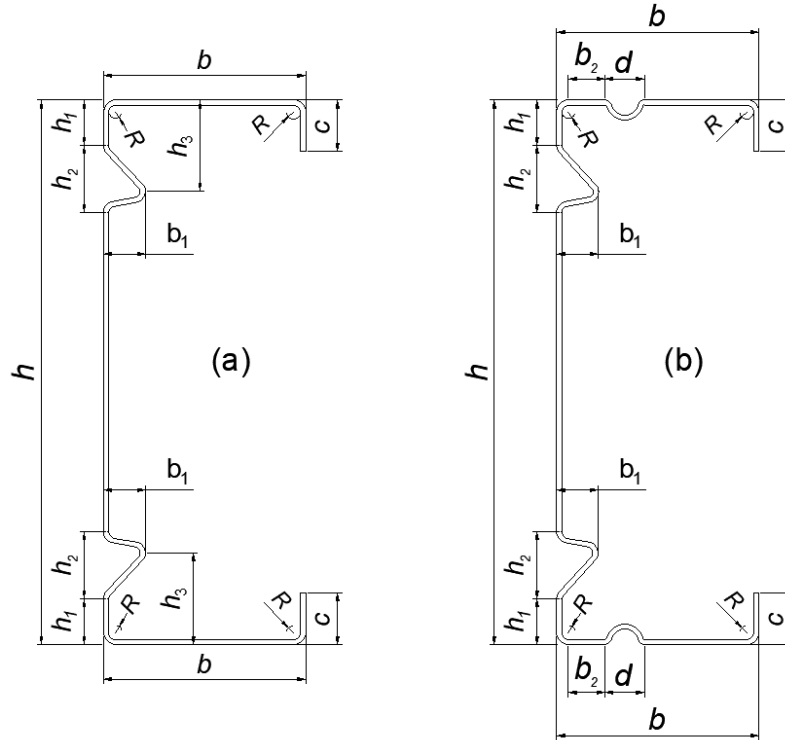


Figure 4.1. Dimension parameters of the channel cross section (a) without flange stiffeners, and (b) with flange stiffeners.

### 4.3 Parametric study and optimisation results

This section presents the results of investigating the influence of both the web and flange intermediate stiffeners' positions, shapes, sizes and cold work effect at corners and stiffeners' bends on the section ultimate strengths.

#### 4.3.1 Effect of the position of the web stiffener $h_1/h$

Figure 4.2 shows a graph of variation of the dimensionless ultimate bending moment capacities obtained by FE analysis  $M/M_y$  with variation of the stiffener position on the web  $h_1/h$ . In which  $M_y$  is the yield bending moment of the whole cross section and when the cold work effect is not included  $M$  equals  $M_u$ , when the cold work effect is included  $M$  equals  $M_{uc}$ . The results obtained by DSM are also presented for comparison. Moving down the stiffeners towards the centre of the cross section was the same with increasing  $h_1/h$ . The detailed values are shown in Table 4.1.

For this first parameter, the stress distributions on the sections without and with the cold work effect are made available for use in discussions, as shown in Figure 4.3.

For the same value of  $h_1/h$ ,  $M_{uc}$  was generally greater than  $M_u$ , as also reflected in the greater stresses developed in the sections with the cold work effect (Figure 4.3), indicating the cold work effect on ultimate bending strength of the section, despite the insignificant increase for some values of  $h_1/h$ . For different values of  $h_1/h$ , it was found that the ultimate bending moments  $M_u$  and  $M_{uc}$  reduced by increasing the ratio  $h_1/h$ . The maximum reduction in flexural strength resistance was 5% and 6% for the ultimate moment without cold work and with the cold work effect, respectively. When increasing  $h_1/h$ , it generated new cross sections with a reduction in the section modulus: the sectional modulus  $S_{xx}$  decreased from 27.60 cm<sup>3</sup> for  $h_1/h = 0.00$  to 26.97 cm<sup>3</sup> for  $h_1/h = 0.17$ , as shown in Table 4.1, and this led to a decrease in the ultimate bending moment. In the same time, the new cross sections had an increase in the buckling distortional slenderness: the distortional buckling slenderness  $\lambda_d$  increased from 1.148 for  $h_1/h = 0.00$  to 1.162 for  $h_1/h = 0.17$  as illustrated in Table 4.1, and this also led to a decrease in the ultimate bending moment. In combination, the ultimate bending moment gradually reduced when increasing the ratio  $h_1/h$  due to a product of the increasing effect by the buckling slenderness  $\lambda_d$  and the decreasing effect of the sectional modulus  $S_{xx}$ . Therefore, increasing the ratio  $h_1/h$  ultimately reduced the ultimate bending moments  $M_u$  and  $M_{uc}$ , and dimensionless values  $M_u/M_y$  and  $M_{uc}/M_y$ , as illustrated in Figure 4.2, indicating the sensitivity of the sections to distortional buckling. This suggested that if the stiffeners were placed on the web close to the flange, the buckling and ultimate strengths of the section would increase, and maximum strength could be obtained for this case.

The ultimate bending moments  $M_u$  and  $M_{uc}$  obtained by the DSM had the same trends with the FE results that increasing the ratio  $h_1/h$  reduced  $M_u$  and  $M_{uc}$ , with a clear gap between them, as shown in Figure 4.2. This was due to the assumption of using an average enhanced yield stress for the entire section to take into account the cold work effect, which might not entirely realistic but clearly showed the trend. However, for the same value of  $h_1/h$ , the values obtained by the DSM were smaller than those of the FE analysis with a maximum difference of 7% for both the ultimate bending moments, without the cold work effect and with the cold work effect. It should be noted that the DSM's ultimate bending moments  $M_u$  and  $M_{uc}$  were obtained from the semi-

empirical formulae which were derived based on an extensive amount of testing has been performed on laterally braced beams with geometric limitations for channel sections. In addition, the channel sections with intermediate stiffeners used in this thesis did not specify having pre-qualified for use with the DSM, and the assumption of using an average enhanced yield stress for the entire section to take into account the cold work effect was very approximate. Therefore, the ultimate bending moments  $M_u$  and  $M_{uc}$  obtained by the DSM were approximate values whilst those obtained by the FE analysis could be more accurate and insightful of the section behaviour and the cold work effect.

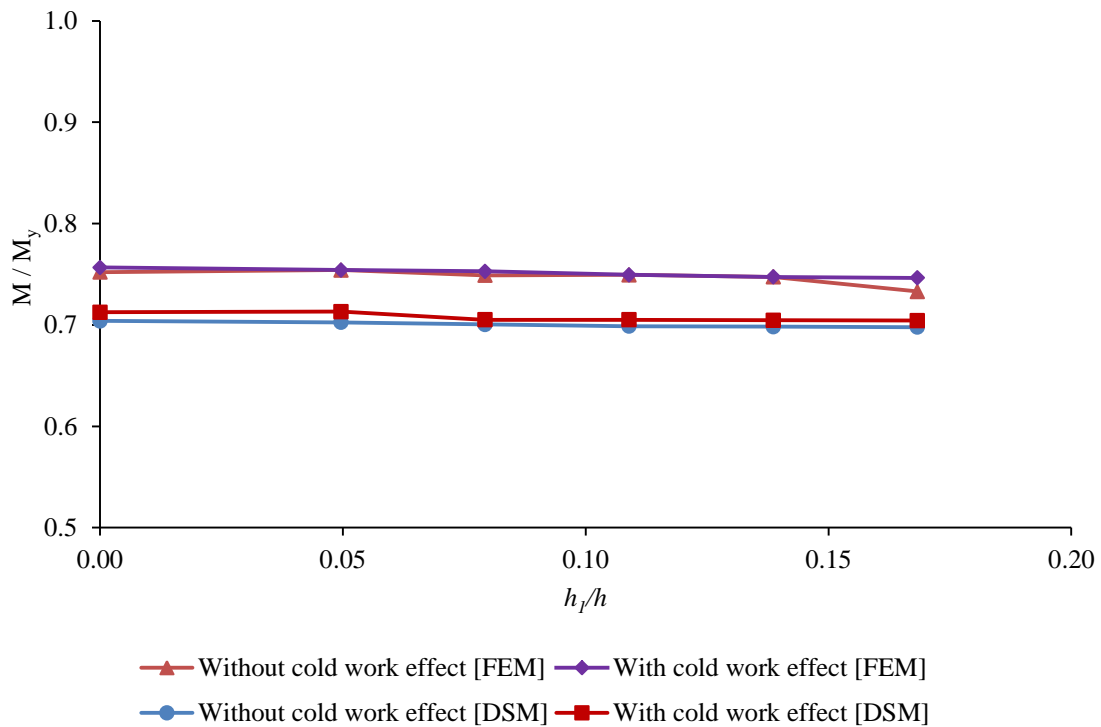


Figure 4.2. Variation in the ultimate moment capacity for different positions of web stiffeners  $h_1/h$  without the cold work effect and with the cold work effect.

**Table 4.1** Variation in ultimate bending moment capacity for different positions of web stiffeners.  $M_u$ ,  $M_{uc}$  stand for ultimate moment capacity without and with the cold work effect, respectively.  $f_{ya}$  is the average yield strength of the whole section.

$h_1/h$	Section properties		DSM					FEM			$\frac{M_u^{FEM}}{M_u^{DSM}}$	$\frac{M_{uc}^{FEM}}{M_{uc}^{DSM}}$
	$S_{xx}$ (cm <sup>3</sup> )	$\lambda_d$	$M_y$ (kNm)	$M_{yc}$ (kNm)	$M_u$ (kNm)	$M_{uc}$ (kNm)	$M_{uc}/M_u$	$M_u$ (kNm)	$M_{uc}$ (kNm)	$M_{uc}/M_u$		
0.00	27.60	1.148	14.35	14.53	10.10	10.23	1.01	10.79	10.86	1.01	1.07	1.06
0.05	27.44	1.151	14.27	14.44	10.03	10.18	1.01	10.76	10.76	1.00	1.07	1.06
0.08	27.31	1.155	14.20	14.38	9.95	10.01	1.01	10.64	10.69	1.01	1.07	1.06
0.11	27.19	1.159	14.14	14.31	9.88	9.97	1.01	10.60	10.60	1.00	1.07	1.06
0.14	27.07	1.161	14.08	14.25	9.83	9.92	1.01	10.52	10.52	1.00	1.07	1.07
0.17	26.97	1.162	14.02	14.20	9.79	9.86	1.01	10.28	10.47	1.02	1.05	1.06

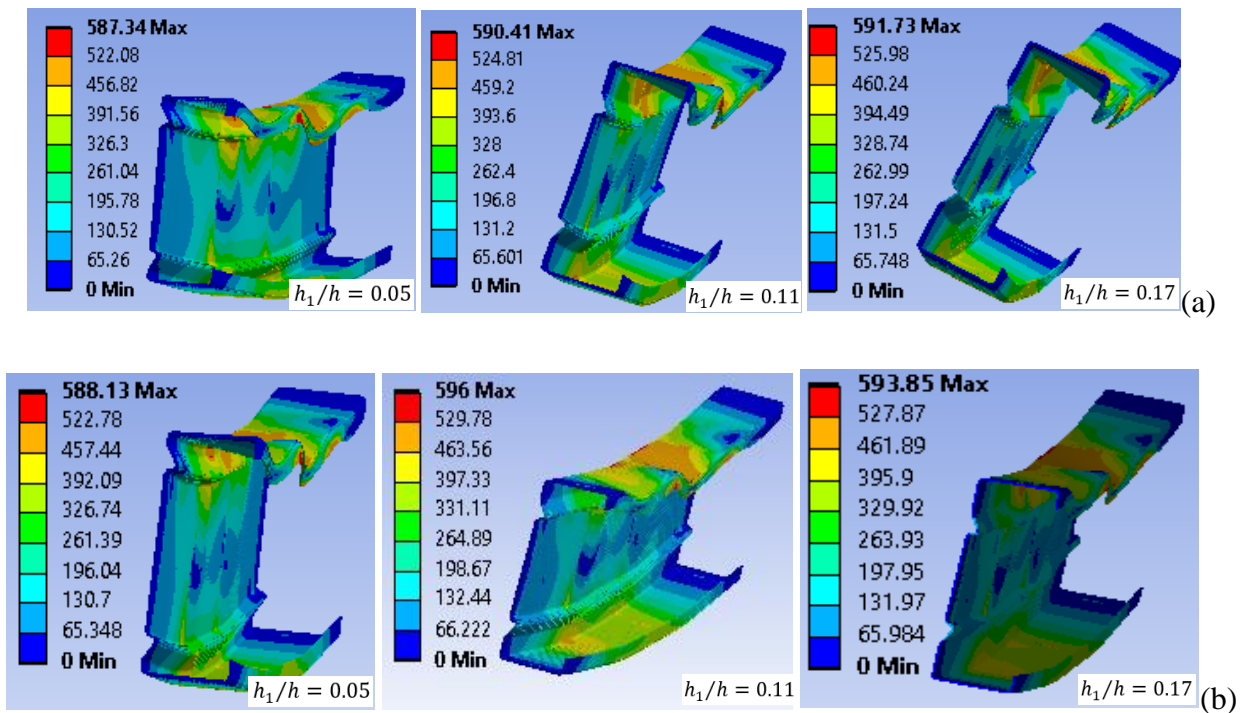


Figure 4.3. Von Mises stress distribution at failure for different web stiffener positions (a) without the cold work effect and (b) with the cold work effect.

### 4.3.2 Effect of the depth of the web stiffener $h_2/h$

Figure 4.4 shows the variation of  $M_u/M_y$  and  $M_{uc}/M_y$  with the variation of the web stiffener's depth  $h_2/h$ . The  $M_u/M_y$  and  $M_{uc}/M_y$  values obtained by DSM are also presented for comparison. The detailed values are shown in Table 4.2.

For the same value of  $h_2/h$ ,  $M_{uc}$  was generally greater than  $M_u$ , confirming the cold work effect on enhancing the section's ultimate bending strength. However, there were small effects at some values of  $h_2/h$  with a maximum difference of 3%, especially it was insignificant with  $h_2/h$  from 0.15 to 0.18. When increasing  $h_2/h$  from 0.07 to 0.13, the ultimate bending moment  $M_u$  and  $M_{uc}$  reduced. It was because the distortional buckling slenderness  $\lambda_d$  increased from 1.142 to 1.155 as illustrated in Table 4.2, and this induced a decrease in the ultimate bending moment. Although, at the same time the ultimate bending moment increased due to an increase in the sectional modulus  $S_{xx}$ , the decreasing effect by the buckling slenderness  $\lambda_d$  was more significant. When increasing  $h_2/h$  from 0.10 to 0.24,  $S_{xx}$  decreased from 27.32 cm<sup>3</sup> to 26.93 cm<sup>3</sup>, as shown in Table 4.2, and this led to a decrease in the ultimate bending moment. In addition,  $\lambda_d$  slightly decreased from 1.155 to 1.153, and this led to an insignificant increase in the ultimate bending moment. As the decreasing effect by the sectional modulus  $S_{xx}$  was more noticeable, the ultimate bending moment slightly increased, as can be seen in Table 4.2 and in Figure 4.4 for  $M_u/M_y$  and  $M_{uc}/M_y$ . The maximum ultimate bending moment increased by the cold work effect was about 1% at  $h_2/h = 0.24$ . The results obtained by the DSM had the same trends with the FE results when increasing the ratio  $h_2/h$ , with a maximum difference of 9%. It is therefore suggested that the web stiffener to have a longer depth than that of the reference section in order to obtain greater bending moment capacity.

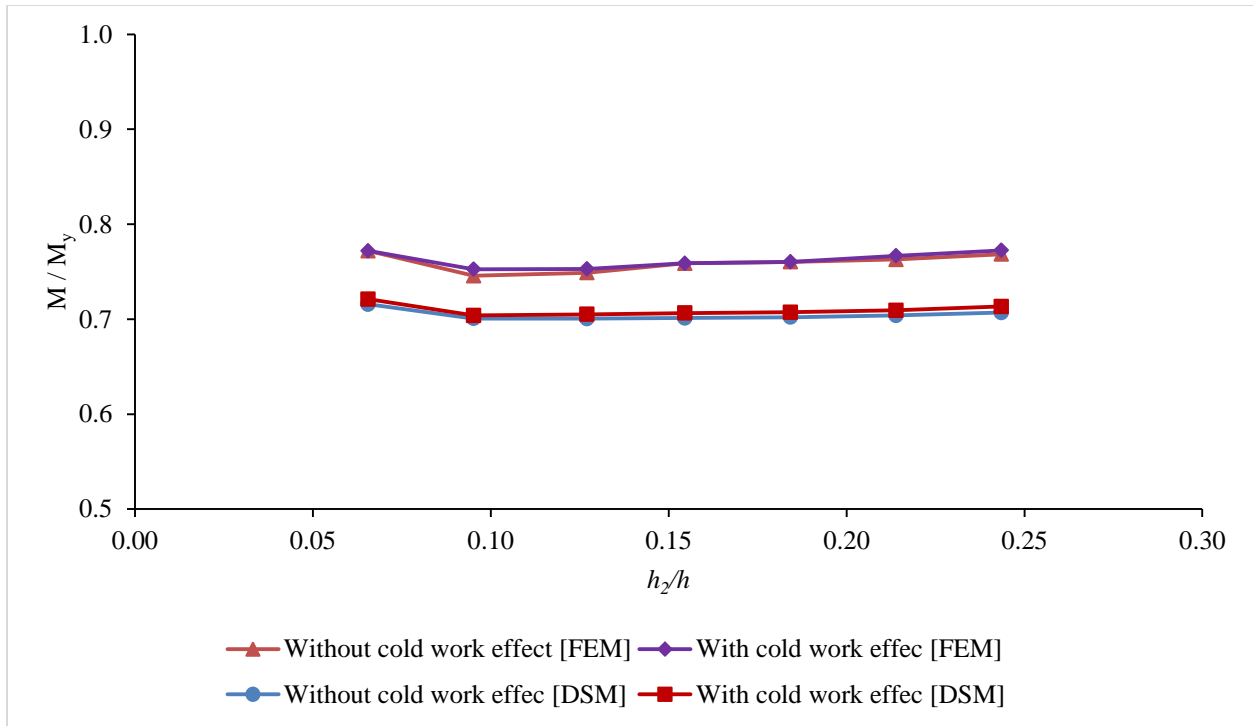


Figure 4.4. Variation in the ultimate moment capacity for different shapes of web stiffeners  $h_2/h$  without and with the cold work effect.

**Table 4.2** Variation in ultimate bending moment capacity for different depths of the web stiffener.

$h_2/h$	Section properties		DSM					FEM			$\frac{M_u^{FEM}}{M_u^{DSM}}$	$\frac{M_{uc}^{FEM}}{M_{uc}^{DSM}}$
	$S_{xx}$ (cm <sup>3</sup> )	$\lambda_d$	$M_y$ (kNm)	$M_{yc}$ (kNm)	$M_u$ (kNm)	$M_{uc}$ (kNm)	$M_{uc}/M_u$	$M_u$ (kNm)	$M_{uc}$ (kNm)	$M_{uc}/M_u$		
0.07	26.89	1.142	13.98	14.15	10.01	10.08	1.01	10.76	10.76	1.00	1.08	1.07
0.10	27.32	1.155	14.21	14.38	9.95	10.00	1.01	10.59	10.69	1.01	1.06	1.07
0.13	27.31	1.155	14.20	14.38	9.95	10.01	1.01	10.64	10.69	1.01	1.07	1.07
0.15	27.2	1.15	14.18	14.35	9.94	10.02	1.01	10.76	10.76	1.00	1.08	1.07



	7	5										
0.18	27.2 2	1.15 2	14.15	14.33	9.94	10.01	1.01	10.76	10.76	1.00	1.08	1.07
0.21	27.1 3	1.15 1	14.11	14.28	9.93	10.01	1.01	10.76	10.82	1.01	1.08	1.08
0.24	26.9 3	1.15 3	14.00	14.18	9.90	9.99	1.01	10.76	10.82	1.01	1.09	1.08

### 4.3.3 Effect of the position of the peak of the web stiffener $h_3/h$

Figure 4.5 shows the variation of  $M_u/M_y$  and  $M_{uc}/M_y$  with the variation of the web stiffener's peak  $h_3/h$  in the vertical direction. Moving down the stiffener's peak away from web-flange junction of the section was the same with increasing  $h_3/h$ . The  $M_u/M_y$  and  $M_{uc}/M_y$  values obtained by DSM are also presented for comparison. The detailed values are shown in Table 4.3.

For the same value of  $h_3/h$ ,  $M_{uc}$  was greater than  $M_u$  with a maximum increase of 1%, confirming the cold work effect on enhancing the section's ultimate bending strength. When increasing  $h_3/h$ , from 0.11 to 0.19, the ultimate bending moment  $M_u$  and  $M_{uc}$  decreased and the rate of decreasing was significantly increased for  $h_3/h$ , from 0.14 to 0.19. It was found that even though increasing  $h_3/h$  reduced the distortional buckling slenderness of the sections (i.e.  $\lambda_d$  reduced from 1.164 to 1.118), the ultimate moment capacity of the sections still reduced due to a more significant reduction in the sectional modulus (i.e.  $S_{xx}$  reduced from 27.51 cm<sup>3</sup> to 26.55 cm<sup>3</sup>), as shown in Table 4.3. The ultimate bending moments  $M_u$  and  $M_{uc}$  obtained by the DSM had the same trends with the FE results, as shown in Figure 4.5 and Table 4.3. However, for the same value of  $h_3/h$ , the values for both the ultimate bending moments, without the cold work effect and with the cold work effect, obtained by the DSM were smaller than those of the FE analysis with a maximum difference of 8%. The reasons were explained previously. It is therefore recommended that the web stiffener's peak should be placed near the web-flange junction in vertical direction in order to have significant strength enhancement, including the case of the cold work effect.

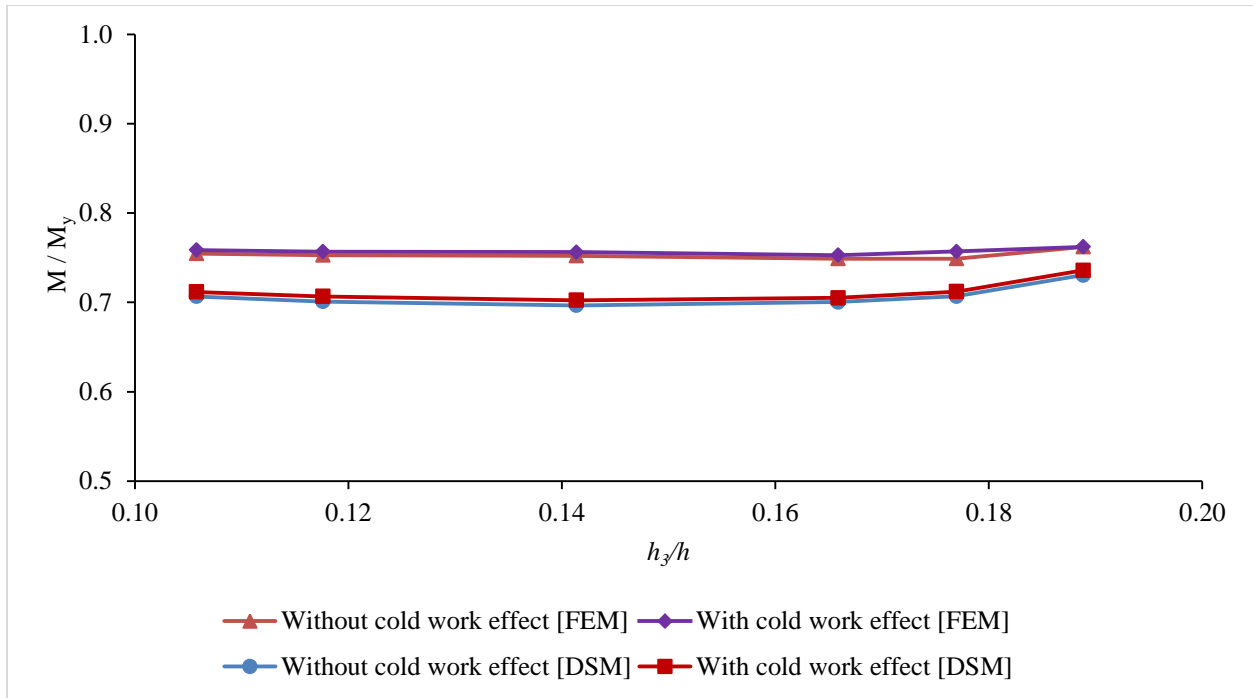


Figure 4.5. Variation in the ultimate moment capacity for different positions of the web stiffener's peak in vertical direction  $h_3/h$  without the cold work effect and with the cold work effect.

**Table 4.3** Variation in ultimate bending moment capacity for different positions of the web stiffener's peak in vertical direction.

$h_3/h$	Section properties		DSM					FEM			$\frac{M_u^{FEM}}{M_u^{DSM}}$	$\frac{M_{uc}^{FEM}}{M_{uc}^{DSM}}$
	$S_{xx}$ (cm <sup>3</sup> )	$\lambda_d$	$M_y$ (kNm)	$M_{yc}$ (kNm)	$M_u$ (kNm)	$M_{uc}$ (kNm)	$M_{uc}/M_u$	$M_u$ (kNm)	$M_{uc}$ (kNm)	$M_{uc}/M_u$		
0.19	26.55	1.118	13.81	13.98	9.92	10.01	1.01	10.52	10.52	1.00	1.06	1.05
0.18	27.02	1.142	14.05	14.22	9.93	10.01	1.01	10.52	10.64	1.01	1.06	1.06
0.17	27.31	1.156	14.20	14.38	9.95	10.01	1.01	10.64	10.69	1.01	1.07	1.07
0.14	27.51	1.164	14.31	14.48	9.97	10.05	1.01	10.76	10.88	1.01	1.08	1.08
0.12	27.4	1.15	14.29	14.47	10.02	10.10	1.01	10.76	10.88	1.01	1.07	1.07

	9	5										
0.11	27.4	1.14	14.26	14.43	10.08	10.15	1.01	10.76	10.88	1.01	1.07	1.07
	2	3										

#### 4.3.4 Effect of the width of the web stiffener $b_1/b$

The variation of the dimensionless ultimate bending moment capacities obtained by FE analysis, without the cold work effect  $M_u/M_y$  and with the cold work effect  $M_{uc}/M_y$ , with variation of the width of the web stiffener  $b_1/b$  is shown in Figure 4.6. Increasing  $b_1/b$  was the same with moving the stiffener's peak away from web in horizontal direction. The  $M_u/M_y$  and  $M_{uc}/M_y$  values obtained by DSM are also presented. The detailed values are shown in Table 4.4.

With the same value of  $b_1/b$ ,  $M_{uc}$  was generally greater than  $M_u$  but the enhancement was very small when  $b_1/b$  was less than 0.05 but was noticeable when  $b_1/b$  increased from 0.05 to 0.32 with a maximum increase of 1%. These were associated with an increase in the stresses in the sections or a decrease in sectional moduli, with a maximum increase of 4% for  $b_1/b = 0.21$ , as can be seen in Table 4.4. Overall, the ultimate moment capacity increased up to certain limit but beyond that the ultimate moment capacity was reduced and the maximum change was 4% and 5% for the ultimate moment without the cold work effect and with the cold work effect, respectively. Detailed values of the ultimate bending moments  $M_u$  and  $M_{uc}$  for different types of sections with different values of  $b_1/b$  are also displayed in bar charts in Figure 4.7. It was observed that  $M_u$  and  $M_{uc}$  increased when the values of  $b_1/b$  increased from 0.00 to 0.21.

When  $b_1/b$  increased from 0.21 to 0.39, however, the FE results showed that sections failed in distortional-global interactive buckling modes as the ultimate bending moment capacities  $M_u$  and  $M_{uc}$  decreased. This reflected through the decreasing values of  $M_u$  and  $M_{uc}$  as shown in Table 4.4 and Figure 4.6. It means that, for this particular range of  $b_1/b$ , the practical bracing length of 900 mm was not sufficient to exhibit pure distortional buckling modes in the sections. It was because the FE results showed that when values of  $b_1/b$  increased from 0.21 to 0.32, 0.39 and 0.47 (for information only, results not shown), the horizontal movement of the compressed web-

flange corner  $d_y$  and the outward compressed flange-lip motion  $d_z$  in post buckling state ( $d_y, d_z$ ) changed from (0 mm, 20 mm) to (0.50 mm, 21 mm), (1 mm, 25 mm) and (2 mm, 26 mm), respectively. In addition, the significant reduction of the sectional modulus  $S_{zz}$  in the minor axis by 70% ( i.e.  $S_{zz}$  reduced significantly from 16.81 cm<sup>3</sup> for  $b_1/b = 0.00$  to 11.07 cm<sup>3</sup> for  $b_1/b = 0.32$  and 9.92 cm<sup>3</sup> for  $b_1/b = 0.39$ ). The noticeable reduction in  $S_{zz}$  from  $b_1/b = 0.21$  could make the sections prone to fail by lateral/global buckling. These clearly indicated the distortional-global buckling interactive failure and consequently led to lower ultimate moment capacities for the beam sections, as confirmed by the FE results shown in Figure 4.6.

For the values of  $b_1/b$  from 0.00 to 0.21, the ultimate bending moments  $M_u$  and  $M_{uc}$  obtained by the DSM had the same trends with the FE results. However, when  $b_1/b$  increased from 0.21 to 0.39, the DSM results showed an increase in the bending moment capacities as shown in Figure 4.6 as they were based on the critical distortional buckling half-wave lengths. For comparison purposes, the FE models with the bracing length the same as the critical distortional buckling half-wave length were developed to model the condition of “fully restrained” for critical distortional buckling failure for values of  $b_1/b$  from 0.21 to 0.39. The ultimate moment capacities  $M_u$  and  $M_{uc}$  are also shown in dash lines in Figure 4.6. The results of these models are compared with the DSM results obtained using the critical distortional buckling modes. It can be seen that the ultimate bending moments  $M_u$  and  $M_{uc}$  obtained by the DSM had the same trends with the FE results. However, for the same value of  $b_1/b$ ,  $M_u$  and  $M_{uc}$  values obtained by the DSM were less than those of the FE analysis with a maximum difference of 8%.

It is therefore suggested that the web stiffener’s peak should be placed further away from the web in horizontal direction to a certain position (up to 20% of the section width) in order to have significant strength enhancement, including the case of the cold work effect.

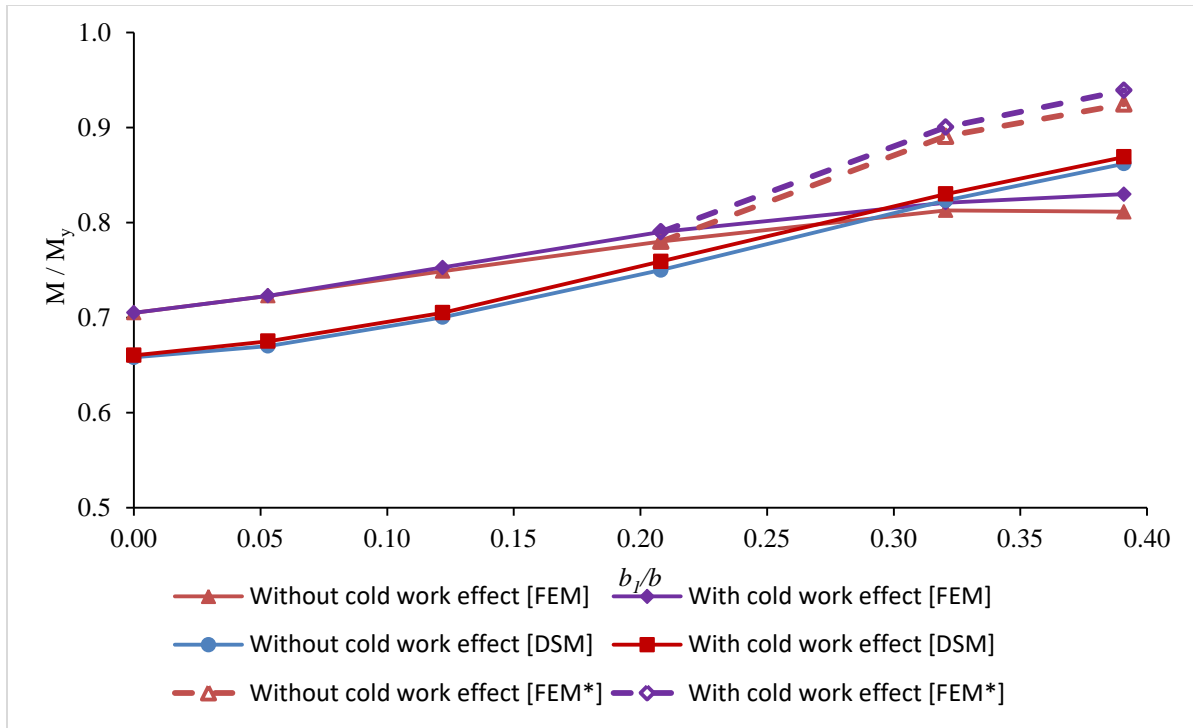


Figure 4.6 Variation in ultimate moment capacity for different widths of the web stiffener  $b_1/b$  of web stiffeners without the cold work effect and with the cold work effect. FEM\* is FEM results with bracing lengths the same with the critical distortional buckling half-wave length.

**Table 4.4** Variation in ultimate bending moment capacity for different widths of the web stiffeners.

$b_1/b$	Section properties		DSM					FEM			$\frac{M_u^{FEM}}{M_u^{DSM}}$	$\frac{M_{uc}^{FEM}}{M_{uc}^{DSM}}$
	$S_{xx}$ (cm <sup>2</sup> )	$\lambda_d$	$M_y$ (kNm)	$M_{yc}$ (kNm)	$M_u$ (kNm)	$M_{uc}$ (kNm)	$M_{uc}/M_u$	$M_u$ (kNm)	$M_{uc}$ (kNm)	$M_{uc}/M_u$		
0.00	28.19	1.247	14.66	14.85	9.68	9.70	1.00	10.34	10.34	1.00	1.07	1.07
0.05	27.98	1.223	14.55	14.68	9.76	9.82	1.01	10.52	10.52	1.00	1.08	1.07
0.12	27.31	1.156	14.20	14.38	9.95	10.01	1.01	10.64	10.69	1.01	1.07	1.07
0.21	26.42	1.055	13.74	13.91	10.31	10.43	1.01	10.72	10.86	1.01	1.04	1.04
0.32	25.44	0.923	13.23	13.39	10.91	10.98	1.01	10.76	10.86	1.01	0.99	0.99
0.39	24.94	0.874	12.97	13.13	11.25	11.34	1.01	10.52	10.76	1.02	0.94	0.95
0.32*	25.44	0.923	13.23	13.39	10.91	10.98	1.01	10.76	11.91	1.01	1.08	1.08
0.39*	24.94	0.874	12.97	13.13	11.25	11.34	1.01	11.99	12.18	1.02	1.07	1.07

\* FE models with bracing lengths the same with the critical distortional buckling half-wave length

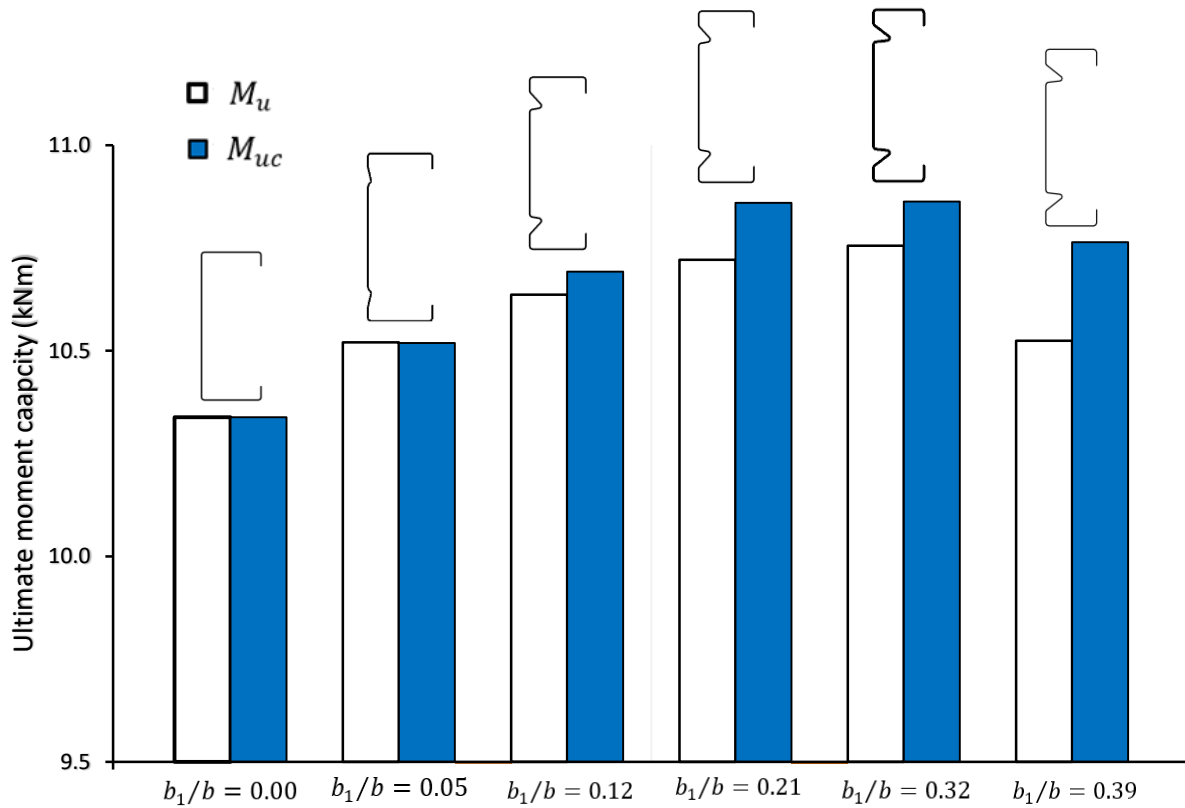


Figure 4.7. Comparison of the ultimate bending moment capacity for different widths of the web stiffeners (when  $b_1/b = 0.32$  and  $0.39$  the sections failed in distortional-global interactive buckling modes).

#### 4.3.5 Effect of the position of the flange stiffeners $b_2/b$

Figure 4.8 shows the variation of  $M_u/M_y$  and  $M_{uc}/M_y$  with the variation of the position of the flange stiffener. Moving the flange stiffeners away from web-flange junction of the section was the same with increasing  $b_2/b$ . The  $M_u/M_y$  and  $M_{uc}/M_y$  values obtained by DSM are also presented for comparison. The detailed values are shown in Table 4.5.

With the same value of  $b_2/b$ ,  $M_{uc}$  was significantly greater than  $M_u$  with a maximum increase of 2%. These were associated with an increase in the stresses in the sections or a decrease in sectional moduli, as can be seen in Table 4.5, with a maximum increase of 5% for  $b_2/b = 0.63$ . When increasing  $b_2/b$ , from 0.06 to 0.63, the ultimate bending moment  $M_u$  and  $M_{uc}$  decreased and the rate of decreasing was not significant with  $b_2/b$  from 0.06 to 0.24, but was significant with  $b_2/b$  from 0.24 to 0.63. It was observed that within the range of  $b_2/b = 0.06$  to 0.63, the sections failed by distortional buckling modes. Values of  $M_u$  and  $M_{uc}$  obtained by the DSM had the same trends with the FE results. This was due to the increase in the distortional buckling slenderness of the sections (i.e. values of  $\lambda_d$  increased from 1.070 for  $b_2/b = 0.06$  to 1.1581 for  $b_2/b = 0.63$ ) whilst the sectional modulus was unchanged (i.e. values of  $S_{xx}$  were the same for all the sections) as shown in Table 4.5. The increase in the distortional buckling slenderness had an inverse effect that reduced the ultimate moment capacity of the sections. It was finally concluded that in the sections with flange stiffeners, distortional buckling failure was more severe when the flange stiffeners shifted away in horizontal direction from the web-flange junction. It is, therefore, suggested that the flange stiffeners need to be placed near the web-flange junction in order to gain maximum bending strength capacity.

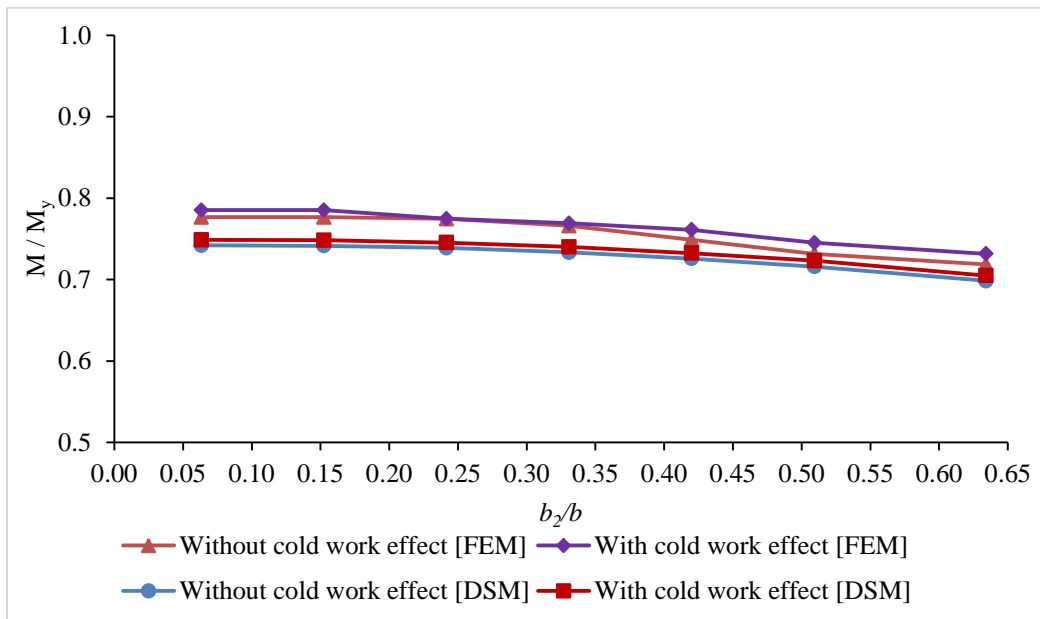


Figure 4.8. Variation in ultimate moment capacity for different positions of flange stiffeners  $b_2/b$  without the cold work effect and with the cold work effect.

**Table 4.5** Variation in ultimate bending moment capacity for different positions of flange-intermediate stiffeners.

$b_2/b$	Section properties		DSM					FEM			$\frac{M_u^{FEM}}{M_u^{DSM}}$	$\frac{M_{uc}^{FEM}}{M_{uc}^{DSM}}$
	$S_{xx}$ (cm <sup>2</sup> )	$\lambda_d$	$M_y$ (kNm)	$M_{yc}$ (kNm)	$M_u$ (kNm)	$M_{uc}$ (kNm)	$M_{uc}/M_u$	$M_u$ (kNm)	$M_{uc}$ (kNm)	$M_{uc}/M_u$		
0.06	27.0 1	1.07 0	14.05	14.25	10.43	10.52	1.01	10.91	11.03	1.01	1.05	1.05
0.15	27.0 1	1.07 2	14.05	14.25	10.42	10.51	1.01	10.91	11.03	1.01	1.05	1.05
0.24	27.0 1	1.07 7	14.05	14.25	10.38	10.47	1.01	10.88	10.88	1.00	1.05	1.04
0.33	27.0 1	1.08 8	14.05	14.25	10.30	10.40	1.01	10.76	10.81	1.01	1.04	1.04
0.42	27.0 1	1.10 2	14.05	14.25	10.20	10.29	1.01	10.52	10.69	1.02	1.03	1.04
0.51	27.0 1	1.12 3	14.05	14.25	10.06	10.16	1.01	10.28	10.47	1.02	1.02	1.03
0.63	27.0 1	1.15 8	14.05	14.25	9.81	10.90	1.01	10.10	10.28	1.02	1.03	1.04

#### 4.3.6 Effect of the size of the flange stiffeners $d/b$

Figure 4.9 shows the influence of changing the size of the flange stiffeners  $d/b$  on the dimensionless ultimate moment capacity  $M_u/M_y$  and  $M_{uc}/M_y$  of the sections. The  $M_u/M_y$  and  $M_{uc}/M_y$  values obtained by DSM are also presented for comparison. The detailed values are shown in Table 4.6.

With the same value of  $d/b$ ,  $M_{uc}$  was significantly greater than  $M_u$  with a maximum increase of 2%. The ultimate moment capacity increased when values of  $d/b$  increased up to certain limit ( $d/b \approx 0.28$ ) beyond which it was slightly reduced. The maximum change in the ultimate moment capacity, for changes in the size of the flange stiffeners, was 7% and 8% in the cases of without the cold work and with the cold work effect, respectively. It was observed that the ultimate moment capacities  $M_u$  and  $M_{uc}$  increased up to certain values because the distortional buckling slenderness  $\lambda_d$  reduced significantly when  $d/b$  increased up to a certain limit ( $d/b = 0.28$ ). Even though the sectional modulus in the major axis  $S_{xx}$  and minor axis  $S_{zz}$  reduced that could reduce the ultimate moment capacities, the influence of the distortional buckling



slenderness  $\lambda_d$  on the ultimate moment capacities were more significant. However, beyond the limit of  $d/b = 0.28$ , the ultimate moment capacities reduced because of the significant reduction of section modulus in the minor axis  $S_{zz}$  (i.e.  $S_{zz}$  reduced significantly from  $14.30 \text{ cm}^3$  for  $d/b = 0.08$  to  $11.87 \text{ cm}^3$  for  $d/b = 0.40$ , which was about 20% in reduction). The reduction in the sectional modulus in the minor axis  $S_{zz}$  caused the sections with values of  $d/b$  greater than 0.28 to fail by distortional-global buckling interaction and that reduced the ultimate moment capacities. This phenomenon was already discussed with FE models and results in Section 4.3.4. The DSM predicted the same trends with FE results for the ultimate moment capacities for the values of  $d/b$  from 0.06 to 0.28, where the FE models also predicted that the sections were failed by the distortional buckling modes. It is therefore suggested that the flange stiffeners should have an increasing diameter up to a certain size (up to 28% of the section width) in order to have maximum bending strength, including the case of the cold work effect. It is also suggested that design guidelines for distortional-global interaction buckling modes need to be included in the DSM procedure.

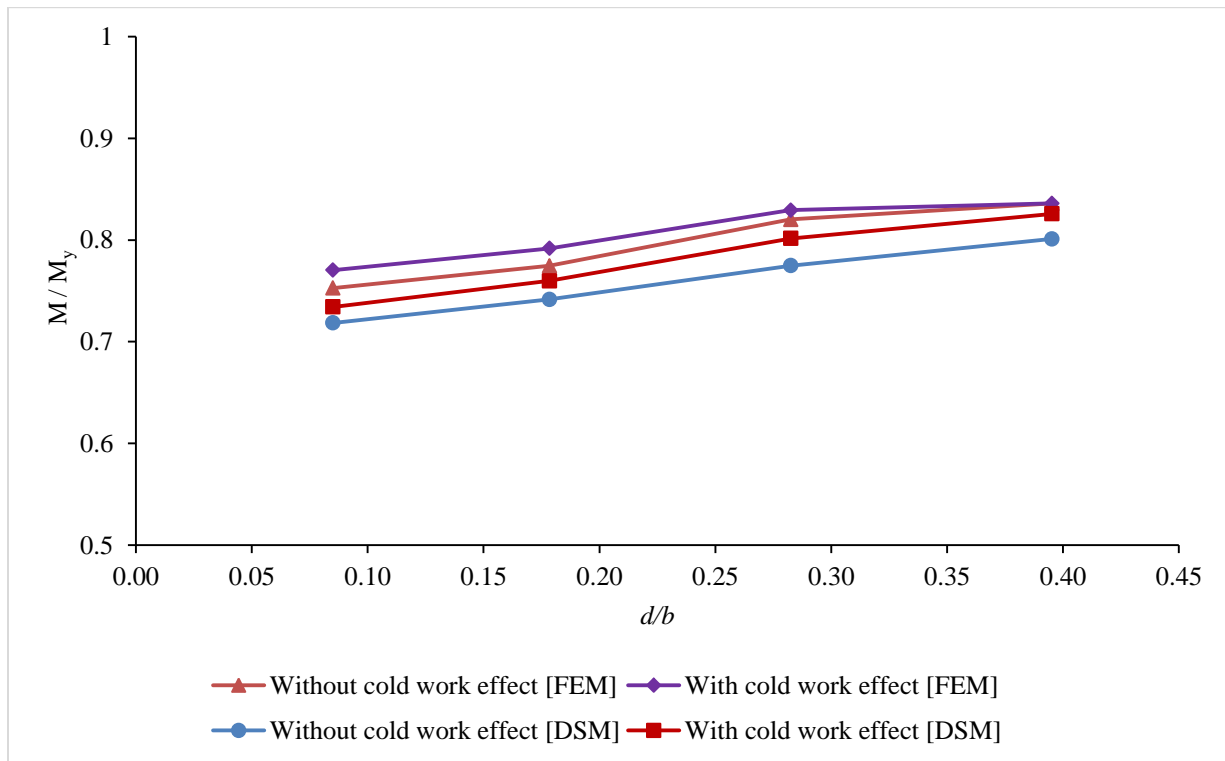


Figure 4.9. Variation in ultimate moment capacity for different sizes of flange stiffeners without the cold work effect and with the cold work effect.

**Table 4.6** Variation in ultimate moment capacity for different sizes of flange stiffeners.

$d/b$	Section properties		DSM					FEM			$\frac{M_u^{FEM}}{M_u^{DSM}}$	$\frac{M_{uc}^{FEM}}{M_{uc}^{DSM}}$
	$S_{xx}$ (cm <sup>3</sup> )	$\lambda_d$	$M_y$ (kNm)	$M_{yc}$ (kNm)	$M_u$ (kNm)	$M_{uc}$ (kNm)	$M_{uc}/M_u$	$M_u$ (kNm)	$M_{uc}$ (kNm)	$M_{uc}/M_u$		
0.08	27.24	1.118	14.16	14.42	10.17	10.29	1.01	10.66	10.91	1.02	1.05	1.06
0.18	27.01	1.072	14.05	14.25	10.42	10.48	1.01	10.88	11.12	1.02	1.04	1.06
0.28	26.63	1.009	13.85	14.04	10.73	10.82	1.01	11.36	11.49	1.01	1.06	1.06
0.40	26.16	0.971	13.60	13.77	10.89	10.98	1.01	11.37	11.37	1.00	1.04	1.04

#### 4.3.7 Effect of the number of stiffeners

The influence of different number of longitudinal stiffeners at the web and the flange on ultimate moment capacities of the sections without and with the cold work effect, was investigated by FE modelling. In this study, there were 6 different cross-section types depending upon different number of longitudinal stiffeners at the web and the flange: (1) the cross-section had no web and flange stiffeners, (2) the cross-section had flange stiffeners, (3) the cross-section had one web stiffener, (4) the cross-section had one web and flange stiffeners, (5) the cross-section had two web stiffeners, and (6) the cross-section had two web and flange stiffeners. Figure 4.10 shows variation of ultimate moment capacities of the sections without and with the cold work effect. These cross-sections were designed to be symmetrical about the major axis for practical purpose and stiffeners had identical shape and size at web and flanges. Overall, the ultimate moment capacities for both cases, without and with the cold work effect, increased in comparison to the cross-section of no web and flange stiffeners, type (1), when the number of stiffeners increased in both the web and/or the flange as shown in the cross-section types (2), (4), (5) and (6), except type (3) where the cross-section had one web stiffener at the mid-height of the web, there was no influence of the web stiffener on the ultimate moment capacity. The maximum enhancement in the ultimate moment capacity without the cold work effect obtained for type (6) in comparison to the standard lipped channel type (1) was 5%. Similarly, the maximum enhancement in the ultimate moment capacity with the cold work effect obtained for type (6) was 7%. For each section type, the cold work effect on ultimate moment capacity was varied between 0% to 1% for most of the cross-sections depending on both distortional buckling slenderness and area

percentage of stiffener bends in the cross-sectional types. For instance, the maximum the cold work effect for type (6) was 1%, in which the section had  $\lambda_d$  of 1.070 and the area percentage of bends of 23% while the cold work effect was insignificant on for type (1) which had  $\lambda_d$  of 1.247 and the area percentage of bends of 5%. Thus, it was concluded that having two symmetrical web stiffeners and one symmetrical flange stiffeners enhanced the ultimate moment capacity of the sections and the cold work effect on the ultimate moment capacity was maximum as in this case the section had the smallest distortional buckling slenderness and the highest area percentage of the stiffener bends.

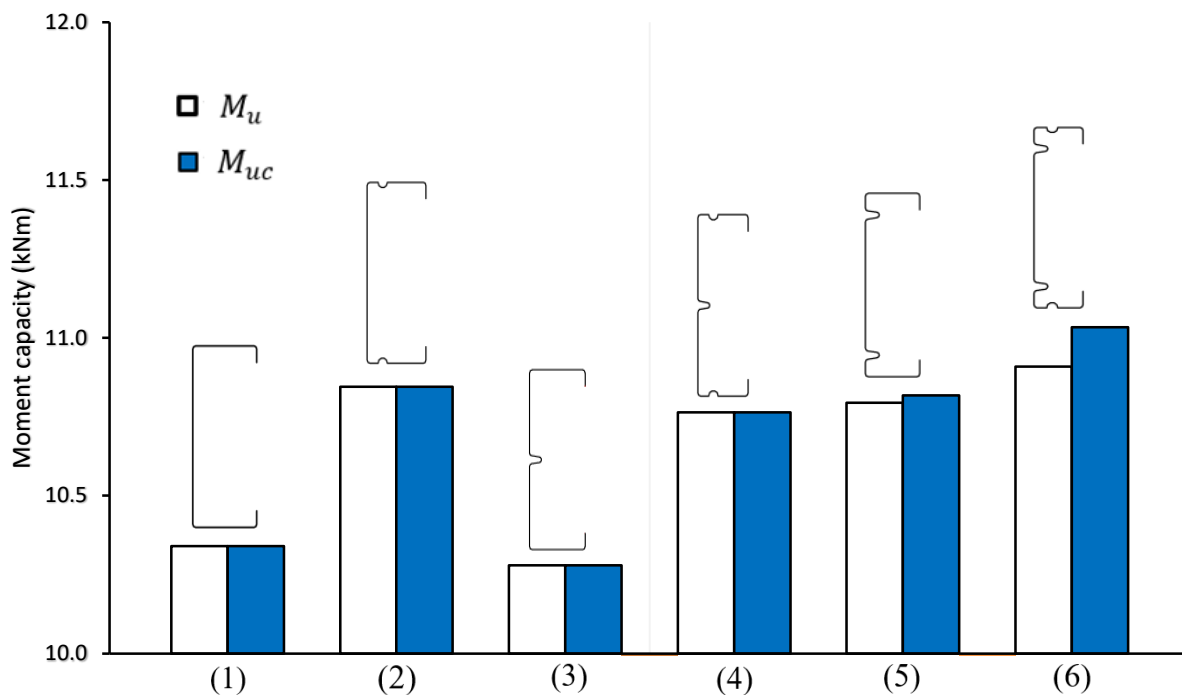


Figure 4.10. Variation in ultimate moment capacity for different numbers of web and flange stiffeners for sections without and with the cold work effect.

**Table 4.7** Variation in ultimate moment capacities for different numbers of web and flange stiffeners.

Section types	Section properties		DSM					FEM		$\frac{M_u^{FEM}}{M_u^{DSM}}$	$\frac{M_{uc}^{FEM}}{M_{uc}^{DSM}}$
	$S_{xx}$ (cm <sup>3</sup> )	$\lambda_d$	$M_y$ (kNm)	$M_u$ (kNm)	$M_{uc}$ (kNm)	$M_{uc}/M_u$	$M_u$ (kNm)	$M_{uc}$ (kNm)	$M_{uc}/M_u$		
Lipped channel (1)	28.19	1.247	14.66	9.68	9.70	1.00	10.34	10.34	1.00	1.07	1.07
One stiffener at flanges (2)	27.90	1.165	14.51	10.10	10.17	1.01	10.84	10.84	1.00	1.07	1.07
One stiffener at web (3)	25.79	1.095	13.41	9.79	9.82	1.00	10.28	10.28	1.00	1.05	1.05
One stiffener at web and one at flanges (4)	25.49	1.013	13.25	10.25	10.33	1.01	10.76	10.76	1.00	1.05	1.05
Two symmetrical stiffeners at web (5)	27.60	1.148	14.35	10.10	10.23	1.01	10.79	10.82	1.00	1.07	1.06
Two symmetrical stiffeners at web and one stiffener at flanges (6)	27.01	1.070	14.05	10.43	10.52	1.01	10.91	11.03	1.01	1.05	1.04

#### 4.3.8 Optimisation results

Based on the above parametric studies of all geometric parameters and the cold work effect, all the maximum positive effects on the section strengths were obtained for the reference section with two web stiffeners and two flange stiffeners (Figure 4.1(b)). Figure 4.11 shows the maximum % increase in the ultimate bending moment capacities for distortional buckling, without and with the cold work effect, against the investigated parameters. It was observed that the maximum percentage of increase in the ultimate moment capacities of the sections without the cold work effect was almost up to 5% when the position of the web stiffeners  $h_1/h = 0.00$  whilst it was about 6% for the ultimate moment capacity with the cold work effect, indicating the cold work effect was noticeable. The maximum percentage of increase in the ultimate moment capacities without and with the cold work effect was about 2% and 3%, respectively, when the depth of the web stiffeners  $h_2/h = 0.24$ , indicating the cold work effect. Similar trends were observed for the maximum percentage of increase in the ultimate moment capacities without and with the cold work effect when changing the position of the peak of the web stiffeners to  $h_3/h = 0.14$ . The maximum percentage of increase in the ultimate moment capacities without and with the cold work effect was about 4% and 5%, respectively, for changing the width of the web stiffeners to the certain value  $b_1/b = 0.21$ , showing that both the stiffeners' shape and the cold work effect were very significant. In terms of changing the positions of the flange stiffeners  $b_2/b$ , the maximum percentage of increase in the ultimate moment capacities without and with the cold work effect was about 8% and 9% at  $b_2/b = 0.06$ , respectively, confirming that both the flange stiffeners' position and the cold work effect were very significant. The maximum percentage of increase in the ultimate moment capacities without and with the cold work effect was about 7% and 8% with the flange stiffeners' size at the certain values  $d/b = 0.28$ , respectively, indicating that both the flange stiffeners' size and the cold work effect were noticeable. Therefore, it was suggested that the optimal shape for the channel section to gain the maximum ultimate moment capacity in distortional buckling had  $h_1/h$  of 0.00 or as much close as possible to the web-flange junction,  $h_2/h$  of at least 0.15 or above,  $h_3/h$  of at least 0.14,  $b_1/b$  of the certain value 0.21,  $b_2/b = 0.06$  or as much close as possible to the web-flange junction, and  $d/b$  of the certain value of 0.28. In addition, the cold work effect had to be included in the FE models for accurately obtaining enhancement in the ultimate moment capacity of the section.

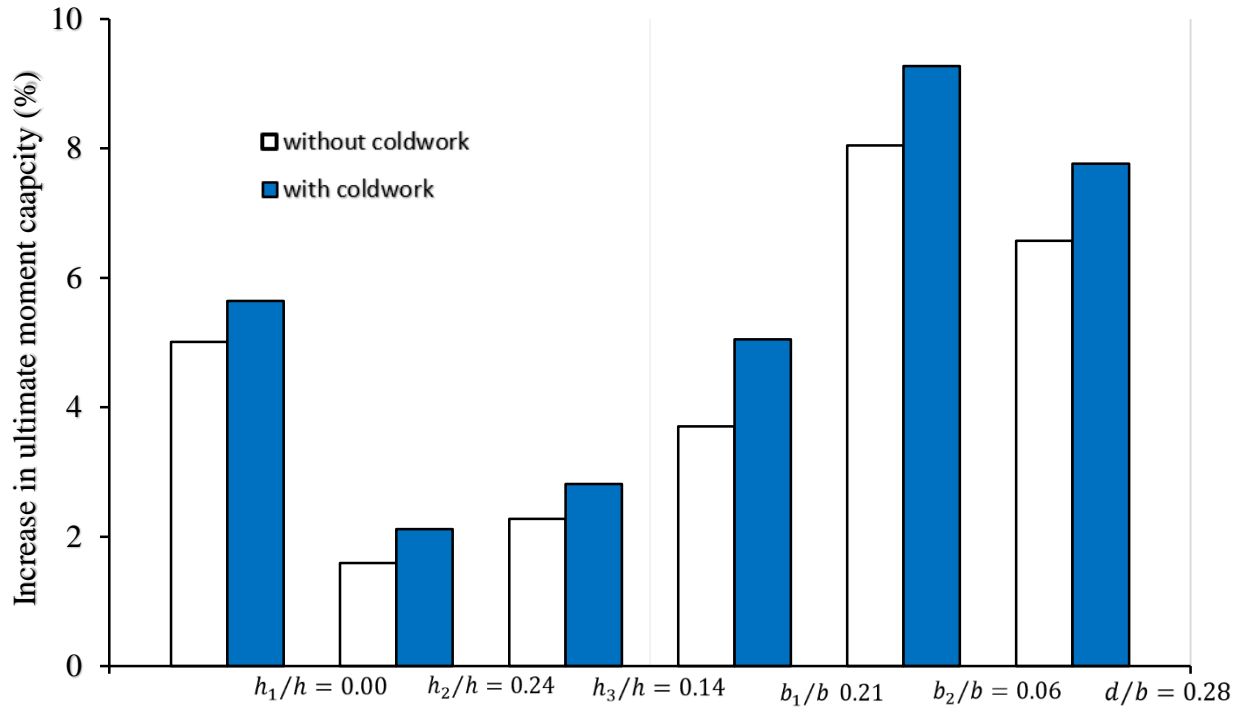


Figure 4.11. The maximum % increase in the ultimate moment capacities without and with the cold work effect, of the channel sections with two web stiffeners and two flange stiffeners, against the geometric parameters.

#### 4.4 Conclusions

This chapter numerically investigated the effect of both the stiffeners' geometry and cold work on the buckling and ultimate bending strength of channel sections with longitudinal web and flange stiffeners. Numerical simulations using Finite Element analysis and design calculations using the Direct Strength Method were developed, which were presented in chapter 3, to replicate four-point bending tests of the channel sections. An optimal shape of the channel section was then achieved through a comprehensive parametric study of all geometric parameters of the stiffeners and their maximum positive effects on the section strengths. The goal was to find the optimum position, shape and size of web stiffeners as well as the position and size of flange stiffeners while considering the influence of cold work in the section corners and stiffeners' bends; this aimed to ultimately enhance the distortional buckling and ultimate strength capacities of the channel sections while keeping the same amount of material and the same height of the sections as required by practical applications. A total of 72 combinations of FE and

DSM analyses was performed and results of ultimate moment capacities, without and with the cold work effect, for different stiffeners' shapes, sizes, positions and the cold work effect on the section's distortional buckling moment capacities were obtained. The results obtained from FE analysis and DSM were compared and evaluated on the capability of modelling the buckling and ultimate strengths of the sections, considering the cold work effect from the cold roll forming process. Based on the results, the following conclusions could be drawn:

- The extent of strength benefit obtained by including variation of stiffeners' position, shape, size and quantity, and the cold work effect induced from the cold roll manufacturing process was found to be dependent on the cross-section shape, the percentage area of the section corners and stiffeners' bends and the distortional buckling slenderness. The lower the distortional buckling slenderness the greater the tendency for the section strength to be influenced by the cold work effect. For the same percentage area of the corners and bends, the sections with lower distortional buckling slenderness gained more strength benefit from the cold work effect.
- The buckling and ultimate strength capacity of the section were changed by moving the position of the web and flange stiffeners. The stiffener's position provided the maximum buckling and ultimate strength capacity at the compression flange was found to be near the web- flange-junction, whereas the stiffener's position at the web was found to be dependent on the shape and size of the stiffeners. The following changes also increased the section's ultimate strength capacity: moving up the web stiffeners towards the web-flange junction; expanding the depth of the web stiffeners beyond a certain value; moving the peak of the web stiffeners towards the cross-section centre in vertical direction; expanding the width of the web stiffeners to a certain value in horizontal direction away from the web; moving the flange stiffeners towards the web-flange junction; increasing the size of the flange stiffeners to a certain value; and allocating two web stiffeners and two flange stiffeners for the channel section. For the same value of each parameter, the section's ultimate strength capacity with the cold work effect was generally greater than that of not including the cold work effect.
- It was revealed that in order to achieve the maximum ultimate strength in distortional buckling, considering both the stiffeners' position, shape, size and quantity, and the cold

work effect, an optimal shape for the channel section could have: (i) the position of the web stiffener ( $h_1/h$ ) was placed as much close as possible to the web-flange junction, (ii) the depth of the web stiffener ( $h_2/h$ ) was at least 15% of the section height, (iii) the position of the peak of the web stiffener ( $h_3/h$ ) was at least 14% of the section height, (iv) the width of the web stiffener ( $b_1/b$ ) was of the certain value of 21% of the flange width and not more than that (as the ultimate strength would reduce due to the distortional-global buckling failure), (v) the position of the flange stiffener  $b_2/b$  was placed as much close as possible to the web-flange junction, (vi) the size of the flange stiffener ( $d/b$ ) was of the certain value of 28% of the flange width and not more than that (as the ultimate strength would reduce due to the distortional-global buckling failure), and (vii) the sections needed to have two web stiffeners and two flange stiffeners. In addition, the cold work effect had to be included in the FE models for accurately obtaining enhancement in the ultimate moment capacity of the section. The cold work effect was most significant when changing the width of the web stiffeners and the position of the flange stiffeners, especially in the sections that are less prone to buckling.

- The DSM results were in good agreement with the FE results and followed the same trends in the sections that failed by distortional buckling. However, the DSM was found to predict lesser distortional buckling slenderness in the sections where the tip of web stiffeners shifted away from the web in horizontal direction, and in the sections where the size (diameter) of the flange stiffeners was large. In fact, there were significant reductions of the sectional modulus in the minor axis that caused the sections failed by distortional-global interaction buckling but it was not captured in DSM. These resulted in overestimate predictions for the ultimate moment capacities of the sections. It was, therefore, concluded that a modification in the DSM design guideline for distortional buckling with web intermediate stiffener is needed in the case of cross-sections with large web intermediate stiffeners.



## Chapter 5 Parametric study of longitudinally stiffened CFS zed sections under bending

This chapter is an extension of chapter 4 but focused on parametric study and the structural behaviour of CFS zed sections under bending.

### 5.1 Introduction

A comprehensive parametric study carried out to investigate the influence of both the web and flange stiffeners' positions, shapes, sizes, and enhanced material properties at corners and stiffeners' bends on the section's buckling and ultimate strengths. The FE model developed and validated in chapter 3 was utilised for the parametric study. The number of the parametric studies and their results were arranged in orders so that all the maximum positive effects on the section strengths when changing parameter values were obtained. The zed section together with its bending setup used in the experimental testing in chapter 3 were defined as “reference section”. The section height  $h$ , thickness  $t$ , internal radius  $R$  and lip length  $c$  were fixed in the parametric study. The total length of the zed cross section was kept unchanged for the optimisation target, that was “obtaining maximum strength of the section while maintaining the same weight”. Changes in parameters relating to the stiffeners' shapes, sizes, positions while considering enhanced material properties at corners and bends by the cold work effect resulted in new zed sections. The material properties at the flat regions, corners and at the stiffeners' bends were assumed to be the same in these new sections. In summary, the reference section had an initial imperfection of  $1.55t$ , an elastic modulus  $E$  of 205 GPa, a Poisson's ratio  $\nu$  of 0.3 and the stress-strain data determined in chapter 3 for the flat, corners and stiffener's bends.

### 5.2 Description of investigated section dimensions and parameters

The section without flange stiffeners is shown in Figure 5.1(a), in which all dimension parameters are also shown and the section with flange stiffeners is shown in Figure 5.1(b). The values for  $h$  and  $t$ ,  $R$ , and  $c$  were taken of the reference section as 170.00 mm, 1.60 mm, 3.00 mm

and 14.98 mm, respectively.  $h_1$  is the position of the web stiffener from the web-flange junction,  $h_2$  is the depth of the web stiffener,  $h_3$  is the position of the peak of the web stiffener in vertical direction from the web-flange junction,  $b_1$  is the width of the web stiffener,  $b_2$  is the position of the flange stiffener,  $d$  is the width and depth of the flange stiffener (assuming the flange stiffener had a circular shape),  $R$  is the radius of the section corners and it was assumed that they had the same radius. For the zed section shown in Figure 5.1(a), a total of 58 combinations with and without cold work between  $h_1/h$ ,  $h_2/h$ ,  $h_3/h$  and  $b_1/b$  were considered with  $h_1/h$  varying from 0.02 to 0.21,  $h_2/h$  varying from 0.09 to 0.21,  $h_3/h$  varying from 0.08 to 0.20 and  $b_1/b$  varying from 0.00 to 0.63. The reference section had  $h_1/h = 0.02$ ,  $h_2/h = 0.15$ ,  $h_3/h = 0.14$ , and  $b_1/b = 0.15$ . Hence, the buckling, ultimate moment capacity with and without cold work for each change were obtained and compared.

For the zed section shown in Figure 5.1(b), the position of flange intermediate stiffener  $b_2$ , size of flange intermediate stiffener  $d$  and flange width  $b$  were changed. A total of 20 combinations with and without cold work between  $b_2/b$  and  $d/b$  were considered with  $b_2/b$  varying from 0.09 to 0.73 and  $d/b$  varying from 0.09 to 0.47. In total, 78 combinations with and without cold work effect were generated through FE models, for different positions  $h_1/h$ , different shapes  $h_2/h$  and  $h_3/h$ , and different sizes  $b_1/b$  of the web stiffeners as well as different positions  $b_2/b$  and different sizes  $d/b$  of the flange stiffeners. Hence, the buckling, ultimate moment capacity with and without cold work for each change were obtained and compared to evaluate the effect of these changes.

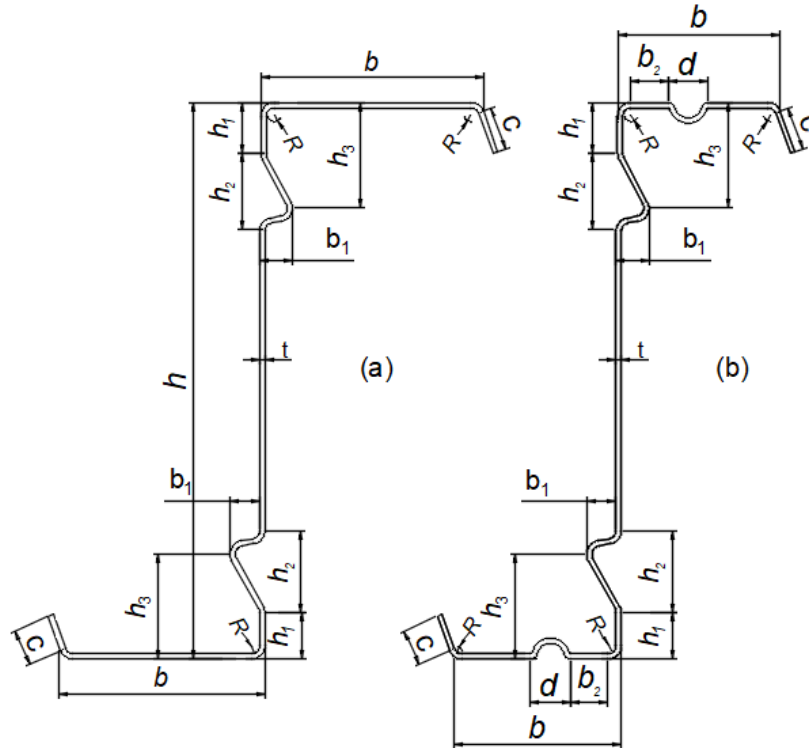


Figure 5.1. Dimension parameters of the zed cross section (a) without flange stiffeners, and (b) with flange stiffeners.

### 5.3 Parametric study and optimisation results

This section presents the results of investigating the influence of both the web and flange intermediate stiffeners' positions, shapes, sizes and cold work effect at corners and stiffeners' bends on the section ultimate strengths.

#### 5.3.1 Effect of the position of the web stiffener $h_1/h$

Figure 5.2 shows a graph of variation of the dimensionless ultimate bending moment capacities obtained by FE analysis  $M/M_y$  with variation of the stiffener position on the web  $h_1/h$ . In which  $M_y$  is the yield bending moment of the whole cross section and when the cold work effect is not included  $M$  equals  $M_u$ , when the cold work effect is included  $M$  equals  $M_{uc}$ . The results obtained by DSM are also presented for comparison. Moving down the stiffeners towards the centre of the

cross section was the same with increasing  $h_1/h$ . The detailed values are shown in Table 5.1. For this first parameter, the stress distributions on the sections without and with the cold work effect are made available for use in discussions, as shown in Figure 5.3.

For the same value of  $h_1/h$ ,  $M_{uc}$  was generally greater than  $M_u$ , as also reflected in the greater stresses developed in the sections with the cold work effect (Figure 5.3), indicating the cold work effect on ultimate bending strength of the section, despite the insignificant increase for some values of  $h_1/h$ . For different values of  $h_1/h$ , it was found that the ultimate bending moments  $M_u$  and  $M_{uc}$  reduced by increasing the ratio  $h_1/h$ . The maximum reduction in flexural strength resistance was 5% and 7% for the ultimate moment without cold work and with the cold work effect, respectively. When increasing  $h_1/h$ , it generated new cross sections with a reduction in the section modulus: the sectional modulus  $S_{xx}$  decreased from 28.22 cm<sup>3</sup> for  $h_1/h = 0.00$  to 27.24 cm<sup>3</sup> for  $h_1/h = 0.21$ , as shown in Table 5.1, and this led to a decrease in the ultimate bending moment. Although the new cross sections had a decrease in the buckling distortional slenderness: the distortional buckling slenderness  $\lambda_d$  decreased from 1.281 for  $h_1/h = 0.00$  to 1.246 for  $h_1/h = 0.21$  as illustrated in Table 5.1, this still led to a decrease in the ultimate bending moment. In combination, the ultimate bending moment gradually reduced when increasing the ratio  $h_1/h$  due to a product of the decreasing effect by the buckling slenderness  $\lambda_d$  and the decreasing effect of the sectional modulus  $S_{xx}$ . Therefore, increasing the ratio  $h_1/h$  ultimately reduced the ultimate bending moments  $M_u$  and  $M_{uc}$ , and dimensionless values  $M_u/M_y$  and  $M_{uc}/M_y$ , as illustrated in Figure 5.2. This suggested that if the stiffeners were placed on the web close to the flange, the ultimate bending strengths of the section would increase, and maximum strength could be obtained for this case.

The ultimate bending moments  $M_u$  and  $M_{uc}$  obtained by the DSM had the same trends with the FE results that increasing the ratio  $h_1/h$  reduced  $M_u$  and  $M_{uc}$ , with a clear gap between them, as shown in Figure 5.2. This was due to the assumption of using an average enhanced yield stress for the entire section to take into account the cold work effect, which might not entirely realistic but clearly showed the trend. However, for the same value of  $h_1/h$ , the values obtained by the DSM were smaller than those of the FE analysis with a maximum difference of 14% for both the ultimate bending moments, without the cold work effect and with the cold work effect. It should be noted that the DSM's ultimate bending moments  $M_u$  and  $M_{uc}$  were obtained from the semi-

empirical formulae which were derived based on an extensive amount of testing has been performed on laterally braced beams with geometric limitations for zed sections. In addition, the zed sections with intermediate stiffeners used in this study did not specify having pre-qualified for use with the DSM, and the assumption of using an average enhanced yield stress for the entire section to take into account the cold work effect was very approximate. Therefore, the ultimate bending moments  $M_u$  and  $M_{uc}$  obtained by the DSM were approximate values whilst those obtained by the FE analysis could be more accurate and insightful of the section behaviour and the cold work effect.

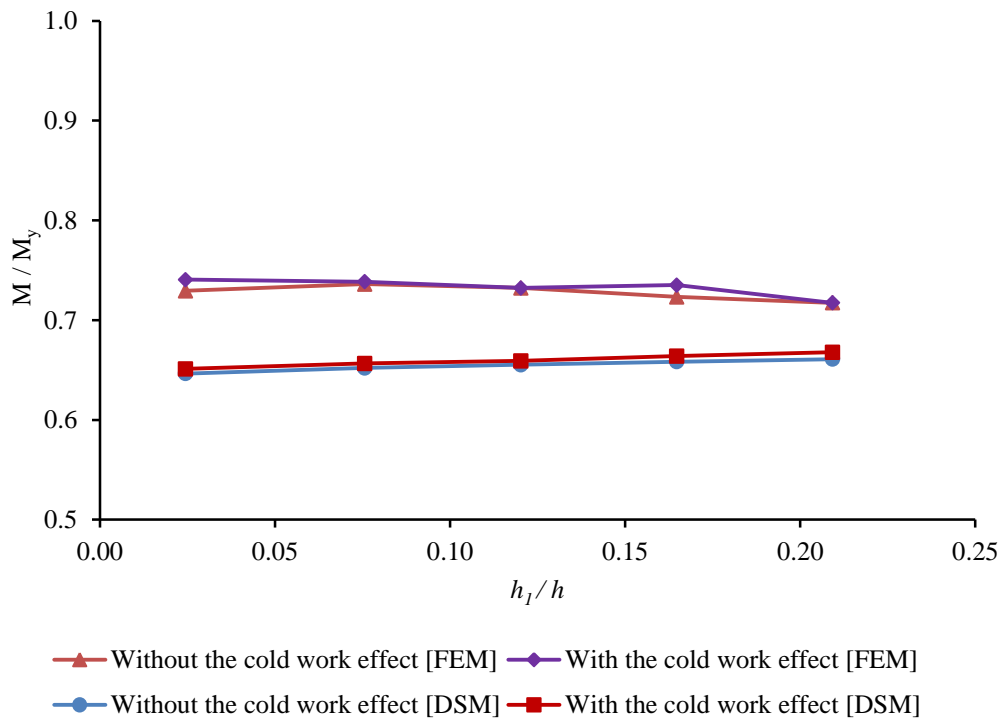


Figure 5.2. Variation in the ultimate moment capacity for different positions of web stiffeners  $h_1/h$  without the cold work effect and with the cold work effect.

**Table 5.1** Variation in ultimate bending moment capacity for different positions of web stiffeners.  $M_u$ ,  $M_{uc}$  stand for ultimate moment capacity without and with the cold work effect, respectively.  $f_{ya}$  is the average yield strength of the whole section.

$h_1/h$	Section properties		DSM					FEM			$\frac{M_u^{FEM}}{M_u^{DSM}}$	$\frac{M_{uc}^{FEM}}{M_{uc}^{DSM}}$
	$S_{xx}$ (cm <sup>3</sup> )	$\lambda_d$	$M_y$ (kNm)	$M_{yc}$ (kNm)	$M_u$ (kNm)	$M_{uc}$ (kNm)	$M_{uc}/M_u$	$M_u$ (kNm)	$M_{uc}$ (kNm)	$M_{uc}/M_u$		
0.02	28.22	1.281	14.68	15.05	9.49	9.56	1.01	10.71	10.87	1.02	1.13	1.14
0.08	27.89	1.267	14.50	14.88	9.46	9.52	1.01	10.67	10.71	1.00	1.13	1.12
0.12	27.64	1.196	14.37	14.74	9.42	9.47	1.01	10.52	10.52	1.00	1.12	1.11
0.16	27.42	1.251	14.26	14.63	9.39	9.47	1.01	10.32	10.48	1.02	1.10	1.11
0.21	27.24	1.246	14.17	14.53	9.36	9.46	1.01	10.17	10.17	1.00	1.09	1.07

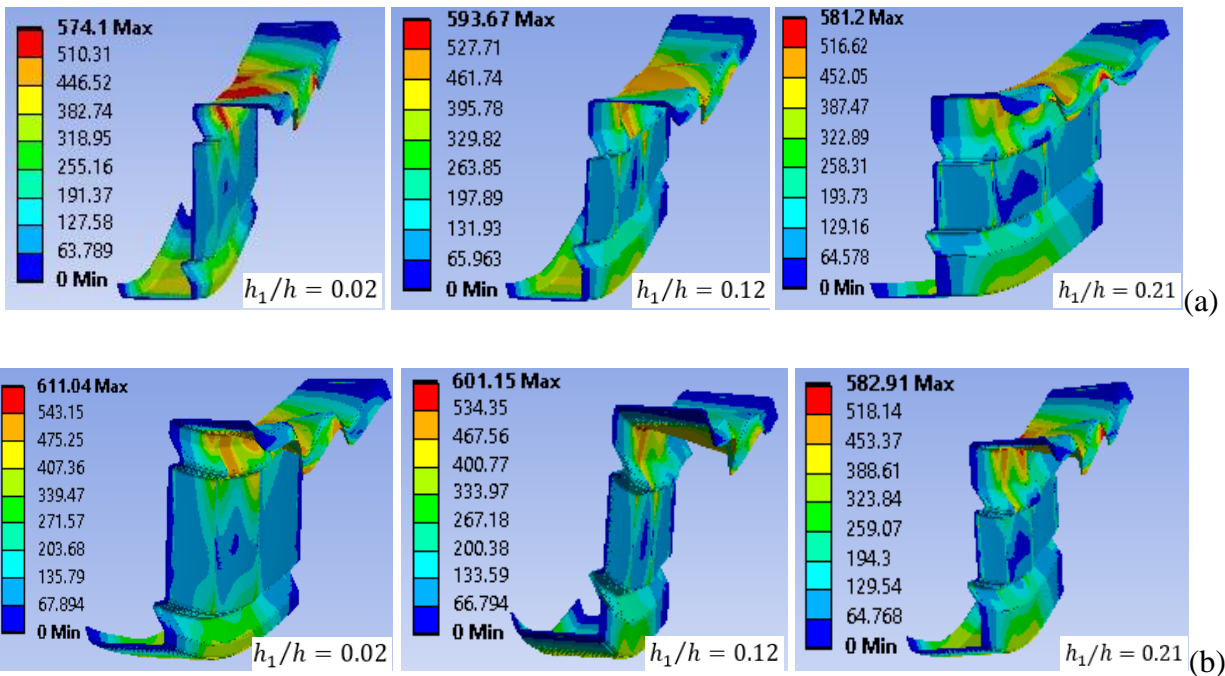


Figure 5.3. Von Mises stress distribution at failure for different web stiffener positions (a) without the cold work effect and (b) with the cold work effect.

### 5.3.2 Effect of the depth of the web stiffener $h_2/h$

Figure 5.4 shows the variation of  $M_u/M_y$  and  $M_{uc}/M_y$  with the variation of the web stiffener's depth  $h_2/h$ . The  $M_u/M_y$  and  $M_{uc}/M_y$  values obtained by DSM are also presented for comparison. The detailed values are shown in Table 5.2.

For the same value of  $h_2/h$ ,  $M_{uc}$  was generally greater than  $M_u$ , confirming the cold work effect on enhancing the section's ultimate bending strength. However, there were small effects at some values of  $h_2/h$  with a maximum difference of 6%, especially it was insignificant with  $h_2/h$  from 0.18 to 0.21. When increasing  $h_2/h$  from 0.09 to 0.15, the ultimate bending moment  $M_u$  and  $M_{uc}$  reduced. It was because the distortional buckling slenderness  $\lambda_d$  increased from 1.176 to 1.281 as illustrated in Table 5.2, and this induced a decrease in the ultimate bending moment. At the same time, the ultimate bending moment decreased due to an decrease in the sectional modulus  $S_{xx}$ , the decreasing effect by the buckling slenderness  $\lambda_d$  was more significant. When increasing  $h_2/h$  from 0.15 to 0.21,  $S_{xx}$  decreased from 28.22 cm<sup>3</sup> to 27.99 cm<sup>3</sup>, as shown in Table 5.2, and this led to a decrease in the ultimate bending moment. In addition,  $\lambda_d$  slightly decreased from 1.281 to 1.265, and this also led to a decrease in the ultimate bending moment, as can be seen in Table 5 and in Figure 5.4 for  $M_u/M_y$  and  $M_{uc}/M_y$ . The maximum ultimate bending moment increased by the cold work effect was about 2% at  $h_2/h = 0.09$ . The results obtained by the DSM had the same trends with the FE results when increasing the ratio  $h_2/h$ , with a maximum difference of 16%. It is therefore suggested that the web stiffener to have a depth similar that of the reference section in order to obtain greater bending moment capacity.

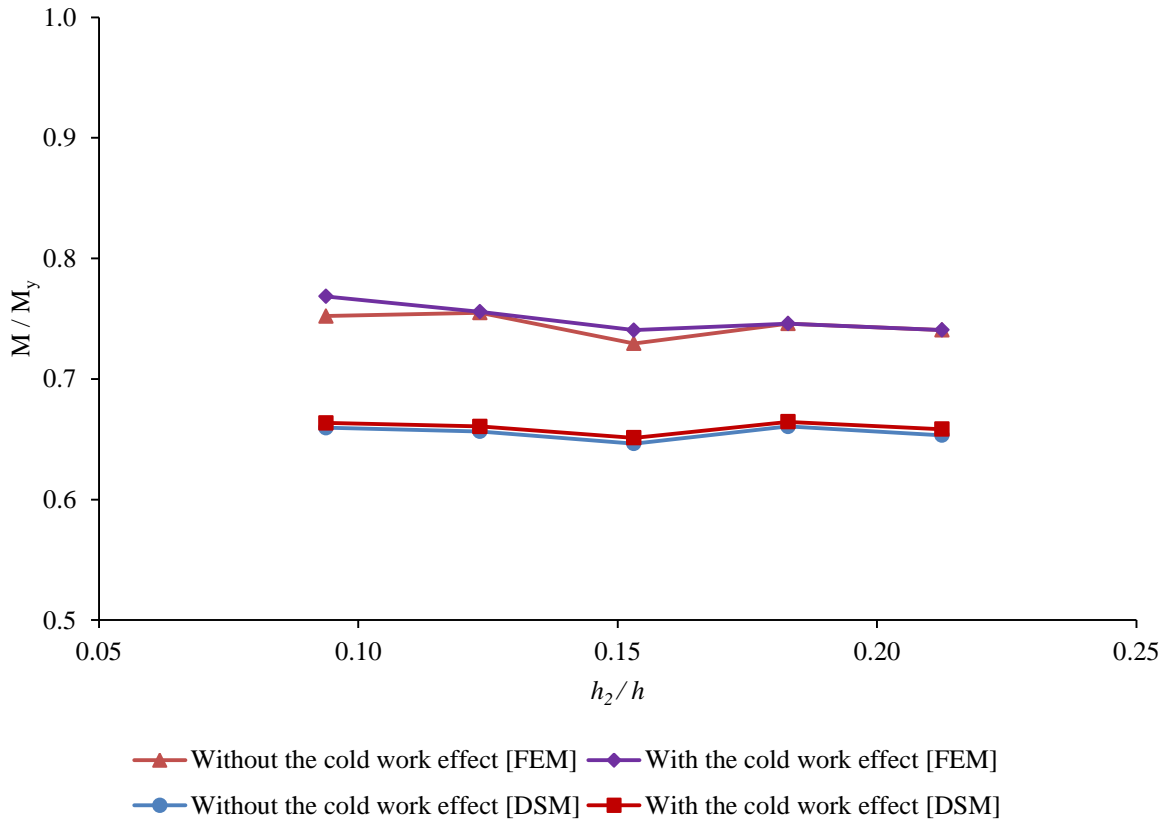


Figure 5.4. Variation in the ultimate moment capacity for different shapes of web stiffeners  $h_2/h$  without and with the cold work effect.

**Table 5.2** Variation in ultimate bending moment capacity for different depths of the web stiffener.

$h_2/h$	Section properties		DSM					FEM			$\frac{M_u^{FEM}}{M_u^{DSM}}$	$\frac{M_{uc}^{FEM}}{M_{uc}^{DSM}}$
	$S_{xx}$ (cm <sup>3</sup> )	$\lambda_d$	$M_y$ (kNm)	$M_{yc}$ (kNm)	$M_u$ (kNm)	$M_{uc}$ (kNm)	$M_{uc}/M_u$	$M_u$ (kNm)	$M_{uc}$ (kNm)	$M_{uc}/M_u$		
0.09	28.49	1.276	14.81	15.19	9.77	9.83	1.01	11.14	11.38	1.02	1.14	1.16
0.12	28.35	1.257	14.74	15.12	9.68	9.74	1.01	11.13	11.14	1.00	1.15	1.14
0.15	28.22	1.281	14.68	15.05	9.49	9.56	1.01	10.71	10.87	1.02	1.13	1.14
0.18	28.10	1.247	14.61	14.99	9.65	9.71	1.01	10.90	10.90	1.00	1.13	1.12
0.21	27.99	1.265	14.55	14.93	9.51	9.58	1.01	10.78	10.78	1.00	1.13	1.13



### 5.3.3 Effect of the position of the peak of the web stiffener $h_3/h$

Figure 5.5 shows the variation of  $M_u/M_y$  and  $M_{uc}/M_y$  with the variation of the web stiffener's peak  $h_3/h$  in the vertical direction. Moving down the stiffener's peak away from web-flange junction of the section was the same with increasing  $h_3/h$ . The  $M_u/M_y$  and  $M_{uc}/M_y$  values obtained by DSM are also presented for comparison. The detailed values are shown in Table 5.3.

For the same value of  $h_3/h$ ,  $M_{uc}$  was greater than  $M_u$  with a maximum increase of 2%, confirming the cold work effect on enhancing the section's ultimate bending strength. When increasing  $h_3/h$ , from 0.08 to 0.20, the ultimate bending moment  $M_u$  and  $M_{uc}$  increased and the rate of increasing was significantly increased for  $h_3/h$ , from 0.17 to 0.20. It was found that even though increasing  $h_3/h$  reduced sectional modulus (i.e.  $S_{xx}$  reduced from 28.62 cm<sup>3</sup> to 25.56 cm<sup>3</sup>), the ultimate moment capacity increased due to significant reduction in distortional buckling slenderness of the sections (i.e.  $\lambda_d$  reduced from 1.265 to 1.093), as shown in Table 5.3. The ultimate bending moments  $M_u$  and  $M_{uc}$  obtained by the DSM had the same trends with the FE results, as shown in Figure 5.5 and Table 5.3. However, for the same value of  $h_3/h$ , the values for both the ultimate bending moments, without the cold work effect and with the cold work effect, obtained by the DSM were smaller than those of the FE analysis with a maximum difference of 18%. The reasons were explained previously. It is therefore recommended that the web stiffener's peak should be placed away from the web-flange junction in vertical direction in order to have significant strength enhancement in this case.

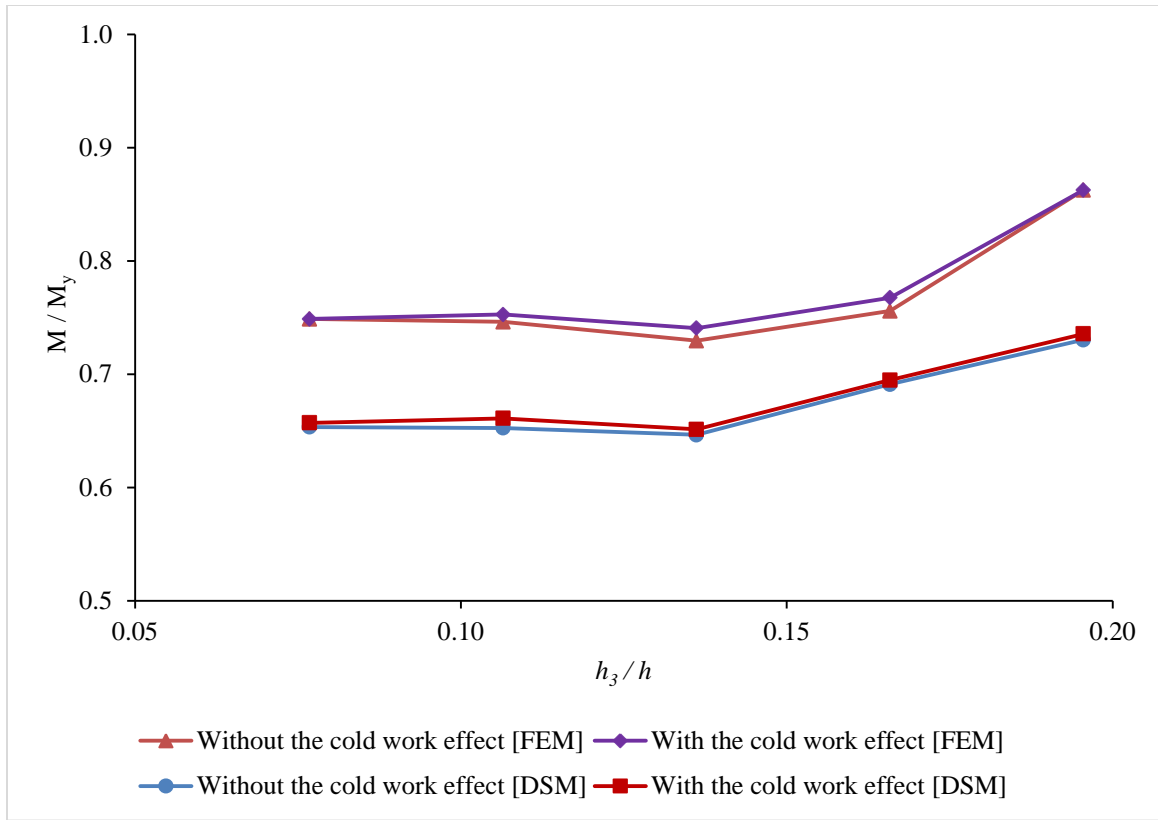


Figure 5.5. Variation in the ultimate moment capacity for different positions of the web stiffener's peak in vertical direction  $h_3/h$  without the cold work effect and with the cold work effect.

**Table 5.3** Variation in ultimate bending moment capacity for different positions of the web stiffener's peak in vertical direction.

$h_3/h$	Section properties		DSM					FEM			$\frac{M_u^{FEM}}{M_u^{DSM}}$	$\frac{M_{uc}^{FEM}}{M_{uc}^{DSM}}$
	$S_{xx}$ (cm <sup>3</sup> )	$\lambda_d$	$M_y$ (kNm)	$M_{yc}$ (kNm)	$M_u$ (kNm)	$M_{uc}$ (kNm)	$M_{uc}/M_u$	$M_u$ (kNm)	$M_{uc}$ (kNm)	$M_{uc}/M_u$		
0.08	28.62	1.265	14.88	15.27	9.72	9.78	1.01	11.14	11.14	1.00	1.15	1.14
0.11	28.21	1.266	14.67	15.04	9.57	9.70	1.01	10.95	11.04	1.01	1.14	1.14
0.14	28.22	1.281	14.68	15.05	9.49	9.56	1.01	10.71	10.87	1.02	1.13	1.14
0.17	27.14	1.171	14.17	14.64	9.79	9.84	1.01	10.71	10.88	1.02	1.09	1.10
0.20	25.56	1.093	13.29	13.63	9.71	9.78	1.01	11.46	11.46	1.00	1.18	1.17

### 5.3.4 Effect of the width of the web stiffener $b_1/b$

The variation of the dimensionless ultimate bending moment capacities obtained by FE analysis, without the cold work effect  $M_u/M_y$  and with the cold work effect  $M_{uc}/M_y$ , with variation of the width of the web stiffener  $b_1/b$  is shown in Figure 5.6. Increasing  $b_1/b$  was the same with moving the stiffener's peak away from web in horizontal direction. The  $M_u/M_y$  and  $M_{uc}/M_y$  values obtained by DSM are also presented. The detailed values are shown in Table 5.4.

With the same value of  $b_1/b$ ,  $M_{uc}$  was generally greater than  $M_u$  but the enhancement was very small when  $b_1/b$  was less than 0.07 but was noticeable when  $b_1/b$  increased from 0.07 to 0.42 with a maximum increase of 2%. These were associated with an increase in the stresses in the sections or a decrease in sectional moduli, with a maximum increase of 10% for  $b_1/b = 0.42$ , as can be seen in Table 5.4. Overall, the ultimate moment capacity increased up to certain limit but beyond that the ultimate moment capacity was reduced and the maximum change was 17% and 19% for the ultimate moment without the cold work effect and with the cold work effect, respectively. Detailed values of the ultimate bending moments  $M_u$  and  $M_{uc}$  for different types of sections with different values of  $b_1/b$  are also displayed in bar charts in Figure 5.7. It was observed that  $M_u$  and  $M_{uc}$  increased when the values of  $b_1/b$  increased from 0.00 to 0.42.

When  $b_1/b$  increased from 0.42 to 0.63, however, the FE results showed that sections failed in distortional-global interactive buckling modes as the ultimate bending moment capacities  $M_u$  and  $M_{uc}$  decreased. This reflected through the decreasing values of  $M_u$  and  $M_{uc}$  as shown in Table 5.4 and Figure 5.6. It means that, for this particular range of  $b_1/b$ , the practical bracing length of 900 mm was not sufficient to exhibit pure distortional buckling modes in the sections. It was because the FE results showed that when values of  $b_1/b$  increased from 0.42 to 0.49, 0.539 and 0.63, the significant reduction of the sectional modulus  $S_{zz}$  in the minor axis by 70% (i.e.  $S_{zz}$  reduced significantly from 8.32 cm<sup>3</sup> for  $b_1/b = 0.00$  to 4.10 cm<sup>3</sup> for  $b_1/b = 0.42$ ). The noticeable reduction in  $S_{zz}$  from  $b_1/b = 0.42$  could make the sections prone to fail by lateral/global buckling. These clearly indicated the distortional-global buckling interactive failure and consequently led to lower ultimate moment capacities for the beam sections, as confirmed by the FE results shown in Figure 5.6.

For the values of  $b_1/b$  from 0.00 to 0.42, the ultimate bending moments  $M_u$  and  $M_{uc}$  obtained by the DSM had the same trends with the FE results. However, when  $b_1/b$  increased from 0.42 to 0.49, the DSM results showed an increase in the bending moment capacities as shown in Figure 5.6 as they were based on the critical distortional buckling half-wave lengths. when  $b_1/b$  increased from 0.49 to 0.63, both the FEM and the DSM results showed a decrease in the bending moment capacities as shown in Figure 5.6 as they were based on the effective length of the beam (i.e. the distance between the bracings in the moment span = 900 mm was used). . However, for the same value of  $b_1/b$ ,  $M_u$  and  $M_{uc}$  values obtained by the DSM were less than those of the FE analysis with a maximum difference of 12%.

It is therefore suggested that the web stiffener's peak should be placed further away from the web in horizontal direction to a certain position (up to 40% of the section width) in order to have significant strength enhancement, including the case of the cold work effect.

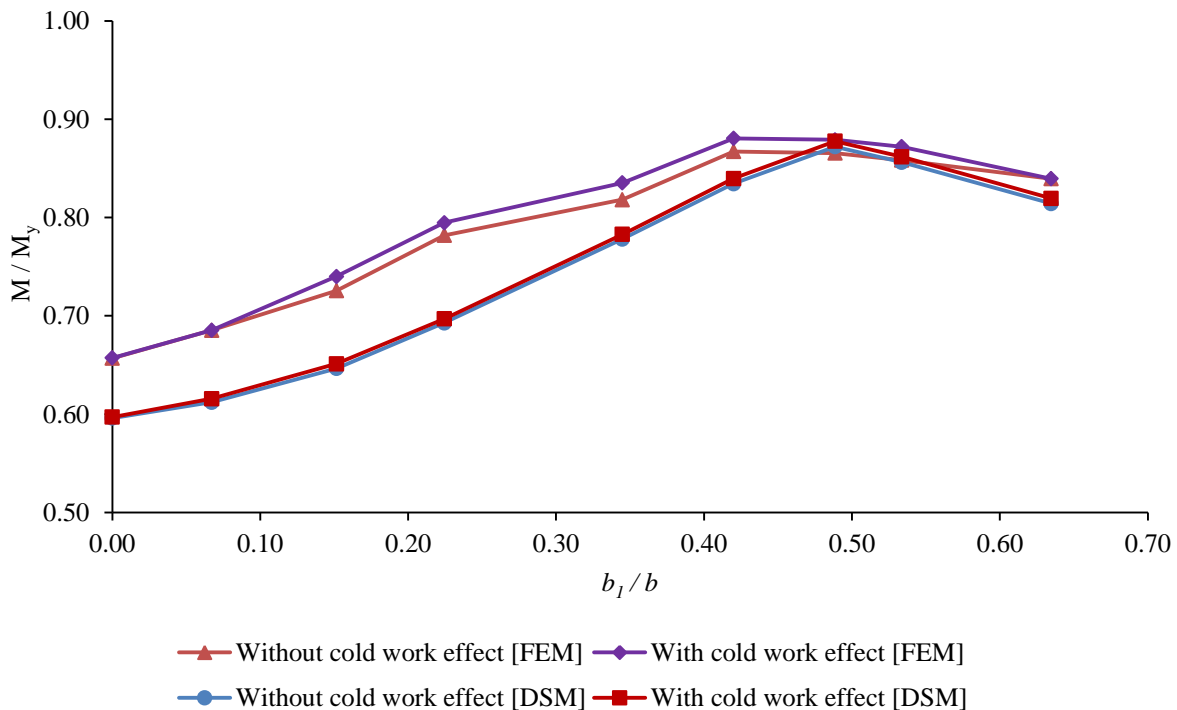


Figure 5.6. Variation in ultimate moment capacity for different widths of the web stiffener  $b_1/b$  of web stiffeners without the cold work effect and with the cold work effect.

**Table 5.4** Variation in ultimate bending moment capacity for different widths of the web stiffeners.

$b_1/b$	Section properties		DSM					FEM			$\frac{M_u^{FEM}}{M_u^{DSM}}$	$\frac{M_{uc}^{FEM}}{M_{uc}^{DSM}}$
	$S_{xx}$ (cm <sup>2</sup> )	$\lambda_d$	$M_y$ (kNm)	$M_{yc}$ (kNm)	$M_u$ (kNm)	$M_{uc}$ (kNm)	$M_{uc}/M_u$	$M_u$ (kNm)	$M_{uc}$ (kNm)	$M_{uc}/M_u$		
0.00	29.21	1.417	15.19	15.33	9.06	9.07	1.00	9.98	9.98	1.00	1.10	1.10
0.07	28.95	1.371	15.05	15.44	9.21	9.27	1.01	10.32	10.32	1.00	1.12	1.11
0.15	28.22	1.281	14.68	15.05	9.49	9.56	1.01	10.65	10.86	1.02	1.12	1.14
0.22	27.85	1.172	14.48	14.85	10.03	10.09	1.01	11.32	11.51	1.02	1.13	1.14
0.34	26.81	1.004	13.94	14.30	10.85	10.91	1.01	11.41	11.64	1.02	1.05	1.07
0.42	26.44	0.928	13.55	13.90	11.31	11.38	1.01	11.75	11.93	1.02	1.04	1.05
0.49	26.05	0.850	13.55	13.90	11.82	11.89	1.01	11.73	11.91	1.02	0.99	1.00
0.53	25.87	0.812	13.45	13.45	11.52	11.59	1.01	11.54	11.73	1.02	1.00	1.01
0.63	25.49	0.750	13.25	13.25	10.79	10.86	1.01	11.12	11.12	1.00	1.03	1.02

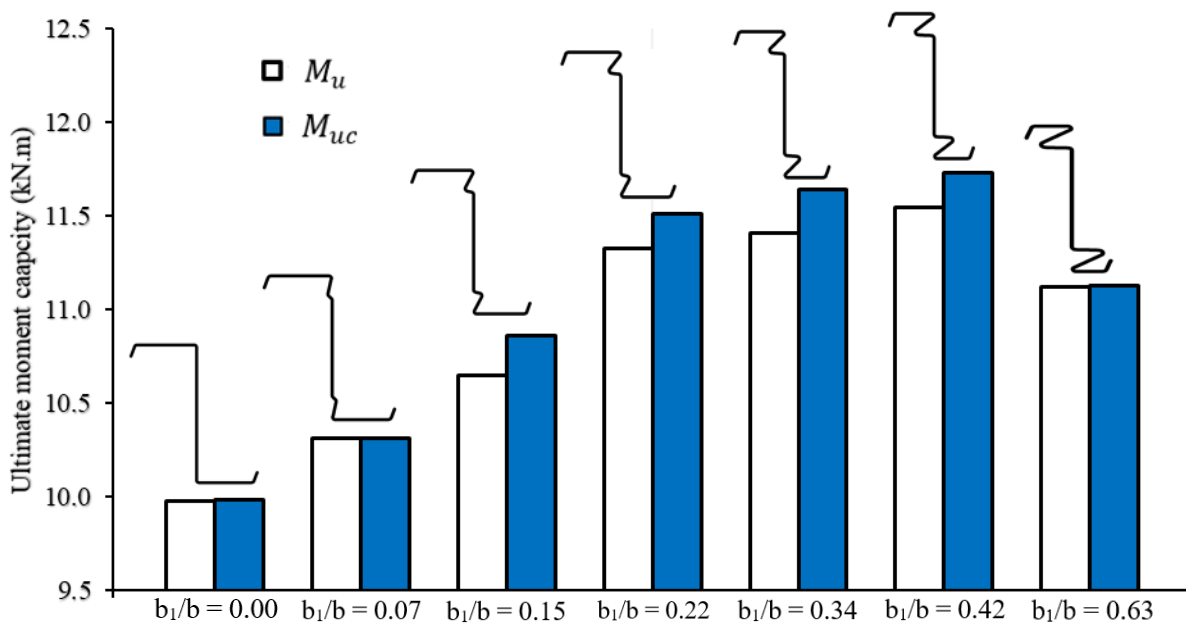


Figure 5.7. Comparison of the ultimate bending moment capacity for different widths of the web stiffeners (when  $b_1/b = 0.53$  and  $0.63$  the sections failed in distortional-global interactive buckling modes).

### 5.3.5 Effect of the position of the flange stiffeners $b_2/b$

Figure 5.8 shows the variation of  $M_u/M_y$  and  $M_{uc}/M_y$  with the variation of the position of the flange stiffener. Moving the flange stiffeners away from web-flange junction of the section was the same with increasing  $b_2/b$ . The  $M_u/M_y$  and  $M_{uc}/M_y$  values obtained by DSM are also presented for comparison. The detailed values are shown in Table 5.5.

With the same value of  $b_2/b$ ,  $M_{uc}$  was greater than  $M_u$  with a maximum increase of 1%. When increasing  $b_2/b$ , from 0.09 to 0.73, the ultimate bending moment  $M_u$  and  $M_{uc}$  decreased and the rate of decreasing was not significant with  $b_2/b$  from 0.09 to 0.22, but was significant with  $b_2/b$  from 0.22 to 0.73. It was observed that within the range of  $b_2/b = 0.09$  to 0.73, the sections failed by distortional buckling modes. Values of  $M_u$  and  $M_{uc}$  obtained by the DSM had the same trends with the FE results. This was due to the increase in the distortional buckling slenderness of the sections (i.e. values of  $\lambda_d$  increased from 1.162 for  $b_2/b = 0.09$  to 1.261 for  $b_2/b = 0.73$ ) whilst the sectional modulus was unchanged (i.e. values of  $S_{xx}$  were the same for all the sections) as shown in Table 5.5. The increase in the distortional buckling slenderness had an inverse effect that reduced the ultimate moment capacity of the sections. It was finally concluded that in the sections with flange stiffeners, distortional buckling failure was more severe when the flange stiffeners shifted away in horizontal direction from the web-flange junction. It is, therefore, suggested that the flange stiffeners need to be placed near the web-flange junction in order to gain maximum bending strength capacity.

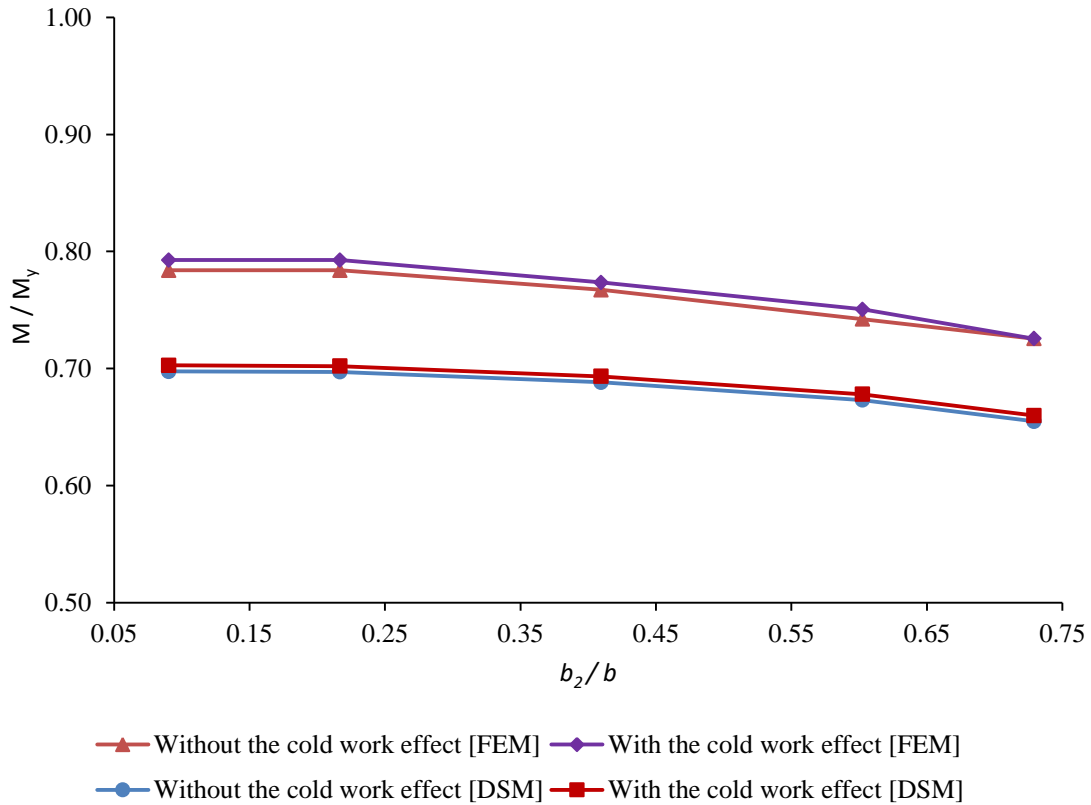


Figure 5.8. Variation in ultimate moment capacity for different positions of flange stiffeners  $b_2/b$  without the cold work effect and with the cold work effect.

**Table 5.5** Variation in ultimate bending moment capacity for different positions of flange-intermediate stiffeners.

$b_2/b$	Section properties		DSM					FEM			$\frac{M_u^{FEM}}{M_u^{DSM}}$	$\frac{M_{uc}^{FEM}}{M_{uc}^{DSM}}$
	$S_{xx}$ (cm <sup>3</sup> )	$\lambda_d$	$M_y$ (kNm)	$M_{yc}$ (kNm)	$M_u$ (kNm)	$M_{uc}$ (kNm)	$M_{uc}/M_u$	$M_u$ (kNm)	$M_{uc}$ (kNm)	$M_{uc}/M_u$		
0.09	27.93	1.162	14.52	15.09	10.13	10.20	1.01	11.38	11.51	1.01	1.12	1.13
0.22	27.93	1.163	14.52	15.09	10.12	10.19	1.01	11.38	11.51	1.01	1.12	1.13
0.41	27.93	1.183	14.52	15.09	9.99	10.07	1.01	11.14	11.23	1.01	1.11	1.12
0.60	27.93	1.217	14.52	15.09	9.77	9.84	1.01	10.78	10.90	1.01	1.10	1.11
0.73	27.93	1.261	14.52	15.09	9.51	9.58	1.01	10.54	10.54	1.00	1.11	1.10

### 5.3.6 Effect of the size of the flange stiffeners $d/b$

Figure 5.9 shows the influence of changing the size of the flange stiffeners  $d/b$  on the dimensionless ultimate moment capacity  $M_u/M_y$  and  $M_{uc}/M_y$  of the sections. The  $M_u/M_y$  and  $M_{uc}/M_y$  values obtained by DSM are also presented for comparison. The detailed values are shown in Table 5.6.

With the same value of  $d/b$ ,  $M_{uc}$  was significantly greater than  $M_u$  with a maximum increase of 2%. The ultimate moment capacity increased when values of  $d/b$  increased up to certain limit ( $d/b \approx 0.40$ ) beyond which it was slightly increased. The maximum change in the ultimate moment capacity, for changes in the size of the flange stiffeners, was 87% and 10% in the cases of without the cold work and with the cold work effect, respectively. It was observed that the ultimate moment capacities  $M_u$  and  $M_{uc}$  increased up to certain values because the distortional buckling slenderness  $\lambda_d$  reduced significantly when  $d/b$  increased up to a certain limit ( $d/b = 0.40$ ). Even though the sectional modulus in the major axis  $S_{xx}$  and minor axis  $S_{zz}$  reduced that could reduce the ultimate moment capacities, the influence of the distortional buckling slenderness  $\lambda_d$  on the ultimate moment capacities were more significant. However, beyond the limit of  $d/b = 0.40$ , the ultimate moment capacities slightly increased because of the significant reduction of section modulus in the minor axis  $S_{zz}$  (i.e.  $S_{zz}$  reduced significantly from 7.30 cm<sup>3</sup> for  $d/b = 0.09$  to 6.04 cm<sup>3</sup> for  $d/b = 0.47$ , which was about 20% in reduction). The reduction in the sectional modulus in the minor axis  $S_{zz}$  caused the sections with values of  $d/b$  greater than 0.40 to fail by distortional-global buckling interaction and that reduced the ultimate moment capacities. This phenomenon was already discussed with FE models and results in Section 5.3.4. The DSM predicted the same trends with FE results for the ultimate moment capacities. It is therefore suggested that the flange stiffeners should have an increasing diameter up to a certain size (up to 40% of the section width) in order to have maximum bending strength, including the case of the cold work effect. It is also suggested that design guidelines for distortional-global interaction buckling modes need to be included in the DSM procedure.



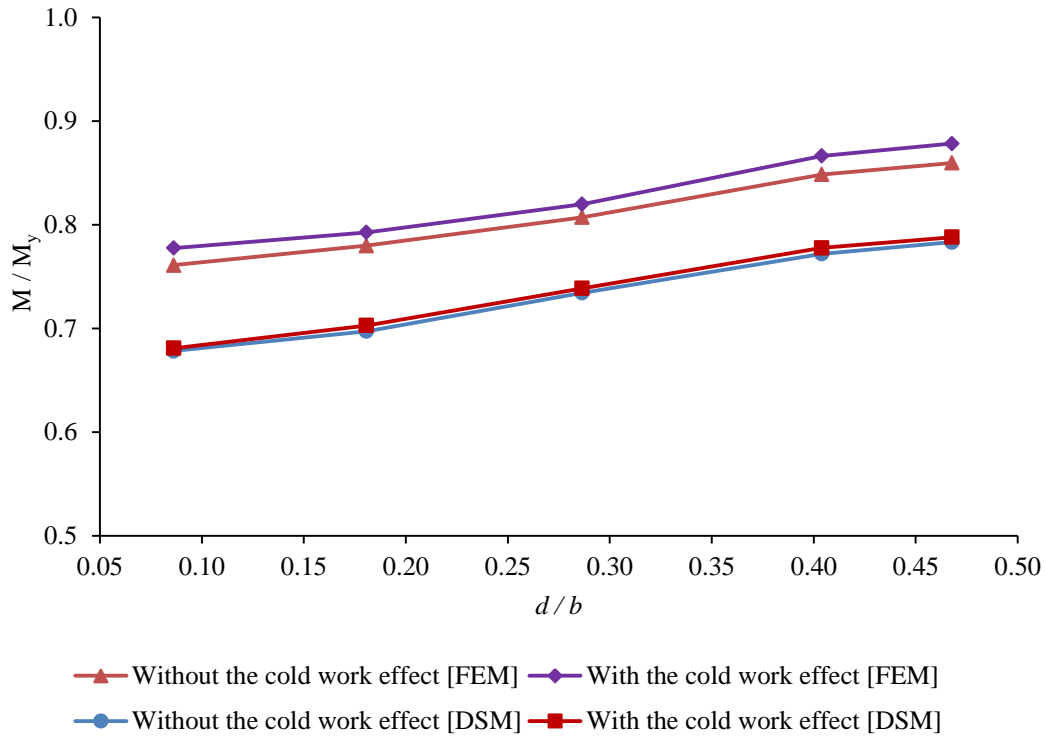


Figure 5.9. Variation in ultimate moment capacity for different sizes of flange stiffeners without the cold work effect and with the cold work effect.

**Table 5.6** Variation in ultimate moment capacity for different sizes of flange stiffeners.

d/b	Section properties		DSM					FEM			$\frac{M_u^{FEM}}{M_u^{DSM}}$	$\frac{M_{uc}^{FEM}}{M_{uc}^{DSM}}$
	$S_{xx}$ (cm <sup>2</sup> )	$\lambda_d$	$M_y$ (kNm)	$M_{yc}$ (kNm)	$M_u$ (kNm)	$M_{uc}$ (kNm)	$M_{uc}/M_u$	$M_u$ (kNm)	$M_{uc}$ (kNm)	$M_{uc}/M_u$		
0.09	28.15	1.205	14.64	15.20	9.93	9.97	1.00	11.14	11.38	1.02	1.12	1.14
0.18	27.93	1.164	14.52	14.61	10.12	10.20	1.01	11.32	11.51	1.02	1.12	1.13
0.29	27.55	1.129	14.33	14.61	10.52	10.58	1.01	11.57	11.75	1.02	1.10	1.11
0.40	27.03	1.019	14.06	14.06	10.85	10.93	1.01	11.93	12.18	1.02	1.10	1.11
0.47	26.72	0.994	13.90	13.90	10.89	10.95	1.01	11.95	12.21	1.02	1.10	1.11

### 5.3.7 Effect of the number of stiffeners

The influence of different number of longitudinal stiffeners at the web and the flange on ultimate moment capacities of the sections without and with the cold work effect, was investigated by FE modelling. In this study, there were 6 different cross-section types depending upon different number of longitudinal stiffeners at the web and the flange: (1) the cross-section had no web and flange stiffeners, (2) the cross-section had flange stiffeners, (3) the cross-section had one web stiffener, (4) the cross-section had one web and flange stiffeners, (5) the cross-section had two web stiffeners, and (6) the cross-section had two web and flange stiffeners. Figure 5.10 shows variation of ultimate moment capacities of the sections without and with the cold work effect. These cross-sections were designed to be symmetrical about the major axis for practical purpose and stiffeners had identical shape and size at web and flanges.

Overall, the ultimate moment capacities for both cases, without and with the cold work effect, increased in comparison to the cross-section of no web and flange stiffeners, type (1), when the number of stiffeners increased in both the web and/or the flange as shown in the cross-section types (2), (3), (4), (5) and (6). The maximum enhancement in the ultimate moment capacity without the cold work effect obtained for type (6) in comparison to the standard lipped zed type (1) was 5%. Similarly, the maximum enhancement in the ultimate moment capacity with the cold work effect obtained for type (6) was 20%. For each section type, the cold work effect on ultimate moment capacity was varied between 0% to 2% for most of the cross-sections depending on both distortional buckling slenderness and area percentage of stiffener bends in the cross-sectional types. For instance, the maximum the cold work effect for type (6) was 2%, in which the section had  $\lambda_d$  of 1.076 and the area percentage of bends of 25% while the cold work effect was insignificant on for type (1) which had  $\lambda_d$  of 1.417 and the area percentage of bends of 7%. Thus, it was concluded that having two symmetrical web stiffeners and one symmetrical flange stiffeners enhanced the ultimate moment capacity of the sections and the cold work effect on the ultimate moment capacity was maximum as in this case the section had the smallest distortional buckling slenderness and the highest area percentage of the stiffener bends.

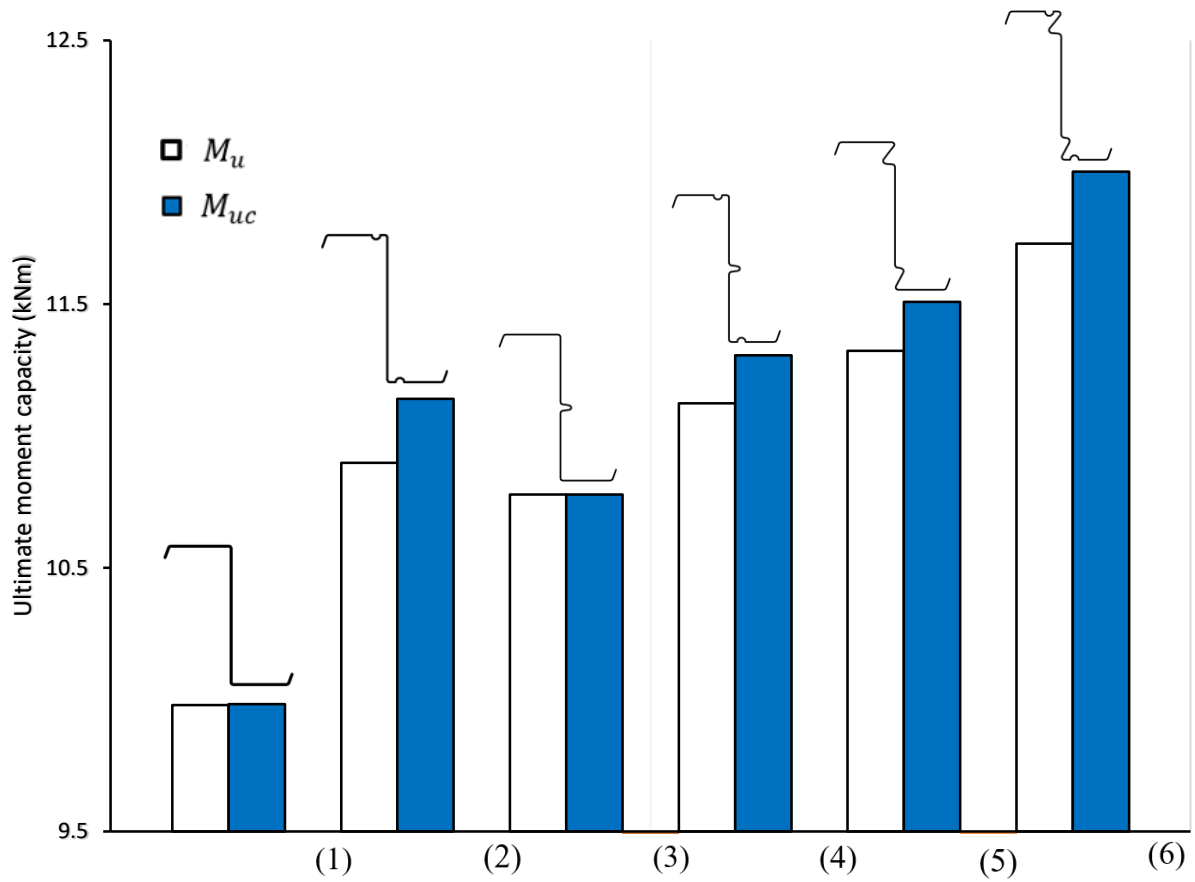


Figure 5.10. Variation in ultimate moment capacity for different numbers of web and flange stiffeners for sections without and with the cold work effect.

**Table 5.7** Variation in ultimate moment capacities for different numbers of web and flange stiffeners.

Section types	Section properties		DSM			FEM			$\frac{M_u^{FEM}}{M_u^{DSM}}$	$\frac{M_{uc}^{FEM}}{M_{uc}^{DSM}}$
	$S_{xx}$ (cm <sup>3</sup> )	$\lambda_d$	$M_u$ (kNm)	$M_{uc}$ (kNm)	$M_{uc}/M_u$	$M_u$ (kNm)	$M_{uc}$ (kNm)	$M_{uc}/M_u$		
Lipped zed section (1)	29.21	1.417	9.06	9.07	1.00	9.98	9.98	1.00	1.10	1.10
One stiffener at flanges (2)	28.91	1.314	9.53	9.56	1.00	10.90	11.14	1.02	1.14	1.17
One stiffener at web (3)	26.81	1.231	9.30	9.35	1.01	10.78	10.78	1.00	1.16	1.15
One stiffener at web and one at flanges (4)	26.51	1.153	9.67	9.82	1.02	11.12	11.31	1.02	1.15	1.15
Two symmetrical stiffeners at web (5)	27.85	1.172	10.03	10.09	1.01	11.32	11.51	1.02	1.13	1.14
Two symmetrical stiffeners at web and one stiffener at flanges (6)	27.55	1.076	10.60	10.68	1.01	11.73	12.00	1.02	1.11	1.12

### 5.3.8 Optimisation results

Based on the above parametric studies of all geometric parameters and the cold work effect, all the maximum positive effects on the section strengths were obtained for the reference section with two web stiffeners and two flange stiffeners (Figure 5.1(b)). Figure 5.11 shows the maximum % increase in the ultimate bending moment capacities for distortional buckling, without and with the cold work effect, against the investigated parameters. It was observed that the maximum percentage of increase in the ultimate moment capacities of the sections without the cold work effect was almost up to 5% when the position of the web stiffeners  $h_1/h = 0.00$  whilst it was about 7% for the ultimate moment capacity with the cold work effect, indicating the cold work effect was noticeable. The maximum percentage of increase in the ultimate moment capacities without and with the cold work effect was about 4% and 6%, respectively, when the depth of the web stiffeners  $h_2/h = 0.09$ , indicating the cold work effect. Similar trends were observed for the maximum percentage of increase in the ultimate moment capacities without and with the cold work effect when changing the position of the peak of the web stiffeners to  $h_3/h = 0.20$ . The maximum percentage of increase in the ultimate moment capacities without and with the cold work effect was about 18% and 19%, respectively, for changing the width of the web stiffeners to the certain value  $b_1/b = 0.42$ , showing that both the stiffeners' shape and the cold work effect were very significant. In terms of changing the positions of the flange stiffeners  $b_2/b$ , the maximum percentage of increase in the ultimate moment capacities without and with the cold work effect was about 8% and 9% at  $b_2/b = 0.09$ , respectively, confirming that both the flange stiffeners' position and the cold work effect were very significant. The maximum percentage of increase in the ultimate moment capacities without and with the cold work effect was about 8% and 10% with the flange stiffeners' size at the certain values  $d/b = 0.47$ , respectively, indicating that both the flange stiffeners' size and the cold work effect were noticeable. Therefore, it was suggested that the optimal shape for the zed section to gain the maximum ultimate moment capacity in distortional buckling had  $h_1/h$  of 0.00 or as much close as possible to the web-flange junction,  $h_2/h$  of at least 0.10,  $h_3/h$  of at least 0.20,  $b_1/b$  of the certain value 0.40,  $b_2/b = 0.09$  or as much close as possible to the web-flange junction, and  $d/b$  of the certain value of 0.47. In addition, the cold work effect had to be included in the FE models for accurately obtaining enhancement in the ultimate moment capacity of the section.

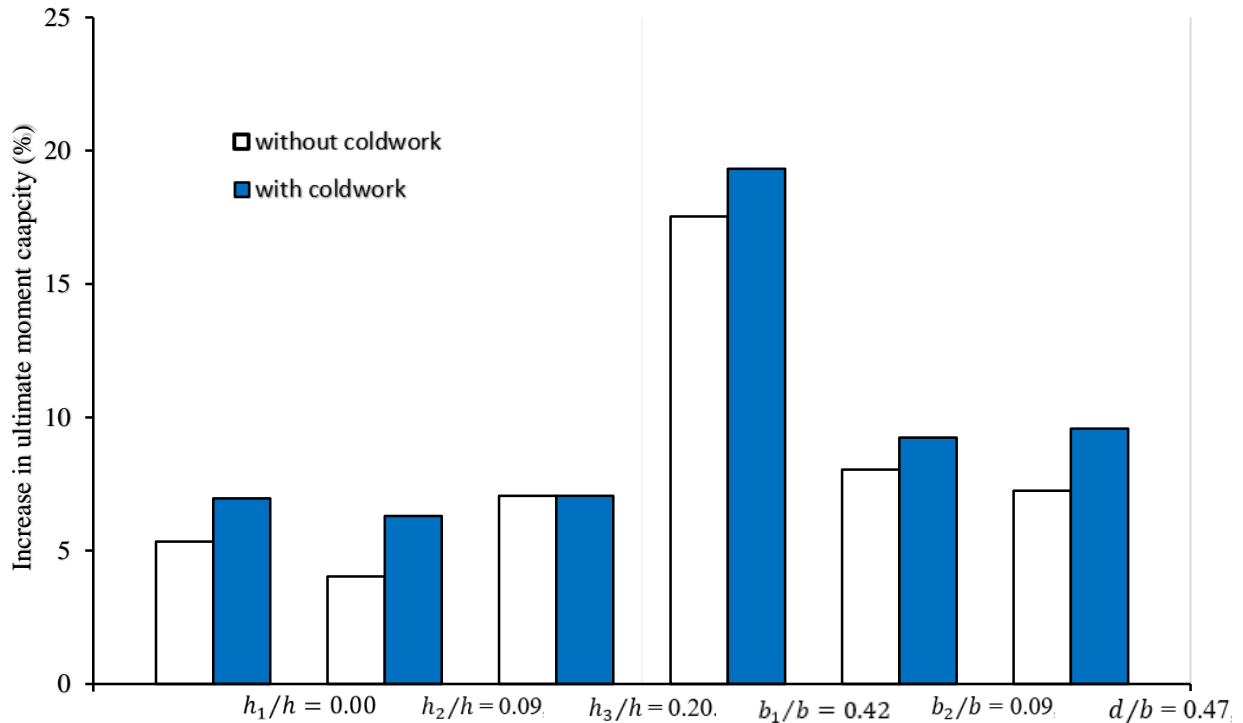


Figure 5.11. The maximum % increase in the ultimate moment capacities without and with the cold work effect, of the zed sections with two web stiffeners and two flange stiffeners, against the geometric parameters.

## 5.4 Conclusions

In this chapter, the effect of both the stiffeners' geometry and cold work on the buckling and ultimate bending strength of zed sections with longitudinal web and flange stiffeners numerically investigated. Numerical simulations using Finite Element analysis and design calculations using the Direct Strength Method were developed, which were presented in chapter 3, to replicate four-point bending tests of the sections. An optimal shape of the zed section was then achieved through a comprehensive parametric study of all geometric parameters of the stiffeners and their maximum positive effects on the section strengths. The goal was to find the optimum position, shape and size of web stiffeners as well as the position and size of flange stiffeners while considering the influence of cold work in the section corners and stiffeners' bends; this aimed to ultimately enhance the distortional buckling and ultimate strength capacities of the zed sections while keeping the same amount of material and the same height of the sections as required by

practical applications. A total of 78 combinations of FE and DSM analyses was performed and results of ultimate moment capacities, without and with the cold work effect, for different stiffeners' shapes, sizes, positions and the cold work effect on the section's distortional buckling moment capacities were obtained. The results obtained from FE analysis and DSM were compared and evaluated on the capability of modelling the buckling and ultimate strengths of the sections, considering the cold work effect from the cold roll forming process. Based on the results, the following conclusions could be drawn:

- The extent of strength benefit obtained by including variation of stiffeners' position, shape, size and quantity, and the cold work effect induced from the cold roll manufacturing process was found to be dependent on the cross-section shape, the percentage area of the section corners and stiffeners' bends and the distortional buckling slenderness. The lower the distortional buckling slenderness the greater the tendency for the section strength to be influenced by the cold work effect. For the same percentage area of the corners and bends, the sections with lower distortional buckling slenderness gained more strength benefit from the cold work effect.
- The buckling and ultimate strength capacity of the sections was changed by moving the position of the web and flange stiffeners. The stiffener's position provided the maximum buckling and ultimate strength capacity at the compression flange was found to be near the web- flange-junction, whereas the stiffener's position at the web was found to be dependent on the shape and size of the stiffeners. The following changes also increased the section's ultimate strength capacity: moving up the web stiffeners towards the web-flange junction; moving the peak of the web stiffeners towards the cross-section centre in vertical direction; expanding the width of the web stiffeners to a certain value in horizontal direction away from the web; moving the flange stiffeners towards the web-flange junction; increasing the size of the flange stiffeners to a certain value; and allocating two web stiffeners and two flange stiffeners for the zed section. For the same value of each parameter, the section's ultimate strength capacity with the cold work effect was generally greater than that of not including the cold work effect.
- It was revealed that in order to achieve the maximum ultimate strength in distortional buckling, considering both the stiffeners' position, shape, size and quantity, and the cold

work effect, an optimal shape for the zed section could have: (i) the position of the web stiffener ( $h_1/h$ ) was placed as much close as possible to the web-flange junction, (ii) the depth of the web stiffener ( $h_2/h$ ) was at least 10% of the section height, (iii) the position of the peak of the web stiffener ( $h_3/h$ ) was at least 20% of the section height, (iv) the width of the web stiffener ( $b_1/b$ ) was of the certain value of 42% of the flange width and not more than that (as the ultimate strength would reduce due to the distortional-global buckling failure), (v) the position of the flange stiffener  $b_2/b$  was placed as much close as possible to the web-flange junction, (vi) the size of the flange stiffener ( $d/b$ ) was of the certain value of 40% of the flange width and and (vii) the sections needed to have two web stiffeners and two flange stiffeners. In addition, the cold work effect had to be included in the FE models for accurately obtaining enhancement in the ultimate moment capacity of the section. The cold work effect was most significant when changing the width of the web stiffeners and the position of the flange stiffeners, especially in the sections that are less prone to buckling.

- The DSM results were in good agreement with the FE results and followed the same trends in the sections that failed by distortional buckling. However, the DSM was found to predict lesser distortional buckling slenderness in the sections where the tip of web stiffeners shifted away from the web in horizontal direction, and in the sections where the size (diameter) of the flange stiffeners was large. In fact, there were significant reductions of the sectional modulus in the minor axis that caused the sections failed by distortional-global interaction buckling but it was not captured in DSM. These resulted in overestimate predictions for the ultimate moment capacities of the sections. It was, therefore, concluded that a modification in the DSM design guideline for distortional buckling with web intermediate stiffener is needed in the case of cross-sections with large web intermediate stiffeners.



## **Chapter 6 Finite Element modelling Optimisation of CFS longitudinally stiffened channel sections under bending**

*This work is based on a conference (in 2020) and journal (in 2021) papers of “Optimization of flexural strength for cold roll formed sections using design of experiments and response surface methodology” by Qadir et al. [152] and “Shape optimisation of cold roll formed sections considering effects of cold working” by Qadir et al., Published in thin-walled structures (2022).*

### **6.1 Introduction**

The focus of the research presented in this chapter was to develop a new practical approach to Optimise CFS channel sections with longitudinal intermediate stiffeners in the flanges and web under bending while considering both the stiffeners’ geometry and cold work influences on the buckling and ultimate bending strength of channel sections. There have been very limited studies on the stiffener’s geometric effects including shape and position of the stiffeners to the section strength under bending [118, 119, 126]. In these numerical studies, it was generally assumed that the material properties at corner and bends of the intermediate stiffeners were the same with those at flat sections. This indicates that the effect of the cold working by the cold roll forming manufacturing process in enhancing the material properties at the stiffener’s corners was not considered. To the best of the author knowledge, there are no optimal design studies on cold roll formed sections that took into account the effects of both the stiffeners’ geometry and the cold working effect on the strength of the sections.

In this chapter, Finite Element analysis, developed and validated in chapter 3, and optimisation using Design Of Experiments (DOE) and response surface methodology were combined as a new approach for finding optimal sections in flexural strength. In particular, the optimisation of cold roll formed channel sections with longitudinal intermediate stiffeners in the flanges and web under bending was obtained, whilst considering both the stiffeners’ geometry and cold working influences on their buckling and ultimate bending strength. A Finite Element model was first developed to replicate four-point bending tests of industrial channel sections in generating distortional buckling failure modes. The sections were then parameterized in terms of geometric dimensions and material properties at section’s stiffener bends and corners using the DOE technique. In this approach, the dimensions, the initial imperfections, and the cold working effect

induced by cold roll forming were defined as input parameters in the Finite Element modelling. In the design of the experiments, these parameters were assigned a range of values to determine sampling points. The values of the buckling and flexural developed stresses were defined as output parameters. Response surfaces were then constructed using these sampling points which combined DOE methods and mathematical statistics, continuously testing the specified points until the relationship between parameters was solved. The Kriging response surface was used to determine the influences of the stiffener's properties on the section distortional buckling and flexural strength including its location, shape, size, and material properties by the cold working at the section corners and stiffener bends. Response surface optimisation was finally used to determine the geometric dimensions and material properties that obtained satisfied the objectives of maximising buckling loads and minimising flexural stresses (sections under the same applied loads), consequently leading to the optimal design of the channel sections with the target performance of a maximum strength to weight ratio. The details of the process are explained in the following sections.

## **6.2 Finite Element modelling**

Qadir et al. [149] presented FE models capable of simulating the buckling and ultimate bending strength of cold rolled steel beam sections. Their FE models, which were developed in ANSYS (ANSYS, Inc.) [141] and verified against earlier experimental testing [142], were used to calculate buckling, developed stresses and ultimate bending strength in this chapter.

All the beams had a total length of 2920 mm, a span of 2691 mm, and a load center of 897 mm (i.e. four-point bending). Lateral bracings were provided to prevent lateral torsional buckling in all FE models. The elastic modulus  $E$  of 205 GPa and material yield strength  $f_y$  of 519.4 MPa were assigned to the flat part of all beam sections and enhanced yield strength at the corners and stiffeners bends of the sections. Two methods were used to generate the shape of initial geometric imperfections namely Finite Element method using ANSYS and Finite Strip Method using CUFSM as well as the 75% of CDF magnitude corresponding to 1.55t was taken for the amplitude of initial imperfections. See chapter 3 for full details on FE modelling.

### 6.3 Optimisation Method

The study was carried out to optimise the influence of both the web and flange stiffeners' positions, shapes, sizes, and enhanced material properties at corners and stiffeners' bends on the section's buckling and ultimate strengths. The FE models developed and validated in Chapter 3 were utilised for the optimisation study. The number of the parameters and the corresponding FE results were arranged in orders so that all the maximum positive effects on the section strengths when changing parameter values were obtained, leading to an optimal design of the section. The channel sections together with their bending setup used in the experimental testing in Chapter 3 and in [142] were defined as "reference sections". The section height  $h$ , thickness  $t$  were fixed. The total length of the channel cross section was kept unchanged for the objective of the optimisation, which was to obtain maximum strength of the section whilst maintaining the same weigh. Changes in parameters relating to the stiffeners' shapes, sizes, positions while considering enhanced material properties at corners and bends by the cold work effect resulted in new sections. The material properties at the flat regions were assumed to be the same in these new sections but varying at corners and at the stiffeners' bends to account for the cold work influence. In summary, the reference section had an initial imperfection of  $1.55t$ , an elastic modulus  $E$  of 205 GPa, a Poisson's ratio  $\nu$  of 0.3 and the stress-strain data determined in Section 2 for the flat, corners and stiffener's bends.

The channel section without and with flange stiffeners are shown in in Figure 6.1 (a) and in Figure 6.1 (b), respectively, with all parameters. The values for  $h$  and  $t$  were taken of the reference section as 170.10 mm and 1.60 mm, respectively.  $p_1$  and  $p_2$  were the position of the web stiffener from the web-flange junction,  $p_3$  was the position of the peak of the web stiffener in horizontal direction from the web-flange junction,  $p_4$  is the width of the edge stiffener,  $p_5$  is the radius of the section corners and it was assumed that they had the same radius,  $p_6$  and  $p_7$  are the angle of rotation of the web stiffener,  $p_8$  is the flange width,  $p_{15}$  is the position of the flange stiffener away from web flange junction, and  $p_{16}$  and  $p_{17}$  are the size of the flange stiffener (assuming the flange stiffener had a circular shape). The reference section had  $p_1 = p_2 = 10.53$  mm,  $p_3 = 13.61$  mm,  $p_4 = 12.35$  mm,  $p_5 = 2.90$  mm,  $p_6 = 0^\circ$  and  $p_7 = 360^\circ$ . In total, 270 combinations between  $p_1, p_2, p_3, p_4, p_5, p_6,$  and  $p_7$  were considered, with values in a range of lower bound of 1.00 mm and upper bound of 40.53 mm for  $p_1$  and  $p_2$ , lower bound of 5.61 mm

and upper bound of 23.61 mm for  $p_3$ , lower bound of 2.90 mm and upper bound of 7.50 mm for  $p_5$ , lower bound of 0° and upper bound of 20° degrees for  $p_6$  and lower bound of 340° degrees and upper bound of 360° degrees (equivalent of 0°) for  $p_7$ . The buckling and flexural strength capacity with the cold work effect for each change were obtained and compared to evaluate the effect of these changes. Ranges of parameter values considered for the optimisation of channel sections are shown in Table 6.1.

**Table 6.1:** Ranges of values considered for the optimisation in (mm for length parameters and degrees for angle parameters).

Parameter	Lower bound	Upper bound	Parameter	Lower bound	Upper bound
$p_1$	1.0	40.5	$p_1$	1.0	40.5
$p_2$	1.0	40.5	$p_2$	1.0	40.5
$p_3$	5.6	23.6	$p_3$	5.6	23.6
$p_4$	12.4	18.4	$p_4$	12.4	18.4
$p_5$	2.9	7.5	$p_5$	2.9	7.5
$p_6$	0°	20°	$p_6$	0°	20°
$p_7$	340°	360°	$p_7$	340°	360°
-	-	-	$p_{15}$	5.0	20.0
-	-	-	$p_{16}$	1.0	5.0
-	-	-	$p_{17}$	1.0	5.0

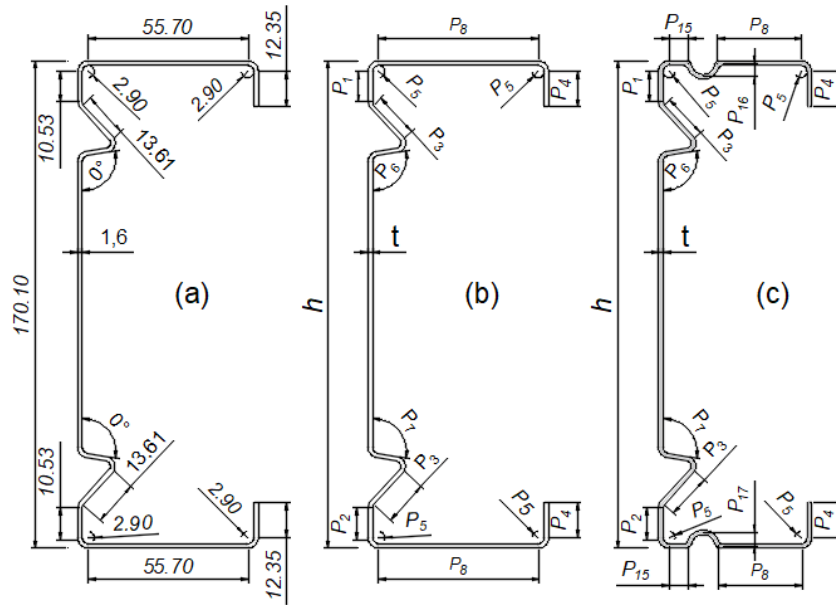


Figure 6.1: Dimension parameters in (mm) and definition of design variables of the channel cross section (a) reference section, (b) without flange stiffeners, and (c) with flange stiffeners

### 6.3.1 Flow chart for FE modelling and Optimisation

Figure 6.2 shows calculation procedures performed in this study. First, the 3-D geometry of the section was built, allowing for the dimensions of the stiffeners and section to be parameterised (the positions, size and shape of web stiffeners, the size of edge stiffeners and section corners, the positions of flange stiffener, and the size of flange stiffener). Next, the Finite Element model was built and linear buckling analysis was carried out on the perfect beam with the reference dimensions before conducting eigenvalue buckling analysis to obtain its buckling mode shapes. Then, the nonlinear post-buckling analysis was performed including geometry and material nonlinearity, initial imperfections, and the cold work effect at section corners and stiffeners' bends assigned via material properties at corners as described in Chapter 3. This linked setup in ANSYS allowed the three analysis systems to share the same resources such as material data, geometry, and boundary condition type definitions. The process of varying all the parameters was carried out with Design Of Experiments in which each parameter was assigned three different values in the range from lower bound to upper bound values. The target responses selected in this study were maximum buckling loads and minimum stresses in the sections. Finally, response surfaces were calculated in which each response was a response surface

function of all parameters and was treated as an objective. The best design candidates (sections) were selected using a multi-objective genetic algorithm.

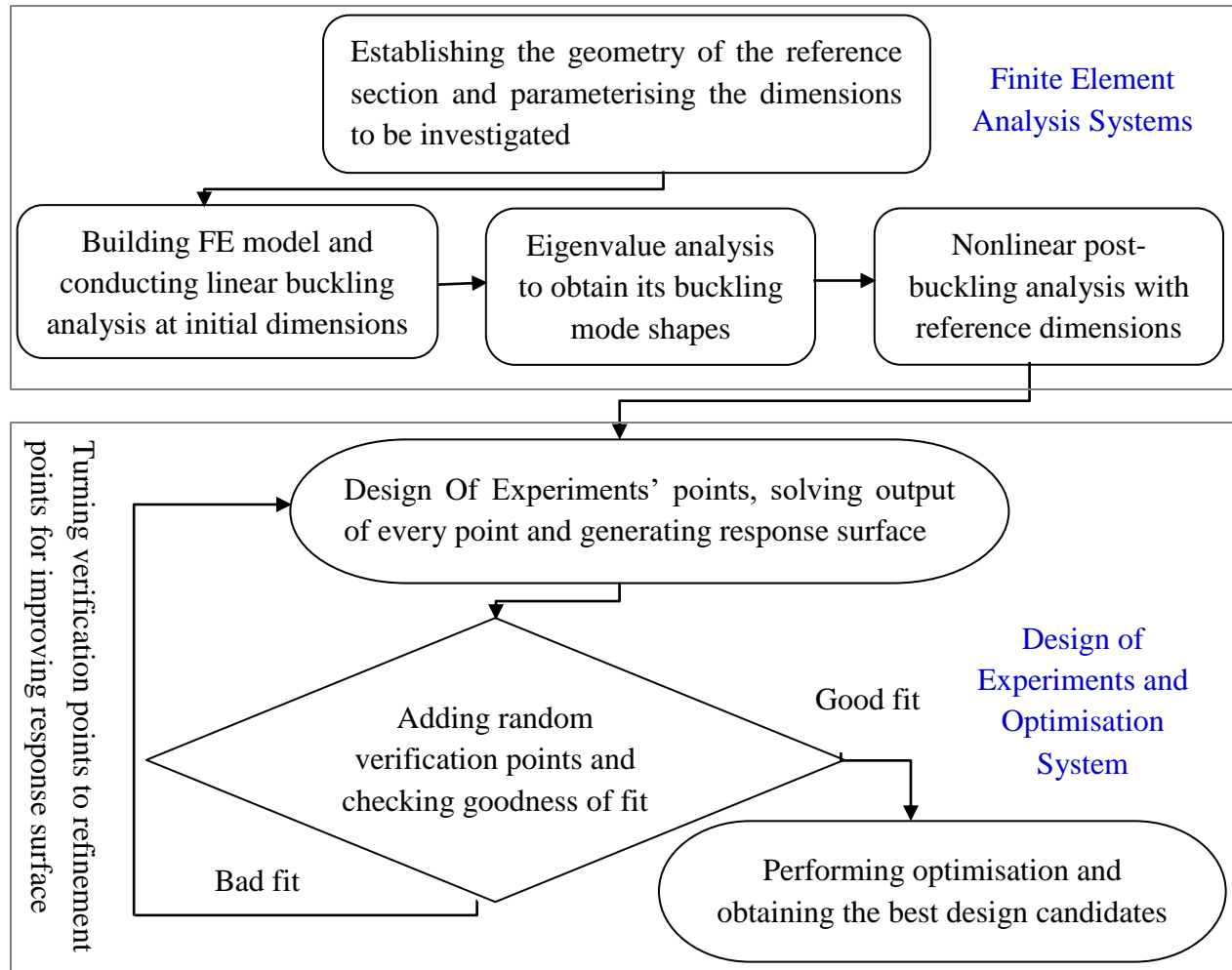


Figure 6.2. The flowchart of the FE modelling and optimisation processes.

### 6.3.2 Design OF Experiment

Design Of Experiments (DoE) is a technique for planning experiments and analysing the information obtained. The technique allows using a minimum number of experiments, in which several experimental parameters are varied systematically and simultaneously to obtain sufficient information. These experiments consist of a series of runs, or tests, in which purposeful changes are made to the input variables. Data are collected at each run and used to identify the process

conditions and product components that affect the investigated quantities, and then determine the factor settings that optimise results. ANSYS provides several DOE types such as Central Composite Design, Optimal Space-Filling Design, Box-Behnken Design, Custom, Custom + Sampling, Sparse Grid Initialization, Latin Hypercube Sampling Design, and External Design of Experiments. All the DOE types have common characteristics, which is to try to locate the sampling points such that the space of random input parameters is explored in the most efficient way and obtain the required information with minimum design points is obtained. Determining efficient locations of sampling points could reduce the required number of design points and increase the accuracy of response surface as well.

In this study, design points of the DOE were manually added to the design points table by introducing the parameters and the desired levels into which they required to be divided (using the Custom DOE in ANSYS). This was used with enough points entered to fill sampling space efficiently so that a good fitting could be created for the response surface. It was therefore possible to efficiently determine the location of sampling points for the geometries of the channel sections with complex immediate stiffeners.

In this approach, the dimensions of the channel sections were defined as geometric parameters in the Finite Element modelling; in the design of experiments, these parameters were assigned a range of values, as shown in Table 6.1, to determine parameter values that achieved the target optimised performance. This was performed under different level of applied loads, searching for the sections that could withstand maximum loads before they failed. In the DOE method, the cross-sectional shapes that resisted maximum applied load were selected as the best design candidates. This means that the optimised sections were chosen from a certain number of alternative solutions, the number of which decided the accuracy.

### 6.3.3 Response surface

Response surfaces (RS) was defined as functions in which the output parameters were described in terms of the input parameters. The sampling points obtained from DOE method were used to construct Response Surface which combined DOE methods and mathematical statistics, continuously testing the specified points until the relationship between parameters was solved. This established the RS and constructed the approximation of target parameters in a global

design space. This could estimate the set of input parameters and yield an optimal response. In this study, Kriging-based response surface method [154, 155] was used as it is an accurate multidimensional interpolation that combines a polynomial model, which provides a “global” model of the design space and local deviation. This enables efficiently interpolating the DOE points. It is a meta-modelling algorithm that provides an improved response quality and fits higher order variations of the output parameter. It is efficient in numerous cases particularly when the output response is highly nonlinear. It can be expressed as

$$Y(x) = f(x) + Z(x) \quad (6.1)$$

Where  $Y(x)$  is the unknown function of interest,  $f(x)$  is a known (usually polynomial) function of  $x$ , and  $Z(x)$  is the realization of a normally distributed Gaussian random process with mean zero, variance  $\sigma^2$ , and non-zero covariance. The  $f(x)$  term is similar to the polynomial model in a response surface and provides a "global" model of the design space.

While  $f(x)$  "globally" approximates the design space,  $Z(x)$  creates "localized" deviations so that the Kriging model interpolates the  $N$  sample data points. The covariance matrix of  $Z(x)$  is given by:

$$\text{Cov}[Z(x^i), Z(x^j)] = \sigma^2 R([r(x^i, x^j)]) \quad (6.2)$$

Where  $R$  is the correlation matrix and  $r(x^i, x^j)$  is the spatial correlation of the function between any two of the  $N$  sample points. The correlation function  $r(x^i, x^j)$  is a Gaussian correlation function:

$$r(x^i, x^j) = \exp\left(-\sum_{k=1}^M \theta_k |x_k^i - x_k^j|^2\right) \quad (6.3)$$

The unknown parameters  $\theta_k$

$$-\frac{[N \ln(\hat{\sigma}^2) + \ln|r|]}{2} \quad (6.4)$$

While any values for  $\theta_k$  create an interpolative model, the “best” Kriging model is found by solving the  $k$ -dimensional unconstrained non-linear optimisation problem given by Eqn. (6.4). The effectiveness of the RS is generally verified by Goodness of Fit metrics and Verification



Points in ANSYS. Kriging fits the RS through all design points, which cannot be verified by only Goodness of Fit metrics. Thus, a randomly generated verification points was used with Goodness of Fit to verify the effectiveness of the RS in this study. The RS was then used to plot the response (output) versus each of the input parameters (i.e. single and double) and to calculate the sensitivities. This could allow the selection of a single parameter to which the outputs (buckling load and flexural stresses) were sensitive. All the input parameters were found to be sensitive to the outputs in this study. Therefore, all the input parameters were included to conduct the optimisation.

#### 6.3.4 Optimisation

Once the response surfaces were generated and the correlations between input and output parameters were obtained, the final step was to optimise the channel sections under bending for the objectives of maximum buckling loads and minimum flexural stresses. In this study, the Response Surface Optimisation using Multi-Objective Genetic Algorithm (MOGA) was adopted to determine the most suitable candidates and ultimately identify the optimal design of the sections. Genetic Algorithm (GA) is an efficient evolutionary optimisation method for finding global optimal solutions in a large domain space [156, 157]. It begins with a random selection of population of solutions, whose individuals are represented in the form of chromosomes and progressed through a process of simulated evolution to obtain the global optimum. It involves chromosome representation, genetic operations and the fitness evaluation of chromosome to efficiently select, crossover and mutate chromosomes, in order to form a new and improved population. The value of fitness function, which is identified by the objective function (the objective function in this research is to maximise buckling loads and minimise the flexural stresses), is used for generation of improved off-springs from the current generation, with the GA operations depending on its value to evaluate the population members performance. The new population replaces previous one in the next iteration and over successive generations, the population evolves toward an optimal solution or Pareto frontier. Multi-objective Genetic Algorithm (MOGA) means optimising several objectives simultaneously. One of the important goals of solving a multi-objective problem is to find a Pareto frontier. Pareto frontier shows the set of the best design points. Each point on the Pareto frontier represents an optimal design point.

Mathematically, the objective function of parameters  $\vec{X} = [x_1, x_2, x_3, \dots, x_n] \in D^n$  for the  $\alpha^{th}$  application can be expressed as  $f_{k\alpha}(\vec{X} \in D^n)$  with  $k = 1, 2, 3, \dots, L_\alpha$  and  $\alpha = 1, 2, 3, \dots, A$ . The best feasible solution for one single objective can be found by  $Min f_{k\alpha}(\vec{X} \in D^n)$  with the constraint  $g_{j\alpha, min} \leq f_{k\alpha}(\vec{X} \in D^n) \leq g_{j\alpha, max}, j = 1, 2, 3, \dots, m_\alpha$ . In which,  $n$  is the total number of design parameters,  $L_\alpha$  is the total number of objective functions,  $m_\alpha$  is the total number of parameters (ANSYS Documents, Version 18.1, ANSYS, Inc.) [141].

In this study, the multi-objective optimisation functions were established as:  $Min F(x) = (f_1(x), f_2(x))$  with the constraint  $a_k \leq x_k \leq b_k, k = 1, 2, \dots, L$ , in which  $f_1(x)$  and  $f_2(x)$  are the maximum buckling load and the minimum flexural stress of the sections, respectively;  $x_k$ , constrained between the lower bound,  $a_k$ , and the upper bound,  $b_k$ , was the  $k$ th design variable. As it was assumed that all objective functions are to be minimised, to maximise an objective function it could be multiplied by minus, or be inversed.

## 6.4 Results and discussion

This section presents the results of investigating the influence of both the web and flange intermediate stiffeners' positions, shapes, sizes and cold work effect at corners and stiffeners' bends on the section buckling and flexural strengths. DOEs were performed to determine the optimal configuration of channel sections, 172 simulations performed for the channel sections without flange stiffeners which are provided in **Appendix A**, and 189 simulations performed for the channel sections with flange stiffeners that are also presented in **Appendix B**. Once the DOEs had completed, the Kriging algorithm was used to construct the response surface without refinement. Then, 30 verification points were simulated and used, along with the DOE points, to check the quality of DOE predictions.

Once the optimal DOE was selected, an analysis of the influences of both the web and flange intermediate stiffeners' positions, shapes, sizes and cold work effect at corners and stiffeners' bends on the section buckling and flexural strengths was performed to observe the effect of

parameters. Finally, Response Surface Optimisation was performed using the MOGA method to determine the design candidates that Optimise the buckling and flexural strength of the channel sections.

#### 6.4.1 Design of experiment quality metrics

Figure 6.3 shows the graph of the comparison between the value of the buckling (Total Deformation Load Multiplier  $p_{13}$ ) and flexural strength (Equivalent Stress Maximum  $p_{14}$ ) of design points as well as the predicted value from response surface. Verification points simulated to check the quality of DOE predictions are also shown in the graph. From the graph, it can be seen that a generated response surface was relatively accurate to achieve good-enough quality criteria. Hence, the response surface could be used for future analysis and Optimisation.

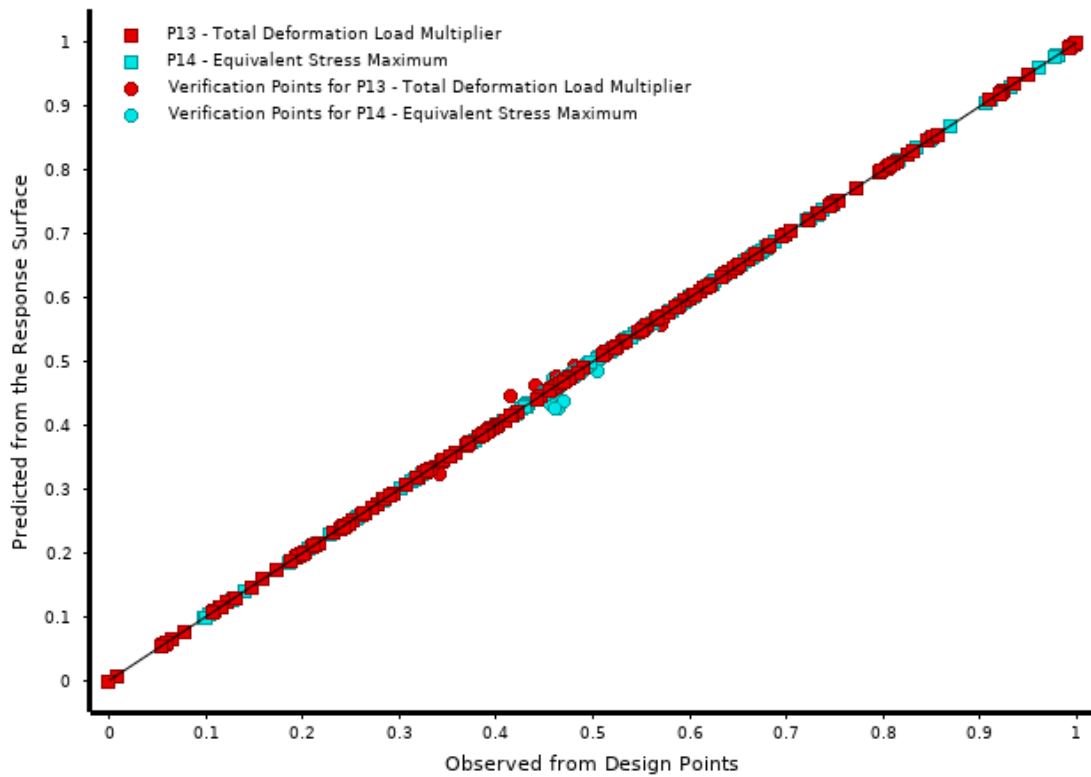


Figure 6.3: Normalized charts of the predicted vs observed values of section buckling and strength for DOE configuration. Square points are the DOE points and circular ones are the verification points. The black line shows the line in which the points could have a predicted value from response surface equal to the observed one in the design points.

## 6.4.2 Response surface results

The buckling loads (Total Deformation Load Multiplier  $p_{13}$ ) and flexural developed stresses (Equivalent Stress Maximum  $p_{14}$ ) results obtained from changing the key parameters are presented in this section. The parameters investigated include the web and flange intermediate stiffeners' positions, shapes, sizes and cold working effect at corners and stiffeners' bends. The results were obtained from performing Eigenvalue buckling analysis under a unite applied load and performing non-linear buckling analysis under applied load of 46 kN (different values of applied load were tested ranging from 40 to 60 kN in the optimisation process for channel sections, but the applied load of 46 kN was selected to obtain results in this study because most of sections were able to withstand this load level just before approaching the ultimate strength and failed). Under this applied load, the sections developed smaller flexural stresses in comparison with those developed greater flexural stresses, indicating that they had higher ultimate loads when the applied load was continuously increased until the sections failed.

Figure 6.4 is the response surfaces of the single parameter in initial values of the channel section with flange stiffeners. It was seen that buckling decreasing gradually to its lowest point and developed stresses increasing gradually to its highest point around  $p_1 = 40 \text{ mm}$ . Increasing ( $p_1$ ) was the same as moving down the stiffeners towards the center of the cross section. The reduction in the buckling and increasing in the developed stresses were due to the fact that when increasing ( $p_1$ ), it generated new cross sections with a reduction in the section modulus and an increase in the buckling slenderness. In combination, the buckling considerably reduced by 4% and the developed stresses considerably increased by 6% when increasing ( $p_1$ ) due to a product of the increasing effect by the buckling slenderness  $\lambda_d$  and the decreasing effect of the sectional modulus  $S_{xx}$ .

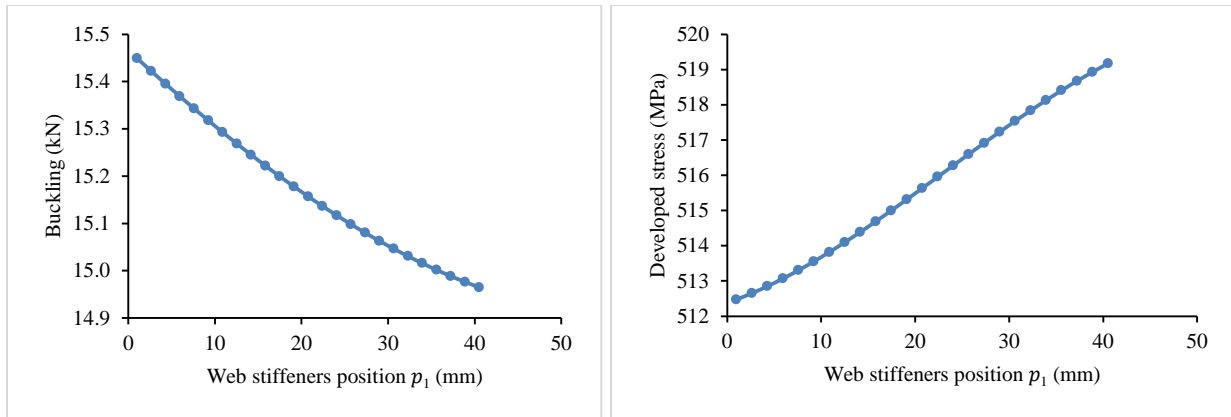


Figure 6.4: Single parameter response for different positions of web stiffeners  $p_1$  (a) buckling loads and (b) Developed stresses.

In general, the local sensitivity reflects the change of the outputs in association of the change of inputs independently. A positive value of the sensitivity indicates that as the input parameter value increases, the output value increases as well. A negative value however means that increasing the input parameter value decreases the output value. Figure 6.5 shows the sensitivities of the main output parameters including the buckling ( $p_{13}$ ) and the flexural strength ( $p_{14}$ ) that were based on the input parameters, namely, the web stiffener's positions from the web-flange junction ( $p_1$  and  $p_2$ ), the web stiffener's sizes ( $p_3$ ), the edge stiffener's sizes ( $p_4$ ), the section corners radiuses ( $p_5$ ), the web stiffener's shapes ( $p_6$  and  $p_7$ ), the flange stiffener's positions ( $p_{15}$ ) and the flange stiffener's sizes ( $p_{16}$  and  $p_{17}$ ) (see Figures. 6.1(b) and 6.1(c)).

It could be seen that for channel sections, increasing the web stiffener's positions from the web-flange junction ( $p_1$  and  $p_2$ ) reduced the buckling loads with a sensitivity of around 4% and increased the flexural stresses with a sensitivity of up to 24%. This meant that placing the stiffeners as much close as possible to the web-flange junction was the effective way to increase the buckling and ultimate strengths of the section. Regarding the section corner's radius ( $p_5$ ), which is linked to the cold working effect, it was observed that reducing the corner's radius values could also be an effective way to increase the section strength. However, it was revealed that increasing the web stiffener's sizes and shapes (through the web stiffener's sizes ( $p_3$ ) and the web stiffener's shapes ( $p_6$  and  $p_7$ )) was the most effective way to increase the section strengths, with up to 38% effect on the buckling loads and 20% effect on the flexural developed stresses.

Increasing the edge stiffener ( $p_4$ ) was also one of the most effective solutions, with up to 38% and 25% effect on increasing the buckling loads and decreasing the flexural stresses, respectively.

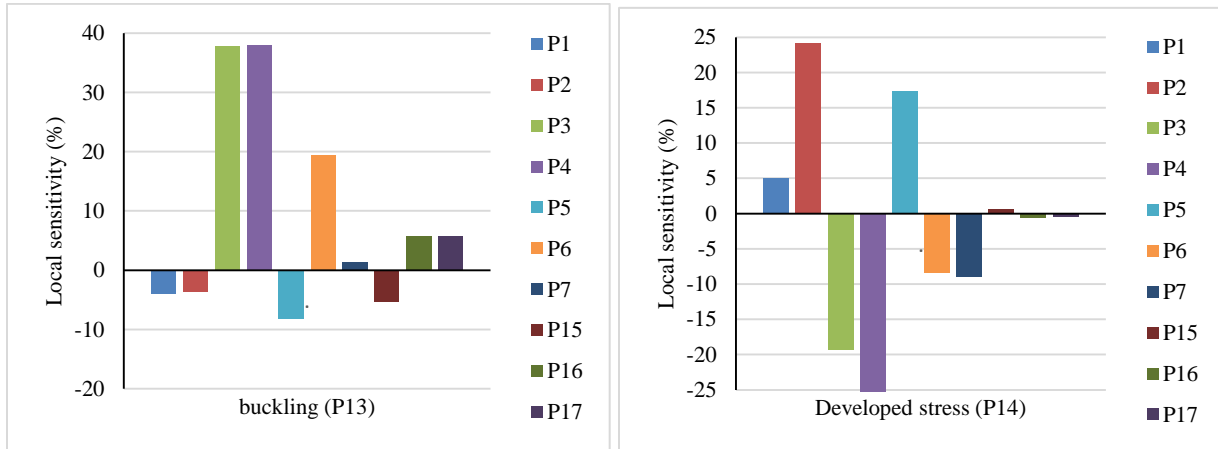


Figure 6.5: The local sensitivity bar chart of single parameters obtained for the channel section with flange stiffeners (a) buckling loads and (b) flexural developed stresses.

Figure 6.6 shows the typical 3-D response surfaces of the buckling loads and flexural stresses for channel sections, which are used to quantify the effect of different combinations of any two input parameters on the buckling loads (denoted by  $p_{13}$ ) and flexural stresses (denoted by  $p_{14}$ ). With the decrease of the values of the parameters  $p_1$  and  $p_2$ , the buckling loads increased (see Figure 6.6(a)), while the flexural stresses decreased (see Figure 6.6(b)). It can be also noted that by increasing the values of the parameters,  $p_3$  and  $p_6$ , the buckling loads increased as shown in Figure 6.6(c), while the flexural stresses decreased as illustrated in Figure 6.6(d).

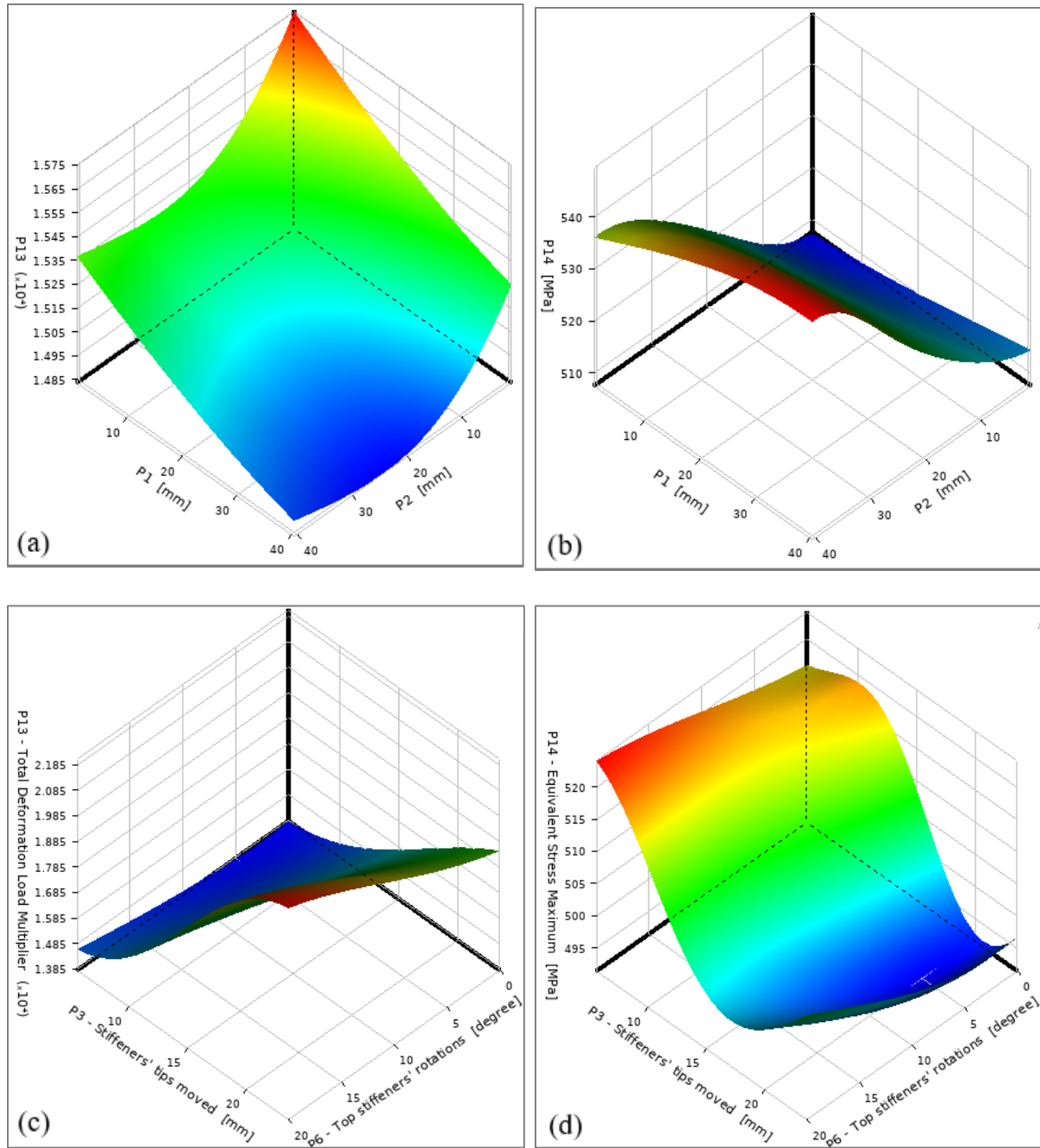


Figure 6.6: Double parameters response of the channel sections for different positions of web stiffeners  $p_1$  and  $p_2$  on (a) buckling loads and (b) flexural developed stresses, and for different sizes of edge and web stiffeners  $p_3$  and  $p_6$  on (c) buckling loads and (d) flexural developed stresses.

### 6.4.3 Optimisation results

Based on the results of the response surface analysis, the Multi-Objective Genetic Algorithm (MOGA) was used as the search engine to find the candidate optimal results to minimise the selected multi-objective function. In this study, for channel sections, the design variables:  $p_1$ ,  $p_2$ ,  $p_3$ ,  $p_4$ ,  $p_5$ ,  $p_6$ ,  $p_7$ ,  $p_{15}$ ,  $p_{16}$ , and  $p_{17}$ , were chosen as the input parameters of the MOGA, the output parameters were the maximum buckling load,  $p_{13}$ , and the minimum flexural developed stress,  $p_{14}$ . Several different scenarios were used to determine optimal design candidates. These included (1) minimising the flexural developed stresses, (2) maximising buckling loads, and (3) minimising the flexural developed stresses and maximising buckling loads at the same time. Table 6.2 shows an example of these scenarios for channel sections with flange stiffeners, where the goal was to maximise the buckling loads ( $p_{13}$ ) and minimise the flexural developed stresses ( $p_{14}$ ). As a result, three design candidates were found with the same design variables. The design candidate was then loaded up to failure to obtain collapse load- displacement curves as indicated in Figure 6.10 for channel sections. This process repeated to obtain other design candidate results for the channel sections (i.e., Candidates 1-5).

Table 6.3 presents the buckling loads and ultimate bending strengths of the channel sections obtained from the MOGA optimisation process (with input parameters shown in Figure 6.1 and Table 6.1). The results in this table were compared with those of the standard lipped channel sections having the same amount of material and the same section height. Candidates 1 and 4 were obtained when the ‘Goal’ was minimising the flexural developed stresses, Candidates 2 and 5 were obtained when the ‘Goal’ was maximising the buckling loads, and Candidates 3 and 6 were obtained when the ‘Goal’ was maximising the buckling and minimising the flexural developed stresses under bending for distortional buckling.



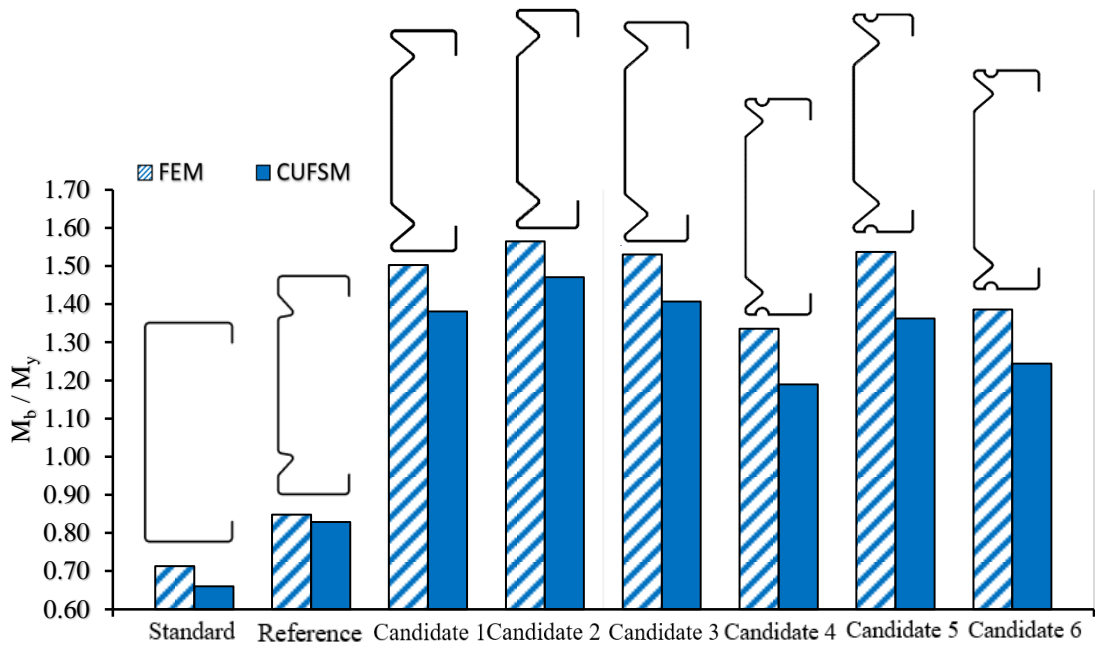
**Table 6.2:** Candidate design when the target objectives were maximizing buckling and minimizing flexural developed stresses (Candidate 6).

Table of Schematic D4: Optimisation			
Optimisation Study			
Minimise $p_{19}$	Goal, Minimise $p_{14}$ (High importance)		
Maximise $p_{18}$	Goal, Maximise $p_{13}$ (Low importance)		
Optimisation Method			
MOGA	The MOGA method (Multi-Objective Genetic Algorithm) is a variant of the popular NSGA-II (Non-dominated Sorted Genetic Algorithm-II) based on controlled elitism concepts. It supports multiple objectives and constrains and aims at finding the global optimum.		
Configuration	Generate 10000 samples initially, 2600 samples per iteration and find 3 candidates in a maximum of 100 iterations.		
Status	Converged after 43214 evaluations.		
Candidate Points			
	Candidate point 1	Candidate point 2	Candidate point 3
$p_1$ - Top stiffeners' position (mm)	1.37	1.79	2.03
$p_2$ - Bottom stiffeners' position (mm)	2.91	1.11	1.81
$p_3$ - Stiffeners' tip moved (mm)	16.16	15.52	15.71
$p_4$ - Edge stiffeners' width (mm)	13.56	13.61	13.67
$p_5$ - Section corner stiffener radiuses (mm)	2.93	3.03	2.97
$p_6$ - Top stiffeners' rotation (degree)	18.39	19.13	16.62
$p_7$ - Bottom stiffeners' rotation (degree)	345.00	340.00	345.00
$p_8$ - Flange width (mm)	28.75	29.08	28.72
$p_9$ - Commands (APDL) 2 ARG 1	571.29	567.15	560.86
$p_{10}$ - Commands (APDL) 2 ARG 1	570.38	568.39	572.14
$p_{15}$ - Flange stiffeners' position (mm)	5.84	5.32	5.58
$p_{16}$ - Top flange stiffeners' size (mm)	4.84	4.49	4.87
$p_{17}$ - Bottom flange stiffeners' size (mm)	4.73	4.82	4.97
$p_{13}$ - Total deformation Load Multiplier	** 21.34	** 21.28	** 20.99
$p_{14}$ - Equivalent Stress Maximum (MPa)	** 456.38	** 456.27	** 455.59

**Table 6.3:** The results of buckling load ( $Pb$ ), flexural developed stresses ( $\sigma$ ) and ultimate moment capacity of channel sections.  $M_u$ ,  $M_{uc}$  stand for ultimate moment capacity without and with the cold working effect, respectively.

Section type	$Pb$ (kN)	$\sigma$ (MPa)	$M_u$ (kNm)	$M_{uc}$ (kNm)	$M_{uc}/M_u$	$M_{uc}/M_{uc}^{standard}$
Standard (a)	11.7	-	10.34	10.34	1.00	1.00
Reference (b)	13.4	546.5	10.64	10.69	1.01	1.03
Candidate 1	22.9	455.3	11.30	11.58	1.03	1.12
Candidate 2	23.5	484.5	10.94	11.07	1.02	1.07
Candidate 3	23.3	460.0	11.34	11.59	1.03	1.12
Reference (c)	15.3	513.8	10.88	11.12	1.02	1.07
Candidate 4	20.8	455.0	11.60	11.87	1.03	1.15
Candidate 5	23.1	517.0	10.96	11.20	1.03	1.08
Candidate 6	21.5	458.0	11.90	12.09	1.02	1.17

The optimal shapes and the comparison between their flexural strength capacities are shown in Figures 6.7-6.9. In which  $M_y$  is the yield bending moment of the whole cross section;  $M$  is the bending moment capacity (when the cold working effect is not included  $M$  equals  $M_u$ , and when the cold working effect is included  $M$  equals  $M_{uc}$ ); and  $Mb$  is the buckling moment capacity. The buckling and ultimate strength results were obtained by FE nonlinear analysis as described in Chapter 3, which is called “FEM” model. The buckling modes were obtained from linear buckling analysis that was conducted with the conventional Finite Element Method (FEM). In addition, another model was developed, in which the desired linear buckling modes obtained from Finite Strip Method using CUFSM software [144] were transferred to the FE analysis, to conduct the nonlinear analysis. This model is called “CUFSM-FEM” model. Both “FEM” and “CUFSM-FEM” models’ results are shown in Figures 6.7-6.9.



(a)

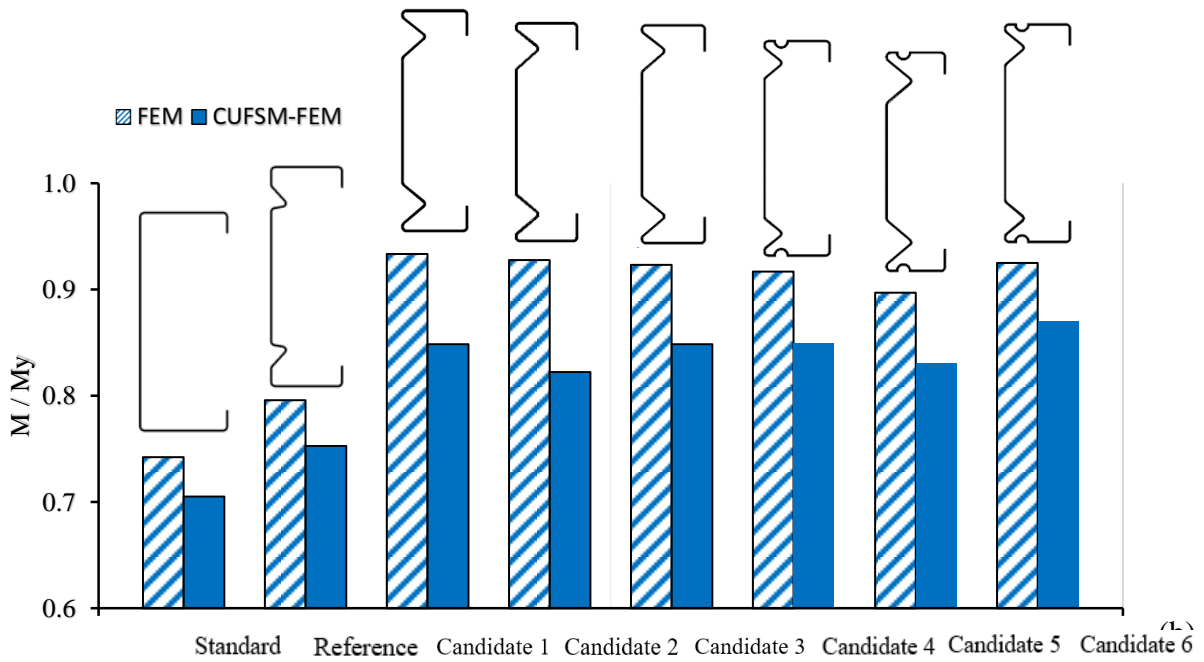


Figure 6.7. Strength results of standard, reference and optimised channel sections for (a) buckling and (b) ultimate moment capacity with the cold working effect included.

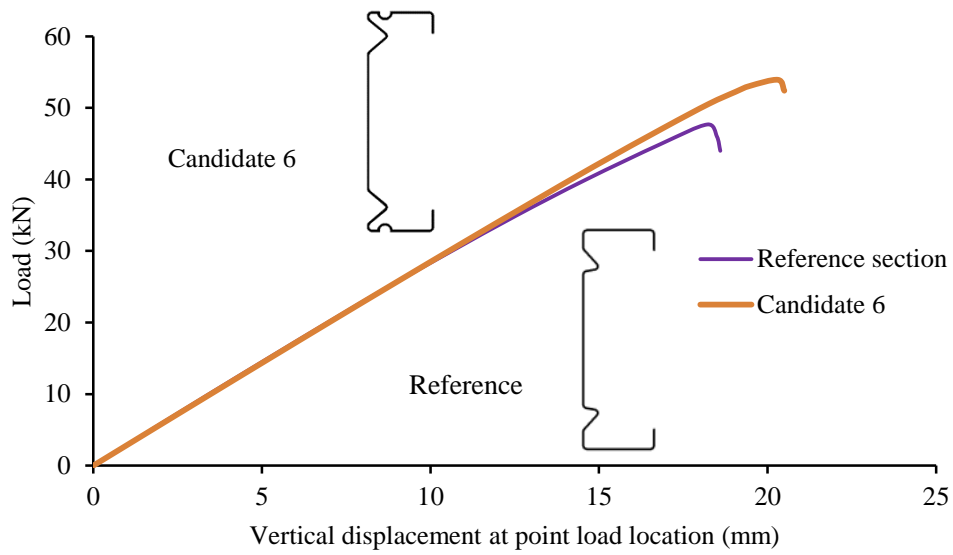


Figure 6.8. Load-displacement curves for the channel reference and design Candidate 6 sections.

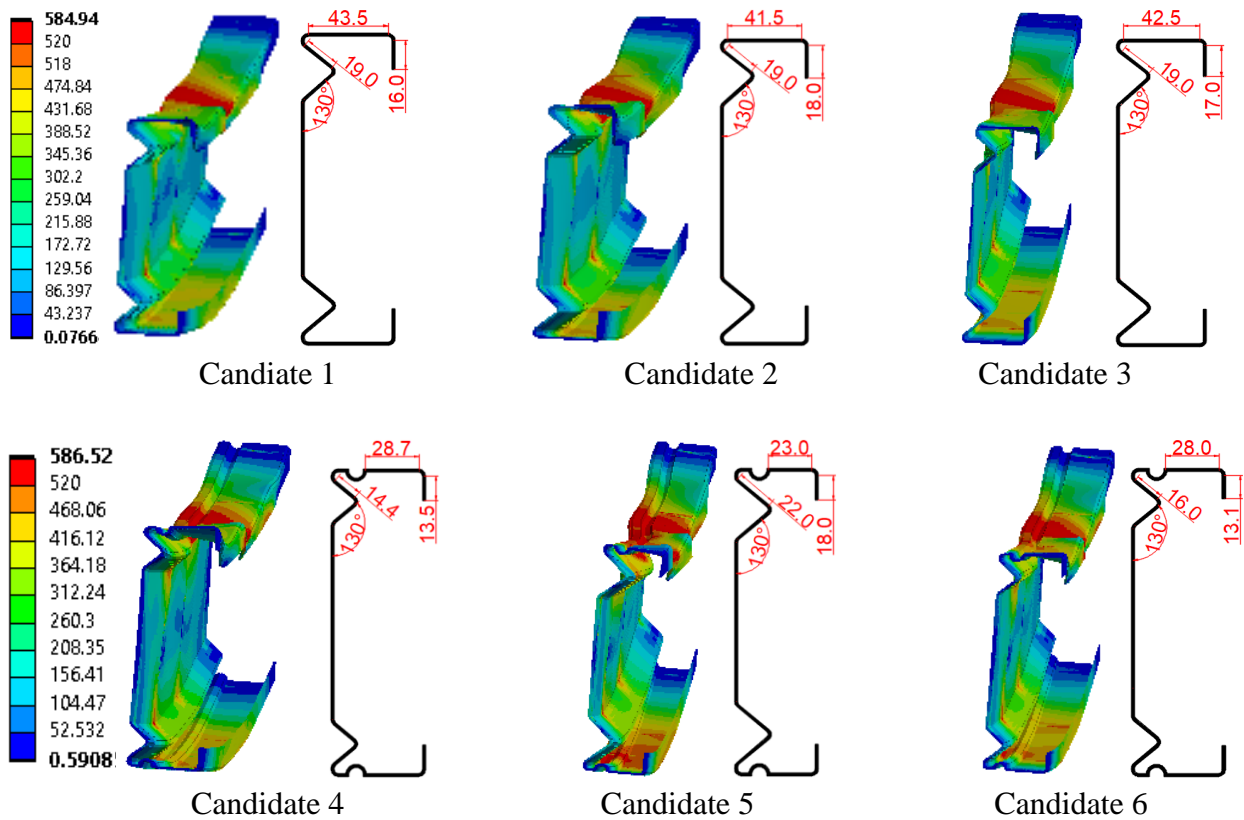


Figure 6.9. Dimensions, deformed shapes and von Mises stress distribution for all design candidates of channel sections.

Several observations were made from Figures 6.7-6.9 and Tables 6.2-6.3 as follows:

- The reference channel section provided considerably greater buckling capacity when compared to the standard lipped channel section by 15%, whereas the ultimate moment capacity was also improved by 3%.
- Adding flange stiffeners to the reference sections further enhanced the buckling and ultimate moment capacities of the channel section by 16% and 4%, respectively.
- By changing the position, size and shape of web stiffeners, lip's length, and section corners' radii as well as including the cold working effect at the sections' corners and stiffeners' bends of the reference channel sections, optimal sections with maximum buckling strengths could be obtained (Candidates 1-3). The gains in buckling strength for the channel Candidates of 1, 2 and 3 were up to 2 times, in comparison with the standard lipped channel. At the same time, the ultimate moment capacities were also improved by 12%, 7% and 12% for the channel sections, respectively.
- The optimal design of the channel was obtained by changing the position, size and shape of web stiffeners, the position and size of flange stiffeners, lip's length, and section corners' radii as well as including the cold working effect at the sections' corners and stiffeners' bends of the reference sections having flange stiffeners (Candidates 4-6). The significant increases in buckling loads for the Candidates 4, 5 and 6 were up to 2 times, in comparison with the standard lipped channel. At the same time, the ultimate moment capacities were also significantly increased by 15%, 8% and 17% for the channel sections, respectively.
- For all design Candidates (1-6), the channel sections strived to increase their buckling and ultimate moment capacities by: (1) decreasing the position of web stiffeners (converged to minimum defined values of  $p1 = 1.0$  mm and  $p2 = 1.0$  mm) or moving web stiffeners toward the web flange junctions as much as possible, (2) reducing the section corners' radii to minimum defined value of  $p5 = 2.9$  mm, and (3) increasing the angle between the web stiffeners and the web ( $p6 = 15$  degrees and  $p7 = 345$  degrees). This was due to the combined effect of (1) increasing the sectional modulus, (2) reducing the distortional buckling slenderness, and (3) the cold working effect in the section corners (smaller corner radius had greater strength enhancement). In general, these observations are consistent with the results presented in Chapter 4.

- As shown in Figure 6.9 for design Candidates (1-3), while the channel sections converged to the same web stiffeners size ( $p_3 = 19.0$  mm), the optimised sections had different lip's lengths and flange widths depending on the target objectives (noted that the total developed length of the channel section and the section height remained constant). For instance, the section tended to converge at shorter lips and wider flanges ( $p_4 = 16.0$  mm and  $p_8 = 43.5$ ) when the target was to minimise flexural developed stresses in the section (Candidate 1), whereas the sections tended to take longer lips and smaller flange widths ( $p_4 = 18.0$  mm and  $p_8 = 41.5$ ) when the target was to maximise buckling loads (Candidate 2).
- As depicted in Figure 6.9 for design Candidates (4-6), while the channel sections tended to have the same position and size of flange stiffeners ( $p_{15} = 5.0$  mm and  $p_{16} = p_{17} = 43.5$ ), the sections had various web stiffeners sizes, lip lengths, and flange widths based on target objectives. Candidate 4 obtained from minimising flexural developed stress had web stiffener size, lip length and flange width of 14.4 mm, 13.5 mm, and 28.7 mm, respectively. However, Candidate 5 obtained from maximising buckling loads had web stiffener size, lip length and flange width of 22.0 mm, 18.0 mm, and 23.0 mm, respectively.
- For all design Candidates (1-6), increasing the web stiffener size and lip length up to certain limit significantly improved the buckling capacities of channel sections which was effective in suppressing section instability, resulting in significantly increased ultimate moment capacities (see Table 6.3). These sections also exhibited a considerably higher stiffnesses (as shown in Figure 6.8), which is a direct result of the stiffeners delaying and mitigating the stiffness degradation due to buckling. It was noted that increasing the stiffeners' size was accounting for the total length of the section, and therefore, the flange width of the design candidates was smaller than that of the reference section. Nevertheless, increasing the stiffeners' sizes beyond a certain limit (Candidates 2 and 5) still considerably improved distortional buckling capacities of the channel sections, whereas it did not have a significant effect on the ultimate moment capacity and it actually noticeably reduced the ultimate moment capacities in design Candidates 2 and 5 when compared to Candidates 1 and 4. This was a result of a significant reduction of the sectional modulus in the minor axis which made these sections prone to the failure due to distortional-global interaction buckling and consequently led to lower ultimate moment capacities for the beam sections. These observations were consistent with Chapter 4.

- The optimal shapes of the channel sections could be obtained when the target objectives were to both minimising the flexural developed stress and maximising the buckling loads in the sections. This led to an optimal design solution (Candidate 6) which had significant increase in bending and ultimate strengths.
- Including the cold working effect in the sections' corners and stiffeners' bends led to noticeable enhancement in the ultimate moment capacities of the optimised channel sections (as indicated in Table 6.3), despite the insignificant effect for the cases where the cold working effect was only present in the sections' corners. The maximum percentage of increase in the ultimate moment capacities with the cold working effect was up to 3%, confirming that the influence of the cold working effect could be significant.
- Figure 6.7 compares the FEM strength capacity results of the optimised sections with the results obtained by transferring buckling mode shapes from CUFSM to the FEM. It was seen that both FEM and CUFSM-FEM methods provided the same trend with an average difference of 15% and 2% in the buckling and ultimate bending moment capacities, respectively.

## 6.5 Conclusions

This chapter presents a practical method to obtain efficient cold roll formed steel channel sections in bending, using FE modelling integrated with Design Of Experiments (DOE) and response surface optimisation. The FE models were first developed to replicate four-point beam bending tests of distortional buckling failure configuration of the channel sections, which included geometrically and materially nonlinear analysis with initial geometric imperfections and the cold working effect. These validated FE models were then utilised to optimise the buckling and ultimate flexural strengths of the sections. In the optimisation process, each section was parameterised in terms of geometric dimensions, imperfections and material properties using DOE technique to determine the buckling loads and flexural stresses at the design points. Kriging-based response surfaces were generated based on the DOE results to study the influences of the stiffener's geometric and material properties on the section buckling loads and flexural stresses including its location, shape, size and material properties by the cold working at the section corners and stiffeners bends. Optimal designs of the channel sections were finally obtained using the multi-objective genetic algorithm method (MOGA). The following conclusions were drawn based on the results of this study:

- By considering both geometry and the cold working effect in the optimisation process, optimal designs of the channel sections could be obtained with significant gain in buckling and ultimate bending strengths. The gains in buckling strength were up to 2 times for the channel sections, when compared to the standard sections using the same amount of material.
- The optimum positions of the web and flange stiffeners was found to be moving towards the web-flange junctions as close as possible during the optimisation process for both channel sections. This was a result of the intermediate stiffeners position increasing the sectional modulus and decreasing the distortional buckling slenderness, which ultimately enhanced the distortional buckling and ultimate strength capacities as well as mitigating the post-buckling stiffness degradation of the optimised sections.
- For the channel sections, the entire sections with decreasing section corners radii resulted in optimal solutions. This was because when reducing the corners radii, the distortional buckling slenderness of the section and the strength enhancement of the corners increased, and consequently the buckling and ultimate bending strength was enhanced.



- Comparisons between the design candidates indicated that by increasing the size of intermediate web, flange and edge stiffeners, a turning point was reached where increasing the stiffeners size reduced the ultimate moment capacities, while marginally improved the distortional buckling loads, resulting in sections fail in distortional-global interactive buckling modes.
- The cold working effect induced from the cold roll manufacturing process was found to be considerable in the optimised channel sections, suggesting that the FE models need to include the cold working effect for accurately obtaining the ultimate moment capacity of the sections. The cold working effect was most significant when the sections were less prone to buckling, especially for distortional and global-distortional interactive buckling modes.
- It was found that both target objective functions, which were maximising buckling loads and minimising flexural developed stresses, had to be deployed in order to obtain the optimal sections with significantly increasing both bending strength capacities and the cold working effect.
- The adequacy of the optimised sections obtained from FEM optimisation process was verified by the results obtained from transferring the CUFSM buckling mode shapes into the FEM using the CUFSM-FEM model. It was found that the FEM results closely followed the trends in the buckling and flexural strength capacities obtained by the CUFSM-FEM results. This demonstrated the reliability of the proposed optimisation procedure using the direct FEM optimisation.

## **Chapter 7 Finite Element modelling Optimisation of CFS longitudinally stiffened zed sections under bending**

*This work is based on a journal (in 2021) paper of “Shape optimisation of cold roll formed sections considering effects of cold working” by Qadir et al., Published in Thin-Walled Structures (2022).*

### **7.1 Introduction**

This chapter provides optimisation of CFS zed sections with longitudinal intermediate stiffeners in the flanges and web under bending while considering both the stiffeners' geometry and cold work influences on the buckling and ultimate bending strength of the sections. FE models developed and validated in chapter 3 and the optimisation approach developed in chapter 6 were applied for the zed sections in this chapter. The section was parameterized in terms of geometric dimensions and material properties using the DOE technique. In this approach, the dimensions, the initial imperfections, and the cold work effect induced from cold roll forming of the zed section were defined as parameters in the Finite Element modelling; in the design of experiments, these parameters were assigned a range of values to determine sampling points. The sampling points obtained from DOE method was used to construct Response Surface (RS) which combined DOE methods and mathematical statistics, continuously testing the specified points until the relationship between parameters was solved. The kriging response surface was used to determine the influences of the stiffener's properties on the section distortional buckling and flexural strength including its location, shape, size, and material properties by the cold work at the section corners and stiffener bends. Response surface Optimisation was finally used to determine the geometric dimensions and material properties that provided the optimal design of the zed sections.

## 7.2 Finite Element modelling

Qadir et al. [149] presented FE models capable of simulating the buckling and ultimate bending strength of cold rolled steel beam sections. Their FE models, which were developed in ANSYS (ANSYS, Inc.) and verified against earlier experimental testing [142], were used to calculate buckling, developed stresses and ultimate bending strength in this chapter. All the beams had a total length of 2920 mm, a span of 2691 mm, and a load centre of 897 mm (i.e. four-point bending). Lateral bracings were provided to prevent lateral torsional buckling in all FE models. The elastic modulus  $E$  of 205 GPa and material yield strength  $f_y$  of 519.4 MPa were assigned to the flat part of all beam sections and enhanced yield strength at the corners and stiffeners bends of the sections. Two methods were used to generate the shape of initial geometric imperfections namely Finite Element method using ANSYS and Finite Strip Method using CUFSM as well as the 75% of CDF magnitude corresponding to 1.55t was taken for the amplitude of initial imperfections. See chapter 3 for full details on FE modelling.

## 7.3 Optimisation Method

Figure 7.1 (a) shows a cross section and general dimensions for the zed sections which was the industrial UltraZED<sup>TM</sup>2 sections (Hadley Industries plc.). The study goal was to find optimal design of the web and flange stiffeners' positions, shapes, sizes, and enhanced material properties at corners and stiffeners' bends, which enhance the section's buckling and ultimate bending strength, leading to an optimal design of the zed sections. The FE model developed and validated in Chapter 3 and [149] was utilised for the optimisation study. The zed section together with their bending setup used in the experimental testing in [142] were defined as "reference section" and shown in Figure 7.1 (b). The section height  $h$  and thickness  $t$  were fixed in the optimisation study.

For the zed section without flange stiffeners is shown in Figure 7.1 (b), in which all dimension parameters are also shown and the zed section with flange stiffeners are shown in Figure 7.1 (c). The values for  $h$  and  $t$  were taken of the reference zed section as 170.0 mm and 1.6 mm,

respectively.  $p_1$  and  $p_2$  are the position of the web stiffeners from the web-flange junctions,  $p_3$  and  $p_4$  are the width of the edge stiffeners,  $p_5$  is the radius of the section corners and it was assumed that they had the same radius,  $p_6$  and  $p_7$  are the position of the peak of the web stiffeners in horizontal direction from the web-flange junction,  $p_8$  and  $p_9$  the angle of rotation of the web stiffeners,  $p_{10}$  and  $p_{11}$  the angle of rotation of the edge stiffeners,  $p_{12}$  and  $p_{13}$  are the width of flanges for the zed section without flange stiffeners, whereas  $p_{12}$  and  $p_{13}$  are the position of the flange stiffeners away from web flange junction for the zed section with flange stiffeners,  $p_{14}$  and  $p_{15}$  are the size of the flange stiffeners (assuming the flange stiffener had a circular shape), and  $p_{16}$  and  $p_{17}$  are the width of flanges.

The total length of the Zed cross section was kept unchanged for the optimisation target, that was “obtaining maximum strength of the section while maintaining the same weight”. Changes in parameters relating to the stiffeners’ shapes, sizes, positions while considering enhanced material properties at corners and bends by the cold work effect resulted in new zed sections. The material properties at the flat regions, corners and at the stiffeners’ bends were assumed to be the same in these new sections.

In summary, the reference section had an initial imperfection of  $1.55t$ , an elastic modulus  $E$  of 205 GPa, a Poisson’s ratio  $\nu$  of 0.3 and the stress-strain data determined for the flat, corners and stiffener’s bends.

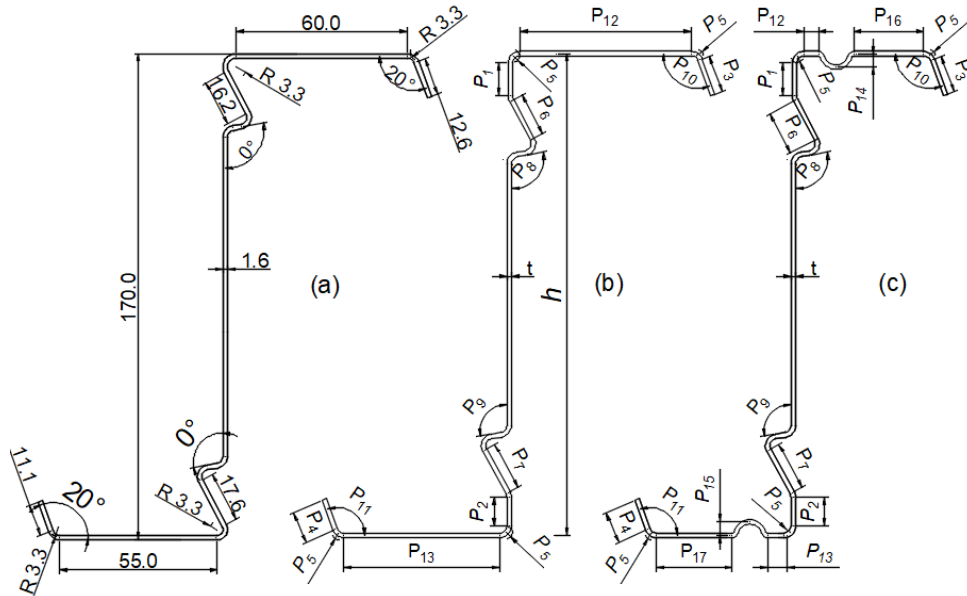


Figure 7.1. Dimension parameters in (mm) and definition of design variables of the zed cross section (a) reference section, (b) without flange stiffeners, and (c) with flange stiffeners.

**Table 7.1** Range of values considered for the optimisation in (mm and degree).

Parameter	Lower bound	Upper bound	Parameter	Lower bound	Upper bound
Zed section without flange stiffeners			Zed section with flange stiffeners		
$p_1$	1.0	10.0	$p_1$	1.0	10.0
$p_2$	1.0	10.0	$p_2$	1.0	10.0
$p_3$	12.6	24.6	$p_3$	12.6	24.6
$p_4$	11.1	23.1	$p_4$	11.1	23.1
$p_5$	3.3	3.3	$p_5$	3.3	3.3
$p_6$	11.2	21.2	$p_6$	11.2	21.2
$p_7$	12.6	22.6	$p_7$	12.6	22.6
$p_8$	0.0°	30.0°	$p_8$	0.0°	40.0°
$p_9$	0.0°	30.0°	$p_9$	0.0°	40.0°
$p_{10}$	0.0°	20.0°	$p_{10}$	0.0°	20.0°
$p_{11}$	0.0°	20.0°	$p_{11}$	0.0°	20.0°
-	-	-	$p_{12}$	5.0	20.0
-	-	-	$p_{13}$	5.0	5.0
-	-	-	$p_{14}$	1.0	5.0
-	-	-	$p_{15}$	1.0	5.0

## 7.4 Results and discussion

This section presents the results of investigating the influence of both the web and flange intermediate stiffeners' positions, shapes, sizes and cold work effect at corners and stiffeners' bends on the section buckling and flexural strengths. DOEs were performed to determine the optimal configuration of zed sections, which provided in **Appendix C** and **Appendix D**. Once the DOEs had completed, the Kriging algorithm was used to construct the response surface without refinement. Then, 20 verification points were simulated and used, along with the DOE points, to check the quality of DOE predictions.

Once the optimal DOE was selected, an analysis of the influences of both the web and flange intermediate stiffeners' positions, shapes, sizes and cold work effect at corners and stiffeners' bends on the section buckling and flexural strengths was performed to observe the effect of parameters. Finally, Response Surface Optimisation was performed using the MOGA method to determine the design candidates that optimise the buckling and flexural strength of the zed sections.

### 7.4.1 Design OF Experiment quality metrics

Figure 7.2 shows the graph of the comparison between the value of the buckling (Total Deformation Load Multiplier  $p_{18}$ ) and flexural developed stresses (Equivalent Stress Maximum  $p_{19}$ ) of design points as well as the predicted value from response surface for the zed section with flanges stiffener. Verification points simulated to check the quality of DOE predictions are also shown in the graph. From the graph, it can be seen that a generated response surface was relatively accurate to achieve good-enough quality criteria. Hence, the response surface could be used for future analysis and optimisation.

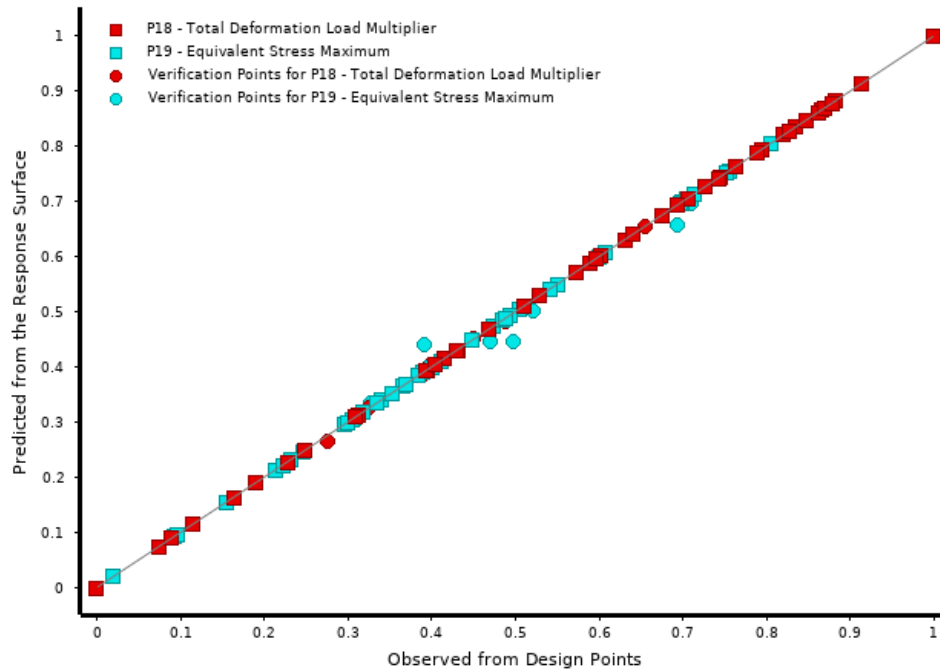


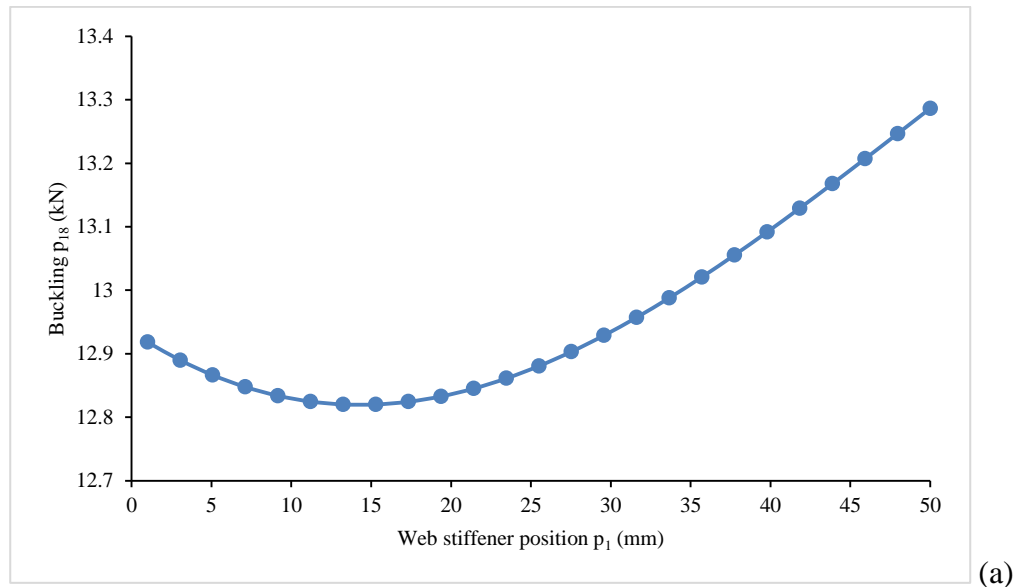
Figure 7.2. Normalised charts of the predicted vs observed values of section buckling and strength for DOE configuration obtained for the zed section with flange and web stiffeners. Square points are the DOE points and circular ones are the verification points. The black line shows the line in which the points could have a predicted value from response surface equal to the observed one in the design points.

#### 7.4.2 Response surface results

The buckling (Total Deformation Load Multiplier  $p_{18}$ ) and flexural developed stresses (Equivalent Stress Maximum  $p_{19}$ ) results obtained from changing different parameters are presented in this section. The parameters investigated include the web and flange intermediate stiffeners' positions, shapes, sizes and cold working effect at corners and stiffeners' bends. The results were obtained from performing Eigenvalue buckling analysis under a unite applied load and performing non-linear buckling analysis under applied load of 46 kN (different values of applied load were tested ranging from 40 to 60 kN in the optimisation process for zed sections, but the applied load of 46 kN was selected to obtain results in this study because most of sections

were able to withstand this load level just before approaching the ultimate strength and failed). Under this applied load, the sections developed smaller flexural stresses in comparison with those developed greater flexural stresses, indicating that they had higher ultimate loads when the applied load was continuously increased until the sections failed.

Figure 7.3 is the response surfaces of the single parameter in initial values of the zed section with web and flange stiffeners. It was seen that the buckling and developed stresses increasing gradually to its highest point around  $p_1 = 50 \text{ mm}$ . Increasing ( $p_1$ ) was the same as moving down the stiffeners towards the centre of the cross section. The increasing in the buckling and developed stresses were due to the fact that when increasing ( $p_1$ ), it generated new cross sections with a reduction in the buckling slenderness and in the section modulus. In combination, the buckling noticeably increased by 4% and the developed stresses slightly increased by 1% when increasing ( $p_1$ ) due to a product of the decreasing effect by the buckling slenderness  $\lambda_d$  and the sectional modulus  $S_{xx}$ .





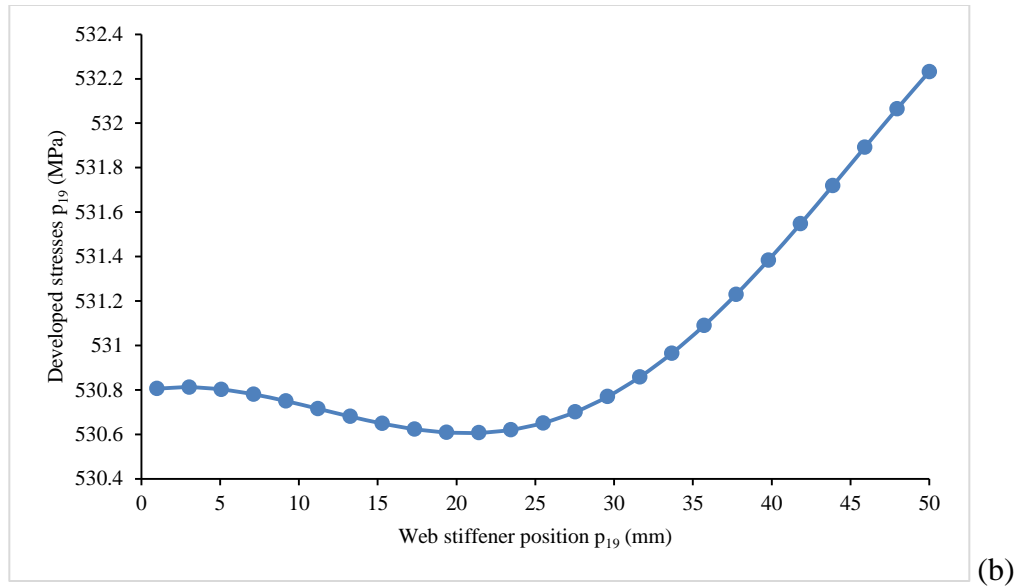


Figure 7.3. Single parameter response for different positions of web stiffeners  $p_1$  (a) buckling loads and (b) Developed stresses.

Local sensitivity represents the change of the outputs based on the change of inputs independently. A positive value of the sensitivity means that as the input parameter increases, the output increases as well; and a negative value means the opposite. Figure 7.4 shows the sensitivities of the zed section with web and flange stiffeners for the main output parameters including the buckling ( $p_{18}$ ) and the flexural developed stresses ( $p_{19}$ ) that were based on the input parameters, namely, the web stiffener's positions from the web-flange junction ( $p_1$  and  $p_2$ ), the edge stiffener's sizes ( $p_3$  and  $p_4$ ), the web stiffener's sizes ( $p_6$  and  $p_7$ ), the angle between web stiffeners and web of the section ( $p_8$  and  $p_9$ ), and the angle between edge stiffeners and flange of the section ( $p_{10}$  and  $p_{11}$ ).

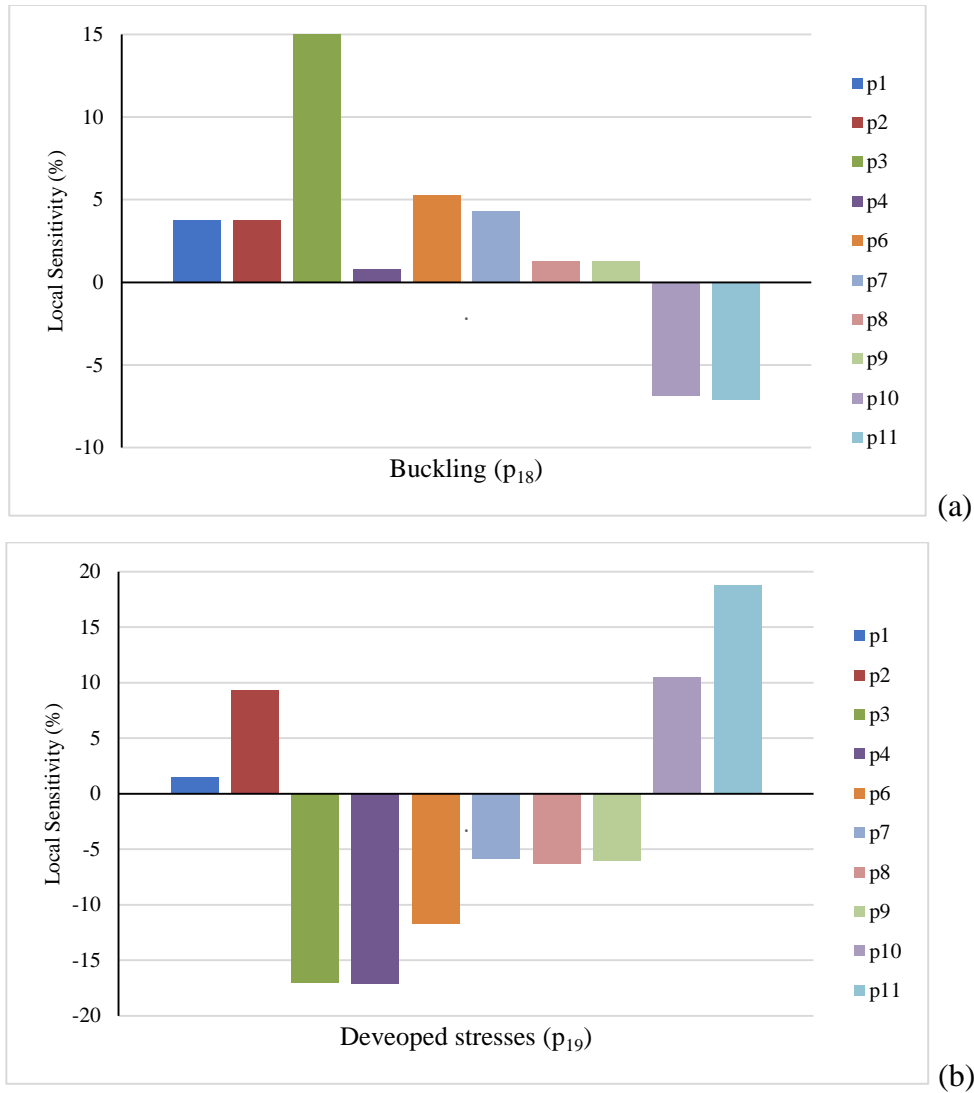
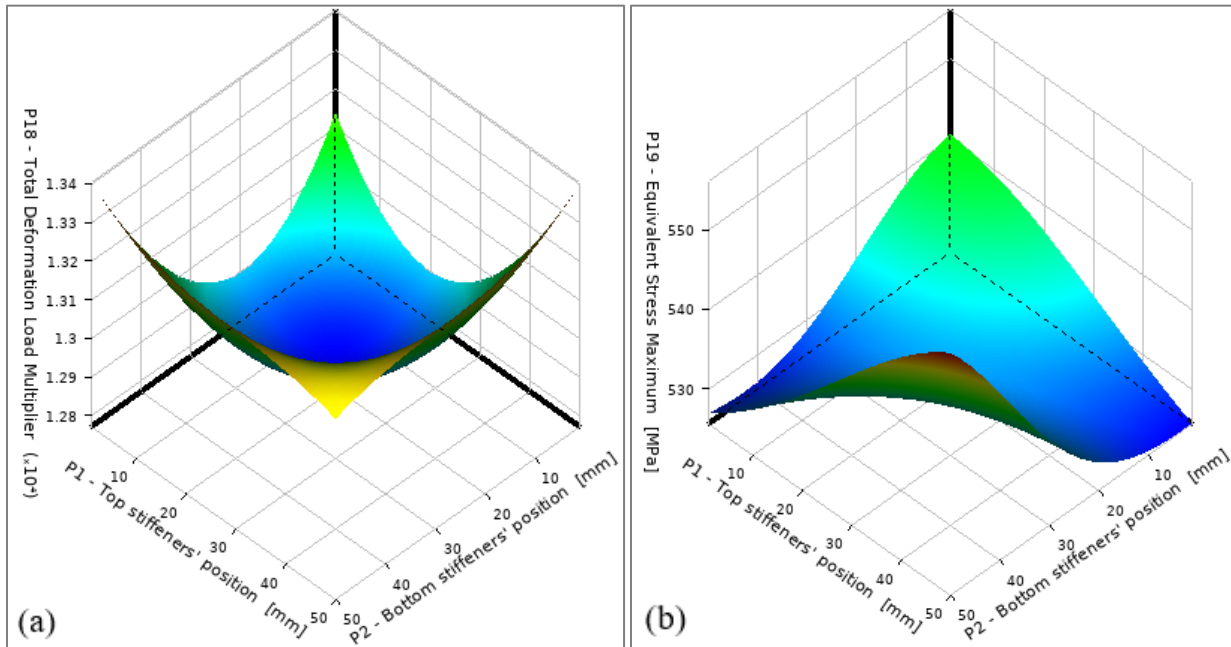


Figure 7.4. Local sensitivity bar of single parameter obtained for the zed section with web and flange stiffeners (a) buckling and (b) developed stresses.

It could be seen that for zed sections, increasing the web stiffener's positions from the web-flange junction ( $p_1$  and  $p_2$ ) reduced the buckling loads with a sensitivity of around 5% and increased the flexural stresses with a sensitivity of up to 9%. It could be seen that increasing the web stiffener's sizes and shapes (through the web stiffener's sizes ( $p_6$  and  $p_7$ ) and the web stiffener's shapes ( $p_8$ )) was one of the most effective ways to increase the section strengths, with up to 5% effect on increasing the buckling loads and 12% effect on decreasing the flexural

stresses. However, increasing the edge stiffener's sizes ( $p_3$  and  $p_4$ ) was the most effective solution, with up to 15% and 17% positive effect on the buckling loads and the flexural stresses, respectively. The sensitivity effect of the angle between flange and edge stiffener ( $p_{10}$  and  $p_{11}$ ) shows that reducing the angle values was also an efficient way to increase the section strength.

Figure 7.5 shows the typical 3-D response surfaces of the buckling loads and flexural stresses for zed sections. These results can quantify the effect of different combinations of any two input parameters on the buckling loads (denoted by  $p_{18}$ ) and flexural stresses (denoted by  $p_{19}$ ). As shown in Figure 7.5 (a), by decreasing the values of the parameters  $p_1$  and  $p_2$ , particularly from 20 mm, the buckling loads increased. Figure 7.5 (b) shows that this also results in a decrease in the flexural stresses. Similarly, by increasing the values of the parameters  $p_6$  and  $p_8$ , the buckling loads decreased as shown in Figure 7.5 (c) and the flexural stresses also decreased as depicted in Figure 7.5 (d).



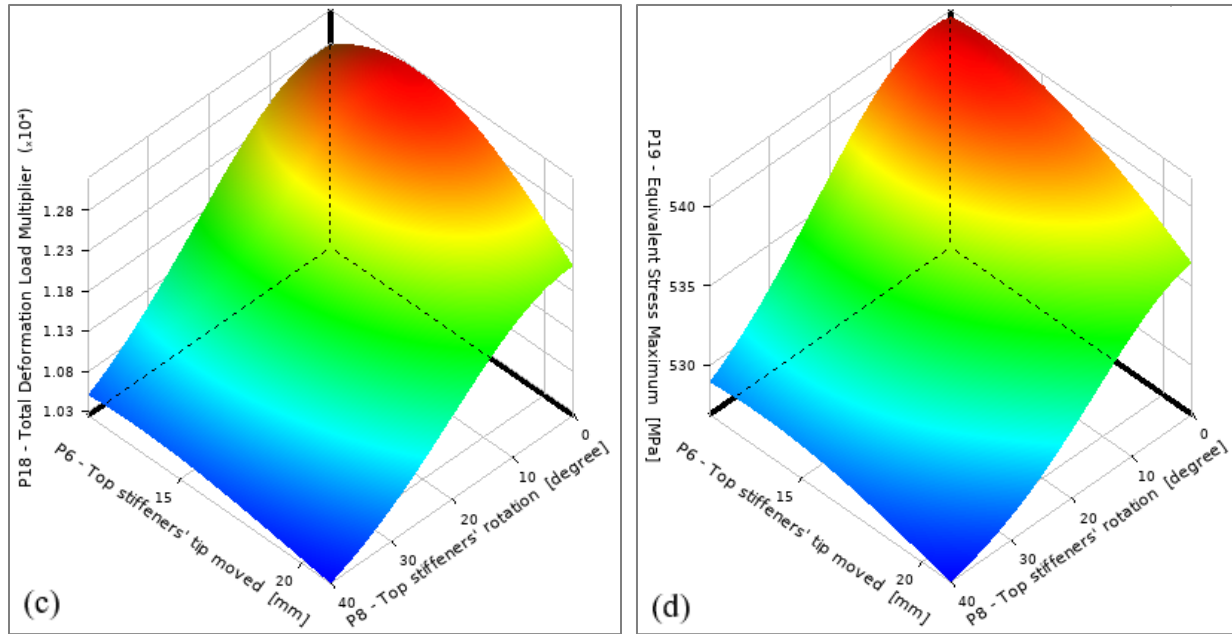


Figure 7.5. Double parameters response of the zed sections for different positions of web stiffeners  $p_1$  and  $p_2$  on (a) buckling loads and (b) flexural developed stresses, and for different web stiffeners through the angle parameters  $p_6$  and  $p_8$  on (c) buckling loads and (d) flexural developed stresses.

### 7.4.3 Optimisation results

Based on the results of the response surface analysis, the Multi-Objective Genetic Algorithm (MOGA) was used as the search engine to find the candidate optimal results to minimise the selected multi-objective function. In this chapter, for zed sections, the design variables were  $p_1$ ,  $p_2$ ,  $p_3$ ,  $p_4$ ,  $p_6$ ,  $p_7$ ,  $p_8$ ,  $p_9$ ,  $p_{10}$ , and  $p_{11}$ , and the output parameters were the maximum buckling load,  $p_{18}$ , and the minimum flexural developed stress,  $p_{19}$ . Several different scenarios were used to determine optimal design candidates. These included (1) minimising the flexural developed stresses, (2) maximising buckling loads, and (3) minimising the flexural developed stresses and maximising buckling loads at the same time. Table 7.2 shows an example of these scenarios for zed sections with flange stiffeners, where the goal was to maximise the buckling loads ( $p_{18}$ ) and minimise the flexural developed stresses ( $p_{19}$ ). As a result, three design candidates were found

with the same design variables. The design candidate was then loaded up to failure to obtain collapse load- displacement curves as indicated in Figure 7.7 for zed sections. This process repeated to obtain other design candidate results for the zed sections (i.e. Candidates 1-5).

Table 7.3 presents the buckling loads and ultimate bending strengths of the channel and zed sections obtained from the MOGA optimisation process (with input parameters shown in Figure 7.1 and Table 7.1). The results in this table were compared with those of the standard lipped channel and zed sections having the same amount of material and the same section height. Candidates 1 and 4 were obtained when the ‘Goal’ was minimising the flexural developed stresses, Candidates 2 and 5 were obtained when the ‘Goal’ was maximising the buckling loads, and Candidates 3 and 6 were obtained when the ‘Goal’ was maximising the buckling and minimising the flexural developed stresses under bending for distortional buckling.

**Table 7.2** Candidate design when the target objectives were maximising buckling and minimising developed stresses (Candidate 6).

Table of Schematic D4: Optimisation			
Optimisation Study			
Minimise $p_{19}$	Goal, Minimise $p_{19}$ (High importance)		
Maximise $p_{18}$	Goal, Maximise $p_{18}$ (Low importance)		
Optimisation Method			
MOGA	The MOGA method (Multi-Objective Genetic Algorithm) is a variant of the popular NSGA-II (Non-dominated Sorted Genetic Algorithm-II) based on controlled elitism concepts. It supports multiple objectives and constrains and aims at finding the global optimum.		
Configuration	Generate 100 samples initially, 100 samples per iteration and find 3 candidates in a maximum of 100 iterations.		
Status	Converged after 2740 evaluations.		
Candidate Points			
	Candidate point 1	Candidate point 2	Candidate point 3
$p_1$ - Top stiffeners' position (mm)	7.55	7.38	7.40
$p_2$ - Bottom stiffeners' position (mm)	3.09	3.29	3.29
$p_3$ - Top edge stiffeners' width (mm)	18.18	18.18	18.20
$p_4$ - Bottom edge stiffeners' width (mm)	16.15	16.19	16.19
$p_6$ - Top stiffeners' tip moved (mm)	12.81	12.82	12.82
$p_7$ - Bottom stiffeners' tip moved (mm)	13.12	13.61	13.60
$p_8$ - Top stiffeners' rotation (degree)	1.32	1.07	1.09
$p_9$ - Bottom stiffeners' rotation (degree)	0.87	1.36	3.13
$p_{10}$ - Top edge stiffeners' rotation (degree)	0.71	0.71	0.73
$p_{11}$ - Bottom edge stiffeners' rotation (degree)	0.71	0.02	0.05
$p_{16}$ - Top flange width (mm)	35.51	35.31	35.50
$p_{17}$ - Bottom flange width (mm)	28.86	29.12	29.12
$p_{18}$ - Total deformation Load Multiplier	** 20.63	** 21.04	** 20.85
$p_{19}$ - Equivalent Stress Maximum (MPa)	** 453.59	** 453.90	** 453.78

**Table 7.3** The results of buckling load ( $P_b$ ), flexural developed stresses ( $\sigma$ ) and ultimate moment capacity of zed sections.  $M_u$ ,  $M_{uc}$  stand for ultimate moment capacity without and with the cold working effect, respectively.

Section type	$P_b$ (kN)	$\sigma$ (MPa)	$M_u$ (kNm)	$M_{uc}$ (kNm)	$M_{uc}/$ $M_u$	$M_{uc}/$ $M_{uc}^{standard}$
Standard	9.6	-	9.98	9.98	1.00	1.00
Reference (b)	11.6	570.0	10.66	10.86	1.02	1.09
Candidate 1	19.7	466.2	11.81	12.29	1.05	1.23
Candidate 2	21.1	496.4	10.76	10.88	1.02	1.09
Candidate 3	20.2	462.8	12.34	12.45	1.01	1.25
Reference (c)	13.3	542.2	11.38	11.51	1.02	1.15
Candidate 4	18.8	449.8	11.81	12.13	1.03	1.21
Candidate 5	20.3	460.6	11.73	12.23	1.05	1.22
Candidate 6	19.8	450.4	11.97	12.35	1.04	1.24

The optimal shapes and the comparison between their flexural strength capacities are shown in Figures 7.6-6.8. In which  $M_y$  is the yield bending moment of the whole cross section;  $M$  is the bending moment capacity (when the cold working effect is not included  $M$  equals  $M_u$ , and when the cold working effect is included  $M$  equals  $M_{uc}$ ); and  $M_b$  is the buckling moment capacity. The buckling and ultimate strength results were obtained by FE nonlinear analysis as described in Chapter 3, which is called “FEM” model. The buckling modes were obtained from linear buckling analysis that was conducted with the conventional Finite Element Method (FEM). In addition, another model was developed, in which the desired linear buckling modes obtained from Finite Strip Method using CUFSM software [144] were transferred to the FE analysis, to conduct the nonlinear analysis. This model is called “CUFSM-FEM” model. Both “FEM” and “CUFSM-FEM” models’ results are shown in Figures 6.6-6.8.

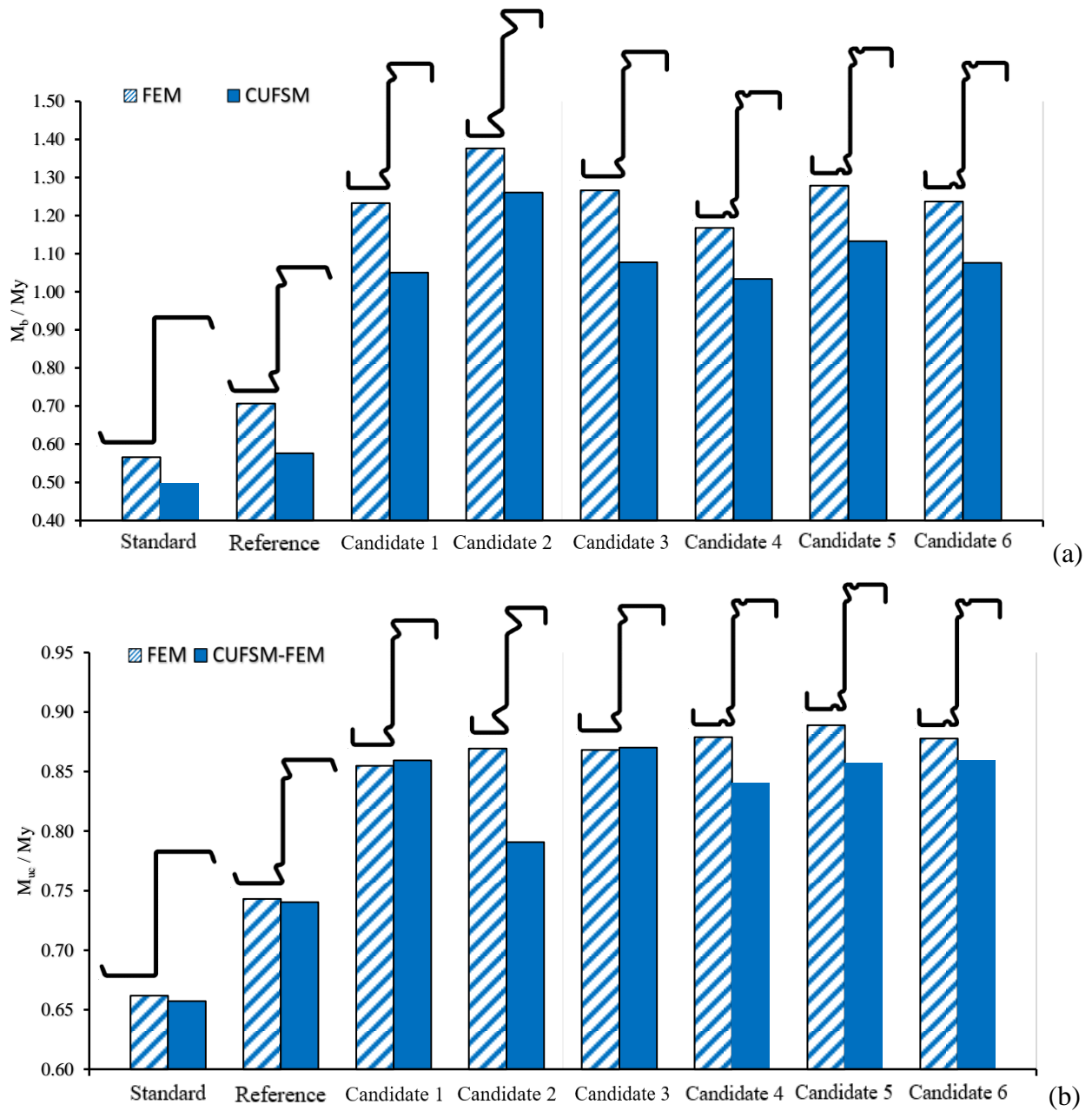


Figure 7.6. Strength results of standard, reference and optimised of the zed sections for (a) buckling and (b) ultimate moment capacities with the cold work effect included.



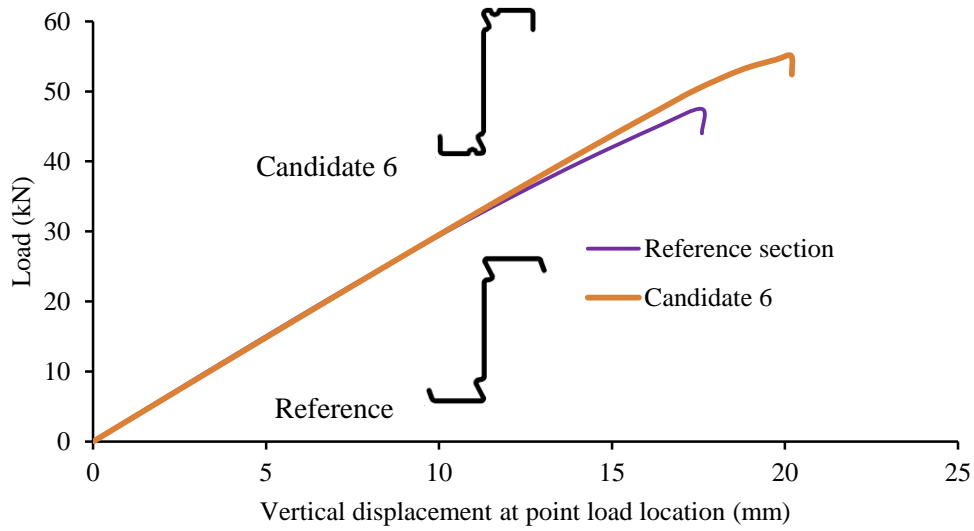


Figure 7.7. Load-displacement curves for the zed reference and design Candidate 6 sections.

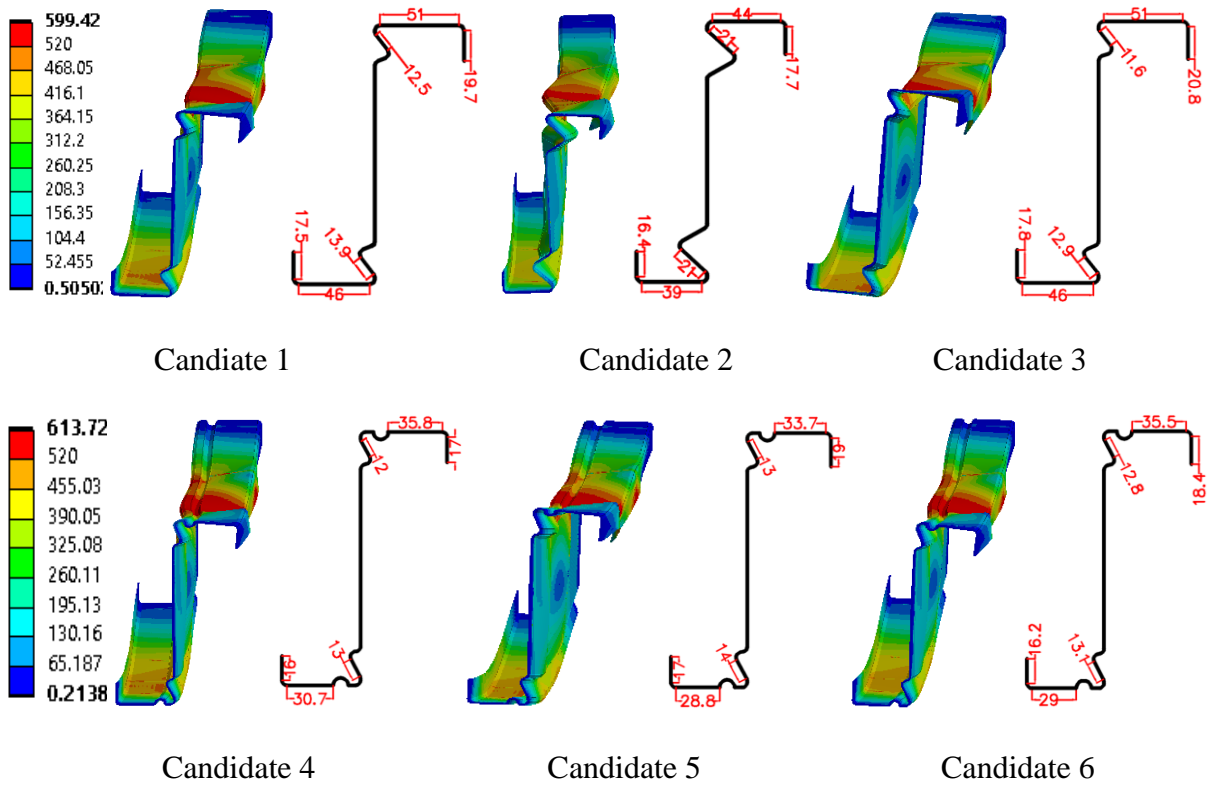


Figure 7.8. Dimensions, deformed shapes and von Mises stress distribution for all design candidates of zed sections.

A number of observations were made from Figures 7.6-7.8 and Table 7.3 as follows:

- The reference zed section provided considerably greater buckling capacity when compared to the standard lipped zed section by 21%, whereas the ultimate moment capacities was also improved by 9%.
- Adding flange stiffeners to the reference sections further enhanced the buckling and ultimate moment capacities of the zed section by 15% and 6%, respectively.
- By changing the position, size and shape of web stiffeners, lip's length, and section corners' radii as well as including the cold working effect at the sections' corners and stiffeners' bends of the reference zed section, optimal sections with maximum buckling strengths could be obtained (Candidates 1-3). The gains in buckling strength for the zed Candidates of 1, 2 and 3 were up to 2.1 times, when compared to the standard lipped zed sections. At the same time, the ultimate moment capacities were also improved by 23%, 9% and 25% for the zed sections, respectively.
- The optimal design of the zed section was obtained by changing the position, size and shape of web stiffeners, the position and size of flange stiffeners, lip's length, and section corners' radii as well as including the cold working effect at the sections' corners and stiffeners' bends of the reference sections having flange stiffeners (Candidates 4-6). The significant increases in buckling loads for the Candidates 4, 5 and 6 were up to 2.1 times, when compared to the standard lipped zed sections. At the same time, the ultimate moment capacities were also significantly increased by 21%, 22% and 24%, respectively.
- For all design Candidates (1-6), the zed sections strived to increase their buckling and ultimate moment capacities by: (1) decreasing the position of web stiffeners (converged to minimum defined vales of  $p_1 = 1.0$  mm and  $p_2 = 1.0$  mm) or moving web stiffeners toward the web flange junctions as much as possible, (2) reducing the section corners' radiuses to

minimum defined value of  $p_5 = 3.3$  mm, (3) keeping the angle between the web stiffeners and the web the same as the reference one ( $p_6 = 0$  degree and  $p_7 = 0$  degree), and (4) reducing the angle between the lip stiffener and the flange (the optimal angles obtained from the process were all close to 90 degrees). This was due to the combined effect of (1) increasing the sectional modulus, (2) reducing the distortional buckling slenderness, and (3) the cold working effect in the section corners (smaller corner radius had greater strength enhancement). In general, these observations are consistent with the results presented in Chapter 5.

- It is shown in Figure 7.8 that for design Candidates (1-3), the optimised zed sections had different web stiffener's sizes, and lip and flange widths depending on the target objectives (note that the total developed length of the zed section and the section height remain constant). For instance, the sections tended to converge to smaller web stiffener's size and longer lips and larger flange widths ( $p_3 = 19.7$  mm,  $p_4 = 17.5$  mm,  $p_6 = 12.5$  mm,  $p_7 = 13.9$  mm,  $p_{12} = 51.0$  mm and  $p_{13} = 46.0$  mm) when the target was to minimise flexural developed stresses in the section (Candidate 1), whereas the section tended to take larger web stiffener's size and shorter lips and smaller flange widths ( $p_3 = 17.7$  mm,  $p_4 = 16.4$  mm,  $p_6 = 21.0$  mm,  $p_7 = 21.0$  mm,  $p_{12} = 44.0$  mm and  $p_{13} = 39.0$  mm) when the target was changed to maximise buckling loads (Candidate 2). However, the section had smaller web stiffener's size and longer lips and larger flange widths ( $p_3 = 20.8$  mm,  $p_4 = 17.8$  mm,  $p_6 = 11.6$  mm,  $p_7 = 12.9$  mm,  $p_{12} = 51.0$  mm and  $p_{13} = 46.0$  mm) when the targets were maximising buckling loads and minimising flexural developed stresses (Candidate 3).
- Considering the design Candidates (4-6) shown in Figure 7.8, while the zed sections tended to have the same position and size of flange stiffeners ( $p_{12} = p_{13} = 5.0$  mm and  $p_{14} = p_{15} = 5.0$ ), the sections had various web stiffeners sizes, lip lengths, and flange widths based on target objectives. Candidate 4 obtained from minimising flexural developed stresses had the web stiffener size, lip length and flange width of 12.0 mm, 17.0 mm, and 35.8 mm,

respectively, for the upper part of the section as well as the web stiffener size, lip length and flange width of 13.0 mm, 16.0 mm, and 30.7 mm, respectively, for the lower part of the section. However, Candidate 5 obtained from maximising buckling loads had web stiffener size, lip width and flange width of 13.0 mm, 19.0 mm, and 33.7 mm, respectively, for the upper part of the section as well as the web stiffener size, lip length and flange width of 14.0 mm, 17.0 mm, and 28.8 mm, respectively, for the lower part of the section.

- For all design Candidates (1-6), increasing the web stiffener size and lip length up to certain limit significantly improved the buckling capacities of zed sections which was effective in suppressing section instability, resulting in significantly increased ultimate moment capacities (see Table 7.3). These sections also exhibited a considerably higher stiffnesses (as shown in Figure 7.7), which is a direct result of the stiffeners delaying and mitigating the stiffness degradation due to buckling. It was noted that increasing the stiffeners' size was accounting for the total length of the section, and therefore, the flange width of the design candidates was smaller than that of the reference section. Nevertheless, increasing the stiffeners' sizes beyond a certain limit (Candidates 2 and 5) still considerably improved distortional buckling capacities of the zed sections, whereas it did not have a significant effect on the ultimate moment capacity and it actually noticeably reduced the ultimate moment capacities in design Candidates 2 and 5 when compared to Candidates 1 and 4. This was a result of a significant reduction of the sectional modulus in the minor axis which made these sections prone to the failure due to distortional-global interaction buckling and consequently led to lower ultimate moment capacities for the beam sections. These observations were consistent with those in Chapter 5.
- The optimal shapes of the zed sections could be obtained when the target objectives were to both minimising the flexural developed stress and maximising the buckling loads in the sections. This led to an optimal design solution (Candidate 6) which had significant increase in bending and ultimate strengths.

- Including the cold working effect in the sections' corners and stiffeners' bends led to noticeable enhancement in the ultimate moment capacities of the optimised zed sections (as indicated in Table 7.3), despite the insignificant effect for the cases where the cold working effect was only present in the sections' corners. The maximum percentage of increase in the ultimate moment capacities with the cold working effect was up to 5%, confirming that the influence of the cold working effect could be significant.
- Figure 7.6 compares the FEM strength capacity results of the optimised sections with the results obtained by transferring buckling mode shapes from CUFSM to the FEM. It was seen that both FEM and CUFSM-FEM methods provided the same trend with an average difference of 15% and 2% in the buckling and ultimate bending moment capacities, respectively.

## 7.5 Conclusions

This chapter presents an optimisation of CFS longitudinally stiffened zed sections using detailed Finite Element (FE) modelling and Response Surface Optimisation. The FE models were first developed to replicate four-point beam bending tests of distortional buckling failure configuration of the zed sections, which included geometrically and materially nonlinear analysis with initial geometric imperfections and the cold working effect. These validated FE models were then utilised to optimise the buckling and ultimate flexural strengths of the sections. In the optimisation process, each section was parameterised in terms of geometric dimensions, imperfections and material properties using DOE technique to determine the buckling loads and flexural stresses at the design points. Kriging-based response surfaces were generated based on the DOE results to study the influences of the stiffener's geometric and material properties on the section buckling loads and flexural stresses including its location, shape, size and material properties by the cold working at the section corners and stiffeners bends. Optimal designs of the zed sections were finally obtained using the multi-objective genetic algorithm method (MOGA). The following conclusions were drawn based on the results of this study:

- By considering both geometry and the cold working effect in the optimisation process, optimal designs of the zed sections could be obtained with significant gain in buckling and ultimate bending strengths. The gains in buckling strength were up to 2.1 times for the zed sections, when compared to the standard sections using the same amount of material.
- The optimum positions of the web and flange stiffeners was found to be moving towards the web-flange junctions as close as possible during the optimisation process for zed sections. This was a result of the intermediate stiffeners position increasing the sectional modulus and decreasing the distortional buckling slenderness, which ultimately enhanced the distortional buckling and ultimate strength capacities as well as mitigating the post-buckling stiffness degradation of the optimised sections.
- For the zed sections, the entire sections with decreasing section corners radii resulted in optimal solutions. This was because when reducing the corners radii, the distortional

buckling slenderness of the section and the strength enhancement of the corners increased, and consequently the buckling and ultimate bending strength was enhanced.

- Comparisons between the design candidates indicated that by increasing the size of intermediate web, flange and edge stiffeners, a turning point was reached where increasing the stiffeners size reduced the ultimate moment capacities, while marginally improved the distortional buckling loads, resulting in sections fail in distortional-global interactive buckling modes.
- The cold working effect induced from the cold roll manufacturing process was found to be considerable in the optimised zed sections, suggesting that the FE models need to include the cold working effect for accurately obtaining the ultimate moment capacity of the sections. The cold working effect was most significant when the sections were less prone to buckling, especially for distortional and global-distortional interactive buckling modes.
- It was found that both target objective functions, which were maximising buckling loads and minimising flexural developed stresses, had to be deployed in order to obtain the optimal sections with significantly increasing both bending strength capacities and the cold working effect.
- The adequacy of the optimised sections obtained from FEM optimisation process was verified by the results obtained from transferring the CUFSM buckling mode shapes into the FEM using the CUFSM-FEM model. It was found that the FEM results closely followed the trends in the buckling and flexural strength capacities obtained by the CUFSM-FEM results. This demonstrated the reliability of the proposed optimisation procedure using the direct FEM optimisation.

## **Chapter 8 The influence of cold work effects on material properties and flexural strength of CFS beam sections**

*This work is based on a journal paper of “Qadir, S. J., et al. “The influence of cold work effects on material properties and flexural strength of CFS beam sections”, Paper in preparation to be submitted.*

### **8.1 Introduction**

The work in this chapter was driven by the need to explore the influence of cold work effects on mechanical properties and flexural strength of the cold roll formed sections by physical testing and combined detailed (FE) models and optimisation. A material test programme on a total of four cold roll formed structural longitudinally stiffened sections, including two channel section and two zed sections was provided, which performed in this research. The experimental programme was fully described: techniques implemented, data generated and analysis methods adopted. The cold work effect in the corner and stiffener bend regions of cold roll formed sections was analysed and the applicability of existing predictive models was evaluated. The strength enhancement obtained in the section corners and stiffener’s bends were then used to accurately obtain the bending strength of the CFS sections using FE models. Optimal cross-sectional shape of the longitudinally stiffened channel and zed sections was finally selected and proposed.



## **8.2 The cold work effects on mechanical properties of CFS sections**

### **8.2.1 Tensile coupon tests carried out in this research**

The material properties of flat and curved coupons extracted from the cold roll formed steel sections in each group of specimens were determined from tensile tests. The tensile specimens were cut from the centre of the web/flange plates in the longitudinal direction of the finished specimens, and belonged to the same production batch as the beam test specimens. Tensile specimens were also cut from the same coil material, as the beam specimens, prior to section forming. Flat and curved steel coupon specimens had the ‘dog bone’ shape and were prepared according to the appropriate specifications of the relevant European standard ISO 6892-1 (ISO 2009). The flat coupons had a nominal width of 12.5 mm, while the curved coupons had different widths depending on the positions and sizes of the cross-sections. The positions of the extracted coupons from within the steel sections are shown in Figure 8.1. The coupon identification system begins with the coupon type, followed by the coupon location and, finally, for repeated tests, the test number with reference to Figure 8.1.

The cross-section specimens were labelled, a channel section specimen label begins with C whilst a zed section specimen begins with Z. For example, a specimen labelled as C-W145T1.2 is described as follows: C: Channel specimen; W: Web, 145: Nominal web height or beam depth (mm); T: Thickness, 1.2: Nominal plate thickness (mm).

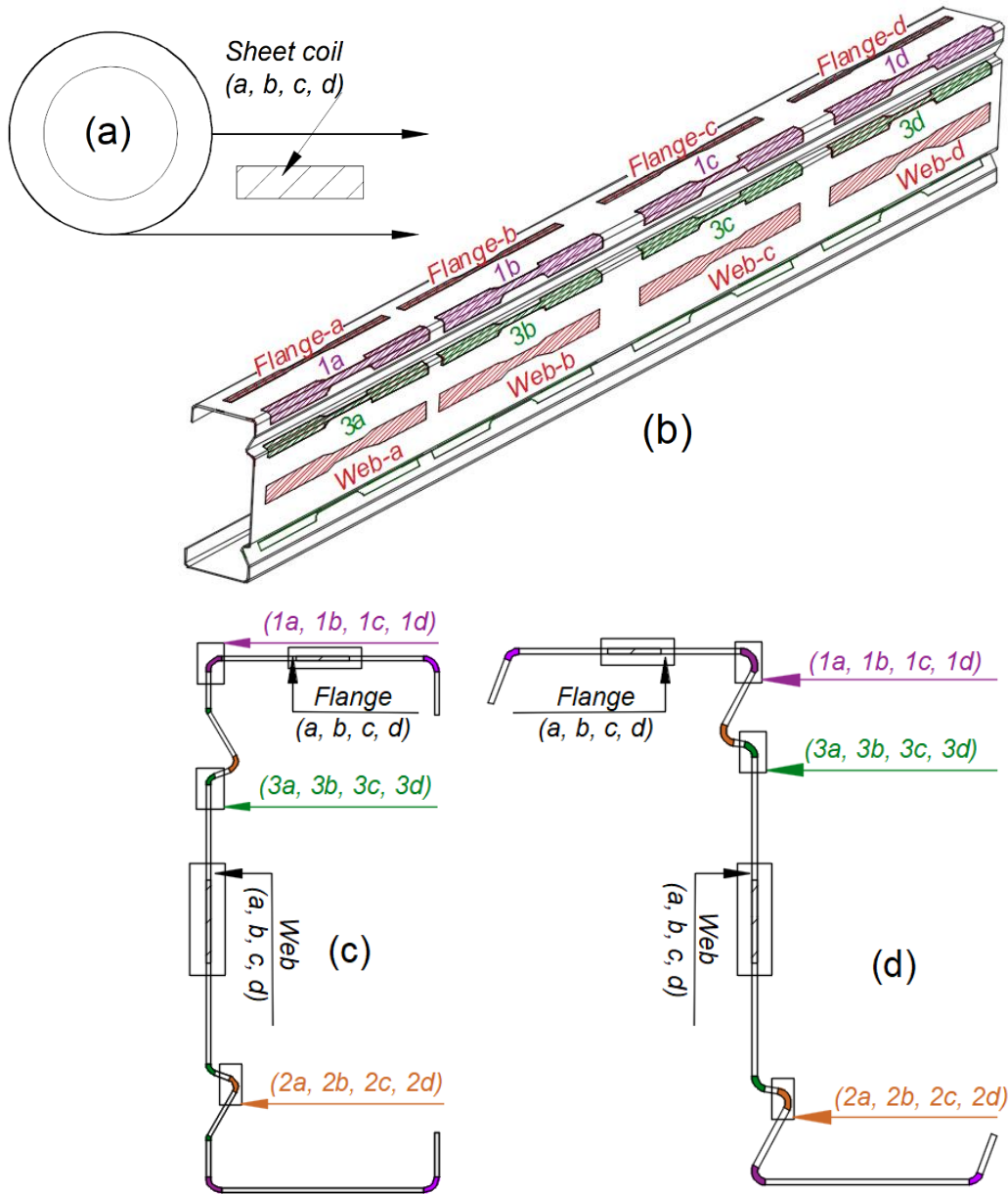


Figure 8.1. Locations of extracted tensile coupons (a) pre-cold rolled sheet coil, (b) longitudinal channel section, (c) channel cross-section, and (d) Zed cross-section.

The dimensions of each specimen were measured before testing. For the flat specimens, the initial cross-sectional area was calculated from the width and thickness, measured using a micrometre. For the curved specimens, the cross-sectional areas were determined by taking a

macro photograph of the cross section using the reversed lens technique. The images were then imported into AutoCAD software version 20.1 and scaled based on the measurement of the width of the gripped end of the coupon, as illustrated in Figure 8.2. The measured width of the coupon along the gauge length was then superimposed on the photograph, allowing the area to be automatically calculated by the software. The process was repeated with pictures taken from the other end of the coupon and a difference in the calculated areas of less than 1% was obtained for all coupons. The stress was calculated using the measured force divided by the initial cross-sectional area and the strain was obtained from the strain gauges and the extensometer measurements.

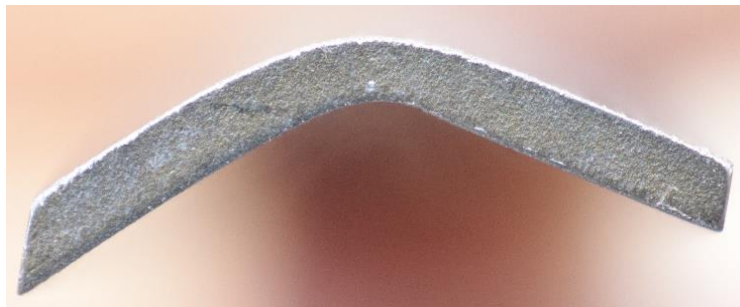


Figure 8.2. Macro photograph of the cross section of a typical curved coupon

All coupons were instrumented with an extensometer of 50 mm gauge length. In addition, each flat coupon was instrumented with one linear 10-mm strain gauge on each side of the coupon at mid-length to the centre of both faces of each coupon using TML strain gauge adhesive of CN series to measure the strains in the initial part of the stress-strain curve, while each curved coupon was instrumented with a 10-mm or 5-mm linear strain gauge on the outside of the corner. Due to the asymmetric shape of the curved coupons, they were tested in pairs with a special round bar placed between the gripped ends of the coupons, as illustrated in Figures 8.3-8.4. This avoided the need to flatten the coupon ends, which could have introduced unwanted bending moments into the coupons.



Figure 8.3. Typical tensile test setup (a) flat coupon and (b) Curved coupons





Figure 8.4. Typical curved coupons before and after testing attached with strain gauges for the cross-section Z-W200T2.0 (Extracted from curved location 1a, 1b, 1c and 1d).

The tensile coupons were tested in a 300-kN Shimadzu AGS-X (Kyoto, Japan) universal testing machine at the University of Sheffield, while applying a displacement rate of 1 mm/min. Each test was halted for 2 min at regular intervals in order to allow the load to settle down to static values and eliminate strain rate effects [150]. Comparing with the readings obtained from the extensometers, the strain gauge readings are more accurate, but for a much smaller range. The resulting stress-strain curves were plotted and the yield stress was obtained at a strain level of 0.2%, while the important material property, initial Young's modulus ( $E$ ), was determined by the readings obtained from strain gauges.

## 8.2.2 Predictive models

The material properties at corners and stiffener's bends affected by the cold work could be obtained from the material properties of virgin coil material by using formulae from the North American specification [3] for Cold-formed steel structural members. The equation for

determining the tensile yield strength,  $f_{yc}$ , of the corner was based on the equation (8.1) which was empirically derived from tests by Karren [28]. The equations (8.1-8.3) are referred to hereinafter as the “AISI Specification” [3].

$$F_{yc} = \frac{B_c F_{yv}}{\left(\frac{R}{t}\right)^m} \quad (8.1)$$

In which

$$m = 0.192 \frac{F_{uw}}{F_{yv}} - 0.068 \quad (8.2)$$

$$B_c = 3.69 \frac{F_{uw}}{F_{yv}} - 0.819 \left(\frac{F_{uw}}{F_{yv}}\right)^2 - 1.79 \quad (8.3)$$

Where:  $F_{yv}$  and  $F_{uw}$  are yield stress and ultimate strength of the flat region material,  $R$  is inside corner/bend radius and  $t$  is the plate thickness.

The AISI Specification assumes that the strength enhancement in the corner regions of cold-formed steel sections is dependent on (i) the ratio of the ultimate tensile strength ( $f_u$ ) to the yield strength ( $f_y$ ) of the unformed (virgin) material, which is indicative of the potential for cold-working, and (ii) the ratio of the inner corner radius ( $R$ ) to the thickness of the steel sheet ( $t$ ), which is indicative of the induced level of plastic strain. Note that values of  $f_y$  and  $f_u$  are provided in mill certificates but, for design purposes, the values given in material specifications should be adopted.

Gardner et al. [151] modified the predictive model given in the AISI Specification [Equations. (8.2), (8.3)] based on test results on corner material extracted from cold-formed steel box sections, and the revised values of coefficients are given in Equations (8.4), (8.5). They found that the modified predictive model provided more accurate and consistent corner yield strength predictions than those obtained from the AISI Specification for cold-formed square and rectangular hollow sections.

$$m = 0.23 \frac{F_{uw}}{F_{yv}} - 0.041 \quad (8.4)$$

$$B_c = 2.9 \frac{F_{uw}}{F_{yv}} - 0.752 \left( \frac{F_{uw}}{F_{yv}} \right)^2 - 1.09 \quad (8.5)$$

The tensile coupon tests carried out by the author in this study for section's corners and stiffeners bends were compared to the above two models and the results are presented in Section 8.5.2 to evaluate the predictive model's accuracy.

### 8.3 Finite Element modelling and optimisation

#### 8.3.1 Tensile test

The Finite Element modelling of flat coupon and curved coupons were performed. In the FE modelling, only the parallel part of the tensile specimen was simulated (the flat coupon has the length, width and thickness of 75 mm, 12.50 mm and 2.0 mm, respectively, the cross sectional area of curved coupon obtained from microphotography. The flat coupon was modelled by 1898 solid elements and the curved coupons were modelled by 3000 elements; they are 20-node 3D structural solid elements. One end of the coupons was fixed and a small incremental displacement was applied at the other end to stretch the coupon to failure.

#### 8.3.2 Four-point beam bending test

Qadir et al. [149] presented FE models capable of simulating the buckling and ultimate bending strength of cold rolled steel beam sections. Their FE models, which were developed in ANSYS (ANSYS, Inc.) and verified against earlier experimental testing [142], were used to calculate buckling and ultimate bending strength in this chapter.

All the beams had a total length of 2920 mm, a span of 2691 mm, and a load centre of 897 mm (i.e. four-point bending). Lateral bracings were provided to prevent lateral torsional buckling in all FE models. Two methods were used to generate the shape of initial geometric imperfections namely Finite Element method using ANSYS and Finite Strip Method using CUFSM as well as

the 75% of CDF magnitude corresponding to 1.55t was taken for the amplitude of initial imperfections. The elastic modulus  $E$  of 205 GPa and material yield strength  $f_y$  of 519.4 MPa were assigned to the flat part of all beam sections while the material properties at corners and stiffener's bends affected by the cold work were obtained from the material properties of flat regions by using formulae from the North American specification for Cold-formed steel structural members. The equation for determining the tensile yield strength,  $f_{yc}$ , of the corner was based on the equation (8.1) in section 8.2.2. The constitutive stress-strain model proposed by Hadarali and Nethercot [143] was employed, in which the plastic region of the stress-strain curve was modelled with a straight line with a constant slope of  $E/50$ , where  $E$  is the elastic modulus obtained from material tests. See chapter 3 for full details on FE modelling.

**In this chapter, however, the measured material properties obtained from tensile coupon tests carried out by the author** are employed in FE modelling to accurately quantify the effects of geometry and the cold work induced from the cold roll forming process. Figures 8.5 (a–b) show both the measured engineering stress-strain curves and the true stress-strain curves, determined using the following equations:

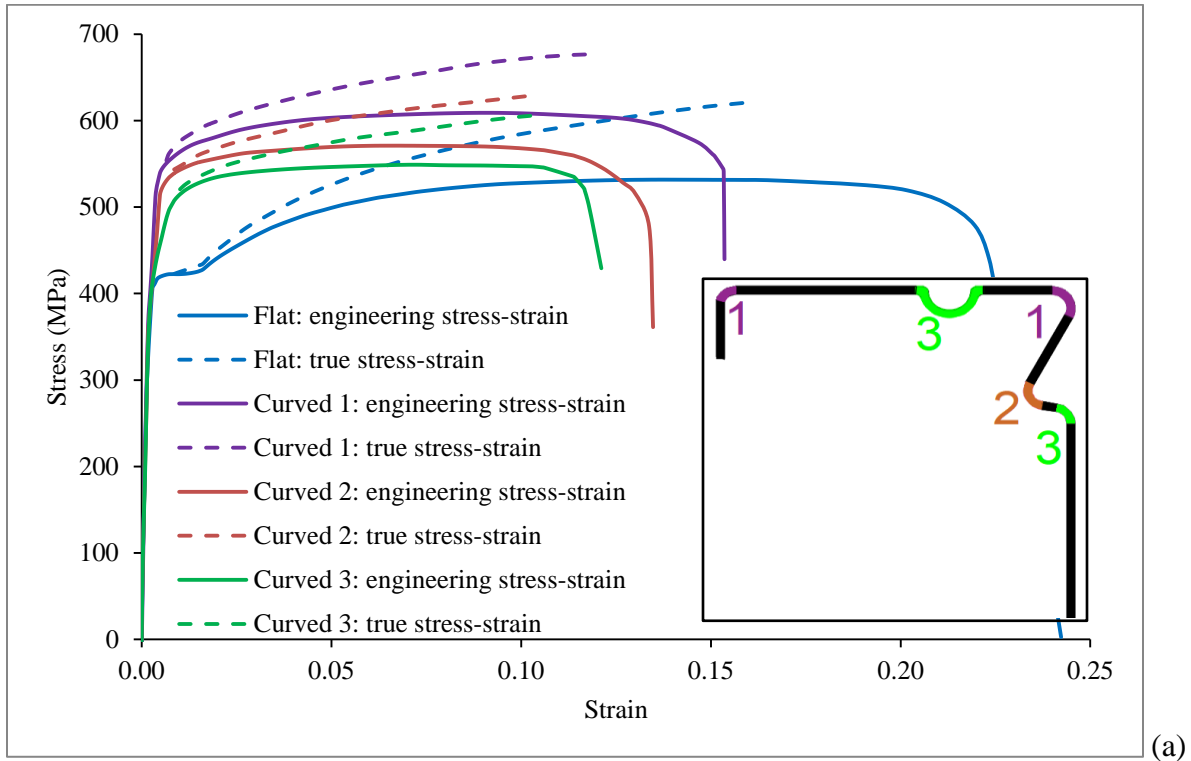
$$\sigma_{true} = \sigma_{eng} (1 + \varepsilon_{eng}) \quad (8.1)$$

$$\varepsilon_{true}^{pl} = \ln (1 + \varepsilon_{eng}) - \frac{\sigma_{eng}}{E} \quad (8.2)$$

where  $\sigma_{eng}$  and  $\varepsilon_{eng}$  = engineering stress and strain, respectively, based on the original cross-sectional area and the original gauge length of the coupons; and  $\sigma_{true}$  and  $\varepsilon_{true}^{pl}$  are the true stress and the true strain, respectively. Equations (8.1) and (8.2) could only be valid as long as stresses and strains are uniform over the gauge length, in other words, true stress and true strain does not have a negative slope. Therefore, the true stress-strain curves are only presented in Figures 8.5(a–b) to the peak point of the engineering curves. The zed section was defined with 10 corners and bends, as shown in Figure 8.5a, but only material properties at five corners and bends in the upper part of the section were considered as the others in the lower part were



assumed to be the same due to symmetry. On the other hand, the channel section was defined with 12 corners and bends, as shown in Figure 8.5b, but only material properties at six corners and bends in the upper part of the section were considered as the others in the lower part were assumed to be the same due to symmetry.



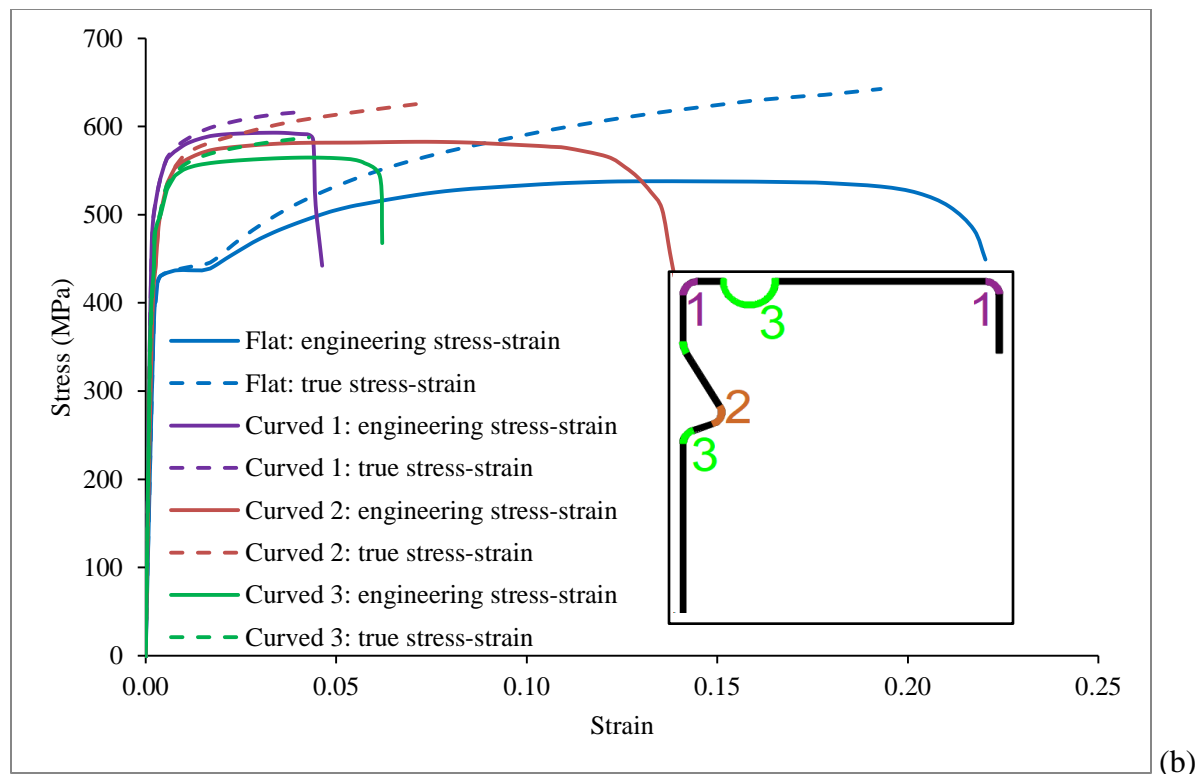


Figure 8.5. The measured stress-strain curves of the flat and curved coupons carried out in this study, and used in the FEM (a) Z-W200T2.0 and (b) C-W200T2.0.

## 8.4 Optimisation

The optimal cross-sectional shapes investigated in this chapter, were optimised based on an optimisation framework developed by the Qadir et al. [152] for the purpose of producing more efficient and optimal design of CFS sections, see chapters 6 and 7. The proposed optimisation framework took the buckling and bending strength of CFS sections as objective function. In this approach, a nonlinear finite element model was first developed for a referenced channel and zed sections subjected to four-point bending tests and these reference sections were then parameterized in terms of geometric dimensions and material properties using the DOE technique. In the next step, a response surface was used to determine the influences of the stiffener's properties on the section distortional buckling and ultimate strength including its location, shape, size and material properties by the cold work at the section corners and stiffener

bends. Response surface design optimisation was then used to determine the geometric dimensions and material properties of optimised sections. The new optimised sections were then applied loading up to failure to obtain ultimate bending strengths.

Figure 8.6 (a) shows a cross section and general dimensions for the channel sections which was the industrial UltraBeam™2 sections (Hadley Industries plc.), respectively, whereas Figure 8.7 (a) shows a cross section and general dimensions for the zed sections which was the industrial UltraZED™2 sections (Hadley Industries plc.). The study goal was to find optimal design of the web and flange stiffeners' positions, shapes, sizes, and enhanced material properties at corners and stiffeners' bends, which enhance the section's buckling and ultimate bending strength, leading to an optimal design of the sections. The FE model developed and validated in chapter 3 was utilised for the optimisation study. The sections together with their bending setup used in the experimental testing in [142] were defined as “reference section” and shown in Figure 8.6 (b) and Figure 8.7 (b). The section height  $h$  and thickness  $t$  were fixed in the optimisation study.

The channel section without flange stiffeners is shown in Figure 8.6 (b), in which all dimension parameters are also shown and the channel section with flange stiffeners is shown in Figure 8.6 (c). The values for  $h$  and  $t$  were taken of the reference channel section as 170.1 mm and 1.6 mm, respectively.  $p_1$  and  $p_2$  are the position of the web stiffeners from the web-flange junctions,  $p_3$  is the position of the peak of the web stiffeners in horizontal direction from the web-flange junction,  $p_4$  is the width of the edge stiffener,  $p_5$  is the radius of the section corners and it was assumed that they had the same radius,  $p_6$  and  $p_7$  are the angle of rotation of the web stiffener,  $p_8$  is the flange width,  $p_{15}$  is the position of the flange stiffener away from web flange junction, and  $p_{16}$  and  $p_{17}$  are the size of the flange stiffener (assuming the flange stiffener had a circular shape).

For the zed section without flange stiffeners is shown in Figure 8.7 (b), in which all dimension parameters are also shown and the zed section with flange stiffeners are shown in Figure 8.7 (c). The values for  $h$  and  $t$  were taken of the reference zed section as 170.1 mm and 1.6 mm, respectively.  $p_1$  and  $p_2$  are the position of the web stiffeners from the web-flange junctions,  $p_3$

and  $p_4$  are the width of the edge stiffeners,  $p_5$  is the radius of the section corners and it was assumed that they had the same radius,  $p_6$  and  $p_7$  are the position of the peak of the web stiffeners in horizontal direction from the web-flange junction,  $p_8$  and  $p_9$  the angle of rotation of the web stiffeners,  $p_{10}$  and  $p_{11}$  the angle of rotation of the edge stiffeners,  $p_{12}$  and  $p_{13}$  are the width of flanges for the zed section without flange stiffeners, whereas  $p_{12}$  and  $p_{13}$  are the position of the flange stiffeners away from web flange junction for the zed section with flange stiffeners,  $p_{14}$  and  $p_{15}$  are the size of the flange stiffeners (assuming the flange stiffener had a circular shape), and  $p_{16}$  and  $p_{17}$  are the width of flanges.

The total length of the cross section was kept unchanged for the optimisation target, that was “obtaining maximum strength of the section while maintaining the same weight”. Changes in parameters relating to the stiffeners’ shapes, sizes, positions while considering enhanced material properties at corners and bends by the cold work effect resulted in new channel and zed sections. The material properties at the flat regions, corners and at the stiffeners’ bends were assumed to be the same in these new sections.

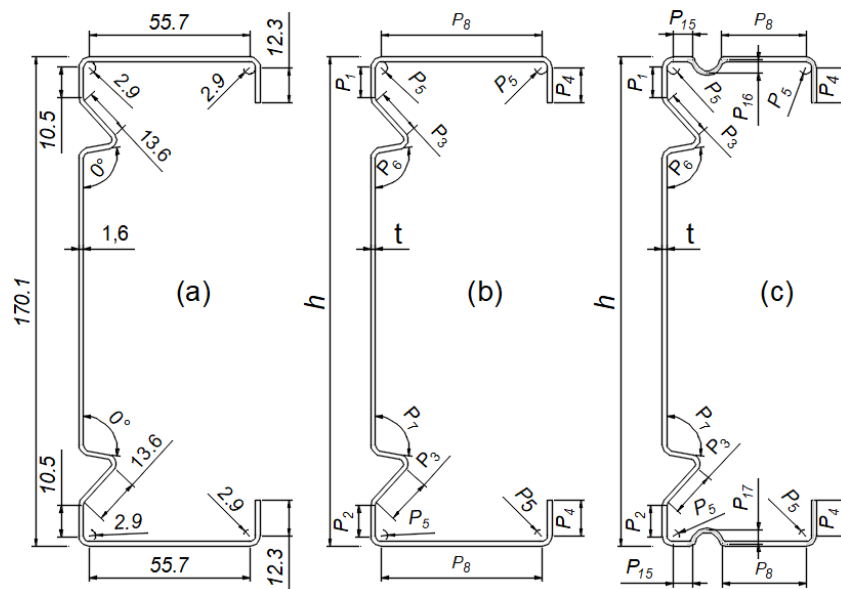


Figure 8.6. Dimension parameters in (mm) and definition of design variables of the channel cross section (a) reference section, (b) without flange stiffeners, and (c) with flange stiffeners

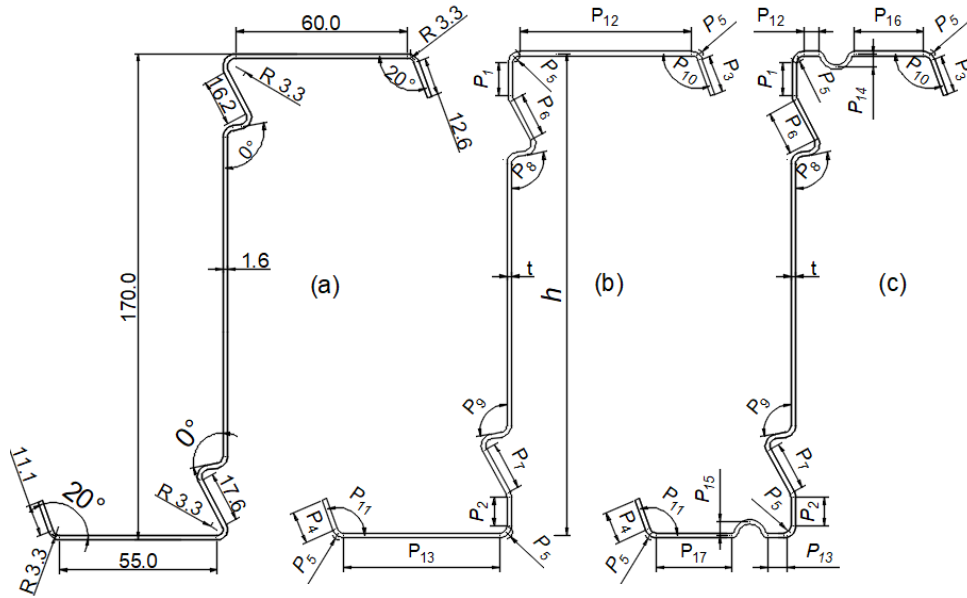


Figure 8.7. Dimension parameters in (mm) and definition of design variables of the zed cross section (a) reference section, (b) without flange stiffeners, and (c) with flange stiffeners

Figure 8.8 shows calculation procedures which were performed in chapter 6 and [152]. First, the three dimensional of the zed section beams was built, allowing for the parameters to be parameterised. Next, the linear buckling analysis was carried out in the Static Structural analysis at the initial dimensions (i.e. the reference section dimensions) before conducting eigenvalue buckling analysis. Then, the nonlinear buckling analysis was performed including geometry and material nonlinearity, initial imperfections, and the cold work effect at section corners and stiffeners' bends. This linked setup allowed the three analysis systems to share resources such as engineering data, geometry, and boundary condition type definitions made in Static Structural analysis. Finally, the response surfaces were calculated, and the best design candidates were selected using a multi-objective genetic algorithm. See chapter 6 for full details on Optimisation approach.

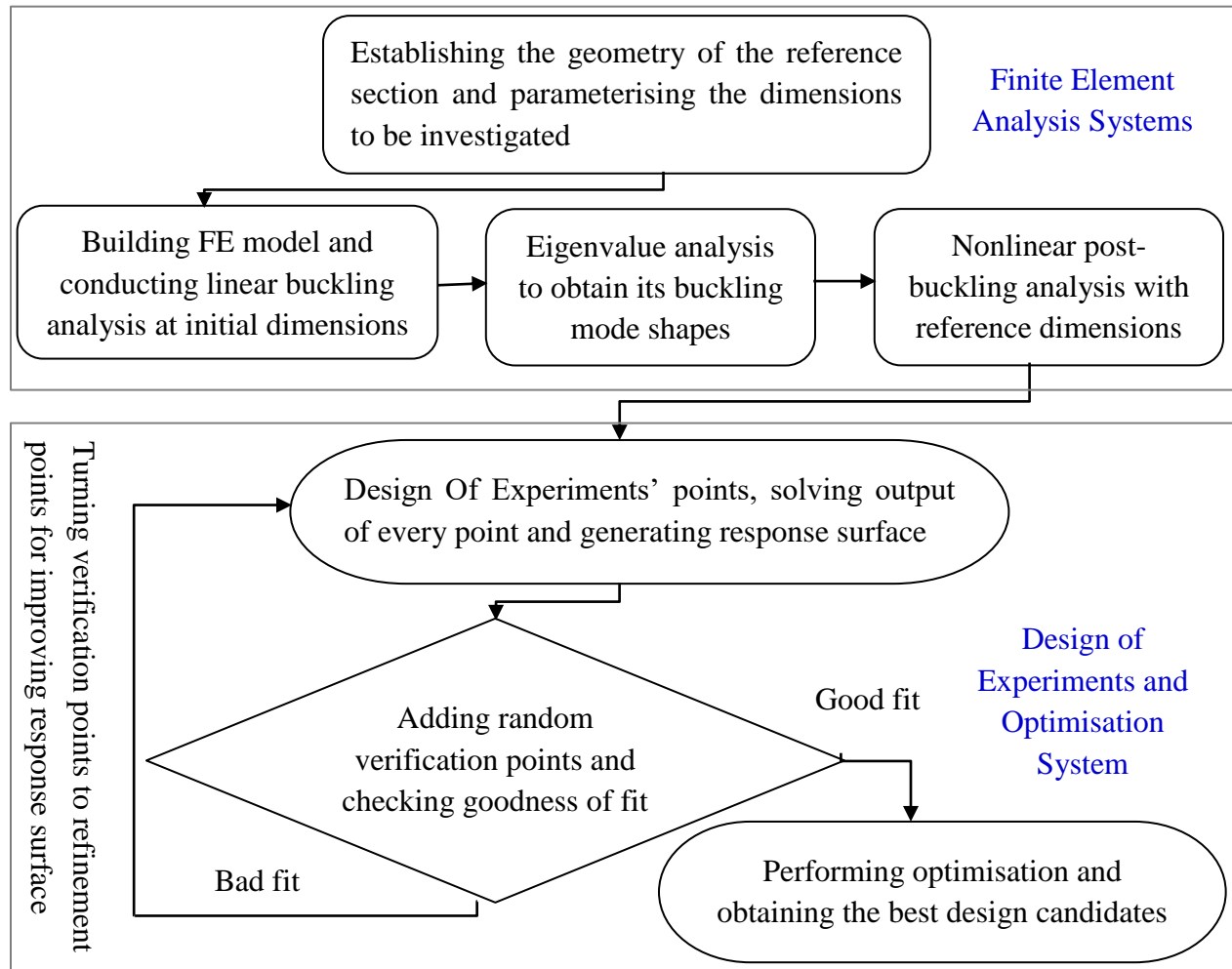


Figure 8.8. The flowchart of the FE modelling and optimisation processes [152].

The dimensions of the cross-sections for the numerical study in this chapter are presented in Tables 8.1-8.2. All the dimensions in the Tables are defined by the centre-to-centre surface. The nine types of cross-sections were labelled referenced to Figures 8.6-8.7. The cross-section “Standard” was a standard commercially available cross-section, which provided a basis for comparison. Reference (b) and Reference (c) were the sections without and with flange stiffeners. Candidate 1-6 are optimised sections obtained based on different target objectives. Candidate 1 and 4 obtained when the ‘target’ was to minimise maximum developed stresses, Candidate 2 and 5 obtained when the ‘target’ was to maximise buckling, and Candidate 3 and 6

obtained when the ‘target’ was to minimise maximum developed stresses and maximise buckling in the cross-sections.

**Table 8.1** Cross-section dimensions of standard, reference and optimised CFS channel sections.

Parameter	Standard	Reference		Candidate					
		(b)	(c)	1	2	3	4	5	6
P1 (mm)		10.5	10.5	1.0	1.0	1.0	1.0	1.0	1.0
P2 (mm)		10.5	10.5	1.0	1.0	1.0	1.0	1.0	1.0
P3 (mm)		13.6	13.6	19.0	19.0	19.0	14.4	22.0	16.0
P4 (mm)	12.3	12.3	12.3	16.0	18.0	17.0	13.5	18.0	13.1
P5 (mm)	2.9	2.9	2.9	2.9	2.9	2.9	2.9	2.9	2.9
P6 (degree)		0.0	0.0	15.0	15.0	15.0	15.0	15.0	15.0
P7 (degree)		360.0	360.0	345.0	345.0	345.0	345.0	345.0	345.0
P8 (mm)	62	55.7	35.2	43.5	41.5	42.5	28.7	23.0	28.0
P15 (mm)			5.0				5.0	5.0	5.0
P16 (mm)			5.0				5.0	5.0	5.0
P17 (mm)			5.0				5.0	5.0	5.0

**Table 8.2** Cross-section dimensions of standard, reference and optimised CFS zed sections.

Parameter	Standard	Reference		Candidate					
		(b)	(c)	1	2	3	4	5	6
P1 (mm)		0.0	0.0	0.0	0.0	0.0	0.0	0.0	0.0
P2 (mm)		0.0	0.0	0.0	0.0	0.0	0.0	0.0	0.0
P3 (mm)	12.6	12.6	12.6	19.7	17.7	20.8	17.0	19.0	18.4
P4 (mm)	11.1	11.1	11.1	17.5	16.4	17.8	16.0	17.0	16.2
P5 (mm)	3.3	3.3	3.3	3.3	3.3	3.3	3.3	3.3	3.3
P6 (mm)		16.2	16.2	12.5	21.0	11.6	12.0	13.0	12.8
P7 (mm)		17.6	17.6	13.9	21.0	12.9	13.0	14.0	13.1
P8 (degree)		0.0	0.0	0.0	0.0	0.0	0.0	0.0	0.0
P9 (degree)		0.0	0.0	0.0	0.0	0.0	0.0	0.0	0.0
P10 (degree)		20.0	20.0	0.0	0.0	0.0	0.0	0.0	0.0
P11 (degree)		20.0	20.0	0.0	0.0	0.0	0.0	0.0	0.0
P12 (mm)	68.6	60.0	5.0	51.0	44.0	51.0	5.0	5.0	5.0
P13 (mm)	63.0	55.0	5.0	46.0	39.0	46.0	5.0	5.0	5.0
P14 (mm)			5.0				5.0	5.0	5.0
P15 (mm)			5.0				5.0	5.0	5.0
P16 (mm)			39.3				35.8	33.7	35.5
P17 (mm)			34.3				30.7	28.8	29.0

## 8.5 Results and discussion

### 8.5.1 Tensile coupon test carried out in this research

A total of 96 tensile coupon specimens obtained from 4 cross-sections was tested to determine the mechanical properties of the material. This included the 16 tensile coupons extracted from the pre-cold rolled sheet coils (virgin materials), 16 coupons extracted from the web of the sections, 16 coupons extracted from the flanges of the sections, and 48 coupons extracted from the section corners and stiffener's bends. The key measured material properties (static engineering values) obtained for each flat coupon and each set of curved coupons as well as average values for corresponding 4 coupons are listed in Tables 8.3-8.6, where E is the Young's



modulus,  $f_y$  is the 0.2% proof stress,  $f_u$  is the ultimate tensile strength, and  $\epsilon_f$  is the elongation after fracture, measured over a gauge length of 50 mm.

From the Tables 8.3-8.6, it may be seen that the measured virgin material (sheet coil) properties and the flat coupons extracted from the complete sections are similar. The limited results presented in this study indicate modest levels of strength enhancement in the flat faces of web and flanges of the steel channel and Zed sections during the cold roll forming process—an average increase in strength of around 1% to 4% over the virgin value was observed. These were consistent with previous studies [145, 146]. However, it is well known that the mechanical properties of section corners and stiffener’s bend could significantly change due to work hardening that arises from plastic deformations induced during section-forming.

**Table 8.3** Measured material properties of tensile coupon for Z-W200T2.0.

Coupon location	$E$ (GPa)		$f_y$ (MPa)		$f_u$ (MPa)		$\epsilon_f$ (%)	
	Ind.	Avg.	Ind.	Avg.	Ind.	Avg.	Ind.	Avg.
Flat coupon								
Sheet coil-a	209	208	430	428	537	538	23	24
Sheet coil-b	208		428		538		24	
Sheet coil-c	208		424		539		24	
Sheet coil-d	208		430		538		24	
Web-a	210	206	435	436	540	544	24	24
Web-b	207		446		554		24	
Web-c	205		430		541		24	
Web-d	201		432		541		24	
Flange-a	206	207	445	443	547	546	24	24
Flange-b	208		438		547		24	
Flange-c	205		444		545		24	
Flange-d	209		446		544		24	
1ab	217	218	535	550	610	618	15	14
1cd	219		565		625		13	

2ab	219	220	520	525	570	575	14	14
2cd	220		530		580		14	
3ab	220	225	490	500	550	560	11	11
3cd	229		510		570		11	

**Table 8.4** Measured material properties of tensile coupon for Z-W145T1.2.

Coupon location	$E$ (GPa)		$f_y$ (MPa)		$f_u$ (MPa)		$\epsilon_f$ (%)	
	Ind.	Avg.	Ind.	Avg.	Ind.	Avg.	Ind.	Avg.
Flat coupon								
Sheet coil-a	208	207	421	425	527	529	25	25
Sheet coil-b	204		427		529		25	
Sheet coil-c	211		424		528		25	
Sheet coil-d	204		429		530		25	
Web-a	211	207	436	435	537	535	25	25
Web-b	211		433		534		25	
Web-c	202		436		534		25	
Web-d	202		434		533		25	
Flange-a	202	203	435	432	530	532	25	25
Flange-b	203		431		533		25	
Flange-c	201		429		532		25	
Flange-d	204		431		532		25	
1ab	235	224	500	510	590	593	11	11
1cd	213		520		595		11	
2ab	230	225	515	510	600	595	17	15
2cd	220		505		590		13	
3ab	220	225	500	505	550	555	5	5
3cd	229		510		560		5	

**Table 8.5** Measured material properties of tensile coupon for C-W200T2.0.

Coupon location	$E$ (GPa)		$f_y$ (MPa)		$f_u$ (MPa)		$\epsilon_f$ (%)	
	Ind.	Avg.	Ind.	Avg.	Ind.	Avg.	Ind.	Avg.
Flat coupon								
Sheet coil-a	204	207	439	438	545	542	26	25
Sheet coil-b	210		437		541		24	
Sheet coil-c	210		437		541		24	
Sheet coil-d	205		439		539		25	
Web-a	208	207	442	435	549	546	23	24
Web-b	206		435		545		25	
Web-c	206		431		544		25	
Web-d	208		432		545		24	
Flange-a	192	206	444	441	547	547	25	25
Flange-b	211		434		549		26	
Flange-c	210		443		547		26	
Flange-d	209		442		543		22	
1ab	232	228	534	540	598	602	4	5
1cd	223		545		605		5	
2ab	239	240	520	527	585	598	13	14
2cd	241		534		610		14	
3ab	257	243	505	515	556	561	6	6
3cd	228		525		565		6	

**Table 8.6** Measured material properties of tensile coupon for C-W145T1.2.

Coupon location	$E$ (GPa)		$f_y$ (MPa)		$f_u$ (MPa)		$\epsilon_f$ (%)	
	Ind.	Avg.	Ind.	Avg.	Ind.	Avg.	Ind.	Avg.
Flat coupon								
Sheet coil-a	193	208	330	330	428	428	26	25
Sheet coil-b	207		330		428		23	
Sheet coil-c	223		328		426		26	
Sheet coil-d	207		332		428		26	
Web-a	211	204	340	336	431	429	26	26
Web-b	204		340		432		26	
Web-c	190		335		427		26	
Web-d	211		329		425		26	
Flange-a	210	207	334	331	430	428	26	26
Flange-b	203		335		430		26	
Flange-c	208		328		426		26	
Flange-d	208		325		424		26	
1ab	217	218	430	427	452	452	4	4
1cd	219		423				4	
2ab	230	225	412	421	450	453	4	4
2cd	220		430		455		4	
3ab	215	220	402	401	450	452	4	4
3cd	225		400		454		4	

It is important to note that although the 0.2% proof stresses listed in the Tables 8.3-8.6 are often lower than the nominally specified values (i.e. 450 MPa for sections C-W200T2.0, Z-W145T1.2 and Z-W200T2.0, and 350 MPa for section C-W145T1.2), the values listed in the tables correspond to the ‘static’ 0.2% proof stresses, reduced to zero strain rate. The nominal values reported in practice are based on ‘dynamic’ values (with strain rates within the limits set by the

standards). As an example, Figure 8.9 shows the ('static' and 'dynamic') stress-strain curves of one of the flat coupons and the pair of curved coupons taken from the cross-section Z-W200T2.0. Stresses and strains shown in this figure are conventional 'engineering' values.

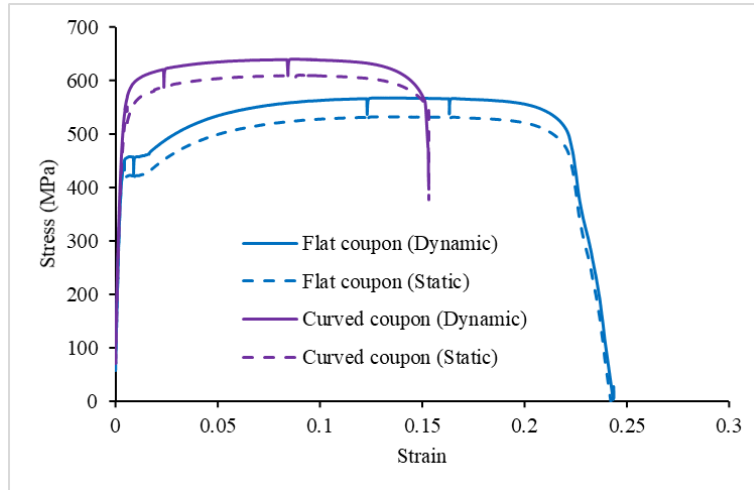
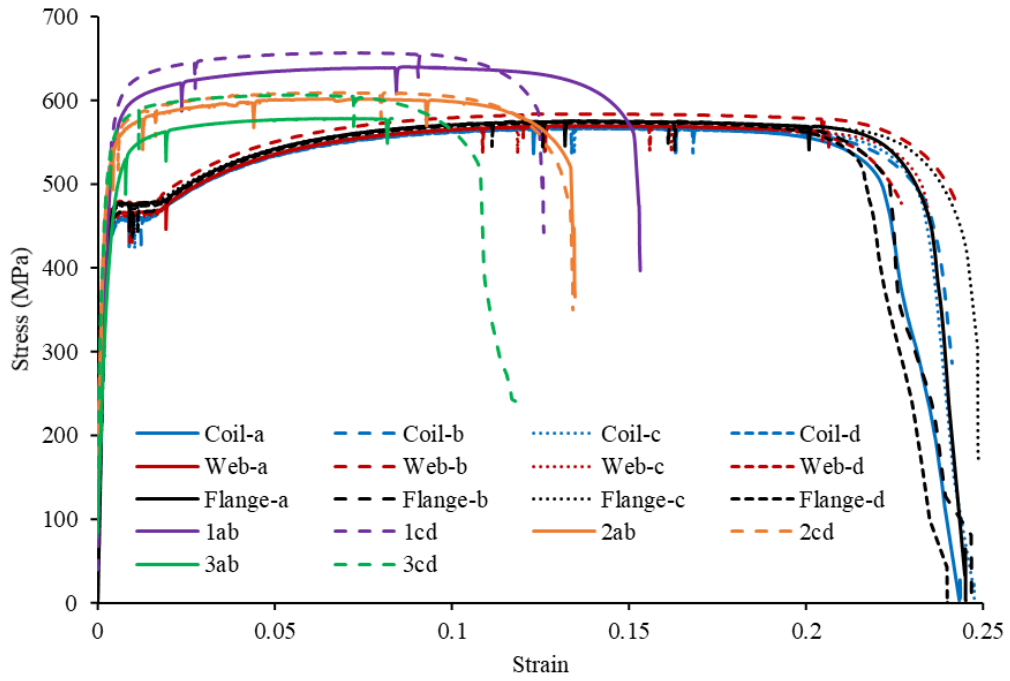
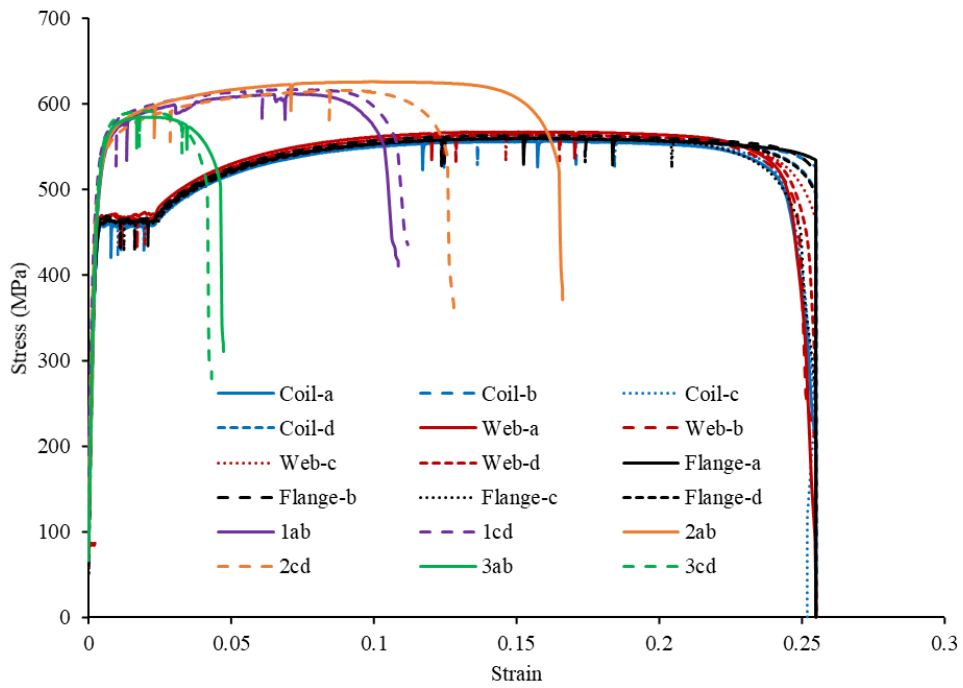


Figure 8.9. Engineering stress–strain relationships of the tensile tests for the cross-section Z-W200T2.0 (Typical flat and curved coupon test results).

Figures 8.10 (a-d) present all stress–strain curves of sheet coil, web, flange and curved specimens. Compared to the flat specimens the yield and tensile strengths were increased by 17–29% and 5–15% in the curved specimens respectively, the percentage of elongation decreased by 40–84%. The cold work by the cold roll forming process produces a significant increase in the yield and tensile strengths and a decrease in ductility of the section corners and stiffener's bends. The effect of the cold work on the mechanical properties of web and flange specimens, however, was very small, compared to the amount of cold work in the curved locations so that it could be neglected.



(a)



(b).

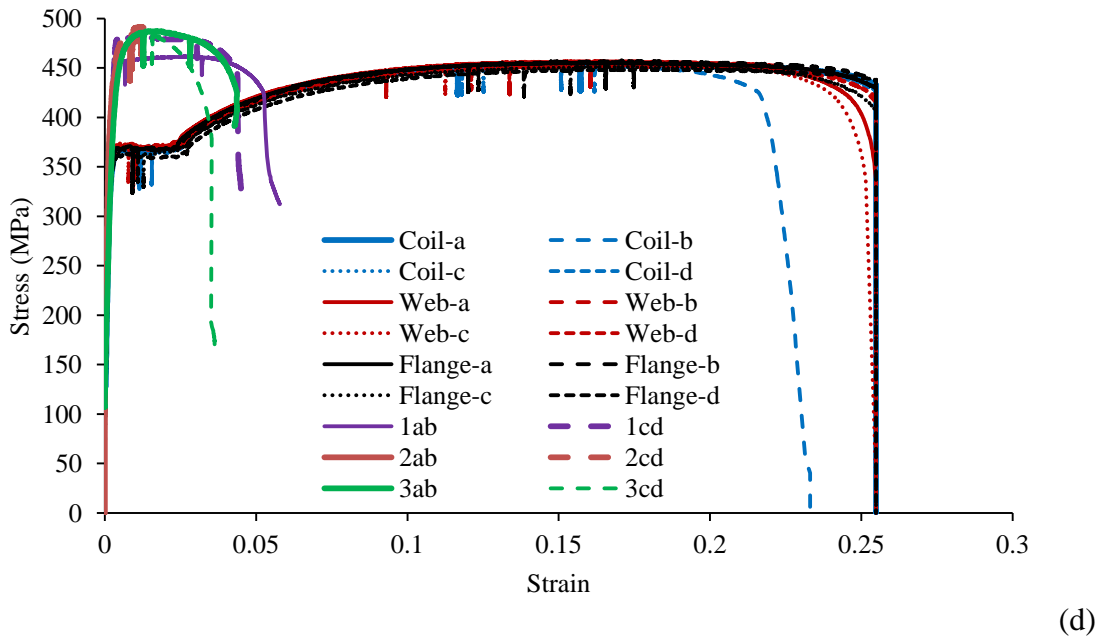
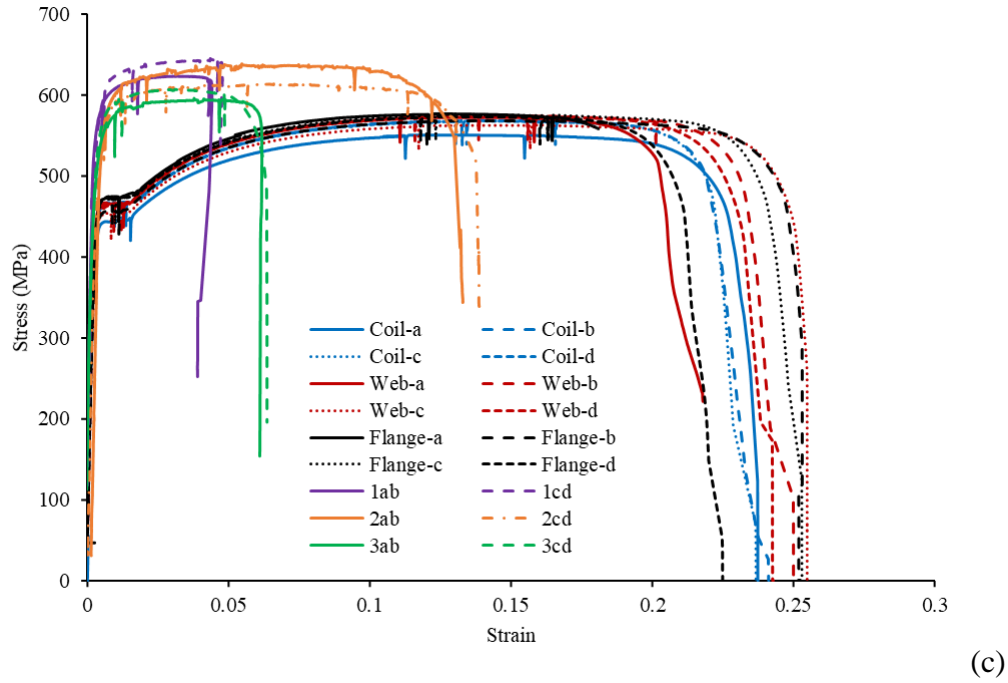


Figure 8.10. Engineering stress–strain relationships of the tensile tests for the section (a) Z-W200T2.0, (b) Z-W145T1.2, (c) C-W200T2.0 and (d) C-W145T1.2.

Figures 8.11 and 8.14 show the strength enhancement over the cross sections due to the influence of cold work effects. The thickness of the test specimens ranged between about 1 and 2 mm, while the corner radii ranged between about 2 and 5 mm. The measured yield strength of the section's corner and stiffener's bend material  $f_{yc}$  was normalised by the yield strength of the virgin material  $f_{y, mill}$  to indicate the level of strength enhancement due to corner and stiffener forming as (%), while in Figures 8.12 and 8.14 are presented the ultimate tensile strength distribution for the same profiles. The values presented in Figures 8.11-8.14 represent the average values of experimentally obtained values of each tested coupon for yield strength and ultimate limit increase.

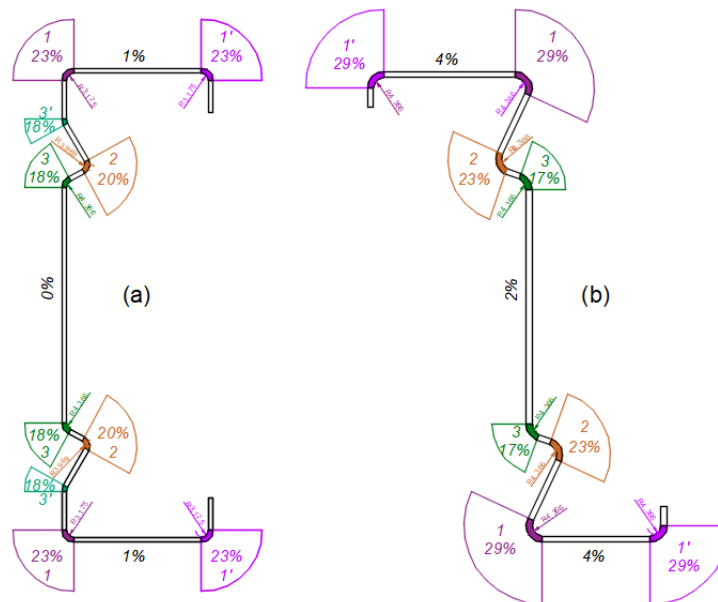


Figure 8.11. Yield strength enhancement due to cold roll forming (a) channel cross-section C-W200T2.0, and (b) Zed cross-section Z-W200T2.0.



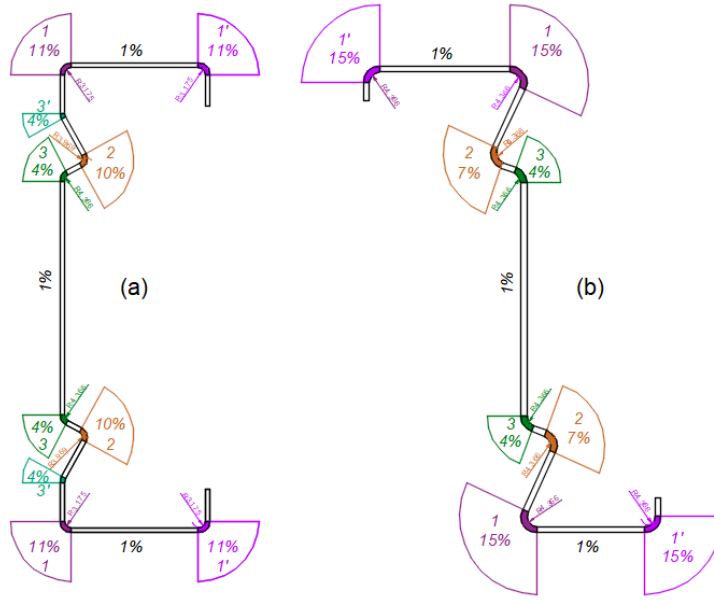


Figure 8.12. Ultimate strength enhancement due to cold roll forming (a) channel cross-section C-W200T2.0, and (b) Zed cross-section Z-W200T2.0.

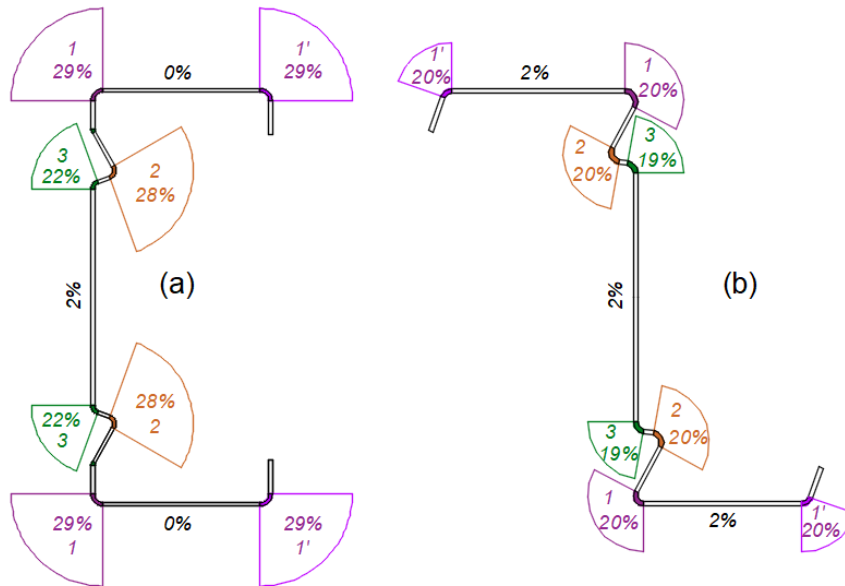


Figure 8.13. Yield strength enhancement due to cold roll forming (a) channel cross-section C-W145T1.2, and (b) Zed cross-section Z-W145T1.2.

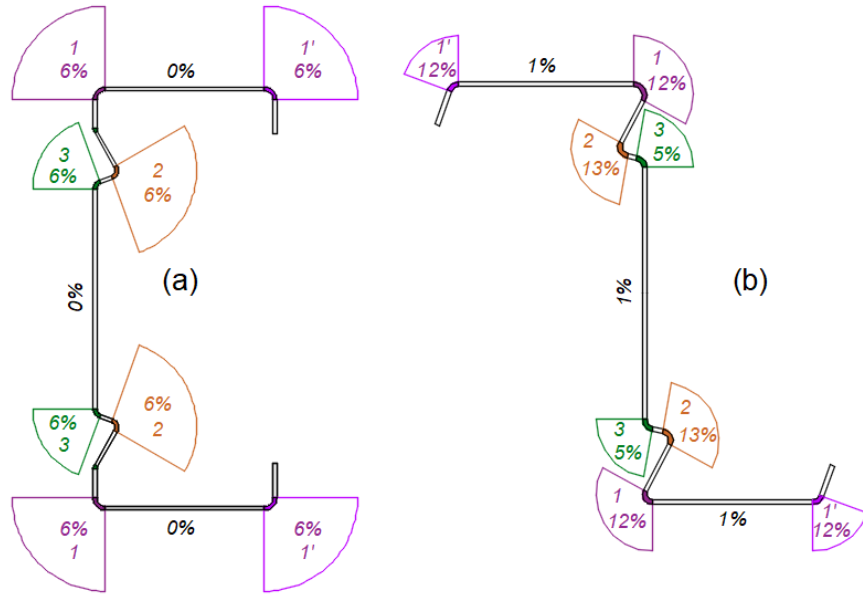


Figure 8.14. Ultimate strength enhancement due to cold roll forming (a) channel cross-section C-W145T1.2, and (b) Zed cross-section Z-W145T1.2.

## 8.5.2 Comparisons of predictive models with measured increased yield stresses

Representative comparisons between the corner yield strengths determined from the experiments  $f_{yc,test}$  carried out by the author with those obtained using the two different predictive models  $f_{yc,pred}$ , presented in terms of the predicted-to-test ratios, are shown in Table 8.7. The accuracy of the two different predictive models described earlier, for the determination of the increased yield strength of section corner and stiffener bend materials extracted from the three locations of four cold-formed steel sections, was assessed herein. Overall, it was observed that the section corner and stiffener bend yield strength was significantly higher than that of the virgin material, with an average enhancement in yield strength of around 22% for the measured test data carried out in this study. Note that the strength enhancement in the flat faces of cold-formed steel sections was relatively small due to the limited amount of cold-work induced during the roll-forming process.

For all the corner and stiffener bend regions, the results obtained from both predictive models the AISI Specification [3] and Gardner et al. [151], confirmed that the yield strength of the materials were considerably improved compared to the virgin sheet coil materials. As indicated in Table 8.6, the predictive model set out in the AISI Specification provided relatively over predictions of  $f_{yc,test}$ , in terms of the average ( $f_{yc,pred} / f_{yc,test}$ ) by about 12%, while the model proposed by Gardner et al. [151] under-estimated  $f_{yc,test}$  on the average by about 6%. Though the later method was calibrated based on cold rolled hollow sections, the former [3] model was more universally applicable and was thus recommended for predicting the corner yield strength of cold-formed steel sections in the lack of test data. The former predictive model, which was used for determining the tensile 0.2% proof strength of cold-formed sections and was based on the tensile material properties of the flat coupon cut from either the same cold-formed steel section or the virgin/sheet material, was selected and used to account for the cold work effects in order to conduct further investigations in this study.

**Table 8.7** Comparison of the proposed predictive models and representative test data for the 0.2% proof strength of curved regions of cold-formed sections ( $f_{yc,pred} / f_{yc,test}$ ). The tensile tests conducted by the author in this study.

Curved coupon location	$t$ (mm)	$R$ (mm)	$f_{yc,test}$ ( $N/mm^2$ )	$f_{yc,pred} / f_{yc,test}$	
				AISI specification	Gardner et al.
Z-W200T2.0-1	1.934	4.366	550	1.05	0.87
Z-W200T2.0-2	1.942	4.366	525	1.08	0.91
Z-W200T2.0-3	1.952	4.366	500	1.14	0.98
Z-W145T1.2-1	1.259	2.381	510	1.15	0.96
Z-W145T1.2-2	1.243	2.381	510	1.14	0.96
Z-W145T1.2-3	1.225	2.778	505	1.12	0.95
C-W200T2.0-1	1.994	3.175	540	1.14	0.98
C-W200T2.0-2	1.948	3.969	527	1.12	0.94
C-W200T2.0-3	1.964	4.366	515	1.13	0.94
C-W145T1.2-1	1.241	3.175	427	1.05	0.85
C-W145T1.2-2	1.242	1.984	421	1.16	0.98
C-W145T1.2-3	1.185	2.778	401	1.14	0.95
Average				1.12	0.94
St. dev.				0.035	0.039

### 8.5.3 FE modelling

#### 8.5.3.1 Tensile test

Typical FE stress–strain curves of flat and curved coupons are shown in Figure 8.15, which also presents the stress–strain curves from the tests. The lack of a yield plateau in the case of curved steel coupon is the result of the strain hardening generated during the cold roll forming process. This could make the curved regions much stronger than they had previously been in flat form.

However, residual stresses were not measured and its influence to the mechanical properties of curved steel coupon was not considered but assumed to be implicitly presented in the stress-strain behaviour of the coupon tensile test results as the coupons were cut from the final sections.

The yield and ultimate forces predicted using FE modelling in the curved coupon were less than 1% greater than the experimental results, respectively; the predicted yield and ultimate force in the flat coupon were about 1% less than the experimental ones. The stiffness of both flat and curved coupons obtained from FE modelling, however, was slightly greater than the experimental ones around the proportional limit and yielding regions of the material. Overall, it showed that the stiffness and strength values predicted by the FE modelling were in excellent agreement with the experimental ones.

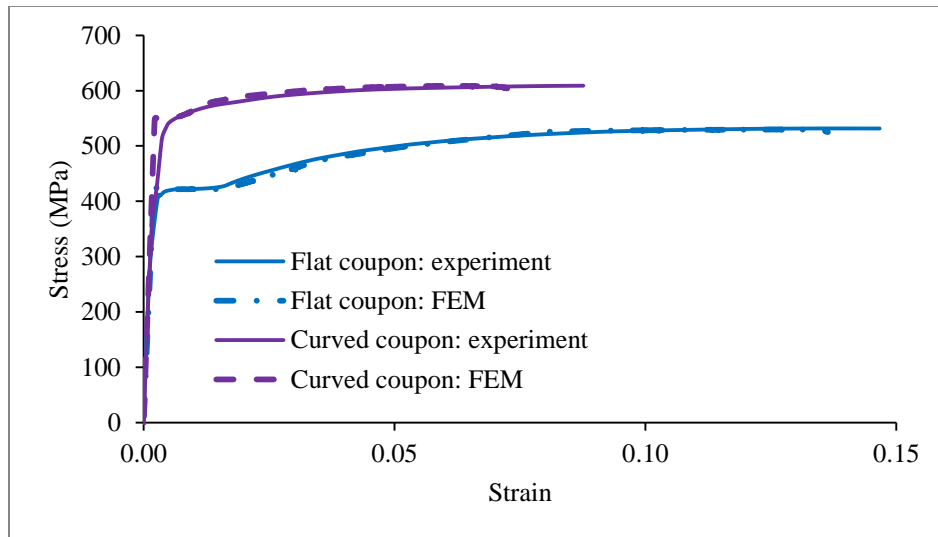


Figure 8.15. FE and experimental stress–strain curves of the typical flat and curved coupon specimens.

### 8.5.3.2 FE result validation

Further validation of FE models was carried out for four-point beam bending tests and compared with various experiments performed by Nguyen et al. [142] to understand the cold work effects on bending strength of the beams. FE simulations were performed using both the measured

material properties carried out by the author in this study and the AISI specification calculated values for strength enhancement in the section corner and stiffeners bend regions. The FE model results were then compared with the experimental beam bending tests in [142].

A comparison of ultimate moment capacity for beams with different span lengths is summarized in Table 8.8,  $M_u$ ,  $M_{uc}$  stand for ultimate moment capacity without and with the cold work effect, respectively. The two sections selected from Nguyen et al. [142] are the zed section with depth = 145 mm, top flange width = 67 mm, bottom flange width = 61 mm and thickness = 1.2 mm, and the channel section with depth = 255 mm, flange width = 63 mm and thickness = 2.3 mm. These two sections were selected from [142] as they had consistent material properties with current material properties obtained from coupon tests presented in this chapter carried out by the author. The ultimate moment capacities from experimental tests [142] and FEM results and the ratios between two methods for each section are also presented in the Table.

**Table 8.8** Ultimate moment capacity obtained from experimental tests [142] and FE models.  $M_u$ ,  $M_{uc1}$ ,  $M_{uc2}$  stand for ultimate moment capacity without and with the cold work effect using both the measured material properties conducted by the author in this research and the AISI specification predicted values, respectively.

Cross-section types	Span length (m)	$M_{test}$ (kNm) [142]	FEM			$M_{test}/M_u$	$M_{test}/M_{uc1}$	$M_{test}/M_{uc2}$
			$M_u$ (kNm)	$M_{uc1}$ (kNm)	$M_{uc2}$ (kNm)			
Zed section	2295	7.29	6.73	7.06	7.05	1.08	1.03	1.03
Channel section	3879	23.82	25.18	25.71	25.71	0.94	0.93	0.93

It was seen from Table 8.8 that that the cold work influence on bending strength of the channel section beams was insignificant about 1% due to the fact that the distortional buckling slenderness in the section was very high and the beam failed by distortional buckling stress before it reached its yield strength capacity. For the zed section beams, the cold work effect was significant on bending strength of the beam using both the measured material properties and the

AISI specification calculated values about 5% as the sections gained their full strength and the generated stresses reached the plastic region.

#### 8.5.3.3 Four-point beam bending test

Table 8.8 summarises the buckling and ultimate bending strength of the cross-sectional geometries obtained from the optimisation process (which reference to Figures 8.6 and 8.7 and Tables 8.1 and 8.2 for the optimal parameters presented in this chapter) and compare them with the standard lipped channel section with the same amount of material and the same section height taken as a starting point. The resulting cross-sectional shapes and comparison between flexural strength capacity with the cold work effects and without the cold work effects, using the measured material properties performed by the author in this research from the tensile coupon tests at flat, corner and stiffener bend regions, of the various optimal design candidate points are also shown in Figure 8.16.

The main purpose of this exercise was to (1) accurately quantify both geometry and the cold work effects on the buckling and bending strength in the cross-sectional shapes, and (2) ultimately select and propose the optimal design of the longitudinally stiffened channel and zed sections. The following observations could be made from Table 8.8 and Figures 8.16 and 8.17:

- The extent of improved distortional buckling and ultimate bending strength benefit obtained from geometry and the cold work effects was dependent on the cross-section shape and dimensions, and the percentage area of the section corners and stiffeners' bends in the sections.
- Adding two longitudinal stiffeners to the web of the standard channel and zed sections (reference (b)) provided considerably better buckling compared to the standard sections by 15% and 21%, respectively, whereas the ultimate moment capacity was noticeably improved by 2% and 8%, respectively. The cold work had noticeable effect by 2% on the reference section bending strengths.

- Having two longitudinal stiffeners in the web and one at the flanges of the standard sections (reference (c)) resulted in further enhancement in the buckling and ultimate moment capacity by 15% and 8% for the channel section, respectively, and by 21% and 17% for the zed section, respectively. The cold work had considerably more effect by around 6% due to further improved buckling load and increased bend regions in the sections.
- The optimised sections with two longitudinal web stiffeners in the web (Candidate 3) could provide with significant enhancement in the buckling of the channel sections due geometry effects which were about 100%, whereas it only considerably increased the ultimate moment capacity by 4% and extra 4% was also obtained in the ultimate moment capacity when the cold work effects were also considered. For the zed section, Candidate 3 gained significant increase in buckling, ultimate moment capacity without the cold work effects and with the cold work effects included by 110%, 17% and 23%, respectively.
- The Candidate 6 was the optimal solutions for both the channel and zed sections gained significant buckling, ultimate moment capacity without the cold work effects and with the cold work effects included by 84%, 13% and 20% for the channel section, respectively, and 105%, 17% and 23% for the zed section, respectively.
- The Candidate 6 also exhibited a considerably increased stiffness compared to the reference sections (as shown in Figure 8.16) for both the channel and zed sections, which was a direct result of the stiffeners delaying and mitigating the stiffness degradation due to buckling. It was noted that the stiffeners size was accounting for in the total developed length of the section and that, therefore, the flange width of the design candidate 6 was less than that of the reference section.



**Table 8.9** Buckling and ultimate moment capacity of standard and optimised CFS channel and zed sections.  $M_u$ ,  $M_{uc}$  stand for ultimate moment capacity without and with the cold work effect, respectively. The measured material properties carried out by the author was employed in the FE models to obtain buckling and ultimate moment capacities of the sections.

Cross-section types	$P_b$ (kN)	$M_{uc}$ (kNm)	$M_{uc}$ (kNm)	$M_{uc}/M_u$	$M_{uc}/M_{uc}^{standard}$
Channel					
Standard	11.7	9.48	9.48	1.00	1.00
Reference (b)	13.4	9.48	9.63	1.02	1.02
Candidate 1	22.9	9.89	10.25	1.04	1.08
Candidate 2	23.5	9.62	9.87	1.03	1.04
Candidate 3	23.3	9.91	10.26	1.04	1.08
Reference (c)	15.3	9.67	10.26	1.07	1.08
Candidate 4	20.8	10.18	10.85	1.07	1.14
Candidate 5	23.1	10.31	10.96	1.07	1.16
Candidate 6	21.5	10.69	11.40	1.07	1.20
Zed					
Standard	9.6	9.03	9.03	1.00	1.00
Reference (b)	11.6	9.61	9.77	1.02	1.08
Candidate 1	19.7	10.38	10.55	1.02	1.17
Candidate 2	21.1	9.52	9.74	1.02	1.08
Candidate 3	20.2	10.52	11.11	1.06	1.23
Reference (c)	13.3	9.98	10.54	1.06	1.17
Candidate 4	18.8	10.38	10.91	1.05	1.21
Candidate 5	20.3	10.30	10.94	1.06	1.21
Candidate 6	19.8	10.52	11.11	1.06	1.23

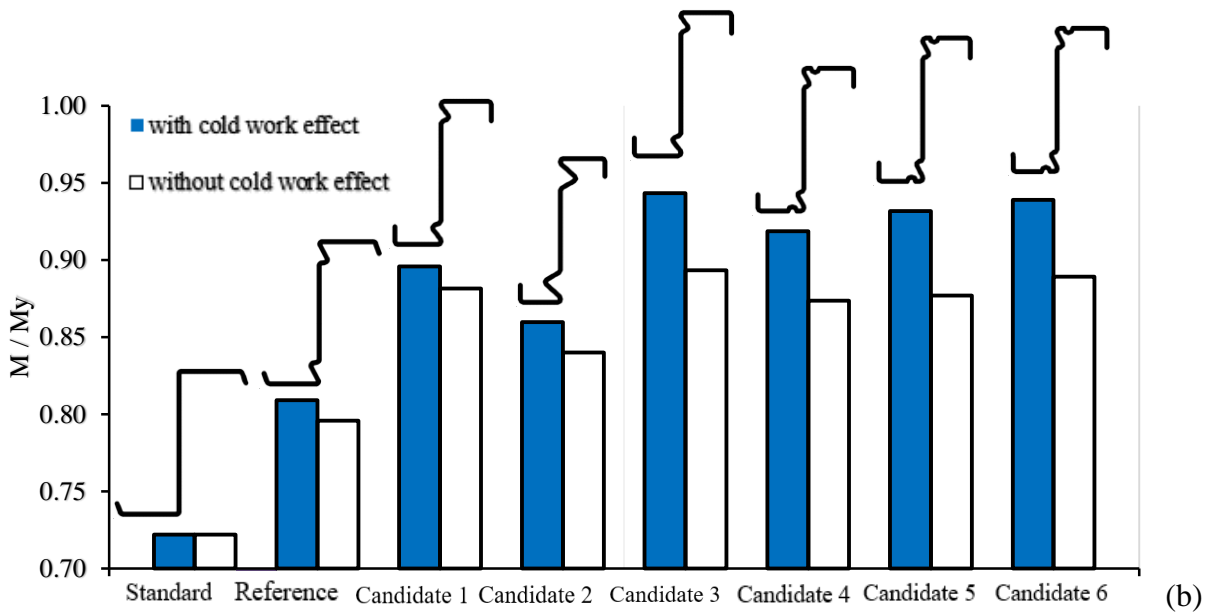
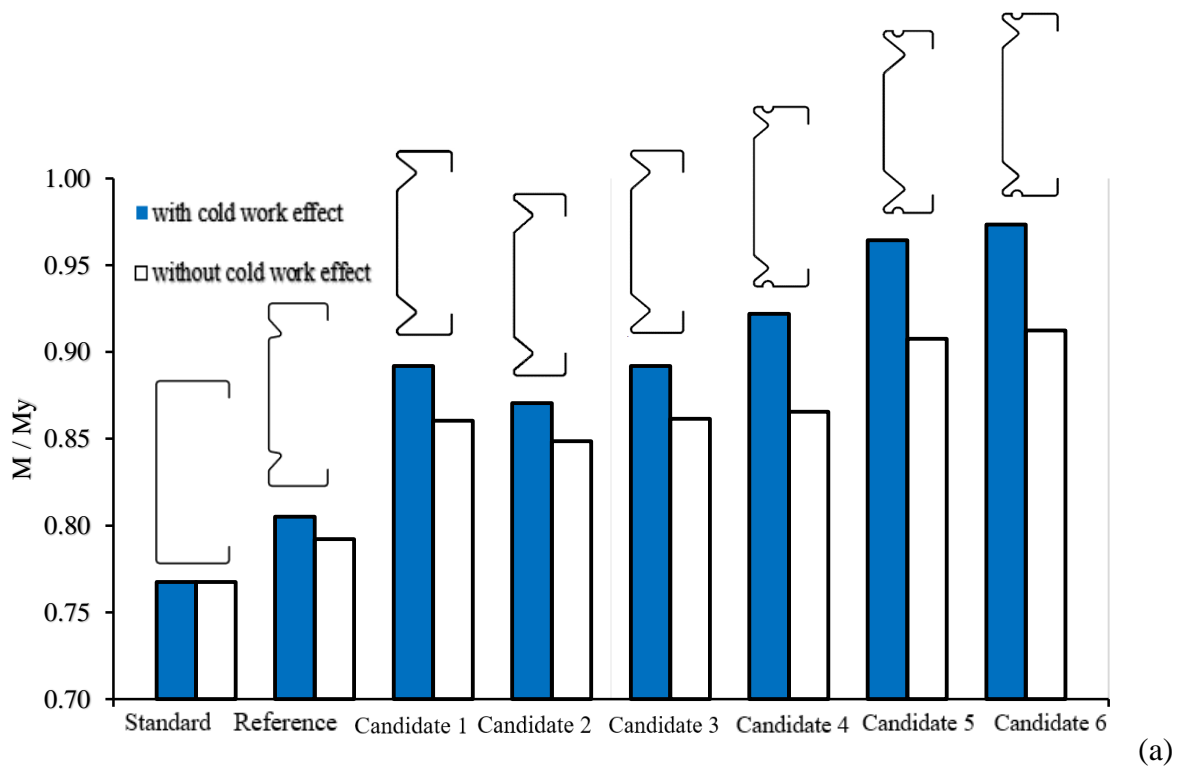


Figure 8.16. Ultimate bending strength to yield ratio with the cold work effects and without the cold work effects for (a) the channel cross sections and (b) the Zed cross sections.

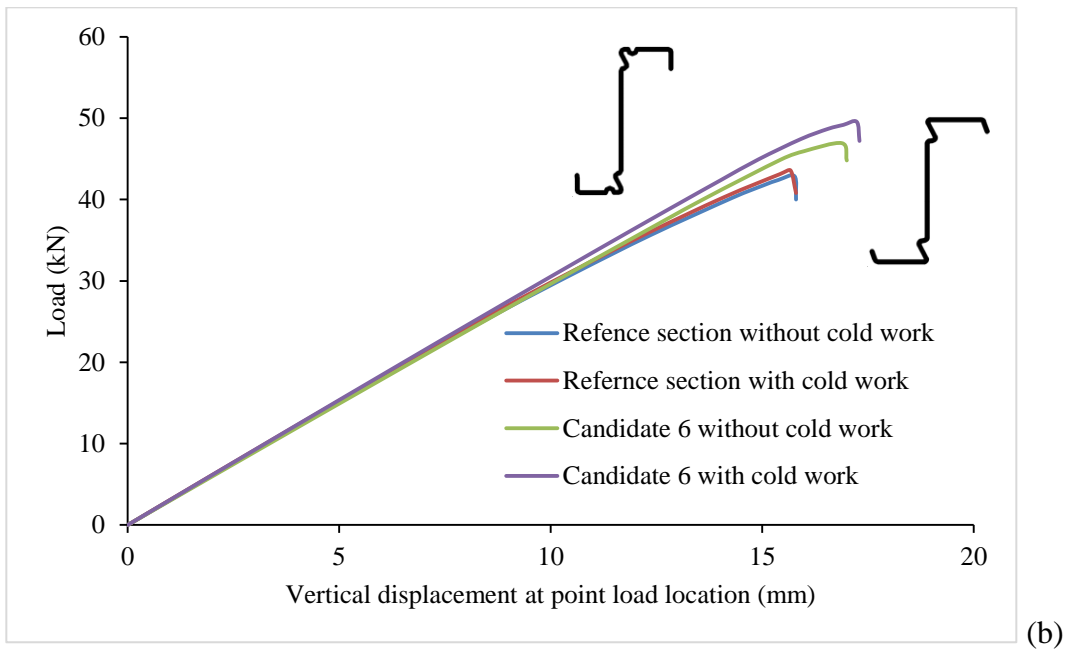
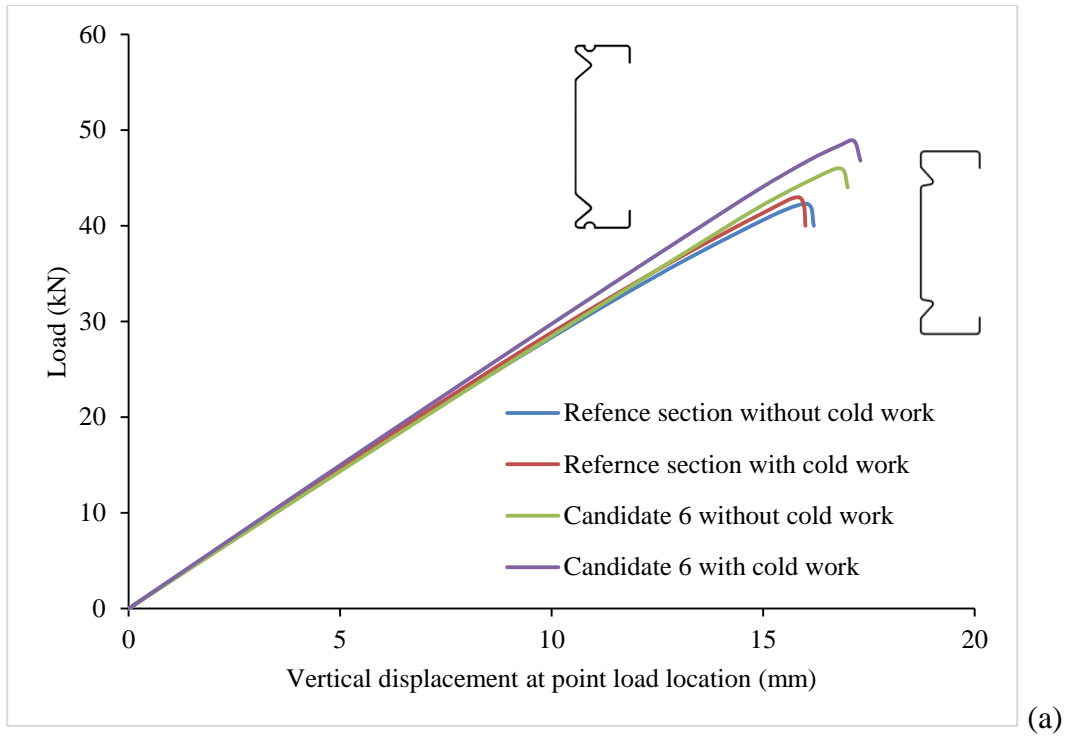


Figure 8.17. Load-displacement curves for the reference section and design candidate 6 results for (a) the channel sections and (b) the zed sections.

It was noted that the measured material properties carried out in this study (as shown in Tables 8.3-8.6) might provide only a limited representation of the expected material properties for CFS sections. Gardner et al. [153] performed a data collection from over 700 experimental stress-strain curves on cold-formed steels from the global literature and found the ratio ( $f_u/f_y$ ) about up to 40%. Therefore, to gain more inside the cold work effects on bending strengths, new FE models were developed by considering different ratio of ultimate to yield tensile strength of the material ( $f_u/f_y$ ) for the flat part of the sections and the enhanced yield strength at section corner and stiffener bend regions determined based on the formulars in the AISI Specification. The constitutive stress-strain model proposed by Hadarali and Nethercot [143] was employed, in which the plastic region of the stress-strain curve was modelled with a straight line with a constant slope of  $E/50$ , where  $E$  is the elastic modulus obtained from material tests. In Figure 8.18, the ( $f_u/f_y$ ) ratio is plotted versus the bending strength with the cold work effects ( $M_{uc}$ ) normalized by ( $M_u$ ) for the reference and optimised sections.

A comparison between the  $M_{uc}$  and  $M_u$  results indicated that the strength variation caused by the strain hardening of the material in the corner and stiffener bend regions had noticeable effect on bending strength of the reference channel and zed sections about 1% and 3%, respectively. The main reason for the low contribution of the strain hardening could be the higher distortional buckling slenderness and the relatively small area of the rounded corners compared to the total cross section area in the reference sections. On the other hand, by comparing the predicted bending strength  $M_{uc}$  and  $M_u$  of the optimised sections, it was shown that the cold work effects had significant effects on the predicted flexural strength capacity (up to 8% and 7% variation for channel and zed sections, respectively) and it actually linearly increased the bending strength for different ratio of ( $f_u/f_y$ ). This confirmed the fact that the cold work effect had to be included in the FE models for accurately obtaining enhancement in the ultimate moment capacity of the section, especially in the sections that are less prone to buckling and have higher ( $f_u/f_y$ ) ratio.

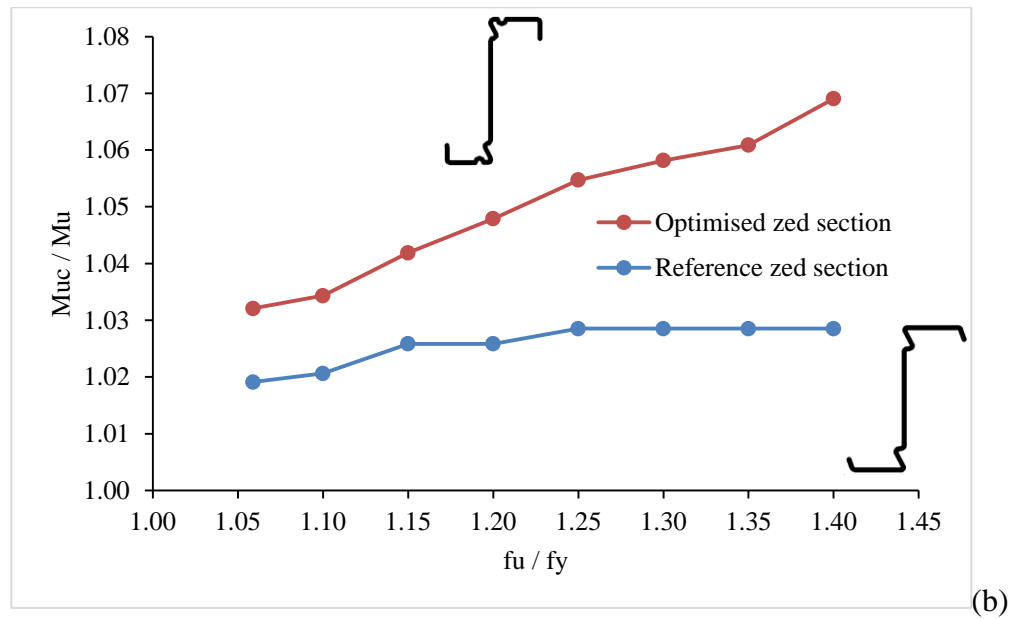
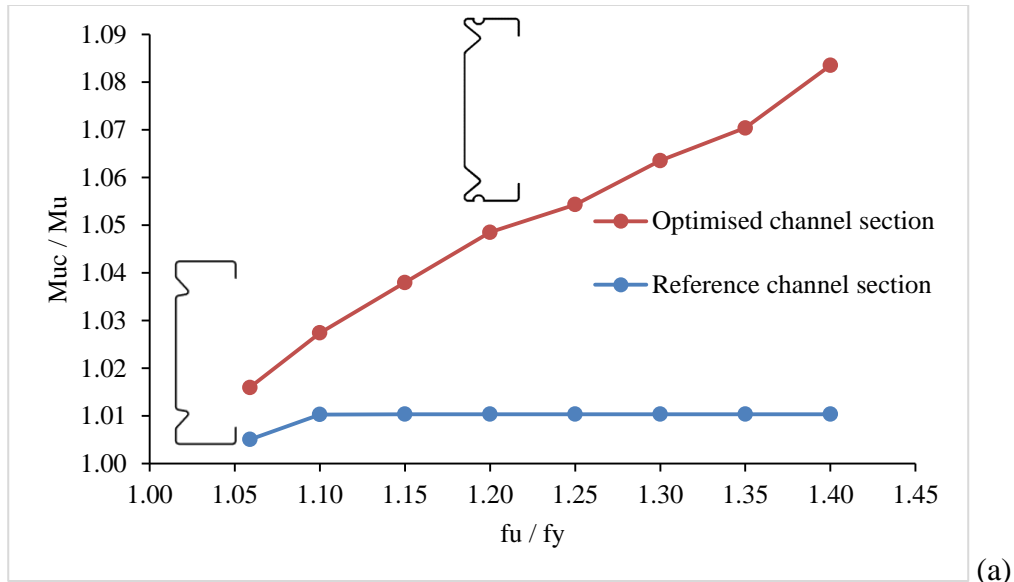


Figure 8.18. Bending strength enhancement due to cold roll forming process obtained for different ratios of ultimate tensile strength to yield strength of the materials for the reference and optimised sections (a) channel sections and (b) zed sections. The material properties at flat parts obtained from [142] and the material properties at corners  $f_{yc}$  was determined using the North the AISI Specification.

## 8.6 Conclusions

In this chapter, the influence of cold work effects on mechanical properties and flexural strength of the cold roll formed sections were studied by experimental testing and detailed Finite Element (FE) modelling. A material test programme on a total of four cold roll formed structural longitudinally stiffened sections, including two channel section and two zed sections was described that performed in this research. The results from tensile tests on 16 sheet coil coupons, 32 flat coupons, and 48 corner and stiffener bend coupons were presented. The cold work effect in the corner and stiffener bend regions of cold roll formed sections was analysed and the applicability of existing predictive models was evaluated. The strength enhancement obtained in the section corners and stiffener's bends were then used to accurately obtain the bending strength of the CFS sections. Optimal cross-sectional shape of the longitudinally stiffened channel and zed sections was finally selected and proposed. The following conclusions were drawn based on the results of this chapter:

- The cold work had modest effect in material strength in the flat regions of cold roll formed steel sections by on average 2.5%, but significantly enhanced material strength in the corner and stiffener bend regions by on average 22%.; the results were compared with two predictive models and both of the models provided reasonable results.
- The results revealed the efficiency of the adopted optimisation approach to increase the bending strength of CFS sections. The ultimate moment capacity of the optimised CFS sections obtained from validated FE models were significantly higher than their standard and reference counterparts with the same amount of material used for both channel and zed sections. This improvement was more evident for the zed sections which they are less prone to distortional-global buckling failure mode.
- The cold work effect in the corner and stiffener areas was insignificant on bending strength in the standard sections and only had a relevant influence at reference sections bending

strength. The main reason for the low contribution of the cold work effects can be the higher distortional buckling slenderness and the relatively small area of the rounded corners compared to the total cross section area in the sections. On the other hand, the cold work effect significantly increased the stiffness and bending strength of the optimised sections up to 7% and 6% for the channel and zed sections, respectively. In the optimised sections, several parts of the cross-section presented an equivalent strain higher than the yield strain, so the increase of the yield strength in corner areas produced an increase of the flexural strength of the beams.

- By considering both geometry and the cold work effects in the optimisation process, optimal cross-sectional shape could be obtained with significant gain in distortional buckling and ultimate bending strength up to 84% and 20%, respectively, for the optimised channel section compared to the standard lipped channel, and up to 105% and 23%, respectively, for the optimised zed section compared to the standard lipped zed section using the same amount of material and the same height of the sections.
- The optimal cross-sectional shape recommended having two longitudinal stiffeners at the web placed as much close as possible to the web-flange junctions, one longitudinal flange stiffeners placed near the web flange junctions as much as possible, and the relative dimensions of the sections as proposed in this thesis. The proposed shape could gain significant benefit from the geometry and the cold work effects.

## Chapter 9 Conclusions

This research study has developed an optimal strength design that takes into consideration key ‘geometry’ and ‘manufacturing process’ effects to the material and structural properties into the design of cold formed steel (CFS) structural members. Numerical methods such as Finite Element modelling were developed and validated against earlier experimental data to model the final members subjected to loads in building applications. In addition, experimental measurements and testing of the materials were carried out to investigate the cold work effects, and their results were used for the validation of numerical simulations. This study came from the motivation of deploying a novel practice orientated design approach to optimise CFS sections with longitudinal intermediate stiffeners in the flanges and web under bending that led to more economical and sustainable alternative cross sections in the CFS industry. The cross-sectional shapes considered in this research were channel and zed sections as they are widely used in building construction applications.

The **scientific novelties, contributions to the existing knowledge** and **impacts** of this doctoral research study are explained below:

### 9.1 Numerical validation

A validated FE model for an industrial channel and zed section beam subjected to four-point bending tests was developed. Two different arrangements were considered for the purpose of validation in the FE models: (1) a full model in which the two beam specimens were modelled similar to the actual setup in the experimental test, and (2) a half model in which only one beam specimen was modelled, and appropriate boundary conditions were used to model the symmetry about the longitudinal axis of the full system. The results obtained from full models were compared to those of the half model with symmetry conditions for verification purpose and found that the difference in maximum load capacity was very small, 0.07%, which could be



negligible. Therefore, the half model setup was used to conduct all numerical investigations in this study.

Two different methods were used to model the elastic buckling analysis in order to take the shape and distribution of initial imperfections for FE models of beam bending tests: (1) conducting elastic buckling analysis with the conventional Finite Element Model (FEM) via ANSYS, and (2) conducting elastic buckling analysis with Finite Strip Method (FSM) using CUFSM. The FEM first buckling mode was often the smallest buckling mode and could be selected for nonlinear buckling analysis. Therefore, the first buckling mode shape was selected to generate imperfections. In the second method, the first linear buckling mode obtained from FSM using CUFSM were then transferred to the FEM via the software ANSYS to conduct the nonlinear buckling analysis. Schafer and Peköz suggested the cumulative distribution function (CDF) values for the maximum imperfections be used for type 1 (local buckling  $d_1$ ) and type 2 (distortional buckling  $d_2$ ). It was observed that the FE results with the imperfection value of 1.55t were the closest in agreement with the experimental results with less than 1% difference in the slope and strength values. The 75% CDF amplitude corresponded to an initial imperfection amplitude of 1.55t was, therefore, adopted for the parametric study and optimisation in this research.

The material properties of flat regions were obtained from previous experimental tensile tests and the material properties at corners and stiffener's bends affected by the cold work were obtained from the material properties of flat regions by using formulae from the North American specification for Cold-formed steel structural members. The constitutive stress-strain model proposed by Hadarali and Nethercot was employed, in which the plastic region of the stress-strain curve was modelled with a straight line with a constant slope of  $E/50$ , where  $E$  is the elastic modulus obtained from material tests. Therefore, different stress-strain models of corners and stiffeners' bends were used for the channel and zed sections in the FE simulations.

It was concluded that the FE results of four-points bending tests of the channel and zed sections were in excellent agreement with the experimental, indicating that the buckling and nonlinear

buckling behaviour of cold roll formed sections, considering the imperfections and the cold work effect, was accurately represented by the FE models. The validated FE models were then employed to conduct comprehensive parametric studies and optimisations of cold formed steel channel and zed sections.

## **9.2 Parametric study and current design standard**

A comprehensive parametric study of the channel beam sections under bending conducted to investigate the effects of a stiffener's properties on the section strength including its position, shape, size and material properties by the cold work at bends. Several different cold rolled channel sections having longitudinal intermediate stiffeners at web and flanges with and without the cold work effect on material properties at the stiffener's bends were considered for this investigation. The goal was to find the optimum position, shape and size of web stiffeners as well as the position and size of flange stiffeners while considering the influence of cold work in the section corners and stiffeners' bends; this aimed to ultimately enhance the distortional buckling and ultimate strength capacities of the channel sections while keeping the same amount of material and the same height of the sections as required by practical applications. A total of 72 combinations of FE and DSM analyses were performed and results of ultimate moment capacities, without and with the cold work effect, for different stiffeners' shapes, sizes, positions and the cold work effect on the section's distortional buckling moment capacities were obtained and compared.

It was revealed that an optimal shape for the channel section achieved the maximum ultimate strength in distortional buckling, considering both the stiffeners' position, shape, size and quantity, and the cold work effect, should have the following parameters: the position of the web stiffener was placed as close as possible to the web-flange junction, the depth of the web stiffener was at least 15% of the section height, the position of the peak of the web stiffener was at least 14% of the section height, the width of the web stiffener was of the certain value of 20% of the flange width and not more than that (as the ultimate strength would reduce due to the distortional-global buckling failure), the position of the flange stiffener was placed as much close

as possible to the web-flange junction, the size of the flange stiffener was of the certain value of 28% of the flange width and not more than that (as the ultimate strength would reduce due to the distortional-global buckling failure), and the sections needed to have two web stiffeners and two flange stiffeners. The cold work effect was most significant when changing the width of the web stiffeners and the position of the flange stiffeners, especially in the sections that are less prone to buckling.

The validated FE models and the DSM were then used to conduct a parametric study of the zed sections under bending to understand and gain inside into their structural performance. The same parameters investigated for the channel sections were also considered for the zed sections included both stiffener's geometry and the cold work effects so as to maximise the buckling and ultimate bending strength of the sections. A total of 78 combinations of FE and DSM analyses were performed and results of ultimate moment capacities, without and with the cold work effect, for different stiffeners' shapes, sizes, positions and the cold work effect on the section's buckling moment capacities were obtained and compared. An optimal shape of the zed section, considering both the stiffeners' position, shape, size and quantity, and the cold work effect, resulted in the maximum ultimate bending strength could have: the position of the web stiffener was placed as much close as possible to the web-flange junction, the depth of the web stiffener was at least 10% of the section height, the position of the peak of the web stiffener was at least 20% of the section height, the width of the web stiffener was of the certain value of 40% of the flange width and not more than that (as the ultimate strength would reduce due to the distortional-global buckling failure), the position of the flange stiffener was placed as much close as possible to the web-flange junction, the size of the flange stiffener was of the certain value of 40% of the flange width and the sections needed to have two web stiffeners and two flange stiffeners

The suitability of a design method, the Direct Strength Method (DSM), in predicting the ultimate moment capacity for cold-formed steel beam channel and zed sections was assessed using the FE analyses results. It was found that the DSM results were in good agreement with the FE results

and followed the same trends in most of the channel and zed sections. However, as the statistical correlation between a cross-sectional slenderness parameter and the ultimate strength capacity was used to develop the DSM equations, the DSM predictions was found significantly cross-sectional dependent, resulted in providing more accurate prediction for certain cross-sections than for others. The DSM also ignored distortional-global buckling interactions. This could be significantly problematic as the DSM results may not be correct in their prediction. This was found in the channel and zed sections where the tip of web stiffeners shifted away from the web in horizontal direction. In fact, there were significant reductions of the sectional modulus in the minor axis that caused the sections failed by distortional-global interaction buckling but it was not accounted for in DSM design rules. It was, therefore, concluded that the distortional-global interaction buckling needs to be included in the DSM design guideline.

It should be noted that the above parametric studies gained inside into the structural behaviour of CFS longitudinally stiffened channel and zed sections, investigated the effects of cold-working from the manufacturing process on ultimate bending strength of the beam sections, and evaluated the suitability of the current codified DSM for the channel and zed sections with web and flange stiffeners and suggested the inclusion of distortional-global interaction buckling into current codified DSM design rules. On the other hand, an attempt was made to achieve the optimal shape of the channel and zed sections by changing single parameter. The single parameter response surface is always used for conventional optimisation design since it is easily obtained by an orthogonal test. However, it is insufficient for optimisation if one does not understand the interaction between parameters.

The majority of previous studies on the optimisation of CFS sections investigated the interaction between the parameters (optimising the relative dimension of the sections) but limited to use the current design methods to maximise the buckling and ultimate strength of the conventional sections. As thin-walled CFS sections have very complicated behaviour, which they are prone to different buckling failures such as local, distortional, global buckling mode and the interactive buckling failure between these modes. The current design methods (the EWM and the DSM)

available in the standards and specifications are typically not applicable for all the cross-sectional shapes. This was confirmed through the comprehensive parametric studies conducted in this thesis, which gained insight into the structural behaviour of the channel and zed sections with intermediate stiffeners and evaluated the current design methods. It was concluded that, based on the parametric study results and literature reviews performed in this thesis, the previous optimisation procedures employed the design methods may not lead to optimal design of the cross-sectional shape.

### **9.3 New design optimisation approach**

A new practical design optimisation approach considering key ‘geometry’ and ‘manufacturing process’ effects was developed toward an optimal design of CFS sections. In this approach, detailed nonlinear FE models were first developed for referenced channel and zed sections subjected to four-point bending tests and these reference sections were then parameterized in terms of geometric dimensions and material properties using the DOE technique. In the next step, a response surface was used to determine the influences of the stiffener’s properties on the section distortional buckling and ultimate bending strength including its location, shape, size and enhanced material properties by the cold work at the section corners and stiffener bends. Response surface design optimisation was then used to determine the geometric dimensions and material properties of optimised channel and zed sections. The adequacy of the optimised sections obtained from FEM optimisation process was verified by the results obtained from transferring CUFSM buckling mode shapes into the FEM (i.e., CUFSM-FEM). It was found that the FEM candidate results closely followed the increasing or decreasing trends in the buckling and flexural strength capacity obtained by the CUFSM-FEM results. This demonstrates the reliability of the proposed optimisation procedure using the direct FEM optimisation.

It was also found that both target objectives constrain, which were maximising buckling and minimising maximum developed stress, had to be applied in order to obtain the optimal design of the sections with significantly increasing both stiffness and bending strength and the cold work effects. Comparison between the optimised candidates indicated that when increasing the size of

intermediate web and flange stiffeners and edge stiffeners, a turning point was reached where increasing the stiffeners size reduced the ultimate moment capacity, while marginally improved the distortional buckling, resulting in sections failed in distortional-global interactive buckling modes. The optimum position of the web and flange stiffeners found to be moved toward the web-flange junctions as much as possible during the optimisation process resulted in the optimised cross-sectional shapes for the channel and zed sections. This was a result of the intermediate stiffeners position both increasing the sectional modulus and decreasing the distortional buckling slenderness, which led to ultimately enhance the distortional buckling and ultimate strength capacities as well as mitigating the post-buckling stiffness degradation of the optimised sections.

FEM optimisation of cold formed steel channel sections in bending considering key geometry and manufacturing effects. The following findings could be summarised for the channel sections. The reference channel section provided considerably greater buckling compared to the standard lipped channel by 15%, whereas the ultimate moment capacity was noticeably improved by 3%. Adding flange stiffeners to the reference section resulted in further enhancement in the buckling and ultimate moment capacity by 16% and 4%, respectively. By changing the position, size and shape of web stiffeners, lip width, and section corners' radiuses as well as including the cold work effect at the sections' corners and stiffeners' bends of the reference channel section, optimised sections could be obtained (Candidate 1-3) with significantly greater buckling. The gains for the candidates of 1, 2 and 3 were 96%, 101% and 100%, respectively, compared to the standard lipped channel. At the same time, the ultimate moment capacity was also improved by 12%, 7% and 12%, respectively. Similarly, the optimal design of the channel sections was obtained by changing the position, size and shape of web stiffeners, the position and size of flange stiffeners, lip width, and section corners' radiuses as well as including the cold work effect at the sections' corners and stiffeners' bends of the reference section with having flange stiffeners (Candidate 4-6). The significant increases in buckling for the candidate 4, 5 and 6 were 78%, 98% and 84%, respectively. At the same time, the ultimate moment capacity was also significantly increased by 15%, 8% and 17%, respectively.

FEM optimisation of CFS zed sections in bending performed considering key geometry and manufacturing effects. The findings obtained for the zed sections could be summarised as the following: The reference zed section provided considerably better buckling compared to the standard lipped zed section by 21%, whereas the ultimate moment capacity was considerably improved by 9%. Adding flange stiffeners to the reference section resulted in further enhancement in the buckling and ultimate moment capacity by 15% and 6%, respectively. By changing the position, size and shape of web stiffeners, lip width, and section corners' radiuses as well as including the cold work effect at the sections' corners and stiffeners' bends of the reference zed section, optimised sections could be obtained (Candidate 1-3) with significantly better buckling. The gains for the candidates of 1, 2 and 3 were 105%, 120% and 110%, respectively, compared to the standard lipped zed section. At the same time, the ultimate moment capacity was also significantly improved by 23%, 9% and 25%, respectively. Similarly, the optimal design of the zed sections was obtained by changing the position, size and shape of web stiffeners, the position and size of flange stiffeners, lip width, and section corners' radiuses as well as including the cold work effect at the sections' corners and stiffeners' bends of the reference section with having flange stiffeners (Candidate 4-6). The significant increases in buckling for the candidate 4, 5 and 6 were 95%, 112% and 105%, respectively. At the same time, the ultimate moment capacity was also significantly increased by 21%, 22% and 24%, respectively.

#### **9.4 Experimental measurement and material testing**

A total of 96 tensile coupon specimens obtained from 4 cross-sections was tested to determine the mechanical properties of the material. This included the 16 tensile coupons extracted from the pre-cold rolled sheet coils (virgin materials), 16 coupons extracted from the web of the sections, 16 coupons extracted from the flanges of the sections, and 48 coupons extracted from the section corners and stiffener's bends. The results from the current test programme were used to investigate the cold work effects in the corner and stiffener bend regions of cold roll formed sections and the accuracy of existing predictive models was evaluated. The strength

enhancement obtained in the section corners and stiffener's bends were then used to accurately obtain the bending strength of the CFS sections. The findings could be summarised as the following.

The cold work had modest effect in material strength in the flat regions of cold roll formed steel sections by on average 2.5%, but significantly enhanced material strength in the corner and stiffener bend regions by on average 22%.; the results were compared with two predictive models and both of the models provided reasonable results. The cold work effect in the corner and stiffener areas was insignificant on bending strength in the standard sections and only had a relevant influence at reference sections bending strength. The main reason for the low contribution of the cold work effects can be the higher distortional buckling slenderness and the relatively small area of the rounded corners compared to the total cross section area in the sections. On the other hand, the cold work effect significantly increased the bending strength of the optimised channel and zed sections up to 7% and 6%, respectively. In the optimised sections, several parts of the cross-section presented an equivalent strain higher than the yield strain, so the increase of the yield strength in corner areas produced an increase of the flexural strength of the beams. The optimal cross-sectional shape recommended to have two longitudinal stiffeners at the web placed as much close as possible to the web-flange junctions, one longitudinal flange stiffeners placed near the web flange junctions as much as possible, and the relative dimensions of the sections should be as proposed in this thesis. The proposed shape could gain significant benefit from both the 'geometry' and the 'manufacturing process' effects.

## **9.5 Recommendations for future research**

Even though the study objectives have been achieved in this research, a number of new questions during the study become essential to be answered, which can be considered as recommendations for future research:

- Even though the current codified DSM for predicting bending strength of CFS sections with web and flange intermediate stiffener provided relatively safe results in most of the



cross-sections considered for distortional buckling, a more refined validated method is still important to account for other modal interactive buckling failures particularly distortional-global interaction failures.

- It is desirable to conduct experiments for both reference sections and optimised sections and compares the results with the achieved numerical ones in this study.
- The new optimisation method developed and applied for structural beam member in this PhD study, it can be easily applied and extended for other structural members such as column and beam-column members.
- The focus of this study was on optimising CFS sections considering key geometry and manufacturing effects particularly channel and zed sections. Other cross-sectional shapes (rack sections, hollow sections and angles) are also required to be optimised for geometry and manufacturing effects to achieve more efficient sections. Optimising cold formed stainless-steel sections may experience, in general, more changes from manufacturing effects and can be highly recommended.
- The CFS sections were optimised for the bending strength in this study, but they are highly likely to be optimal for the shear strength and energy dissipation. Optimising the new channel and zed sections under shear and cyclic loads is also required to be studied.

The overall recommendations for further research studies can be presented as that it is important to conduct extensive research to perform experimental study to validate the optimised sections developed in this research. In addition, the optimisation of CFS sections for shear strength and energy dissipation are highly recommended to be numerically and experimentally studied for the channel and zed sections with web and flange intermediate stiffeners.

# Appendices

Appendices present Finite Element modelling results performed to obtain the buckling loads and flexural developed stresses when changing the parameters of the cross-sections in the optimisation process.

## Appendix A

Experimental Design points for longitudinally web stiffened channel sections

Name	P1	P2	P3	P4	P5	P6	P7	P8	P9	P10	P11	P12	P13	P14
DP 0	40.5	40.5	13.61	12.35	2.9	0	0	55.7	574	574	3.48	-10000	13098	482
DP 1	10.5	10.5	13.61	12.35	2.9	0	0	55.7	574	574	3.48	-10000	13419	446
DP 2	25.5	25.5	13.61	12.35	2.9	0	0	55.7	574	574	3.48	-10000	13167	454
DP 3	40.5	40.5	13.61	12.35	2.9	0	0	55.7	574	574	3.48	-10000	13098	482
DP 4	10.5	10.5	5.61	12.35	2.9	0	0	59.4	574	574	3.48	-10000	12168	500
DP 5	25.5	25.5	5.61	12.35	2.9	0	0	59.4	574	574	3.48	-10000	12081	497
DP 6	40.5	40.5	5.61	12.35	2.9	0	0	59.4	574	574	3.48	-10000	12066	500
DP 7	10.5	10.5	18.61	12.35	2.9	0	0	52.8	574	574	3.48	-10000	14888	426
DP 8	25.5	25.5	18.61	12.35	2.9	0	0	52.8	574	574	3.48	-10000	14474	454
DP 9	40.5	40.5	18.61	12.35	2.9	0	0	52.8	574	574	3.48	-10000	14247	518
DP 10	10.5	10.5	13.61	15.35	2.9	0	0	52.7	574	574	3.48	-10000	16113	430
DP 11	25.5	25.5	13.61	15.35	2.9	0	0	52.7	574	574	3.48	-10000	15771	455
DP 12	40.5	40.5	13.61	15.35	2.9	0	0	52.7	574	574	3.48	-10000	15708	486
DP 13	10.5	10.5	5.61	15.35	2.9	0	0	56.4	574	574	3.48	-10000	14904	437
DP 14	25.5	25.5	5.61	15.35	2.9	0	0	56.4	574	574	3.48	-10000	14789	444
DP 15	40.5	40.5	5.61	15.35	2.9	0	0	56.4	574	574	3.48	-10000	14776	449
DP 16	10.5	10.5	18.61	15.35	2.9	0	0	49.8	574	574	3.48	-10000	17544	403
DP 17	25.5	25.5	18.61	15.35	2.9	0	0	49.8	574	574	3.48	-10000	17003	425
DP 18	40.5	40.5	18.61	15.35	2.9	0	0	49.8	574	574	3.48	-10000	16833	516
DP 19	10.5	10.5	13.61	18.35	2.9	0	0	49.7	574	574	3.48	-10000	18411	421
DP 20	25.5	25.5	13.61	18.35	2.9	0	0	49.7	574	574	3.48	-10000	17987	437
DP 21	40.5	40.5	13.61	18.35	2.9	0	0	49.7	574	574	3.48	-10000	17965	488
DP 22	10.5	10.5	5.61	18.35	2.9	0	0	53.4	574	574	3.48	-10000	17413	447
DP 23	25.5	25.5	5.61	18.35	2.9	0	0	53.4	574	574	3.48	-10000	17276	453
DP 24	40.5	40.5	5.61	18.35	2.9	0	0	53.4	574	574	3.48	-10000	17261	457
DP 25	10.5	10.5	18.61	18.35	2.9	0	0	46.8	574	574	3.48	-10000	19672	419

DP 26	25.5	25.5	18.61	18.35	2.9	0	0	46.8	574	574	3.48	-10000	19019	441
DP 27	40.5	40.5	18.61	18.35	2.9	0	0	46.8	574	574	3.48	-10000	18926	516
DP 28	10.5	10.5	13.61	12.35	5	0	0	57.2	534	534	3.48	-10000	12576	470
DP 29	25.5	25.5	13.61	12.35	5	0	0	57.2	534	534	3.48	-10000	12337	463
DP 30	40.5	40.5	13.61	12.35	5	0	0	57.2	534	534	3.48	-10000	12260	480
DP 31	10.5	10.5	5.61	12.35	5	0	0	60.9	534	534	3.48	-10000	11515	507
DP 32	25.5	25.5	5.61	12.35	5	0	0	60.9	534	534	3.48	-10000	11433	504
DP 33	40.5	40.5	5.61	12.35	5	0	0	60.9	534	534	3.48	-10000	11414	501
DP 34	10.5	10.5	18.61	12.35	5	0	0	54.3	534	534	3.48	-10000	13828	443
DP 35	25.5	25.5	18.61	12.35	5	0	0	54.3	534	534	3.48	-10000	13437	450
DP 36	40.5	40.5	18.61	12.35	5	0	0	54.3	534	534	3.48	-10000	13224	516
DP 37	10.5	10.5	13.61	15.35	5	0	0	54.2	534	534	3.48	-10000	15292	434
DP 38	25.5	25.5	13.61	15.35	5	0	0	54.2	534	534	3.48	-10000	14968	451
DP 39	40.5	40.5	13.61	15.35	5	0	0	54.2	534	534	3.48	-10000	14882	486
DP 40	10.5	10.5	5.61	15.35	5	0	0	57.9	534	534	3.48	-10000	14188	478
DP 41	25.5	25.5	5.61	15.35	5	0	0	57.9	534	534	3.48	-10000	14083	486
DP 42	40.5	40.5	5.61	15.35	5	0	0	57.9	534	534	3.48	-10000	14057	492
DP 43	10.5	10.5	18.61	15.35	5	0	0	51.3	534	534	3.48	-10000	16567	414
DP 44	25.5	25.5	18.61	15.35	5	0	0	51.3	534	534	3.48	-10000	16046	430
DP 45	40.5	40.5	18.61	15.35	5	0	0	51.3	534	534	3.48	-10000	15858	516
DP 46	10.5	10.5	13.61	18.35	5	0	0	51.2	534	534	3.48	-10000	17797	411
DP 47	25.5	25.5	13.61	18.35	5	0	0	51.2	534	534	3.48	-10000	17391	425
DP 48	40.5	40.5	13.61	18.35	5	0	0	51.2	534	534	3.48	-10000	17309	486
DP 49	10.5	10.5	5.61	18.35	5	0	0	54.9	534	534	3.48	-10000	16766	444
DP 50	25.5	25.5	5.61	18.35	5	0	0	54.9	534	534	3.48	-10000	16636	449
DP 51	40.5	40.5	5.61	18.35	5	0	0	54.9	534	534	3.48	-10000	16608	453
DP 52	10.5	10.5	18.61	18.35	5	0	0	48.3	534	534	3.48	-10000	19050	419
DP 53	25.5	25.5	18.61	18.35	5	0	0	48.3	534	534	3.48	-10000	18397	439
DP 54	40.5	40.5	18.61	18.35	5	0	0	48.3	534	534	3.48	-10000	18238	516
DP 55	10.5	10.5	13.61	12.35	7.5	0	0	58.7	519	519	3.48	-10000	11685	524
DP 56	25.5	25.5	13.61	12.35	7.5	0	0	58.7	519	519	3.48	-10000	11459	519
DP 57	40.5	40.5	13.61	12.35	7.5	0	0	58.7	519	519	3.48	-10000	11373	524
DP 58	10.5	10.5	5.61	12.35	7.5	0	0	62.4	519	519	3.48	-10000	10783	541
DP 59	25.5	25.5	5.61	12.35	7.5	0	0	62.4	519	519	3.48	-10000	10705	540
DP 60	40.5	40.5	5.61	12.35	7.5	0	0	62.4	519	519	3.48	-10000	10682	536
DP 61	10.5	10.5	18.61	12.35	7.5	0	0	55.8	519	519	3.48	-10000	12729	521
DP 62	25.5	25.5	18.61	12.35	7.5	0	0	55.8	519	519	3.48	-10000	12359	507
DP 63	40.5	40.5	18.61	12.35	7.5	0	0	55.8	519	519	3.48	-10000	12179	521

DP 64	10.5	10.5	13.61	15.35	7.5	0	0	55.7	519	519	3.48	-10000	14338	488
DP 65	25.5	25.5	13.61	15.35	7.5	0	0	55.7	519	519	3.48	-10000	14036	486
DP 66	40.5	40.5	13.61	15.35	7.5	0	0	55.7	519	519	3.48	-10000	13934	502
DP 67	10.5	10.5	5.61	15.35	7.5	0	0	59.4	519	519	3.48	-10000	13375	489
DP 68	25.5	25.5	5.61	15.35	7.5	0	0	59.4	519	519	3.48	-10000	13279	493
DP 69	40.5	40.5	5.61	15.35	7.5	0	0	59.4	519	519	3.48	-10000	13250	498
DP 70	10.5	10.5	18.61	15.35	7.5	0	0	52.8	519	519	3.48	-10000	15442	477
DP 71	25.5	25.5	18.61	15.35	7.5	0	0	52.8	519	519	3.48	-10000	14959	476
DP 72	40.5	40.5	18.61	15.35	7.5	0	0	52.8	519	519	3.48	-10000	14768	516
DP 73	10.5	10.5	13.61	18.35	7.5	0	0	52.7	519	519	3.48	-10000	16913	470
DP 74	25.5	25.5	13.61	18.35	7.5	0	0	52.7	519	519	3.48	-10000	16542	476
DP 75	40.5	40.5	13.61	18.35	7.5	0	0	52.7	519	519	3.48	-10000	16425	490
DP 76	10.5	10.5	5.61	18.35	7.5	0	0	56.4	519	519	3.48	-10000	15946	476
DP 77	25.5	25.5	5.61	18.35	7.5	0	0	56.4	519	519	3.48	-10000	15832	484
DP 78	40.5	40.5	5.61	18.35	7.5	0	0	56.4	519	519	3.48	-10000	15796	488
DP 79	10.5	10.5	18.61	18.35	7.5	0	0	49.8	519	519	3.48	-10000	18054	459
DP 80	25.5	25.5	18.61	18.35	7.5	0	0	49.8	519	519	3.48	-10000	17450	477
DP 81	40.5	40.5	18.61	18.35	7.5	0	0	49.8	519	519	3.48	-10000	17250	516
DP 82	10.5	10.5	13.61	12.35	2.9	10	350	50	574	574	3.48	-10000	14350	443
DP 83	25.5	25.5	13.61	12.35	2.9	10	350	50	574	574	3.48	-10000	15103	429
DP 84	40.5	40.5	13.61	12.35	2.9	10	350	50	574	574	3.48	-10000	15683	536
DP 85	10.5	10.5	5.61	12.35	2.9	10	350	53.6	574	574	3.48	-10000	12916	485
DP 86	25.5	25.5	5.61	12.35	2.9	10	350	53.6	574	574	3.48	-10000	13204	473
DP 87	40.5	40.5	5.61	12.35	2.9	10	350	53.6	574	574	3.48	-10000	13806	532
DP 88	10.5	10.5	18.61	12.35	2.9	10	350	47.2	574	574	3.48	-10000	16003	428
DP 89	25.5	25.5	18.61	12.35	2.9	10	350	47.2	574	574	3.48	-10000	16922	437
DP 90	40.5	40.5	18.61	12.35	2.9	10	350	47.2	574	574	3.48	-10000	17118	542
DP 91	10.5	10.5	13.61	15.35	2.9	10	350	47	574	574	3.48	-10000	16798	434
DP 92	25.5	25.5	13.61	15.35	2.9	10	350	47	574	574	3.48	-10000	17502	442
DP 93	40.5	40.5	13.61	15.35	2.9	10	350	47	574	574	3.48	-10000	18349	536
DP 94	10.5	10.5	5.61	15.35	2.9	10	350	50.6	574	574	3.48	-10000	15498	430
DP 95	25.5	25.5	5.61	15.35	2.9	10	350	50.6	574	574	3.48	-10000	15735	431
DP 96	40.5	40.5	5.61	15.35	2.9	10	350	50.6	574	574	3.48	-10000	16388	533
DP 97	10.5	10.5	18.61	15.35	2.9	10	350	44.2	574	574	3.48	-10000	18274	421
DP 98	25.5	25.5	18.61	15.35	2.9	10	350	44.2	574	574	3.48	-10000	19202	427
DP 99	40.5	40.5	18.61	15.35	2.9	10	350	44.2	574	574	3.48	-10000	19851	542
DP 100	10.5	10.5	13.61	18.35	2.9	10	350	44	574	574	3.48	-10000	18631	424
DP 101	25.5	25.5	13.61	18.35	2.9	10	350	44	574	574	3.48	-10000	19183	430

DP 102	40.5	40.5	13.61	18.35	2.9	10	350	44	574	574	3.48	-10000	20265	535
DP 103	10.5	10.5	5.61	18.35	2.9	10	350	47.6	574	574	3.48	-10000	17715	452
DP 104	25.5	25.5	5.61	18.35	2.9	10	350	47.6	574	574	3.48	-10000	17834	453
DP 105	40.5	40.5	5.61	18.35	2.9	10	350	47.6	574	574	3.48	-10000	18538	534
DP 106	10.5	10.5	18.61	18.35	2.9	10	350	41.2	574	574	3.48	-10000	19704	438
DP 107	25.5	25.5	18.61	18.35	2.9	10	350	41.2	574	574	3.48	-10000	20413	442
DP 108	40.5	40.5	18.61	18.35	2.9	10	350	41.2	574	574	3.48	-10000	21497	541
DP 109	10.5	10.5	13.61	12.35	2.9	20	340	44.7	574	574	3.48	-10000	15438	443
DP 110	25.5	25.5	13.61	12.35	2.9	20	340	44.7	574	574	3.48	-10000	17773	433
DP 111	40.5	40.5	13.61	12.35	2.9	20	340	44.7	574	574	3.48	-10000	18459	537
DP 112	10.5	10.5	5.61	12.35	2.9	20	340	47.9	574	574	3.48	-10000	13675	489
DP 113	25.5	25.5	5.61	12.35	2.9	20	340	47.9	574	574	3.48	-10000	15136	453
DP 114	40.5	40.5	5.61	12.35	2.9	20	340	47.9	574	574	3.48	-10000	16555	536
DP 115	10.5	10.5	18.61	12.35	2.9	20	340	45	574	574	3.48	-10000	16689	434
DP 116	25.5	25.5	18.61	12.35	2.9	20	340	45	574	574	3.48	-10000	18948	455
DP 117	40.5	40.5	18.61	12.35	2.9	20	340	45	574	574	3.48	-10000	18884	538
DP 118	10.5	10.5	13.61	15.35	2.9	20	340	41.7	574	574	3.48	-10000	17448	451
DP 119	25.5	25.5	13.61	15.35	2.9	20	340	41.7	574	574	3.48	-10000	19755	440
DP 120	40.5	40.5	13.61	15.35	2.9	20	340	41.7	574	574	3.48	-10000	21312	538
DP 121	10.5	10.5	5.61	15.35	2.9	20	340	44.9	574	574	3.48	-10000	16051	440
DP 122	25.5	25.5	5.61	15.35	2.9	20	340	44.9	574	574	3.48	-10000	17407	428
DP 123	40.5	40.5	5.61	15.35	2.9	20	340	44.9	574	574	3.48	-10000	19298	537
DP 124	10.5	10.5	18.61	15.35	2.9	20	340	39	574	574	3.48	-10000	18823	455
DP 125	25.5	25.5	18.61	15.35	2.9	20	340	39	574	574	3.48	-10000	21162	438
DP 126	40.5	40.5	18.61	15.35	2.9	20	340	39	574	574	3.48	-10000	22581	538
DP 127	10.5	10.5	13.61	18.35	2.9	20	340	38.7	574	574	3.48	-10000	18549	451
DP 128	25.5	25.5	13.61	18.35	2.9	20	340	38.7	574	574	3.48	-10000	20319	443
DP 129	40.5	40.5	13.61	18.35	2.9	20	340	38.7	574	574	3.48	-10000	22550	538
DP 130	10.5	10.5	5.61	18.35	2.9	20	340	41.9	574	574	3.48	-10000	17769	457
DP 131	25.5	25.5	5.61	18.35	2.9	20	340	41.9	574	574	3.48	-10000	18842	454
DP 132	40.5	40.5	5.61	18.35	2.9	20	340	41.9	574	574	3.48	-10000	21050	536
DP 133	10.5	10.5	18.61	18.35	2.9	20	340	36	574	574	3.48	-10000	19006	475
DP 134	25.5	25.5	18.61	18.35	2.9	20	340	36	574	574	3.48	-10000	20630	479
DP 135	40.5	40.5	18.61	18.35	2.9	20	340	36	574	574	3.48	-10000	22922	538
DP 136	10.5	10.5	13.61	12.35	2.9	0	0	55.7	574	574	3.48	-11500	13419	546
DP 137	25.5	25.5	13.61	12.35	2.9	0	0	55.7	574	574	3.48	-11500	13167	552
DP 138	40.5	40.5	13.61	12.35	2.9	0	0	55.7	574	574	3.48	-11500	13092	554
DP 139	10.5	10.5	5.61	12.35	2.9	0	0	59.4	574	574	3.48	-11500	12168	574

DP 140	25.5	25.5	5.61	12.35	2.9	0	0	59.4	574	574	3.48	-11500	12081	575
DP 141	40.5	40.5	5.61	12.35	2.9	0	0	59.4	574	574	3.48	-11500	12066	575
DP 142	10.5	10.5	18.61	12.35	2.9	0	0	52.8	574	574	3.48	-11500	14888	516
DP 143	25.5	25.5	18.61	12.35	2.9	0	0	52.8	574	574	3.48	-11500	14474	522
DP 144	40.5	40.5	18.61	12.35	2.9	0	0	52.8	574	574	3.48	-11500	14247	531
DP 145	10.5	10.5	13.61	15.35	2.9	0	0	52.7	574	574	3.48	-11500	16113	519
DP 146	25.5	25.5	13.61	15.35	2.9	0	0	52.7	574	574	3.48	-11500	15771	519
DP 147	40.5	40.5	13.61	15.35	2.9	0	0	52.7	574	574	3.48	-11500	15708	520
DP 148	10.5	10.5	5.61	15.35	2.9	0	0	56.4	574	574	3.48	-11500	14904	527
DP 149	25.5	25.5	5.61	15.35	2.9	0	0	56.4	574	574	3.48	-11500	14789	529
DP 150	40.5	40.5	5.61	15.35	2.9	0	0	56.4	574	574	3.48	-11500	14776	531
DP 151	10.5	10.5	18.61	15.35	2.9	0	0	49.8	574	574	3.48	-11500	17544	488
DP 152	25.5	25.5	18.61	15.35	2.9	0	0	49.8	574	574	3.48	-11500	17003	516
DP 153	40.5	40.5	18.61	15.35	2.9	0	0	49.8	574	574	3.48	-11500	16833	521
DP 154	10.5	10.5	13.61	18.35	2.9	0	0	49.7	574	574	3.48	-11500	18411	513
DP 155	25.5	25.5	13.61	18.35	2.9	0	0	49.7	574	574	3.48	-11500	17987	519
DP 156	40.5	40.5	13.61	18.35	2.9	0	0	49.7	574	574	3.48	-11500	17965	519
DP 157	10.5	10.5	5.61	18.35	2.9	0	0	53.4	574	574	3.48	-11500	17413	519
DP 158	25.5	25.5	5.61	18.35	2.9	0	0	53.4	574	574	3.48	-11500	17276	520
DP 159	40.5	40.5	5.61	18.35	2.9	0	0	53.4	574	574	3.48	-11500	17261	523
DP 160	10.5	10.5	18.61	18.35	2.9	0	0	46.8	574	574	3.48	-11500	19672	501
DP 161	25.5	25.5	18.61	18.35	2.9	0	0	46.8	574	574	3.48	-11500	19019	519
DP 162	40.5	40.5	18.61	18.35	2.9	0	0	46.8	574	574	3.48	-11500	18926	520
DP 163	10.5	10.5	13.61	12.35	5	0	0	57.2	534	534	3.48	-11500	12576	543
DP 164	25.5	25.5	13.61	12.35	5	0	0	57.2	534	534	3.48	-11500	12337	535
DP 165	40.5	40.5	13.61	12.35	5	0	0	57.2	534	534	3.48	-11500	12260	533
DP 166	10.5	10.5	5.61	12.35	5	0	0	60.9	534	534	3.48	-11500	11515	552
DP 167	25.5	25.5	5.61	12.35	5	0	0	60.9	534	534	3.48	-11500	11433	564
DP 168	40.5	40.5	5.61	12.35	5	0	0	60.9	534	534	3.48	-11500	11414	566
DP 169	10.5	10.5	18.61	12.35	5	0	0	54.3	534	534	3.48	-11500	13828	545
DP 170	25.5	25.5	18.61	12.35	5	0	0	54.3	534	534	3.48	-11500	13437	534
DP 171	40.5	40.5	18.61	12.35	5	0	0	54.3	534	534	3.48	-11500	13224	534
DP 172	10.5	10.5	13.61	15.35	5	0	0	54.2	534	534	3.48	-11500	15292	523
DP 173	25.5	25.5	13.61	15.35	5	0	0	54.2	534	534	3.48	-11500	14968	524
DP 174	40.5	40.5	13.61	15.35	5	0	0	54.2	534	534	3.48	-11500	14882	523
DP 175	10.5	10.5	5.61	15.35	5	0	0	57.9	534	534	3.48	-11500	14188	523
DP 176	25.5	25.5	5.61	15.35	5	0	0	57.9	534	534	3.48	-11500	14083	523
DP 177	40.5	40.5	5.61	15.35	5	0	0	57.9	534	534	3.48	-11500	14057	523

DP 178	10.5	10.5	18.61	15.35	5	0	0	51.3	534	534	3.48	-11500	16567	516
DP 179	25.5	25.5	18.61	15.35	5	0	0	51.3	534	534	3.48	-11500	16046	516
DP 180	40.5	40.5	18.61	15.35	5	0	0	51.3	534	534	3.48	-11500	15858	522
DP 181	10.5	10.5	13.61	18.35	5	0	0	51.2	534	534	3.48	-11500	17797	502
DP 182	25.5	25.5	13.61	18.35	5	0	0	51.2	534	534	3.48	-11500	17391	516
DP 183	40.5	40.5	13.61	18.35	5	0	0	51.2	534	534	3.48	-11500	17309	519
DP 184	10.5	10.5	5.61	18.35	5	0	0	54.9	534	534	3.48	-11500	16766	518
DP 185	25.5	25.5	5.61	18.35	5	0	0	54.9	534	534	3.48	-11500	16636	521
DP 186	40.5	40.5	5.61	18.35	5	0	0	54.9	534	534	3.48	-11500	16608	524
DP 187	10.5	10.5	18.61	18.35	5	0	0	48.3	534	534	3.48	-11500	19050	509
DP 188	25.5	25.5	18.61	18.35	5	0	0	48.3	534	534	3.48	-11500	18397	518
DP 189	40.5	40.5	18.61	18.35	5	0	0	48.3	534	534	3.48	-11500	18238	520
DP 190	10.5	10.5	13.61	12.35	7.5	0	0	58.7	519	519	3.48	-11500	11685	546
DP 191	25.5	25.5	13.61	12.35	7.5	0	0	58.7	519	519	3.48	-11500	11459	537
DP 192	40.5	40.5	13.61	12.35	7.5	0	0	58.7	519	519	3.48	-11500	11373	536
DP 193	10.5	10.5	5.61	12.35	7.5	0	0	62.4	519	519	3.48	-11500	10783	567
DP 195	40.5	40.5	5.61	12.35	7.5	0	0	62.4	519	519	3.48	-11500	10682	570
DP 196	10.5	10.5	18.61	12.35	7.5	0	0	55.8	519	519	3.48	-11500	12729	546
DP 197	25.5	25.5	18.61	12.35	7.5	0	0	55.8	519	519	3.48	-11500	12359	536
DP 198	40.5	40.5	18.61	12.35	7.5	0	0	55.8	519	519	3.48	-11500	12179	534
DP 199	10.5	10.5	13.61	15.35	7.5	0	0	55.7	519	519	3.48	-11500	14338	546
DP 200	25.5	25.5	13.61	15.35	7.5	0	0	55.7	519	519	3.48	-11500	14036	522
DP 201	40.5	40.5	13.61	15.35	7.5	0	0	55.7	519	519	3.48	-11500	13934	521
DP 202	10.5	10.5	5.61	15.35	7.5	0	0	59.4	519	519	3.48	-11500	13375	524
DP 203	25.5	25.5	5.61	15.35	7.5	0	0	59.4	519	519	3.48	-11500	13279	522
DP 204	40.5	40.5	5.61	15.35	7.5	0	0	59.4	519	519	3.48	-11500	13250	525
DP 205	10.5	10.5	18.61	15.35	7.5	0	0	52.8	519	519	3.48	-11500	15442	542
DP 206	25.5	25.5	18.61	15.35	7.5	0	0	52.8	519	519	3.48	-11500	14959	521
DP 207	40.5	40.5	18.61	15.35	7.5	0	0	52.8	519	519	3.48	-11500	14768	520
DP 208	10.5	10.5	13.61	18.35	7.5	0	0	52.7	519	519	3.48	-11500	16913	531
DP 209	25.5	25.5	13.61	18.35	7.5	0	0	52.7	519	519	3.48	-11500	16542	521
DP 210	40.5	40.5	13.61	18.35	7.5	0	0	52.7	519	519	3.48	-11500	16425	521
DP 211	10.5	10.5	5.61	18.35	7.5	0	0	56.4	519	519	3.48	-11500	15946	522
DP 212	25.5	25.5	5.61	18.35	7.5	0	0	56.4	519	519	3.48	-11500	15832	522
DP 213	40.5	40.5	5.61	18.35	7.5	0	0	56.4	519	519	3.48	-11500	15796	521
DP 214	10.5	10.5	18.61	18.35	7.5	0	0	49.8	519	519	3.48	-11500	18054	527
DP 215	25.5	25.5	18.61	18.35	7.5	0	0	49.8	519	519	3.48	-11500	17450	522
DP 216	40.5	40.5	18.61	18.35	7.5	0	0	49.8	519	519	3.48	-11500	17250	521

DP 217	10.5	10.5	13.61	12.35	2.9	10	350	50	574	574	3.48	-11500	14350	530
DP 218	25.5	25.5	13.61	12.35	2.9	10	350	50	574	574	3.48	-11500	15103	525
DP 219	40.5	40.5	13.61	12.35	2.9	10	350	50	574	574	3.48	-11500	15683	543
DP 220	10.5	10.5	5.61	12.35	2.9	10	350	53.7	574	574	3.48	-11500	12921	556
DP 221	25.5	25.5	5.61	12.35	2.9	10	350	53.7	574	574	3.48	-11500	13206	554
DP 222	40.5	40.5	5.61	12.35	2.9	10	350	53.7	574	574	3.48	-11500	13804	552
DP 223	10.5	10.5	18.61	12.35	2.9	10	350	52.8	574	574	3.48	-11500	14920	514
DP 224	25.5	25.5	18.61	12.35	2.9	10	350	52.8	574	574	3.48	-11500	15597	522
DP 225	40.5	40.5	18.61	12.35	2.9	10	350	52.8	574	574	3.48	-11500	15737	542
DP 226	10.5	10.5	13.61	15.35	2.9	10	350	47	574	574	3.48	-11500	16798	523
DP 227	25.5	25.5	13.61	15.35	2.9	10	350	47	574	574	3.48	-11500	17502	519
DP 228	40.5	40.5	13.61	15.35	2.9	10	350	47	574	574	3.48	-11500	18349	543
DP 229	10.5	10.5	5.61	15.35	2.9	10	350	50.7	574	574	3.48	-11500	15487	522
DP 230	25.5	25.5	5.61	15.35	2.9	10	350	50.7	574	574	3.48	-11500	15724	521
DP 231	40.5	40.5	5.61	15.35	2.9	10	350	50.7	574	574	3.48	-11500	16370	533
DP 232	10.5	10.5	18.61	15.35	2.9	10	350	49.8	574	574	3.48	-11500	17551	487
DP 233	25.5	25.5	18.61	15.35	2.9	10	350	49.8	574	574	3.48	-11500	18269	494
DP 234	40.5	40.5	18.61	15.35	2.9	10	350	49.8	574	574	3.48	-11500	18680	542
DP 235	10.5	10.5	13.61	18.35	2.9	10	350	44	574	574	3.48	-11500	18631	505
DP 236	25.5	25.5	13.61	18.35	2.9	10	350	44	574	574	3.48	-11500	19183	512
DP 237	40.5	40.5	13.61	18.35	2.9	10	350	44	574	574	3.48	-11500	20265	541
DP 238	10.5	10.5	5.61	18.35	2.9	10	350	47.7	574	574	3.48	-11500	17729	519
DP 239	25.5	25.5	5.61	18.35	2.9	10	350	47.7	574	574	3.48	-11500	17846	519
DP 240	40.5	40.5	5.61	18.35	2.9	10	350	47.7	574	574	3.48	-11500	18545	533
DP 241	10.5	10.5	18.61	18.35	2.9	10	350	46.8	574	574	3.48	-11500	19646	500
DP 242	25.5	25.5	18.61	18.35	2.9	10	350	46.8	574	574	3.48	-11500	20287	515
DP 243	40.5	40.5	18.61	18.35	2.9	10	350	46.8	574	574	3.48	-11500	21018	543
DP 244	10.5	10.5	13.61	12.35	2.9	20	340	44.7	574	574	3.48	-11500	15438	529
DP 245	25.5	25.5	13.61	12.35	2.9	20	340	44.7	574	574	3.48	-11500	17773	510
DP 246	40.5	40.5	13.61	12.35	2.9	20	340	44.7	574	574	3.48	-11500	18459	545
DP 247	10.5	10.5	5.61	12.35	2.9	20	340	47.9	574	574	3.48	-11500	13675	567
DP 248	25.5	25.5	5.61	12.35	2.9	20	340	47.9	574	574	3.48	-11500	15136	527
DP 249	40.5	40.5	5.61	12.35	2.9	20	340	47.9	574	574	3.48	-11500	16555	584
DP 250	10.5	10.5	18.61	12.35	2.9	20	340	45	574	574	3.48	-11500	16689	523
DP 251	25.5	25.5	18.61	12.35	2.9	20	340	45	574	574	3.48	-11500	18948	509
DP 252	40.5	40.5	18.61	12.35	2.9	20	340	45	574	574	3.48	-11500	18884	584
DP 253	10.5	10.5	13.61	15.35	2.9	20	340	41.7	574	574	3.48	-11500	17448	527
DP 254	25.5	25.5	13.61	15.35	2.9	20	340	41.7	574	574	3.48	-11500	19755	515



DP 255	40.5	40.5	13.61	15.35	2.9	20	340	41.7	574	574	3.48	-11500	21312	540
DP 256	10.5	10.5	5.61	15.35	2.9	20	340	44.9	574	574	3.48	-11500	16051	525
DP 257	25.5	25.5	5.61	15.35	2.9	20	340	44.9	574	574	3.48	-11500	17407	511
DP 258	40.5	40.5	5.61	15.35	2.9	20	340	44.9	574	574	3.48	-11500	19298	539
DP 259	10.5	10.5	18.61	15.35	2.9	20	340	39	574	574	3.48	-11500	18823	523
DP 260	25.5	25.5	18.61	15.35	2.9	20	340	39	574	574	3.48	-11500	21162	521
DP 261	40.5	40.5	18.61	15.35	2.9	20	340	39	574	574	3.48	-11500	22581	583
DP 262	10.5	10.5	13.61	18.35	2.9	20	340	38.7	574	574	3.48	-11500	18549	536
DP 263	25.5	25.5	13.61	18.35	2.9	20	340	38.7	574	574	3.48	-11500	20319	520
DP 264	40.5	40.5	13.61	18.35	2.9	20	340	38.7	574	574	3.48	-11500	22550	540
DP 265	10.5	10.5	5.61	18.35	2.9	20	340	41.9	574	574	3.48	-11500	17769	520
DP 266	25.5	25.5	5.61	18.35	2.9	20	340	41.9	574	574	3.48	-11500	18842	522
DP 267	40.5	40.5	5.61	18.35	2.9	20	340	41.9	574	574	3.48	-11500	21050	539
DP 268	10.5	10.5	18.61	18.35	2.9	20	340	36	574	574	3.48	-11500	19006	555
DP 269	25.5	25.5	18.61	18.35	2.9	20	340	36	574	574	3.48	-11500	20630	553
DP 270	40.5	40.5	18.61	18.35	2.9	20	340	36	574	574	3.48	-11500	22922	581
DP 271	10.5	10.5	23.61	12.35	2.9	0	0	50.7	574	574	3.48	-11500	16734	495
DP 272	25.5	25.5	23.61	12.35	2.9	0	0	50.7	574	574	3.48	-11500	16022	514
DP 273	40.5	40.5	23.61	12.35	2.9	0	0	50.7	574	574	3.48	-11500	15454	536
DP 274	10.5	10.5	23.61	15.35	2.9	0	0	47.7	574	574	3.48	-11500	19440	486
DP 275	25.5	25.5	23.61	15.35	2.9	0	0	47.7	574	574	3.48	-11500	18604	521
DP 276	40.5	40.5	23.61	15.35	2.9	0	0	47.7	574	574	3.48	-11500	18125	537
DP 277	10.5	10.5	23.61	18.35	2.9	0	0	44.7	574	574	3.48	-11500	21377	479
DP 278	25.5	25.5	23.61	18.35	2.9	0	0	44.7	574	574	3.48	-11500	20383	494
DP 279	40.5	40.5	23.61	18.35	2.9	0	0	44.7	574	574	3.48	-11500	20102	537
DP 280	10.5	10.5	23.61	12.35	2.9	10	350	45.7	574	574	3.48	-11500	17964	489
DP 281	25.5	25.5	23.61	12.35	2.9	10	350	45.7	574	574	3.48	-11500	18659	516
DP 282	40.5	40.5	23.61	12.35	2.9	10	350	45.7	574	574	3.48	-11500	18230	546
DP 283	10.5	10.5	23.61	15.35	2.9	10	350	42.7	574	574	3.48	-11500	20119	498
DP 284	25.5	25.5	23.61	15.35	2.9	10	350	42.7	574	574	3.48	-11500	20933	503
DP 285	40.5	40.5	23.61	15.35	2.9	10	350	42.7	574	574	3.48	-11500	21129	546
DP 286	10.5	10.5	23.61	18.35	2.9	10	350	39.7	574	574	3.48	-11500	20965	512
DP 287	25.5	25.5	23.61	18.35	2.9	10	350	39.7	574	574	3.48	-11500	21579	524
DP 288	40.5	40.5	23.61	18.35	2.9	10	350	39.7	574	574	3.48	-11500	22524	547
DP 289	10.5	10.5	23.61	12.35	2.9	20	340	39.7	574	574	3.48	-11500	19450	520
DP 290	25.5	25.5	23.61	12.35	2.9	20	340	39.7	574	574	3.48	-11500	21650	524
DP 291	40.5	40.5	23.61	12.35	2.9	20	340	39.7	574	574	3.48	-11500	21074	586
DP 292	10.5	10.5	23.61	15.35	2.9	20	340	36.7	574	574	3.48	-11500	19981	536

DP 293	25.5	25.5	23.61	15.35	2.9	20	340	36.7	574	574	3.48	-11500	21711	545
DP 294	40.5	40.5	23.61	15.35	2.9	20	340	36.7	574	574	3.48	-11500	23472	586
DP 295	10.5	10.5	23.61	18.35	2.9	20	340	33.7	574	574	3.48	-11500	19071	575
DP 296	25.5	25.5	23.61	18.35	2.9	20	340	33.7	574	574	3.48	-11500	20301	578
DP 297	40.5	40.5	23.61	18.35	2.9	20	340	33.7	574	574	3.48	-11500	22736	585
DP 298	1	1	18.61	15.5	2.9	20	340	44	574	574	3.48	-11500	22393	463
DP 299	10.5	10.5	18.61	15.5	2.9	20	340	44	574	574	3.48	-11500	21279	474
DP 300	25.5	25.5	18.61	15.5	2.9	20	340	44	574	574	3.48	-11500	20499	521
DP 301	40.5	40.5	18.61	15.5	2.9	20	340	44	574	574	3.48	-11500	19673	540
DP 302	25.5	1	18.61	15.5	2.9	20	340	44	574	574	3.48	-11500	20668	484
DP 303	1	25.5	18.61	15.5	2.9	20	340	44	574	574	3.48	-11500	22623	508
DP 304	25.5	10.5	18.61	15.5	2.9	20	340	44	574	574	3.48	-11500	20616	491
DP 305	10.5	25.5	18.61	15.5	2.9	20	340	44	574	574	3.48	-11500	21308	504
DP 306	25.5	10.5	13.61	12.35	2.9	0	0	55.7	574	574	3.48	-11500	13151	551
DP 307	10.5	25.5	13.61	12.35	2.9	0	0	55.7	574	574	3.48	-11500	13444	549
DP 308	40.5	10.5	13.61	12.35	2.9	0	0	55.7	574	574	3.48	-11500	13063	554
DP 309	10.5	40.5	13.61	12.35	2.9	0	0	55.7	574	574	3.48	-11500	13464	551
DP 310	5	5	13.61	12.35	2.9	0	0	55.7	574	574	3.48	-11500	13593	548
DP 311	1	1	22	18	2.9	20	340	40	574	574	3.48	-11500	24047	500
DP 312	1	1	22	18	2.9	20	340	45	574	574	3.48	-11500	24656	477

## Appendix B

Experimental Design points for longitudinally web and flange stiffened channel sections

Name	P1	P2	P3	P4	P5	P6	P7	P8	P9	P10	P12	P15	P16	P17	P13	P14
DP 0	41	41	14	12	2.9	0	0	35	574	574	-11500	5	5	5	14904	550
DP 1	11	11	14	12	2.9	0	0	35	574	574	-11500	5	5	5	15298	514
DP 2	26	26	14	12	2.9	0	0	35	574	574	-11500	5	5	5	14969	534
DP 3	41	41	14	12	2.9	0	0	35	574	574	-11500	5	5	5	14904	550
DP 4	11	11	5.6	12	2.9	0	0	39	574	574	-11500	5	5	5	13868	528
DP 5	26	26	5.6	12	2.9	0	0	39	574	574	-11500	5	5	5	13764	530
DP 6	41	41	5.6	12	2.9	0	0	39	574	574	-11500	5	5	5	13745	531
DP 7	11	11	19	12	2.9	0	0	32	574	574	-11500	5	5	5	17010	475
DP 8	26	26	19	12	2.9	0	0	32	574	574	-11500	5	5	5	16464	481
DP 9	41	41	19	12	2.9	0	0	32	574	574	-11500	5	5	5	16238	520
DP 10	11	11	14	15	2.9	0	0	32	574	574	-11500	5	5	5	17984	476
DP 11	26	26	14	15	2.9	0	0	32	574	574	-11500	5	5	5	17575	482
DP 12	41	41	14	15	2.9	0	0	32	574	574	-11500	5	5	5	17532	511
DP 13	11	11	5.6	15	2.9	0	0	36	574	574	-11500	5	5	5	16668	475
DP 14	26	26	5.6	15	2.9	0	0	36	574	574	-11500	5	5	5	16524	478
DP 15	41	41	5.6	15	2.9	0	0	36	574	574	-11500	5	5	5	16521	481
DP 16	11	11	19	15	2.9	0	0	29	574	574	-11500	5	5	5	19572	470
DP 17	26	26	19	15	2.9	0	0	29	574	574	-11500	5	5	5	18872	475
DP 18	41	41	19	15	2.9	0	0	29	574	574	-11500	5	5	5	18737	520
DP 19	11	11	14	18	2.9	0	0	29	574	574	-11500	5	5	5	20048	475
DP 20	26	26	14	18	2.9	0	0	29	574	574	-11500	5	5	5	19545	519
DP 21	41	41	14	18	2.9	0	0	29	574	574	-11500	5	5	5	19552	532
DP 22	11	11	5.6	18	2.9	0	0	33	574	574	-11500	5	5	5	19108	478
DP 23	26	26	5.6	18	2.9	0	0	33	574	574	-11500	5	5	5	18943	480
DP 24	41	41	5.6	18	2.9	0	0	33	574	574	-11500	5	5	5	18951	482
DP 25	11	11	19	18	2.9	0	0	26	574	574	-11500	5	5	5	21215	495
DP 26	26	26	19	18	2.9	0	0	26	574	574	-11500	5	5	5	20387	501
DP 27	41	41	19	18	2.9	0	0	26	574	574	-11500	5	5	5	20388	521
DP 28	11	11	14	12	5	0	0	37	534	534	-11500	5	5	5	14664	535
DP 29	26	26	14	12	5	0	0	37	534	534	-11500	5	5	5	14347	528
DP 30	41	41	14	12	5	0	0	37	534	534	-11500	5	5	5	14267	521
DP 31	11	11	5.6	12	5	0	0	40	534	534	-11500	5	5	5	13358	531

DP 32	26	26	5.6	12	5	0	0	40	534	534	-11500	5	5	5	13249	534
DP 33	41	41	5.6	12	5	0	0	40	534	534	-11500	5	5	5	13238	533
DP 34	11	11	19	12	5	0	0	34	534	534	-11500	5	5	5	16233	549
DP 35	26	26	19	12	5	0	0	34	534	534	-11500	5	5	5	15708	519
DP 36	41	41	19	12	5	0	0	34	534	534	-11500	5	5	5	15470	520
DP 37	11	11	14	15	5	0	0	34	534	534	-11500	5	5	5	17440	516
DP 38	26	26	14	15	5	0	0	34	534	534	-11500	5	5	5	17001	518
DP 39	41	41	14	15	5	0	0	34	534	534	-11500	5	5	5	16935	519
DP 40	11	11	5.6	15	5	0	0	37	534	534	-11500	5	5	5	16146	513
DP 41	26	26	5.6	15	5	0	0	37	534	534	-11500	5	5	5	16020	519
DP 42	41	41	5.6	15	5	0	0	37	534	534	-11500	5	5	5	16001	520
DP 43	11	11	19	15	5	0	0	31	534	534	-11500	5	5	5	18960	527
DP 44	26	26	19	15	5	0	0	31	534	534	-11500	5	5	5	18249	521
DP 45	41	41	19	15	5	0	0	31	534	534	-11500	5	5	5	18079	528
DP 46	11	11	14	18	5	0	0	31	534	534	-11500	5	5	5	19726	521
DP 47	26	26	14	18	5	0	0	31	534	534	-11500	5	5	5	19212	519
DP 48	41	41	14	18	5	0	0	31	534	534	-11500	5	5	5	19171	526
DP 49	11	11	5.6	18	5	0	0	34	534	534	-11500	5	5	5	18707	524
DP 50	26	26	5.6	18	5	0	0	34	534	534	-11500	5	5	5	18559	524
DP 51	41	41	5.6	18	5	0	0	34	534	534	-11500	5	5	5	18550	527
DP 52	11	11	19	18	5	0	0	28	534	534	-11500	5	5	5	20982	528
DP 53	26	26	19	18	5	0	0	28	534	534	-11500	5	5	5	20163	528
DP 54	41	41	19	18	5	0	0	28	534	534	-11500	5	5	5	20068	521
DP 55	11	11	14	12	7.5	0	0	38	519	519	-11500	5	5	5	13952	547
DP 56	26	26	14	12	7.5	0	0	38	519	519	-11500	5	5	5	13638	534
DP 57	41	41	14	12	7.5	0	0	38	519	519	-11500	5	5	5	13552	534
DP 58	11	11	5.6	12	7.5	0	0	42	519	519	-11500	5	5	5	12765	556
DP 59	26	26	5.6	12	7.5	0	0	42	519	519	-11500	5	5	5	12667	533
DP 60	41	41	5.6	12	7.5	0	0	42	519	519	-11500	5	5	5	12639	533
DP 61	11	11	19	12	7.5	0	0	35	519	519	-11500	5	5	5	15349	584
DP 62	26	26	19	12	7.5	0	0	35	519	519	-11500	5	5	5	14839	524
DP 63	41	41	19	12	7.5	0	0	35	519	519	-11500	5	5	5	14618	523
DP 64	11	11	14	15	7.5	0	0	35	519	519	-11500	5	5	5	16681	548
DP 65	26	26	14	15	7.5	0	0	35	519	519	-11500	5	5	5	16286	523
DP 66	41	41	14	15	7.5	0	0	35	519	519	-11500	5	5	5	16196	526
DP 67	11	11	5.6	15	7.5	0	0	39	519	519	-11500	5	5	5	15511	522
DP 68	26	26	5.6	15	7.5	0	0	39	519	519	-11500	5	5	5	15387	524
DP 69	41	41	5.6	15	7.5	0	0	39	519	519	-11500	5	5	5	15358	525

DP 70	11	11	19	15	7.5	0	0	32	519	519	-11500	5	5	5	18038	582
DP 71	26	26	19	15	7.5	0	0	32	519	519	-11500	5	5	5	17385	528
DP 72	41	41	19	15	7.5	0	0	32	519	519	-11500	5	5	5	17192	523
DP 73	11	11	14	18	7.5	0	0	32	519	519	-11500	5	5	5	19104	547
DP 74	26	26	14	18	7.5	0	0	32	519	519	-11500	5	5	5	18600	525
DP 75	41	41	14	18	7.5	0	0	32	519	519	-11500	5	5	5	18528	524
DP 76	11	11	5.6	18	7.5	0	0	36	519	519	-11500	5	5	5	18069	523
DP 77	26	26	5.6	18	7.5	0	0	36	519	519	-11500	5	5	5	17924	522
DP 78	41	41	5.6	18	7.5	0	0	36	519	519	-11500	5	5	5	17896	522
DP 79	11	11	19	18	7.5	0	0	29	519	519	-11500	5	5	5	20383	566
DP 80	26	26	19	18	7.5	0	0	29	519	519	-11500	5	5	5	19574	526
DP 81	41	41	19	18	7.5	0	0	29	519	519	-11500	5	5	5	19429	529
DP 82	11	11	14	12	2.9	10	350	33	574	574	-11500	5	5	5	16587	477
DP 83	26	26	14	12	2.9	10	350	33	574	574	-11500	5	5	5	16185	491
DP 84	41	41	14	12	2.9	10	350	33	574	574	-11500	5	5	5	16062	526
DP 85	11	11	5.6	12	2.9	10	350	37	574	574	-11500	5	5	5	14318	532
DP 86	26	26	5.6	12	2.9	10	350	37	574	574	-11500	5	5	5	14090	532
DP 87	41	41	5.6	12	2.9	10	350	37	574	574	-11500	5	5	5	14016	531
DP 88	11	11	19	12	2.9	10	350	30	574	574	-11500	5	5	5	18901	466
DP 89	26	26	19	12	2.9	10	350	30	574	574	-11500	5	5	5	18295	478
DP 90	41	41	19	12	2.9	10	350	30	574	574	-11500	5	5	5	17775	537
DP 91	11	11	14	15	2.9	10	350	30	574	574	-11500	5	5	5	19100	472
DP 92	26	26	14	15	2.9	10	350	30	574	574	-11500	5	5	5	18607	517
DP 93	41	41	14	15	2.9	10	350	30	574	574	-11500	5	5	5	18560	531
DP 94	11	11	5.6	15	2.9	10	350	34	574	574	-11500	5	5	5	17107	472
DP 95	26	26	5.6	15	2.9	10	350	34	574	574	-11500	5	5	5	16830	482
DP 96	41	41	5.6	15	2.9	10	350	34	574	574	-11500	5	5	5	16735	492
DP 97	11	11	19	15	2.9	10	350	27	574	574	-11500	5	5	5	21074	487
DP 98	26	26	19	15	2.9	10	350	27	574	574	-11500	5	5	5	20518	492
DP 99	41	41	19	15	2.9	10	350	27	574	574	-11500	5	5	5	20334	537
DP 100	11	11	14	18	2.9	10	350	27	574	574	-11500	5	5	5	20774	494
DP 101	26	26	14	18	2.9	10	350	27	574	574	-11500	5	5	5	20159	501
DP 102	41	41	14	18	2.9	10	350	27	574	574	-11500	5	5	5	20259	518
DP 103	11	11	5.6	18	2.9	10	350	31	574	574	-11500	5	5	5	19456	479
DP 104	26	26	5.6	18	2.9	10	350	31	574	574	-11500	5	5	5	19104	486
DP 105	41	41	5.6	18	2.9	10	350	31	574	574	-11500	5	5	5	19016	487
DP 106	11	11	19	18	2.9	10	350	24	574	574	-11500	5	5	5	21623	500
DP 107	26	26	19	18	2.9	10	350	24	574	574	-11500	5	5	5	21190	506

DP 108	41	41	19	18	2.9	10	350	24	574	574	-11500	5	5	5	21467	538
DP 109	11	11	14	12	2.9	20	340	30	574	574	-11500	5	5	5	18183	473
DP 110	26	26	14	12	2.9	20	340	30	574	574	-11500	5	5	5	17644	477
DP 111	41	41	14	12	2.9	20	340	30	574	574	-11500	5	5	5	17284	554
DP 112	11	11	5.6	12	2.9	20	340	36	574	574	-11500	5	5	5	14753	532
DP 113	26	26	5.6	12	2.9	20	340	36	574	574	-11500	5	5	5	14446	527
DP 114	41	41	5.6	12	2.9	20	340	36	574	574	-11500	5	5	5	14394	518
DP 115	11	11	19	12	2.9	20	340	27	574	574	-11500	5	5	5	21440	477
DP 116	26	26	19	12	2.9	20	340	27	574	574	-11500	5	5	5	20429	506
DP 117	41	41	19	12	2.9	20	340	27	574	574	-11500	5	5	5	19343	540
DP 118	11	11	14	15	2.9	20	340	27	574	574	-11500	5	5	5	20515	474
DP 119	26	26	14	15	2.9	20	340	27	574	574	-11500	5	5	5	19870	479
DP 120	41	41	14	15	2.9	20	340	27	574	574	-11500	5	5	5	19750	552
DP 121	11	11	5.6	15	2.9	20	340	33	574	574	-11500	5	5	5	17515	469
DP 122	26	26	5.6	15	2.9	20	340	33	574	574	-11500	5	5	5	17110	486
DP 123	41	41	5.6	15	2.9	20	340	33	574	574	-11500	5	5	5	17063	488
DP 124	11	11	19	15	2.9	20	340	24	574	574	-11500	5	5	5	22431	495
DP 125	26	26	19	15	2.9	20	340	24	574	574	-11500	5	5	5	21972	500
DP 126	41	41	19	15	2.9	20	340	24	574	574	-11500	5	5	5	21677	540
DP 127	11	11	14	18	2.9	20	340	24	574	574	-11500	5	5	5	21533	504
DP 128	26	26	14	18	2.9	20	340	24	574	574	-11500	5	5	5	20838	512
DP 129	41	41	14	18	2.9	20	340	24	574	574	-11500	5	5	5	21014	554
DP 130	11	11	5.6	18	2.9	20	340	30	574	574	-11500	5	5	5	19723	483
DP 131	26	26	5.6	18	2.9	20	340	30	574	574	-11500	5	5	5	19216	490
DP 132	41	41	5.6	18	2.9	20	340	30	574	574	-11500	5	5	5	19164	493
DP 135	41	41	19	18	2.9	20	340	21	574	574	-11500	5	5	5	21984	540
DP 136	11	11	14	12	2.9	0	0	20	574	574	-11500	20	5	5	14640	509
DP 137	26	26	14	12	2.9	0	0	20	574	574	-11500	20	5	5	14394	523
DP 138	41	41	14	12	2.9	0	0	20	574	574	-11500	20	5	5	14317	525
DP 139	11	11	5.6	12	2.9	0	0	24	574	574	-11500	20	5	5	13340	538
DP 140	26	26	5.6	12	2.9	0	0	24	574	574	-11500	20	5	5	13257	542
DP 141	41	41	5.6	12	2.9	0	0	24	574	574	-11500	20	5	5	13243	546
DP 142	11	11	19	12	2.9	0	0	17	574	574	-11500	20	5	5	16222	485
DP 143	26	26	19	12	2.9	0	0	17	574	574	-11500	20	5	5	15786	521
DP 144	41	41	19	12	2.9	0	0	17	574	574	-11500	20	5	5	15515	520
DP 145	11	11	14	15	2.9	0	0	17	574	574	-11500	20	5	5	17162	494
DP 146	26	26	14	15	2.9	0	0	17	574	574	-11500	20	5	5	16832	512
DP 147	41	41	14	15	2.9	0	0	17	574	574	-11500	20	5	5	16782	523

DP 148	11	11	5.6	15	2.9	0	0	21	574	574	-11500	20	5	5	15995	513
DP 149	26	26	5.6	15	2.9	0	0	21	574	574	-11500	20	5	5	15870	520
DP 150	41	41	5.6	15	2.9	0	0	21	574	574	-11500	20	5	5	15873	519
DP 151	11	11	19	15	2.9	0	0	14	574	574	-11500	20	5	5	18662	477
DP 152	26	26	19	15	2.9	0	0	14	574	574	-11500	20	5	5	18076	485
DP 153	41	41	19	15	2.9	0	0	14	574	574	-11500	20	5	5	17892	520
DP 154	11	11	14	18	2.9	0	0	14	574	574	-11500	20	5	5	19209	487
DP 155	26	26	14	18	2.9	0	0	14	574	574	-11500	20	5	5	18782	497
DP 156	41	41	14	18	2.9	0	0	14	574	574	-11500	20	5	5	18774	513
DP 157	11	11	5.6	18	2.9	0	0	18	574	574	-11500	20	5	5	18360	514
DP 158	26	26	5.6	18	2.9	0	0	18	574	574	-11500	20	5	5	18209	521
DP 159	41	41	5.6	18	2.9	0	0	18	574	574	-11500	20	5	5	18224	522
DP 160	11	11	19	18	2.9	0	0	11	574	574	-11500	20	5	5	20337	497
DP 161	26	26	19	18	2.9	0	0	11	574	574	-11500	20	5	5	19609	510
DP 162	41	41	19	18	2.9	0	0	11	574	574	-11500	20	5	5	19558	522
DP 163	11	11	14	12	2.9	0	0	40	574	574	-11500	5	2.5	2.5	13988	531
DP 164	26	26	14	12	2.9	0	0	40	574	574	-11500	5	2.5	2.5	13718	551
DP 165	41	41	14	12	2.9	0	0	40	574	574	-11500	5	2.5	2.5	13649	568
DP 166	11	11	5.6	12	2.9	0	0	44	574	574	-11500	5	2.5	2.5	12700	572
DP 167	26	26	5.6	12	2.9	0	0	44	574	574	-11500	5	2.5	2.5	12599	574
DP 168	41	41	5.6	12	2.9	0	0	44	574	574	-11500	5	2.5	2.5	12592	574
DP 169	11	11	19	12	2.9	0	0	37	574	574	-11500	5	2.5	2.5	15523	513
DP 170	26	26	19	12	2.9	0	0	37	574	574	-11500	5	2.5	2.5	15080	513
DP 171	41	41	19	12	2.9	0	0	37	574	574	-11500	5	2.5	2.5	14859	527
DP 172	11	11	14	15	2.9	0	0	37	574	574	-11500	5	2.5	2.5	16709	485
DP 173	26	26	14	15	2.9	0	0	37	574	574	-11500	5	2.5	2.5	16341	497
DP 174	41	41	14	15	2.9	0	0	37	574	574	-11500	5	2.5	2.5	16287	511
DP 175	11	11	5.6	15	2.9	0	0	41	574	574	-11500	5	2.5	2.5	15442	499
DP 176	26	26	5.6	15	2.9	0	0	41	574	574	-11500	5	2.5	2.5	15328	503
DP 177	41	41	5.6	15	2.9	0	0	41	574	574	-11500	5	2.5	2.5	15314	508
DP 178	11	11	14	12	2.9	0	0	44	574	574	-11500	5	1	1	13490	544
DP 179	26	11	14	12	2.9	0	0	44	574	574	-11500	5	1	1	13220	548
DP 180	41	41	14	12	2.9	0	0	44	574	574	-11500	5	1	1	13172	559
DP 181	18	18	14	12	2.9	0	0	35	574	574	-11500	5	5	5	15075	513
DP 182	33	33	14	12	2.9	0	0	35	574	574	-11500	5	5	5	14909	501
DP 183	18	18	5.6	12	2.9	0	0	39	574	574	-11500	5	5	5	13803	530
DP 184	33	33	5.6	12	2.9	0	0	39	574	574	-11500	5	5	5	13748	531
DP 185	18	18	19	12	2.9	0	0	32	574	574	-11500	5	5	5	16660	480

DP 186	33	33	19	12	2.9	0	0	32	574	574	-11500	5	5	5	16337	485
DP 187	18	18	14	15	2.9	0	0	32	574	574	-11500	5	5	5	17706	480
DP 188	33	33	14	15	2.9	0	0	32	574	574	-11500	5	5	5	17507	482
DP 189	18	18	5.6	15	2.9	0	0	36	574	574	-11500	5	5	5	16571	476
DP 190	33	33	5.6	15	2.9	0	0	36	574	574	-11500	5	5	5	16506	479
DP 191	18	18	19	15	2.9	0	0	29	574	574	-11500	5	5	5	19107	474
DP 192	33	33	19	15	2.9	0	0	29	574	574	-11500	5	5	5	18769	475
DP 193	18	18	14	18	2.9	0	0	29	574	574	-11500	5	5	5	19706	478
DP 194	33	33	14	18	2.9	0	0	29	574	574	-11500	5	5	5	19490	487
DP 195	18	18	5.6	18	2.9	0	0	33	574	574	-11500	5	5	5	18999	479
DP 196	33	33	5.6	18	2.9	0	0	33	574	574	-11500	5	5	5	18928	481
DP 197	18	18	19	18	2.9	0	0	26	574	574	-11500	5	5	5	20648	500
DP 198	33	33	19	18	2.9	0	0	26	574	574	-11500	5	5	5	20312	501
DP 202	11	11	9	17	2.9	0	0	33	574	574	-11500	5	5	5	18333	476
DP 203	4	4	19	14	2.9	0	0	31	574	574	-11500	5	5	5	18620	473
DP 204	4	4	19	13	2.9	0	0	32	574	574	-11500	5	5	5	17713	472
DP 205	11	11	9	17	2.9	0	0	33	574	574	-13500	5	5	5	18259	576
DP 206	4	4	19	14	2.9	0	0	31	574	574	-13500	5	5	5	18621	584
DP 207	4	4	19	13	2.9	0	0	32	574	574	-13500	5	5	5	17713	584
DP 208	11	11	24	12	2.9	0	0	30	574	574	-11500	5	5	5	18572	476
DP 209	26	26	24	12	2.9	0	0	30	574	574	-11500	5	5	5	17956	488
DP 210	41	41	24	12	2.9	0	0	30	574	574	-11500	5	5	5	17418	585
DP 211	11	11	24	15	2.9	0	0	27	574	574	-11500	5	5	5	20836	482
DP 212	26	26	24	15	2.9	0	0	27	574	574	-11500	5	5	5	20345	532
DP 213	41	41	24	15	2.9	0	0	27	574	574	-11500	5	5	5	20089	538
DP 214	11	11	24	18	2.9	0	0	24	574	574	-11500	5	5	5	21516	516
DP 215	26	26	24	18	2.9	0	0	24	574	574	-11500	5	5	5	21181	516
DP 216	41	41	24	18	2.9	0	0	24	574	574	-11500	5	5	5	21406	540
DP 217	1	1	24	12	2.9	0	0	30	574	574	-11500	5	5	5	19336	463
DP 218	1	1	24	15	2.9	0	0	27	574	574	-11500	5	5	5	21750	475
DP 219	1	1	24	18	2.9	0	0	24	574	574	-11500	5	5	5	22527	506
DP 220	26	26	19	18	2.9	20	340	21	574	574	-11500	5	5	5	21450	521
DP 221	11	11	19	18	2.9	20	340	21	574	574	-11500	5	5	5	21561	521
DP 222	1	1	14	12	2.9	0	0	35	574	574	-11500	5	5	5	15752	508
DP 223	17	17	14	14	2.9	20	340	29	574	574	-11500	5	5	5	19310	478
DP 224	1	1	14	14	2.9	20	340	29	574	574	-11500	5	5	5	20799	456
DP 225	1	1	23	14	2.9	20	340	23	574	574	-11500	5	5	5	23121	519
DP 226	1	1	16	13	2.9	20	340	28	574	574	-11500	5	5	5	21475	454



# Appendix C

## Experimental Design points for longitudinally web stiffened Zed sections

Name	P1	P2	P3	P4	P5	P6	P7	P8	P9	P10	P11	P12	P13	P14	P15
DP 0	10	10	12.6	11.1	3.3	16.2	18	0	0	20	20	60	55	11207	567
DP 1	10	10	12.6	11.1	3.3	16.2	18	0	0	20	20	60	55	11207	567
DP 2	10	10	15.6	14.1	3.3	16.2	18	0	0	20	20	57	52	13301	556
DP 3	10	10	18.6	17.1	3.3	16.2	18	0	0	20	20	54	49	15195	528
DP 4	10	10	12.6	11.1	3.3	21.2	23	0	0	20	20	58	53	12048	570
DP 5	10	10	15.6	14.1	3.3	21.2	23	0	0	20	20	55	50	14222	547
DP 6	10	10	18.6	17.1	3.3	21.2	23	0	0	20	20	52	47	15938	525
DP 7	10	10	12.6	11.1	3.3	11.2	13	0	0	20	20	63	58	10616	569
DP 8	10	10	15.6	14.1	3.3	11.2	13	0	0	20	20	60	55	12785	565
DP 9	10	10	18.6	17.1	3.3	11.2	13	0	0	20	20	57	52	14815	523
DP 10	10	10	12.6	11.1	3.3	16.2	18	10	10	20	20	57	52	12227	566
DP 11	10	10	15.6	14.1	3.3	16.2	18	10	10	20	20	54	49	14378	541
DP 12	10	10	18.6	17.1	3.3	16.2	18	10	10	20	20	51	46	16076	522
DP 13	10	10	12.6	11.1	3.3	21.2	23	10	10	20	20	53	48	13875	537
DP 14	10	10	15.6	14.1	3.3	21.2	23	10	10	20	20	50	45	15997	523
DP 15	10	10	18.6	17.1	3.3	21.2	23	10	10	20	20	47	42	17400	525
DP 16	10	10	12.6	11.1	3.3	11.2	13	10	10	20	20	60	55	11136	567
DP 17	10	10	15.6	14.1	3.3	11.2	13	10	10	20	20	57	52	13287	557
DP 18	10	10	18.6	17.1	3.3	11.2	13	10	10	20	20	54	49	15291	512
DP 19	10	10	12.6	11.1	3.3	16.2	18	20	20	20	20	54	49	13702	555
DP 20	10	10	15.6	14.1	3.3	16.2	18	20	20	20	20	51	46	15709	522
DP 21	10	10	18.6	17.1	3.3	16.2	18	20	20	20	20	48	43	17131	522
DP 22	10	10	12.6	11.1	3.3	21.2	23	20	20	20	20	50	45	16139	527
DP 23	10	10	15.6	14.1	3.3	21.2	23	20	20	20	20	47	42	18222	508
DP 24	10	10	18.6	17.1	3.3	21.2	23	20	20	20	20	44	39	19324	510
DP 25	10	10	12.6	11.1	3.3	11.2	13	20	20	20	20	57	52	11849	573
DP 26	10	10	15.6	14.1	3.3	11.2	13	20	20	20	20	54	49	13962	528
DP 27	10	10	18.6	17.1	3.3	11.2	13	20	20	20	20	51	46	15808	518
DP 28	10	10	12.6	11.1	3.3	16.2	18	30	30	20	20	51	46	15369	532
DP 29	10	10	15.6	14.1	3.3	16.2	18	30	30	20	20	48	43	17265	510
DP 30	10	10	18.6	17.1	3.3	16.2	18	30	30	20	20	45	40	18479	516
DP 31	10	10	12.6	11.1	3.3	21.2	23	30	30	20	20	46	41	18331	542

DP 32	10	10	15.6	14.1	3.3	21.2	23	30	30	20	20	43	38	20470	541
DP 33	10	10	18.6	17.1	3.3	21.2	23	30	30	20	20	40	35	-20834	523
DP 34	10	10	12.6	11.1	3.3	11.2	13	30	30	20	20	55	50	12826	565
DP 35	10	10	15.6	14.1	3.3	11.2	13	30	30	20	20	52	47	14800	527
DP 36	10	10	18.6	17.1	3.3	11.2	13	30	30	20	20	49	44	16414	523
DP 37	10	10	12.6	11.1	3.3	16.2	18	0	0	0	0	59	54	13246	565
DP 38	10	10	15.6	14.1	3.3	16.2	18	0	0	0	0	56	51	15787	491
DP 39	10	10	18.6	17.1	3.3	16.2	18	0	0	0	0	53	48	18067	490
DP 40	10	10	12.6	11.1	3.3	21.2	23	0	0	0	0	56	51	14169	534
DP 41	10	10	15.6	14.1	3.3	21.2	23	0	0	0	0	53	48	16653	504
DP 42	10	10	18.6	17.1	3.3	21.2	23	0	0	0	0	50	45	18785	501
DP 43	10	10	12.6	11.1	3.3	11.2	13	0	0	0	0	61	56	12538	566
DP 44	10	10	15.6	14.1	3.3	11.2	13	0	0	0	0	58	53	15314	513
DP 45	10	10	18.6	17.1	3.3	11.2	13	0	0	0	0	55	50	17764	474
DP 46	10	10	12.6	11.1	3.3	16.2	18	10	10	0	0	55	50	14339	530
DP 47	10	10	15.6	14.1	3.3	16.2	18	10	10	0	0	52	47	16811	501
DP 48	10	10	18.6	17.1	3.3	16.2	18	10	10	0	0	49	44	18743	501
DP 49	10	10	12.6	11.1	3.3	21.2	23	10	10	0	0	52	47	16077	506
DP 50	10	10	15.6	14.1	3.3	21.2	23	10	10	0	0	49	44	18376	498
DP 51	10	10	18.6	17.1	3.3	21.2	23	10	10	0	0	46	41	19939	503
DP 52	10	10	12.6	11.1	3.3	11.2	13	10	10	0	0	59	54	13227	565
DP 53	10	10	15.6	14.1	3.3	11.2	13	10	10	0	0	56	51	15793	487
DP 54	10	10	18.6	17.1	3.3	11.2	13	10	10	0	0	53	48	18097	486
DP 55	10	10	12.6	11.1	3.3	16.2	18	20	20	0	0	52	47	15822	501
DP 56	10	10	15.6	14.1	3.3	16.2	18	20	20	0	0	49	44	18091	498
DP 57	10	10	18.6	17.1	3.3	16.2	18	20	20	0	0	46	41	19740	500
DP 58	10	10	12.6	11.1	3.3	21.2	23	20	20	0	0	49	44	18451	499
DP 59	10	10	15.6	14.1	3.3	21.2	23	20	20	0	0	46	41	20531	508
DP 60	10	10	18.6	17.1	3.3	21.2	23	20	20	0	0	43	38	21011	521
DP 61	10	10	12.6	11.1	3.3	11.2	13	20	20	0	0	56	51	13930	529
DP 62	10	10	15.6	14.1	3.3	11.2	13	20	20	0	0	53	48	16452	497
DP 63	10	10	18.6	17.1	3.3	11.2	13	20	20	0	0	50	45	18645	494
DP 64	10	10	12.6	11.1	3.3	16.2	18	30	30	0	0	50	45	17721	495
DP 65	10	10	15.6	14.1	3.3	16.2	18	30	30	0	0	47	42	19725	491
DP 66	10	10	18.6	17.1	3.3	16.2	18	30	30	0	0	44	39	20446	518
DP 67	10	10	12.6	11.1	3.3	21.2	23	30	30	0	0	45	40	20833	539
DP 68	10	10	15.6	14.1	3.3	21.2	23	30	30	0	0	42	37	-20545	522
DP 69	10	10	18.6	17.1	3.3	21.2	23	30	30	0	0	39	34	-19293	521

DP 70	10	10	12.6	11.1	3.3	11.2	13	30	30	0	0	54	49	14868	528
DP 71	10	10	15.6	14.1	3.3	11.2	13	30	30	0	0	51	46	17424	498
DP 72	10	10	18.6	17.1	3.3	11.2	13	30	30	0	0	48	43	19208	494
DP 73	1	1	12.6	11.1	3.3	16.2	18	0	0	20	20	60	55	11427	567
DP 74	1	1	15.6	14.1	3.3	16.2	18	0	0	0	0	56	51	16157	481
DP 75	1	1	18.6	17.1	3.3	16.2	18	0	0	0	0	53	48	18556	476
DP 76	1	1	18.6	17.1	3.3	11.2	13	0	0	0	0	55	50	18141	476
DP 77	1	1	15.6	14.1	3.3	11.2	13	10	10	0	0	56	51	16243	481
DP 78	1	1	18.6	17.1	3.3	11.2	13	10	10	0	0	53	48	18680	471
DP 79	1	1	19.6	18.1	3.3	11.2	13	10	10	0	0	52	47	19374	472
DP 80	1	1	20.6	19.1	3.3	11.2	13	10	10	0	0	51	46	20074	466
DP 81	1	1	21.6	20.1	3.3	11.2	13	10	10	0	0	50	45	20599	469
DP 82	1	1	22.6	21.1	3.3	11.2	13	10	10	0	0	49	44	20927	474
DP 83	1	1	23.6	22.1	3.3	11.2	13	10	10	0	0	48	43	20831	566
DP 84	1	1	24.6	23.1	3.3	11.2	13	10	10	0	0	47	42	20596	566
DP 85	1	1	20.6	19.1	3.3	13.2	15	10	10	0	0	49	44	20159	475
DP 86	1	1	19.6	18.1	3.3	13.2	15	10	10	0	0	50	45	19680	497
DP 87	1	1	18.6	17.1	3.3	13.2	15	10	10	0	0	51	46	19037	475
DP 88	1	1	19	17	3.3	11.2	13	15	15	0	0	51	46	19330	465
DP 89	10	10	17.8	16.3	3.3	20.5	22	20	20	0	0	44	39	20723	508

# Appendix D

## Experimental Design points for longitudinally web and flange stiffened Zed sections

Name	P1	P2	P3	P4	P5	P6	P7	P8	P9	P10	P11	P12	P13	P14	P15	P16	P17	P18	P19
DP 0	10	10	13	11	3	16	18	0	0	20	20	5	5	5	5	39	34	12824	537
DP 1	10	10	13	11	3	16	18	0	0	20	20	5	5	5	5	39	34	12824	537
DP 2	25	25	13	11	3	16	18	0	0	20	20	5	5	5	5	39	34	12960	532
DP 3	40	40	13	11	3	16	18	0	0	20	20	5	5	5	5	39	34	13200	543
DP 4	10	10	16	14	3	16	18	0	0	20	20	5	5	5	5	36	31	15026	504
DP 5	10	10	19	17	3	16	18	0	0	20	20	5	5	5	5	33	28	16841	504
DP 6	10	10	13	11	3	21	23	0	0	20	20	5	5	5	5	37	32	13885	537
DP 7	10	10	16	14	3	21	23	0	0	20	20	5	5	5	5	34	29	15967	513
DP 8	10	10	19	17	3	21	23	0	0	20	20	5	5	5	5	31	26	17564	504
DP 9	10	10	13	11	3	11	13	0	0	20	20	5	5	5	5	42	37	12136	565
DP 10	10	10	16	14	3	11	13	0	0	20	20	5	5	5	5	39	34	14429	501
DP 11	10	10	19	17	3	11	13	0	0	20	20	5	5	5	5	36	31	16450	489
DP 12	10	10	13	11	3	16	18	20	20	20	20	5	5	5	5	33	28	15771	530
DP 13	10	10	16	14	3	16	18	20	20	20	20	5	5	5	5	30	25	17678	506
DP 14	10	10	19	17	3	16	18	20	20	20	20	5	5	5	5	27	22	18838	496
DP 15	10	10	13	11	3	21	23	20	20	20	20	5	5	5	5	29	24	18647	508
DP 16	10	10	16	14	3	21	23	20	20	20	20	5	5	5	5	26	21	20266	501
DP 17	10	10	19	17	3	21	23	20	20	20	20	5	5	5	5	23	18	-19472	502
DP 18	10	10	13	11	3	11	13	20	20	20	20	5	5	5	5	37	32	13648	531
DP 19	10	10	16	14	3	11	13	20	20	20	20	5	5	5	5	34	29	15766	507
DP 20	10	10	19	17	3	11	13	20	20	20	20	5	5	5	5	31	26	17412	497
DP 21	10	10	13	11	3	16	18	40	40	20	20	5	5	5	5	28	23	19837	520
DP 22	10	10	16	14	3	16	18	40	40	20	20	5	5	5	5	25	20	-18981	520
DP 23	10	10	19	17	3	16	18	40	40	20	20	5	5	5	5	22	17	-18010	520
DP 24	10	10	13	11	3	21	23	40	40	20	20	5	5	5	5	23	18	-16979	529
DP 25	10	10	16	14	3	21	23	40	40	20	20	5	5	5	5	20	15	-16312	529
DP 26	10	10	19	17	3	21	23	40	40	20	20	5	5	5	5	17	12	-15546	529
DP 27	10	10	13	11	3	11	13	40	40	20	20	5	5	5	5	32	27	16110	530
DP 28	10	10	16	14	3	11	13	40	40	20	20	5	5	5	5	29	24	17953	506
DP 29	10	10	19	17	3	11	13	40	40	20	20	5	5	5	5	26	23	19009	512
DP 30	10	10	13	11	3	16	18	0	0	0	0	5	5	5	5	38	33	14987	492
DP 31	10	10	16	14	3	16	18	0	0	0	0	5	5	5	5	35	30	17632	474

DP 32	10	10	19	17	3	16	18	0	0	0	0	5	5	5	5	32	27	19703	478
DP 33	10	10	13	11	3	21	23	0	0	0	0	5	5	5	5	36	31	16092	484
DP 34	10	10	16	14	3	21	23	0	0	0	0	5	5	5	5	33	28	18537	490
DP 35	10	10	19	17	3	21	23	0	0	0	0	5	5	5	5	30	25	20125	494
DP 36	10	10	13	11	3	11	13	0	0	0	0	5	5	5	5	41	36	14233	530
DP 37	10	10	16	14	3	11	13	0	0	0	0	5	5	5	5	38	33	17011	467
DP 38	10	10	19	17	3	11	13	0	0	0	0	5	5	5	5	35	30	19451	460
DP 39	10	10	13	11	3	16	18	20	20	0	0	5	5	5	5	32	27	18049	486
DP 40	10	10	16	14	3	16	18	20	20	0	0	5	5	5	5	29	24	19953	488
DP 41	10	10	19	17	3	16	18	20	20	0	0	5	5	5	5	26	21	20549	519
DP 42	10	10	13	11	3	21	23	20	20	0	0	5	5	5	5	28	23	-20387	505
DP 43	10	10	16	14	3	21	23	20	20	0	0	5	5	5	5	25	20	-19089	510
DP 44	10	10	19	17	3	21	23	20	20	0	0	5	5	5	5	22	17	-17608	510
DP 45	10	10	13	11	3	11	13	20	20	0	0	5	5	5	5	36	31	15863	476
DP 46	10	10	16	14	3	11	13	20	20	0	0	5	5	5	5	33	28	18356	475
DP 47	10	10	19	17	3	11	13	20	20	0	0	5	5	5	5	30	25	20084	485
DP 48	10	10	19	17	3	14	15	0	0	0	0	5	5	5	5	34	29	19551	470
DP 49	10	10	17	16	3	14	15	0	0	0	0	5	5	5	5	35	30	18445	462
DP 50	10	10	18	16	3	11	13	0	0	0	0	5	5	5	5	36	31	18710	464
DP 51	10	10	15	13	3	21	22	18	18	20	20	5	5	5	5	28	23	19401	494
DP 52	10	10	18	17	3	14	16	18	18	4	4	5	5	5	5	29	24	19759	495
DP 53	10	10	18	16	3	15	17	21	21	2	2	5	5	5	5	27	22	20326	502
DP 54	10	10	19	17	3	11	13	0	0	0	0	5	5	5	5	35	30	19285	510
DP 55	1	1	17	16	3	14	15	0	0	0	0	5	5	5	5	35	30	18978	451
DP 56	1	1	19	17	3	14	15	0	0	0	0	5	5	5	5	34	29	20152	460
DP 57	1	1	18	16	3	11	13	0	0	0	0	5	5	5	5	36	31	19166	449
DP 58	1	1	18	16	3	15	17	21	21	2	2	5	5	5	5	27	22	21343	484
DP 59	10	10	18	17	3	15	16	21	21	3	3	5	5	5	5	27	22	20232	492
DP 60	1	1	13	11	3	16	18	0	0	20	20	5	5	5	5	39	34	13140	541
DP 61	45	45	13	11	3	16	18	0	0	20	20	5	5	5	5	39	34	13251	550
DP 62	50	50	13	11	3	16	18	0	0	20	20	5	5	5	5	39	34	13240	556

## References

- [1] W. Yu, Applications of Cold-Formed Steel in Tall Buildings, Tall Buildings: 2000 and Beyond (1990).
- [2] R. Scharff, Residential steel framing handbook, McGraw-Hill Professional 1996.
- [3] A. Iron, S. Institute, North American specification for the design of cold-formed steel structural members, American Iron & Steel Institute, Committee of Steel Plate Producers ... 2007.
- [4] B.S. BSI, Structural use of steelwork in building, Part 5: Code of practice for design of cold formed thin gauge sections, British Standard Institution (1998).
- [5] E. CEN, 1-3 Eurocode 3: Design of steel structures-Part 1-3: General rules-Supplementary rules for cold-formed members and sheeting, European Committee for Standardization, Brussels (2006).
- [6] V.B. Ginzburg, Flat-rolled steel processes: advanced technologies, CRC Press 2009.
- [7] G.T. Halmos, Roll forming handbook, Crc Press 2005.
- [8] S. Panton, J. Duncan, S. Zhu, Longitudinal and shear strain development in cold roll forming, Journal of materials processing technology 60(1-4) (1996) 219-224.
- [9] S. Panton, S. Zhu, J. Duncan, Geometric constraints on the forming path in roll forming channel sections, Proceedings of the Institution of Mechanical Engineers, Part B: Journal of Engineering Manufacture 206(2) (1992) 113-118.
- [10] Z.-W. Han, C. Liu, W.-P. Lu, L.-Q. Ren, The effects of forming parameters in the roll-forming of a channel section with an outer edge, Journal of Materials Processing Technology 116(2-3) (2001) 205-210.

- [11] Z.-W. Han, C. Liu, W.-P. Lu, L.-Q. Ren, J. Tong, Spline finite strip analysis of forming parameters in roll forming a channel section, *Journal of Materials Processing Technology* 159(3) (2005) 383-388.
- [12] R. Safdarian, H.M. Naeini, The effects of forming parameters on the cold roll forming of channel section, *Thin-Walled Structures* 92 (2015) 130-136.
- [13] B.S. Bidabadi, H.M. Naeini, M.S. Tehrani, H. Barghikar, Experimental and numerical study of bowing defects in cold roll-formed, U-channel sections, *Journal of Constructional Steel Research* 118 (2016) 243-253.
- [14] B.S. Bidabadi, H.M. Naeini, R.A. Tafti, H. Barghikar, Experimental study of bowing defects in pre-notched channel section products in the cold roll forming process, *The International Journal of Advanced Manufacturing Technology* 87(1) (2016) 997-1011.
- [15] Y.Y. Woo, S.W. Han, T.W. Hwang, J.Y. Park, Y.H. Moon, Characterization of the longitudinal bow during flexible roll forming of steel sheets, *Journal of Materials Processing Technology* 252 (2018) 782-794.
- [16] M. Lindgren, Cold roll forming of a U-channel made of high strength steel, *Journal of Materials Processing Technology* 186(1-3) (2007) 77-81.
- [17] J. Wiebenga, M. Weiss, B. Rolfe, A.H. van den Boogaard, Product defect compensation by robust optimisation of a cold roll forming process, *Journal of Materials Processing Technology* 213(6) (2013) 978-986.
- [18] W.-g. Cha, N. Kim, Study on twisting and bowing of roll formed products made of high strength steel, *International Journal of Precision Engineering and Manufacturing* 14(9) (2013) 1527-1533.
- [19] M. Lindgren, Experimental and computational investigation of the roll forming process, Luleå tekniska universitet, 2009.

- [20] M. Weiss, J. Marnette, P. Wolfram, J. Larrañaga, P.D. Hodgson, Comparison of bending of automotive steels in roll forming and in a V-die, *Key Engineering Materials*, Trans Tech Publ, 2012, pp. 797-802.
- [21] P. Groche, M. Henkelmann, Dimensional deviation of roll formed components made of high strength steel, *Key Engineering Materials*, Trans Tech Publ, 2007, pp. 285-292.
- [22] A. Abvabi, B. Rolfe, P. Hodgson, M. Weiss, The influence of residual stress on a roll forming process, *International Journal of Mechanical Sciences* 101 (2015) 124-136.
- [23] O.M. Badr, B. Rolfe, P. Hodgson, M. Weiss, Numerical investigation about the effect of increasing the number of forming passes on the quality of AHSS roll formed products, *AIP Conference Proceedings*, American Institute of Physics, 2013, pp. 872-875.
- [24] O.M. Badr, B. Rolfe, M. Weiss, Effect of the forming method on part shape quality in cold roll forming high strength Ti-6Al-4V sheet, *Journal of Manufacturing Processes* 32 (2018) 513-521.
- [25] S.N.b.M. Saffe, T. Nagamchi, H. Ona, Mechanism of cut end deformation of hat shape channel steel by roll forming, *AIP Conference Proceedings*, American Institute of Physics, 2013, pp. 908-911.
- [26] G. Winter, Strength of thin steel compression flanges, *Trans. ASCE* 112 (1947) 527.
- [27] K.W. Karren, G. Winter, Effects of cold-forming on light-gage steel members, *Journal of the Structural Division* 93(1) (1967) 433-469.
- [28] K.W. Karren, Corner properties of cold-formed shapes, *Journal of the Structural Division* 93(1) (1967) 401-433.
- [29] L.A. Godoy, *Thin-walled structures with structural imperfections*, Elsevier 1996.



- [30] B.W. Schafer, Z. Li, C.D. Moen, Computational modeling of cold-formed steel, *Thin-Walled Structures* 48(10-11) (2010) 752-762.
- [31] B.W. Schafer, M. Grigoriu, T. Peköz, A probabilistic examination of the ultimate strength of cold-formed steel elements, *Thin-walled structures* 31(4) (1998) 271-288.
- [32] F. Bleich, *Buckling strength of metal structures*, Mc Graw-Hill Book Company, Inc., Cardnr. 51-12588 (1952).
- [33] P. Stephen, M.G. James, *Theory of elastic stability*, McGraw-Hill, Inc, 1961.
- [34] W.-F. Chen, T. Atsuta, *Theory of beam-columns, volume 2: space behavior and design*, J. Ross Publishing 2007.
- [35] E. Ellobody, B. Young, Behavior of cold-formed steel plain angle columns, *Journal of Structural Engineering* 131(3) (2005) 457-466.
- [36] B. Young, E. Ellobody, Buckling analysis of cold-formed steel lipped angle columns, *journal of structural engineering* 131(10) (2005) 1570-1579.
- [37] Y. Zhang, C. Wang, Z. Zhang, Tests and finite element analysis of pin-ended channel columns with inclined simple edge stiffeners, *Journal of Constructional Steel Research* 63(3) (2007) 383-395.
- [38] M. Jandera, L. Gardner, J. Machacek, Residual stresses in cold-rolled stainless steel hollow sections, *Journal of Constructional Steel Research* 64(11) (2008) 1255-1263.
- [39] C.D. Moen, T. Igusa, B.W. Schafer, Prediction of residual stresses and strains in cold-formed steel members, *Thin-walled structures* 46(11) (2008) 1274-1289.
- [40] M. Theofanous, L. Gardner, Testing and numerical modelling of lean duplex stainless steel hollow section columns, *Engineering Structures* 31(12) (2009) 3047-3058.

- [41] Y. Huang, B. Young, Material properties of cold-formed lean duplex stainless steel sections, *Thin-walled structures* 54 (2012) 72-81.
- [42] F. Zhou, Y. Chen, B. Young, Cold-formed high strength stainless steel cross-sections in compression considering interaction effects of constituent plate elements, *Journal of Constructional Steel Research* 80 (2013) 32-41.
- [43] M. Bock, I. Arrayago, E. Real, Experiments on cold-formed ferritic stainless steel slender sections, *Journal of constructional steel research* 109 (2015) 13-23.
- [44] M. El Aghoury, M. Hanna, E. Amoush, Experimental and theoretical investigation of cold-formed single lipped sigma columns, *Thin-Walled Structures* 111 (2017) 80-92.
- [45] J. Ye, I. Hajirasouliha, J. Becque, Experimental investigation of local-flexural interactive buckling of cold-formed steel channel columns, *Thin-walled structures* 125 (2018) 245-258.
- [46] B. Schafer, T. Peköz, Computational modeling of cold-formed steel: characterizing geometric imperfections and residual stresses, *Journal of constructional steel research* 47(3) (1998) 193-210.
- [47] S. Chou, G. Chai, L. Ling, Finite element technique for design of stub columns, *Thin-Walled Structures* 37(2) (2000) 97-112.
- [48] D. Dubina, V. Ungureanu, Effect of imperfections on numerical simulation of instability behaviour of cold-formed steel members, *Thin-walled structures* 40(3) (2002) 239-262.
- [49] L. Gardner, D. Nethercot, Numerical modeling of stainless steel structural components—a consistent approach, *Journal of Structural Engineering* 130(10) (2004) 1586-1601.
- [50] M. Ashraf, L. Gardner, D.A. Nethercot, Finite element modelling of structural stainless steel cross-sections, *Thin-walled structures* 44(10) (2006) 1048-1062.

- [51] A. Crisan, V. Ungureanu, D. Dubina, Behaviour of cold-formed steel perforated sections in compression: Part 2—numerical investigations and design considerations, *Thin-Walled Structures* 61 (2012) 97-105.
- [52] J. Bonada, M. Casafont, F. Roure, M. Pastor, Selection of the initial geometrical imperfection in nonlinear FE analysis of cold-formed steel rack columns, *Thin-walled structures* 51 (2012) 99-111.
- [53] M. Pastor, J. Bonada, F. Roure, M. Casafont, Residual stresses and initial imperfections in non-linear analysis, *Engineering structures* 46 (2013) 493-507.
- [54] J. Bonada, M. Pastor, F. Roure, M. Casafont, Influence of the cold work effects in perforated rack columns under pure compression load, *Engineering Structures* 97 (2015) 130-139.
- [55] J. Bonada, M. Pastor, F. Roure, M. Casafont, Distortional influence of pallet rack uprights subject to combined compression and bending, *Structures*, Elsevier, 2016, pp. 275-285.
- [56] J. Ye, S.M. Mojtabaei, I. Hajirasouliha, Local-flexural interactive buckling of standard and optimised cold-formed steel columns, *Journal of constructional steel research* 144 (2018) 106-118.
- [57] A. Huber, L. Beedle, Residual stress and the compressive strength of steel. *Welding Journal*, 33 (12), p. 589-s,(December 1954), Reprint No. 96 (54-3), (1954).
- [58] N. Abdel-Rahman, K. Sivakumaran, Material properties models for analysis of cold-formed steel members, *Journal of Structural Engineering* 123(9) (1997) 1135-1143.
- [59] D.T. Dat, T. Peköz, *The strength of cold-formed steel columns*, (1980).
- [60] T. Davison, P. Birkemoe, Column behaviour of cold-formed hollow structural steel shapes, *Canadian Journal of Civil Engineering* 10(1) (1983) 125-141.

- [61] M. Jandera, J. Machacek, Residual stress influence on material properties and column behaviour of stainless steel SHS, *Thin-Walled Structures* 83 (2014) 12-18.
- [62] P.W. Key, G.J. Hancock, A theoretical investigation of the column behaviour of cold-formed square hollow sections, *Thin-Walled Structures* 16(1-4) (1993) 31-64.
- [63] L. Ingvarsson, Cold-forming residual stresses effect on buckling, (1975).
- [64] W. Quach, J. Teng, K.F. Chung, Effect of the manufacturing process on the behaviour of press-braked thin-walled steel columns, *Engineering Structures* 32(11) (2010) 3501-3515.
- [65] Y.B. Kwon, G.J. Hancock, Tests of cold-formed channels with local and distortional buckling, *Journal of Structural Engineering* 118(7) (1992) 1786-1803.
- [66] V. Nguyen, C. Wang, D. Mynors, M. Castellucci, M. English, Finite element simulation on mechanical and structural properties of cold-formed dimpled steel, *Thin-Walled Structures* 64 (2013) 13-22.
- [67] V. Nguyen, C. Wang, D. Mynors, M. English, M. Castellucci, Compression tests of cold-formed plain and dimpled steel columns, *Journal of Constructional Steel Research* 69(1) (2012) 20-29.
- [68] W. Quach, J. Teng, K. Chung, Effect of the manufacturing process on the behaviour of press-braked thin-walled steel columns, *Engineering structures* 32(11) (2010) 3501-3515.
- [69] F. Wang, Numerical studies of residual stress in cold formed steel sigma sections, University of Birmingham, 2015.
- [70] V.B. Nguyen, D. Mynors, C. Wang, M. Castellucci, M. English, Analysis and design of cold-formed dimpled steel columns using Finite Element techniques, *Finite Elements in Analysis and Design* 108 (2016) 22-31.

- [71] J. Becque, The interaction of local and overall buckling of cold-formed stainless steel columns, (2008).
- [72] M. Pastor, M. Casafont, J. Bonada, F. Roure, Imperfection amplitudes for nonlinear analysis of open thin-walled steel cross-sections used in rack column uprights, *Thin-Walled Structures* 76 (2014) 28-41.
- [73] J.K. Seo, T. Anapayan, M. Mahendran, Initial imperfection characteristics of mono-symmetric LiteSteel beams for numerical studies, *Proceedings of the Fifth International Conference on Thin-Walled Structures: Recent Innovations and Developments*, Queensland University of Technology, 2008, pp. 451-460.
- [74] M. Theofanous, L. Gardner, Experimental and numerical studies of lean duplex stainless steel beams, *Journal of Constructional Steel Research* 66(6) (2010) 816-825.
- [75] N.D. Kankanamge, M. Mahendran, Behaviour and design of cold-formed steel beams subject to lateral-torsional buckling, *Thin-walled structures* 51 (2012) 25-38.
- [76] Y.-L. Pi, B. Put, N.S. Trahair, Lateral buckling strengths of cold-formed channel section beams, *Journal of Structural Engineering* 124(10) (1998) 1182-1191.
- [77] Y.-L. Pi, B. Put, N.S. Trahair, Lateral buckling strengths of cold-formed Z-section beams, *Thin-walled structures* 34(1) (1999) 65-93.
- [78] Y.-L. Pi, N. Trahair, Lateral-distortional buckling of hollow flange beams, *Journal of Structural Engineering* 123(6) (1997) 695-702.
- [79] C.C. Weng, T. Pekoz, Residual stresses in cold-formed steel members, *Journal of Structural Engineering* 116(6) (1990) 1611-1625.

- [80] Q. Liu, J. Yang, L.-y. Li, Pseudo-plastic moment resistance of continuous beams with cold-formed sigma sections at internal supports: An experimental study, *Engineering structures* 33(3) (2011) 947-957.
- [81] J. Ye, S.M. Mojtabaei, I. Hajirasouliha, P. Shepherd, K. Pilakoutas, Strength and deflection behaviour of cold-formed steel back-to-back channels, *Engineering Structures* 177 (2018) 641-654.
- [82] T. Von Kármán, The strength of thin plates in compression, *Trans. ASME* 54 (1932) 53-57.
- [83] C. Yu, T. Lokie, Effective width method based design for distortional buckling, (2006).
- [84] C. Yu, W. Yan, Effective Width Method for determining distortional buckling strength of cold-formed steel flexural C and Z sections, *Thin-walled structures* 49(2) (2011) 233-238.
- [85] S.C. Lau, G.J. Hancock, Distortional buckling formulas for channel columns, *Journal of Structural Engineering* 113(5) (1987) 1063-1078.
- [86] G.J. Hancock, Y.B. Kwon, E.S. Bernard, Strength design curves for thin-walled sections undergoing distortional buckling, *Journal of Constructional Steel Research* 31(2-3) (1994) 169-186.
- [87] B.W. Schafer, T. Pekoz, Direct strength prediction of cold-formed steel members using numerical elastic buckling solutions, (1998).
- [88] B.W. Schafer, The direct strength method of cold-formed steel member design, *Journal of constructional steel research* 64(7-8) (2008) 766-778.
- [89] B. Schafer, Local, distortional, and Euler buckling of thin-walled columns, *Journal of structural engineering* 128(3) (2002) 289-299.
- [90] B.W. Schafer, *Distortional buckling of cold-formed steel columns*, 2000.

- [91] D. Yang, G.J. Hancock, Compression tests of high strength steel channel columns with interaction between local and distortional buckling, *Journal of Structural Engineering* 130(12) (2004) 1954-1963.
- [92] B. Young, N. Silvestre, D. Camotim, Cold-formed steel lipped channel columns influenced by local-distortional interaction: strength and DSM design, *Journal of structural Engineering* 139(6) (2013) 1059-1074.
- [93] D.C. Yap, G.J. Hancock, Experimental study of complex high-strength cold-formed cross-shaped steel section, *Journal of structural engineering* 134(8) (2008) 1322-1333.
- [94] N. Silvestre, D. Camotim, P.B. Dinis, Post-buckling behaviour and direct strength design of lipped channel columns experiencing local/distortional interaction, *Journal of Constructional Steel Research* 73 (2012) 12-30.
- [95] P.B. Dinis, B. Young, D. Camotim, Local–distortional interaction in cold-formed steel rack-section columns, *Thin-Walled Structures* 81 (2014) 185-194.
- [96] P. Dinis, D. Camotim, Cold-formed steel columns undergoing local–distortional coupling: Behaviour and direct strength prediction against interactive failure, *Computers & Structures* 147 (2015) 181-208.
- [97] A. Martins, P. Dinis, D. Camotim, P. Providência, On the relevance of local–distortional interaction effects in the behaviour and design of cold-formed steel columns, *Computers & Structures* 160 (2015) 57-89.
- [98] A.D. Martins, P.B. Dinis, D. Camotim, On the influence of local-distortional interaction in the behaviour and design of cold-formed steel web-stiffened lipped channel columns, *Thin-Walled Structures* 101 (2016) 181-204.
- [99] D.C. Yap, G.J. Hancock, Experimental study of high-strength cold-formed stiffened-web C-sections in compression, *Journal of Structural Engineering* 137(2) (2010) 162-172.

- [100] V.B. Nguyen, C. Wang, D. Mynors, M. English, M. Castellucci, Compression tests of cold-formed plain and dimpled steel columns, *Journal of Constructional Steel Research* 69(1) (2012) 20-29.
- [101] T. Desmond, T. Pekoz, G. Winter, Local and overall buckling of cold formed compression members, Department of Structural Engineering Report, Cornell University (1978).
- [102] R. Papazian, R. Schuster, M. Sommerstein, Multiple stiffened deck profiles, *Proceedings of the Twelfth International Specialty Conference on Cold-Formed Steel Structures*, 1994, pp. 217-228.
- [103] B. Schafer, T. Peköz, The behavior and design of longitudinally stiffened thin-walled compression elements, *Thin-walled structures* 27(1) (1997) 65-78.
- [104] B. Young, J. Chen, Design of cold-formed steel built-up closed sections with intermediate stiffeners, *Journal of Structural Engineering* 134(5) (2008) 727-737.
- [105] J.-H. Zhang, B. Young, Compression tests of cold-formed steel I-shaped open sections with edge and web stiffeners, *Thin-Walled Structures* 52 (2012) 1-11.
- [106] H. Adeli, A. Karim, Neural network model for optimisation of cold-formed steel beams, *Journal of Structural Engineering* 123(11) (1997) 1535-1543.
- [107] J. Lee, S.-M. Kim, H.S. Park, Optimum design of cold-formed steel columns by using micro genetic algorithms, *Thin-Walled Structures* 44(9) (2006) 952-960.
- [108] J. Lee, S.-M. Kim, H.-S. Park, B.-H. Woo, Optimum design of cold-formed steel channel beams using micro Genetic Algorithm, *Engineering Structures* 27(1) (2005) 17-24.
- [109] T. Tran, L.-y. Li, Global optimisation of cold-formed steel channel sections, *Thin-Walled Structures* 44(4) (2006) 399-406.



- [110] K. Magnucki, P. Paczos, Theoretical shape optimisation of cold-formed thin-walled channel beams with drop flanges in pure bending, *Journal of constructional steel research* 65(8-9) (2009) 1731-1737.
- [111] J. Rhodes, J. Zaras, Development and design analysis of a new purlin system, (1988).
- [112] M. Castellucci, I. Pillinger, P. Hartley, G. Deeley, The optimisation of cold rolled formed products, *Thin-Walled Structures* 29(1-4) (1997) 159-174.
- [113] C.H. Pham, G.J. Hancock, Experimental investigation and direct strength design of high-strength, complex C-sections in pure bending, *Journal of Structural Engineering* 139(11) (2013) 1842-1852.
- [114] C.H. Pham, L.A. Bruneau, G.J. Hancock, Experimental study of longitudinally stiffened web channels subjected to combined bending and shear, *Journal of Structural Engineering* 141(11) (2015) 04015018.
- [115] V.B. Nguyen, M. English, M. Castellucci, FE simulation techniques for new process and product developments in metal forming industry, *Proceedings of the 13th International Cold Forming Congress*, 2015, pp. 178-185.
- [116] V.B. Nguyen, P. Wood, M. English, M. Castellucci, *The Design and Development of New Cold Roll Formed Products by Finite Element Modeling and Optimisation*, (2016).
- [117] M.R. Haidarali, D.A. Nethercot, Local and distortional buckling of cold-formed steel beams with both edge and intermediate stiffeners in their compression flanges, *Thin-Walled Structures* 54 (2012) 106-112.
- [118] J. Ye, I. Hajirasouliha, J. Becque, A. Eslami, Optimum design of cold-formed steel beams using Particle Swarm Optimisation method, *Journal of constructional steel research* 122 (2016) 80-93.

- [119] S.M. Mojtabaee, J. Ye, I. Hajirasouliha, Development of optimum cold-formed steel beams for serviceability and ultimate limit states using Big Bang-Big Crunch optimisation, *Engineering Structures* 195 (2019) 172-181.
- [120] V.B. Nguyen, M. English, The optimisation of thin-walled cold rolled products using Finite Element modelling and Design of Experiments, *The 8th International Conference on Thin-Walled Structures (ICTWS 2018)*, , Lisbon, Portugal, 2018.
- [121] K. Magnucki, M. Maćkiewicz, J. Lewiński, Optimal design of a mono-symmetrical open cross section of a cold-formed beam with sinusoidally corrugated flanges, *Thin-Walled Structures* 44(5) (2006) 554-562.
- [122] K. Magnucki, M. Rodak, J. Lewiński, Optimisation of mono-and anti-symmetrical I-sections of cold-formed thin-walled beams, *Thin-Walled Structures* 44(8) (2006) 832-836.
- [123] M. Ostwald, M. Rodak, Multicriteria optimisation of cold-formed thin-walled beams with generalized open shape under different loads, *Thin-walled structures* 65 (2013) 26-33.
- [124] B.P. Gilbert, L.H. Teh, H. Guan, Self-shape optimisation principles: Optimisation of section capacity for thin-walled profiles, *Thin-Walled Structures* 60 (2012) 194-204.
- [125] P. Sharafi, L.H. Teh, M.N. Hadi, Shape optimisation of thin-walled steel sections using graph theory and ACO algorithm, *Journal of Constructional Steel Research* 101 (2014) 331-341.
- [126] W. Ma, J. Becque, I. Hajirasouliha, J. Ye, Cross-sectional optimisation of cold-formed steel channels to Eurocode 3, *Engineering structures* 101 (2015) 641-651.
- [127] J. Ye, I. Hajirasouliha, J. Becque, K. Pilakoutas, Development of more efficient cold-formed steel channel sections in bending, *Thin-walled structures* 101 (2016) 1-13.
- [128] B.P. Gilbert, T.J.-M. Savoyat, L.H. Teh, Self-shape optimisation application: Optimisation of cold-formed steel columns, *Thin-walled structures* 60 (2012) 173-184.

- [129] J. Leng, J.K. Guest, B.W. Schafer, Shape optimisation of cold-formed steel columns, *Thin-Walled Structures* 49(12) (2011) 1492-1503.
- [130] H. Liu, T. Igusa, B. Schafer, Knowledge-based global optimisation of cold-formed steel columns, *Thin-Walled Structures* 42(6) (2004) 785-801.
- [131] J. Madeira, J. Dias, N. Silvestre, Multiobjective optimisation of cold-formed steel columns, *Thin-walled structures* 96 (2015) 29-38.
- [132] M. Moharrami, A. Louhghalam, M. Tootkaboni, Optimal folding of cold formed steel cross sections under compression, *Thin-Walled Structures* 76 (2014) 145-156.
- [133] J.M.S. Franco, J.P. Duarte, E. de Miranda Batista, A. Landesmann, Shape Grammar of steel cold-formed sections based on manufacturing rules, *Thin-Walled Structures* 79 (2014) 218-232.
- [134] J. Leng, Z. Li, J.K. Guest, B.W. Schafer, Shape optimisation of cold-formed steel columns with fabrication and geometric end-use constraints, *Thin-Walled Structures* 85 (2014) 271-290.
- [135] B. Wang, B.P. Gilbert, A.M. Molinier, H. Guan, L.H. Teh, Shape optimisation of cold-formed steel columns with manufacturing constraints using the Hough transform, *Thin-Walled Structures* 106 (2016) 75-92.
- [136] Z. Li, J. Leng, J.K. Guest, B.W. Schafer, Two-level optimisation for a new family of cold-formed steel lipped channel sections against local and distortional buckling, *Thin-Walled Structures* 108 (2016) 64-74.
- [137] H. Parastesh, I. Hajirasouliha, H. Taji, A.B. Sabbagh, Shape optimisation of cold-formed steel beam-columns with practical and manufacturing constraints, *Journal of Constructional Steel Research* 155 (2019) 249-259.

- [138] B. Wang, G.L. Bosco, B.P. Gilbert, H. Guan, L.H. Teh, Unconstrained shape optimisation of singly-symmetric and open cold-formed steel beams and beam-columns, *Thin-Walled Structures* 104 (2016) 54-61.
- [139] P. Pan, M. Ohsaki, H. Tagawa, Shape optimisation of H-beam flange for maximum plastic energy dissipation, *Journal of Structural Engineering* 133(8) (2007) 1176-1179.
- [140] J. Ye, J. Becque, I. Hajirasouliha, S.M. Mojtabaei, J.B. Lim, Development of optimum cold-formed steel sections for maximum energy dissipation in uniaxial bending, *Engineering structures* 161 (2018) 55-67.
- [141] ANSYS Mechanical, (Version 2018-2019-2020).
- [142] V.B. Nguyen, C.H. Pham, B. Cartwright, M. English, Design of new cold rolled purlins by experimental testing and Direct Strength Method, *Thin-Walled Structures* 118 (2017) 105-112.
- [143] M.R. Haidarali, D.A. Nethercot, Finite element modelling of cold-formed steel beams under local buckling or combined local/distortional buckling, *Thin-Walled Structures* 49(12) (2011) 1554-1562.
- [144] B. Schafer, CUFSM Version 3.12, in, Department of Civil Engineering, Johns Hopkins University, 2006.
- [145] M. Ashraf, L. Gardner, D. Nethercot, Strength enhancement of the corner regions of stainless steel cross-sections, *Journal of Constructional Steel Research* 61(1) (2005) 37-52.
- [146] R.B. Cruise, L. Gardner, Strength enhancements induced during cold forming of stainless steel sections, *Journal of constructional steel research* 64(11) (2008) 1310-1316.
- [147] G.J. Hancock, T. Murray, D.S. Ellifrit, *Cold-formed steel structures to the AISI specification*, CRC Press 2001.
- [148] W.-W. Yu, R.A. LaBoube, H. Chen, *Cold-formed steel design*, Wiley Online Library 2010.

- [149] S. Qadir, V.B. Nguyen, I. Hajirasouliha, B. Cartwright, M. English, Optimal design of cold roll formed steel channel sections under bending considering both geometry and cold work effects, *Thin-Walled Structures* 157 (2020) 107020.
- [150] Y. Huang, B. Young, The art of coupon tests, *Journal of Constructional Steel Research* 96 (2014) 159-175.
- [151] L. Gardner, N. Saari, F. Wang, Comparative experimental study of hot-rolled and cold-formed rectangular hollow sections, *Thin-Walled Structures* 48(7) (2010) 495-507.
- [152] S. Qadir, V. Nguyen, I. Hajirasouliha, B. Cartwright, M. English, Optimisation of flexural strength for cold roll formed sections using design of experiments and response surface methodology, (2020).
- [153] L. Gardner, X. Yun, Description of stress-strain curves for cold-formed steels, *Construction and Building Materials* 189 (2018) 527-538.
- [154] G. Matheron, Principles of geostatistics, *Economic geology* 58(8) (1963) 1246-1266.
- [155] J. Sacks, W.J. Welch, T.J. Mitchell, H.P. Wynn, Design and analysis of computer experiments, *Statistical science* (1989) 409-423.
- [156] D.E. Goldberg, *Genetic algorithms in search, Optimization, and MachineLearning* (1989).
- [157] K. Deb, *Multi-objective optimisation using evolutionary algorithms: an introduction, Multi-objective evolutionary optimisation for product design and manufacturing*, Springer 2011, pp. 3-34.